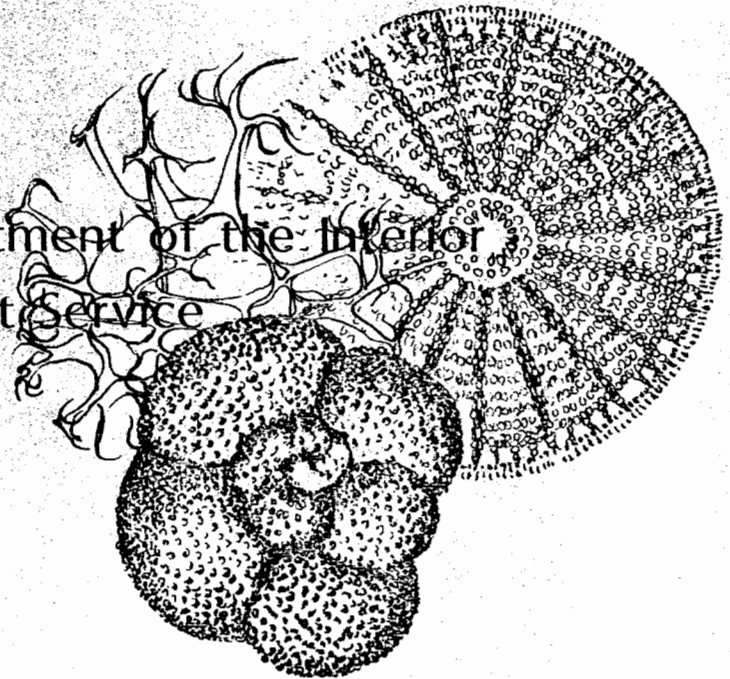


OCS Report MMS 84-0031

August 1984

**Geological and Operational Summary**  
**NAVARIN BASIN COST NO. 1 WELL**  
**Bering Sea, Alaska**

United States Department of the Interior  
Minerals Management Service



**GEOLOGICAL AND OPERATIONAL SUMMARY  
NAVARIN BASIN COST NO. 1 WELL**

**Bering Sea, Alaska**

**Ronald F. Turner (Editor)  
Colleen M. McCarthy  
David A. Steffy  
Maurice B. Lynch  
Gary C. Martin  
Kirk W. Sherwood  
Taber O. Flett  
Allen J. Adams**

**OCS REPORT MMS 84-0031  
August 1984**

**UNITED STATES DEPARTMENT OF THE INTERIOR  
MINERALS MANAGEMENT SERVICE  
Alaska OCS Region**

***Any use of trade names is for descriptive purposes  
only and does not constitute endorsement of these  
products by the Minerals Management Service.***



## CONTENTS

	<u>Page</u>
Introduction	1
Operational Summary	4
Shallow Geology and Geohazards	14
Paleontology and Biostratigraphy	20
Lithology	39
Velocity Analysis in Relation to Time-Depth Conversion	94
Seismic Stratigraphy	103
Bottom-Simulating Reflector	129
Well Log Interpretation	139
Abnormal Formation Pressure	167
Geothermal Gradient	193
Organic Geochemistry	199
Environmental Considerations	222
Summary and Conclusions	230
References	233

## APPENDIXES

Appendix 1. Abbreviations	A-1
2. Well data and consultants reports available for public inspection	A-3

## ILLUSTRATIONS

Figure 1. Lease Sale 83 bid history map	2
2. Location of Navarin Basin planning area	3
3. Final location plat	5
4. Daily drilling progress	7

## ILLUSTRATIONS (cont.)

	<u>Page</u>
5. Casing strings and plugging and abandonment program	8
6. Drilling mud properties	10
7. Lease blocks that exhibit characteristics of active or potential submarine slides	18
8. Siliceous biostratigraphic zonal summary	21
9. Biostratigraphy and paleobathymetry	22
10. Comparison of biostratigraphic summaries of ERT biostrat, BioStratigraphics, and MMS	23
11. Description of conventional core 1	49
12. Description of conventional core 2	50
13. Description of conventional core 3	51
14. Description of conventional core 4	52
15. Description of conventional core 5	52
16. Description of conventional core 6	53
17. Description of conventional core 7	53
18. Description of conventional core 8	54
19. Description of conventional core 9	55
20. Description of conventional core 10	56
21. Description of conventional core 11	57
22. Description of conventional core 12	58
23. Description of conventional core 13	59
24. Description of conventional core 14	60
25. Description of conventional core 15	61
26. Description of conventional core 16	62
27. Description of conventional core 17	63
28. Description of conventional core 18	64

ILLUSTRATIONS (cont.)

	<u>Page</u>
29. Description of conventional core 19	65
30. Description of conventional core 20	66
31. X-ray diffraction data	67
32. Ternary diagrams showing the range of quartz, feldspar, and lithic values, Zones A-1 to D-2	68
33. Ternary diagrams showing the range of quartz, feldspar, and lithic values, Zones E, G, H, and I	69
34. Ternary diagrams showing the range of volcanic, metamorphic, and sedimentary values, Zones A-1 to D-2	70
35. Ternary diagrams showing the range of volcanic, metamorphic, and sedimentary values, Zones E, G, and H	71
36. Comparison between time-depth curves from an integrated LSS log and from seismic reflection data	95
37. Comparison between RMS velocities from an integrated LSS log and from seismic reflection data	97
38. Heterogeneity factor versus RMS velocity	99
39. Interval velocities, anisotropy factor, and Cenozoic lithologic zones	100
40. Location map of Navarin Basin, COST No. 1 well, seismic data coverage, dredge samples, and features of geologic interest	102
41. Seismic line PR 7415 and free-air gravity profile	105
42. Seismic line PR 7418, free-air gravity profile, and filtered magnetics profile	107
43. Synthetic seismogram of the COST No. 1 well and seismic reflection profile	109
44. Seismic sequences and horizons, time-stratigraphic column, lithologic column, and seismic reflection profile	111
45. Seismic line PR 7410a, free-air gravity profile, and filtered magnetics profile	115

ILLUSTRATIONS (cont.)

	<u>Page</u>
46. Structure-contour map of a late Miocene unconformity (horizon A)	117
47. Seismic line PR 7411 and free-air gravity profile	121
48. Structure-contour map of the Oligocene B horizon	123
49. Structure-contour map of an Eocene-Cretaceous unconformity (horizon D)	125
50. Seismic reflection profile of a BSR	131
51. Pattern of decrease in interval transit time for highly diatomaceous rocks and their diagenetic equivalents	136
52. Pattern of porosity reduction and bulk density increase for highly diatomaceous rocks and their diagenetic equivalents	137
53. Neutron-density crossplot of Tertiary sandstone intervals	143
54. Porosity versus permeability for Tertiary sandstones	146
55. Typical pore pressure profile	168
56. Formation pore pressures versus depth	170
57. Typical effect of abnormal formation pressures on shale resistivity, acoustic velocity, and density	172
58. Bering Sea Tertiary shale acoustic transmission as a function of depth	174
59. Shale travel time versus depth, Navarin Basin COST No. 1 well	176
60. Shale interval travel time versus depth, Navarin Basin COST No. 1 well	179
61. Shale density versus depth, Navarin Basin COST No. 1 well	179
62. Pore pressure estimates from drilling parameters, Navarin Basin COST No. 1 well	179
63. Hottmann and Johnson's curve for relationship between shale travel time anomaly and pore pressure	185

## ILLUSTRATIONS (cont.)

	<u>Page</u>
64. Extrapolation of bottom hole temperatures to determine static BHT for logging run 2	194
65. Thermal gradient	197
66. Classification of organic matter	203
67. Modified Van Krevelen diagram	207
68. Indicators of thermal maturity	213
69. Total organic carbon and extractable C <sub>15</sub> + hydrocarbons	219

## PLATES

- Plate 1. Stratigraphic column and summary chart of geologic data
2. Shale resistivity and shale velocity curves, Bering Sea shelf
  3. Pressure plots for Navarin Basin COST No. 1 well
  4. Organic richness and hydrocarbon potential

## TABLES

Table 1. Conventional cores	11
2. Lithology, measured porosity, estimated visible porosity, and measured permeability of samples from sidewall and conventional cores	72
3. X-ray diffraction data from conventional cores, ranges of values for whole rock	90
4. X-ray diffraction data from conventional cores, ranges of values for the fraction finer than 5 microns	91
5. Summary of petrographic data	92
6. Summary of reservoir characteristics	93

TABLES (cont.)

	<u>Page</u>
7. Lithology and age of dredge samples	126
8. Sandstone interval log data and porosity averages, Zone B	151
9. Net sandstone, shale volume, effective porosity, and porosity-feet, Zone B	151
10. Sandstone interval log data and porosity averages, Zone C-1	154
11. Net sandstone, shale volume, effective porosity, and porosity-feet, Zone C-1	154
12. Sandstone interval log data and porosity averages, Zone C-2	156
13. Net sandstone, shale volume, effective porosity, and porosity-feet, Zone C-2	157
14. Suggested threshold values for genetic potential ( $S_1 + S_5$ ) from pyrolysis	215
15. Geochemical characteristics of Demaison's "type B and C" organic facies and analogous values from the Navarin well	221

Geological and Operational Summary  
Navarin Basin COST No. 1 Well  
Bering Sea, Alaska

Ronald F. Turner, Editor

INTRODUCTION

Title 30, Code of Federal Regulations (CFR), paragraph 251.14 stipulates that geological data and processed geological information obtained from Deep Stratigraphic Test wells drilled on the Outer Continental Shelf (OCS) be made available for public inspection 60 calendar days after the issuance of the first Federal lease within 50 nautical miles of the well site or 10 years after the completion of the well if no leases are issued. Tracts within this distance of the Navarin Basin Deep Stratigraphic Test well (designated the ARCO Navarin Basin COST No. 1 Well by the operator) were offered for lease in Sale 83 on April 17, 1984. Four hundred and twenty-five bids on 186 blocks were received. The high bids totaled \$631,228,331. One hundred and eighty bids were accepted and six high bids were rejected (fig. 1). The effective issuance date of the leases is June 1, 1984.

The well was completed on October 22, 1983, in Block 801, located approximately 457 miles southwest of Nome, Alaska (figs. 2 and 3). The well data listed in appendix 2 are available for public inspection at Minerals Management Service, Field Operations, located at 800 "A" Street, Anchorage, Alaska 99501.

Unless otherwise noted, all depths are measured from the Kelly Bushing, which was 85 feet above mean sea level. For the most part, measurements are given in U.S. Customary Units except where scientific convention dictates metric usage. A conversion chart is provided. The interpretations contained herein are chiefly the work of Minerals Management Service (MMS) personnel, although substantial contributions were made by geoscience consulting companies.

EQUIVALENT MEASUREMENT UNITS

1 inch = 2.54 centimeters	1 pound = 0.45 kilogram
1 foot = 0.3048 meter	1 pound/gallon = 119.83 kilograms/ cubic meter
1 statute mile = 1.61 kilometers	1 pound/square inch = 0.07 kilogram/ square centimeter
1 nautical mile = 1.85 kilometers = 1.15 statute miles = 6,080 feet	1 gallon = 3.78 liters (cubic decimeters)
1 knot = 1 nautical mile/hour	1 barrel = 42 U.S. gallons = 0.16 cubic meter
Temperature in degrees Fahrenheit less 32, divided by 1.8 = degrees Celsius	

# NAVARIN BASIN

LEASE SALE 83  
APRIL 1984

-  BLOCKS RECEIVING BIDS IN SALE 83
-  BIDS REJECTED
-  COST WELL
-  SALE AREA BOUNDARY

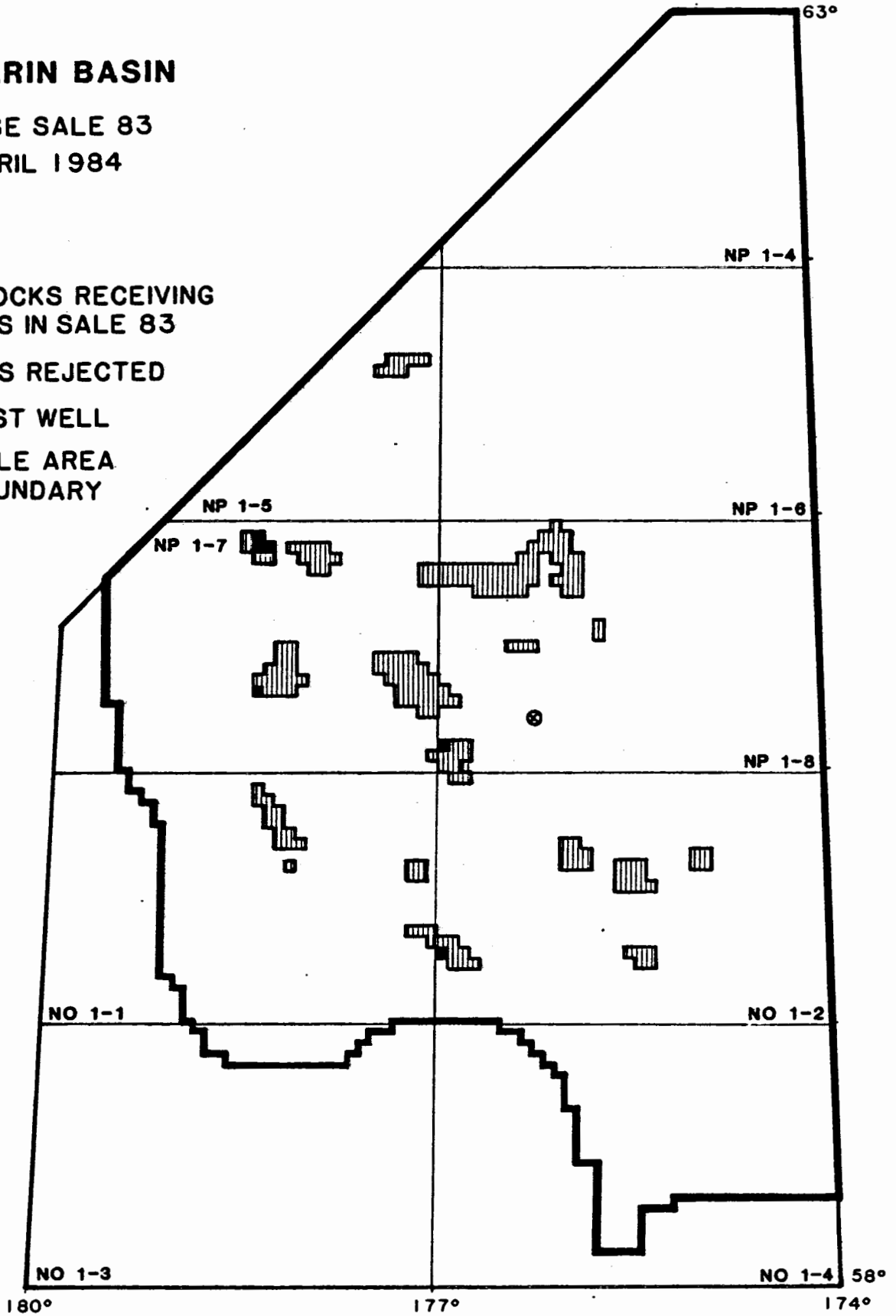
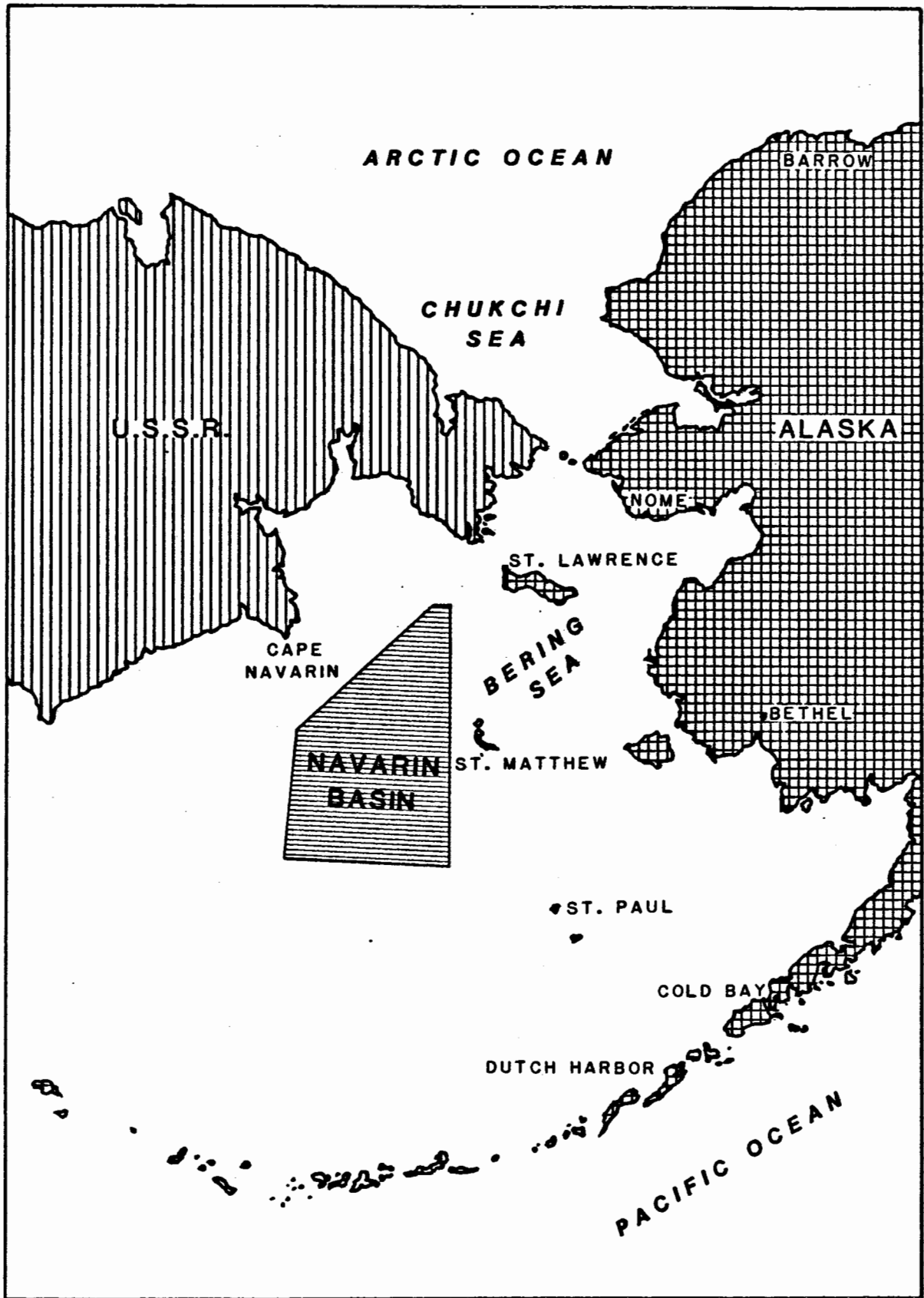


FIGURE 1. LEASE SALE 83 BID HISTORY MAP.



**FIGURE 2. GEOGRAPHIC LOCATION OF NAVARIN BASIN PLANNING AREA.**

OPERATIONAL SUMMARY  
by  
Colleen M. McCarthy

The Navarin Basin COST No. 1 well was drilled by the SEDCO 708, a column-stabilized semisubmersible drilling unit. The SEDCO 708, owned by SEDCO Maritime, Inc., was inspected by Minerals Management Service representatives in October 1981, and the predrill inspection was conducted on May 13, 1983.

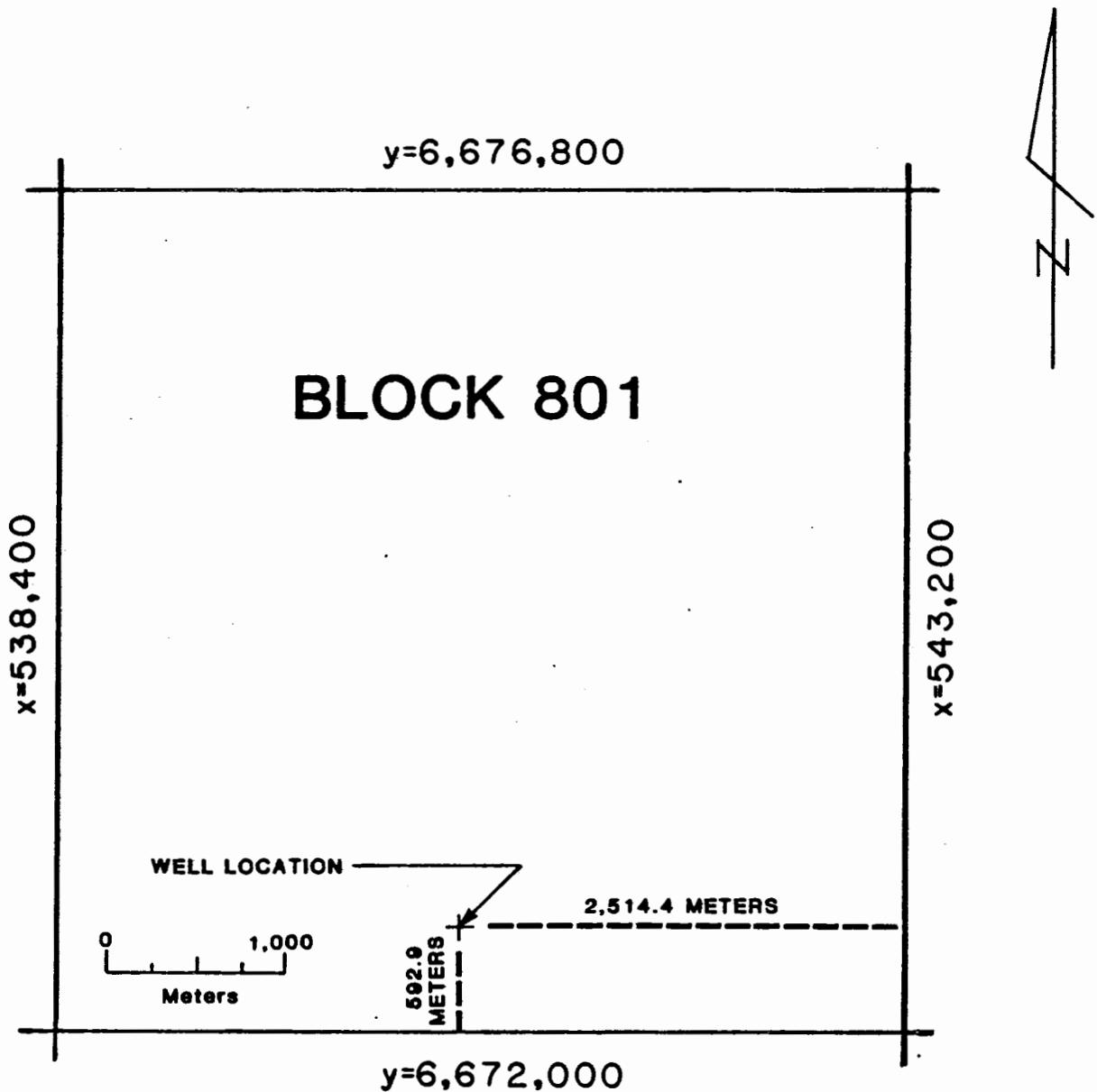
The SEDCO 708 is registered as an A.1 (E) (M) Self-Propelled Column-Stabilized Mobile Drilling Unit. It has been designed to withstand 110-foot waves and 100-knot winds in 600 feet of water. The rated drilling depth is 25,000 feet with a 1500-foot water depth. The American Bureau of Shipping approved extreme operating temperature is  $-22^{\circ}$  F.

Nome, Alaska, which is approximately 457 miles northeast of the well site, was utilized as the shore base for air support operations. Because the distance between the rig and the shore base was so great, a Boeing Chinook 234 helicopter, modified to carry extra fuel, was used to transport personnel, groceries, and lightweight equipment. The Chinook was certified for instrument flight and designed to carry 17 passengers on the 3-hour trip. Personnel, equipment, and supplies were transported between Nome and Anchorage by chartered and commercial air carriers.

Two seagoing supply vessels were used to transport drilling materials and supplies, including fuel, to the rig. They operated out of dock facilities at Dutch Harbor and Kenai. A large seagoing barge was also used to transport some materials from Kenai and was anchored at Dutch Harbor.

The location of the No. 1 well was  $1\text{at } 60^{\circ}11'24.054'' \text{ N.}$ ,  $1\text{ong } 176^{\circ}15'58.979'' \text{ W.}$ , or UTM coordinates (zone 1)  $X = 540,685.6$  meters and  $Y = 6,672,592.9$  meters. The well was located in Block 801 (fig. 3) in a water depth of 432 feet. All depths were measured from the Kelly Bushing (KB), which was 85 feet above the water line and 517 feet above the mud line.

The SEDCO 708 arrived on location at 2130 hours Alaska Standard Time (A.S.T.), May 21, 1983, and the well was spudded on May 26, 1983. On October 3, 1983, the 130th rig day, the total depth of 16,400 feet was reached. The well was plugged and abandoned on October 22, 1983, and the rig was released and undertow by 2055 hours A.S.T., October 14, 1983.



**GEODETTIC POSITION**

LAT. 60° 11' 24.054" N.  
 LONG. 176° 15' 58.979" W.

**UNIVERSAL TRANSVERSE MERCATOR  
 COORDINATES, ZONE 1**

y=6,672,592.9 meters  
 x=540,685.6 meters

**FIGURE 3. FINAL LOCATION PLAT SHOWING THE POSITION OF THE NAVARIN BASIN COST NO. 1 WELL IN OCS PROTRACTION DIAGRAM "NP 1-8."**

Atlantic Richfield acted as the operator for the following 18 petroleum companies which shared expenses for the well:

American Petrofina Company of Texas  
Amoco Production Company  
Chevron, U.S.A., Inc.  
Cities Service Company  
Conoco, Inc.  
Elf Aquitaine, Inc.  
Exxon Company, U.S.A.  
Getty Oil Company  
Gulf Oil Corporation  
Marathon Oil Company  
Mobil Exploration and Producing Service, Inc.  
Murphy Oil Corporation  
Pennzoil Company  
Phillips Petroleum Company  
Shell Oil Company  
Sohio Alaska Petroleum Company  
Texaco, Inc.  
Union Oil Company of California

Regulations and OCS Orders required the operator to provide the Minerals Management Service with all well logs, samples, core slabs, and operational and technical reports, including analyzed geological information, at the same time as industry participants.

#### DRILLING PROGRAM

The No. 1 well was drilled with less than 1 degree deviation from vertical down to 11,411 feet; below this depth the angle gradually increased to a bottom hole deviation of 8.5 degrees. A total of 45 drill bits were used. A 26-inch bit was used to drill the first 642 feet; then the hole was opened with a 36-inch hole-opener assembly. A 12 1/4-inch pilot hole was drilled to 1,536 feet and widened with a 26-inch hole-opener assembly. The well was drilled with 12 1/4-inch bits to 5,048 feet and opened with a 17 1/2-inch assembly. The hole was then deepened with 12 1/4-inch bits to 12,880 feet and with 8 1/2-inch bits to total depth.

The daily drilling progress is shown in figure 4. Drilling rates ranged from 2 to 563 feet/hour, beginning at an average of 125 feet/hour, and gradually decreasing to 50 feet/hour through 9,000 feet. From this depth, the drilling rate decreased to an average of 5 feet/hour at total depth.

The casing and abandonment programs are shown in figure 5. The 30-inch casing was set at 614 feet with 675 sacks of cement; the 20-inch casing was set at 1,508 feet with 1,650

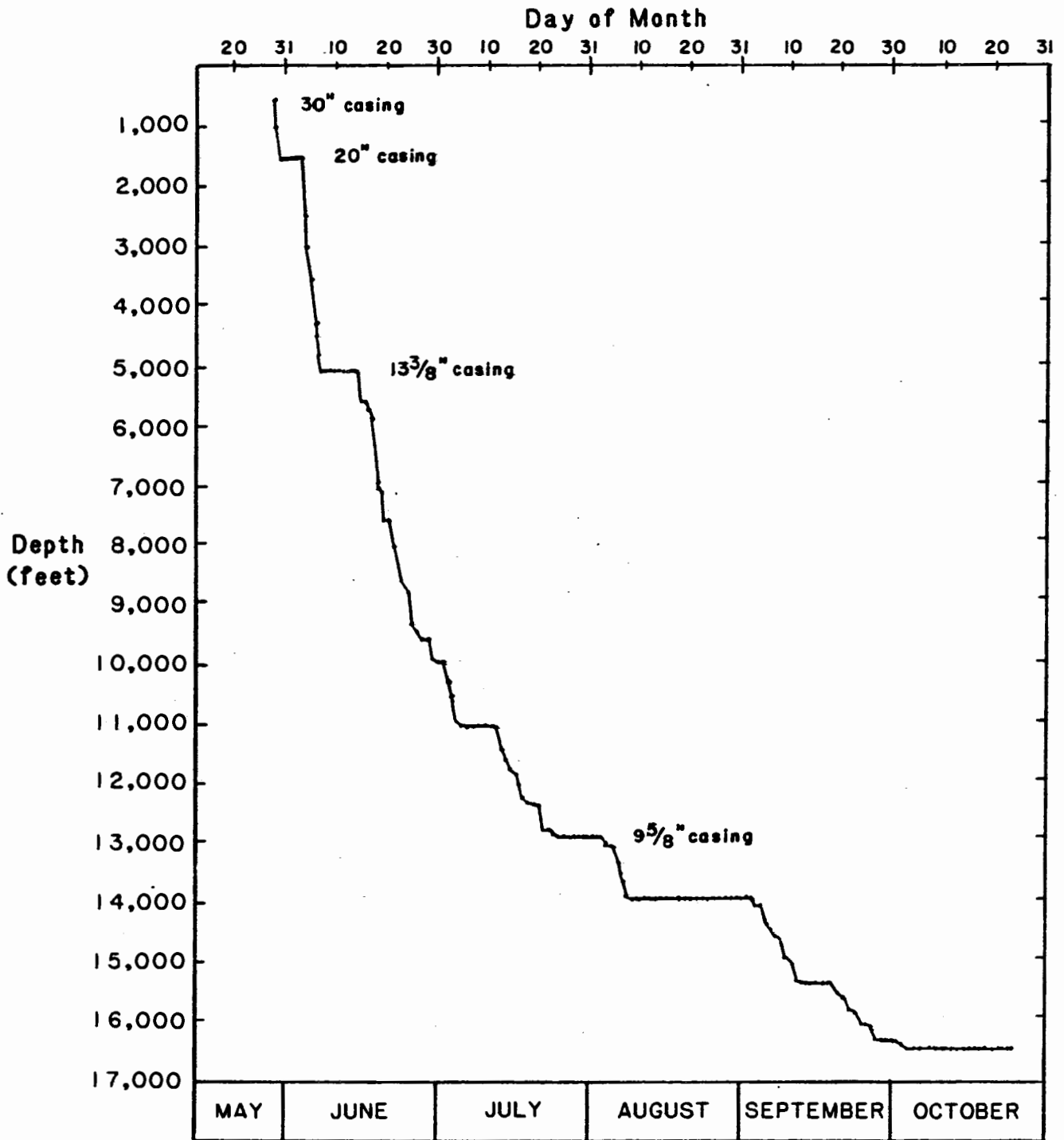


**FIGURE 4.** GRAPH SHOWING DAILY DRILLING PROGRESS FOR THE NAVARIN BASIN COST NO. 1 WELL.

**Kelly Bushing**  
**Water Line 85'**  
**Mud Line 432'**

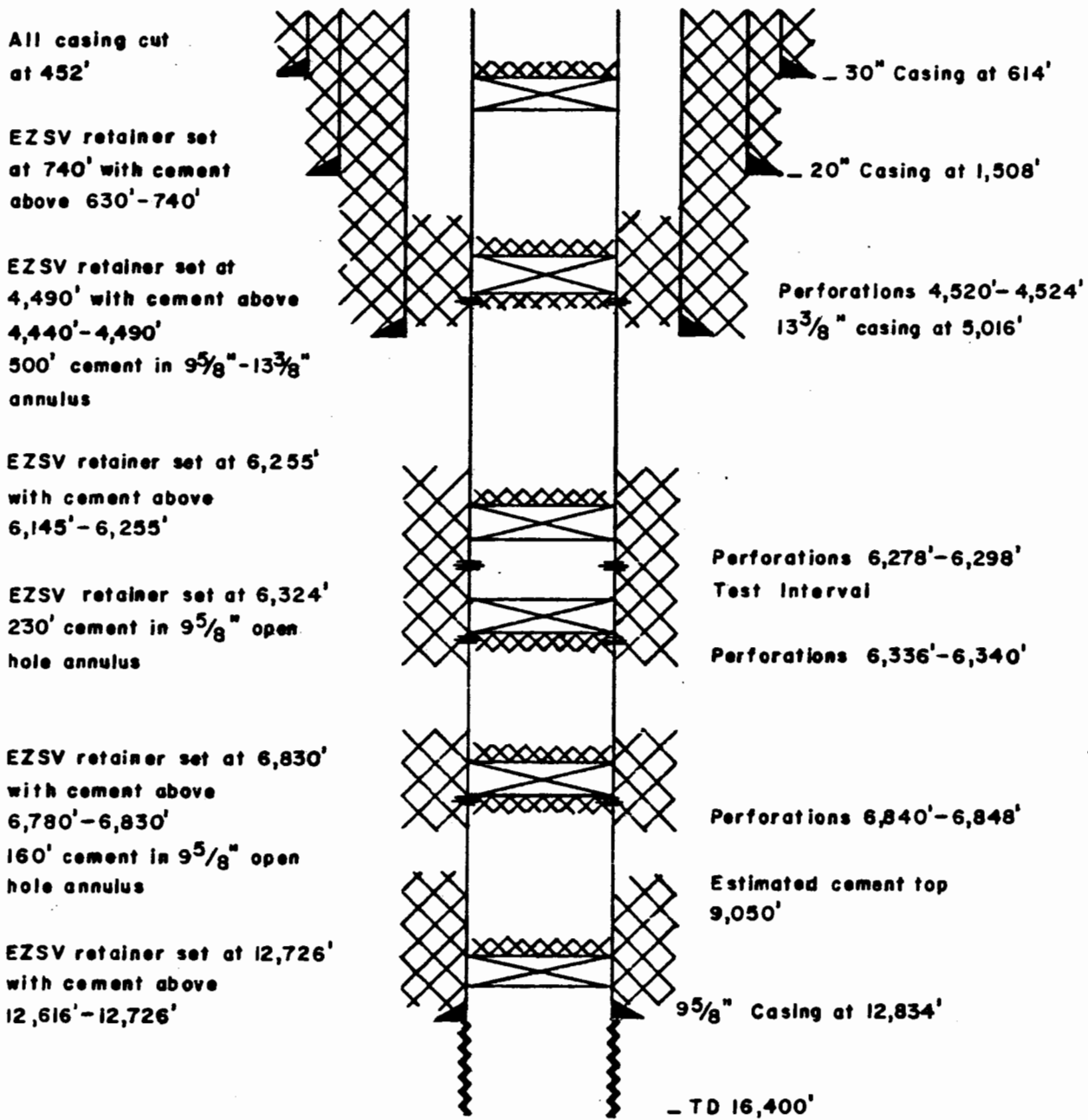


**FIGURE 5. SCHEMATIC DIAGRAM SHOWING CASING STRINGS, PLUGGING AND ABANDONMENT PROGRAM, NAVARIN BASIN COST NO. 1 WELL.**

sacks of cement; the 13 3/8-inch casing was set at 5,016 feet with 1,454 sacks of cement; and the 9 5/8-inch casing was set at 12,834 feet with 1,200 sacks of cement. Class G cement was used for all casing.

The abandonment of the well was begun with the setting of an EZSV (sliding valve) retainer at 12,726 feet and the emplacing of cement above the retainer from 12,616 to 12,726 feet. The 9 5/8-inch casing was then perforated from 6,840 to 6,848 feet with four shots per foot, and an EZSV retainer was set at 6,830 feet. Cement was squeezed to fill approximately 160 feet of the 9 5/8-inch and open hole annulus, with 50 feet of cement fill left above the retainer. The 9 5/8-inch casing was perforated with four shots per foot from 6,336 to 6,340 feet; another EZSV retainer was set at 6,324 feet; 230 feet of cement were squeezed into the 9 5/8-inch and open hole annulus. The test interval from 6,278 to 6,298 feet was perforated, and an EZSV retainer was set at 6,255 feet with 110 feet of cement placed above it. Perforations were then made in the 9 5/8-inch casing from 4,520 to 4,524 feet with four shots per foot, and an EZSV retainer was set at 4,490 feet. Cement was squeezed to fill approximately 500 feet of the 9 5/8-inch and 13 3/8-inch annulus, with 50 feet of cement fill left above the retainer. A surface plug, consisting of a 9 5/8-inch EZSV retainer, was set 740 feet, and a balanced 110-foot plug of cement was placed in the hole above the retainer. All casing strings were cut at 452 feet and recovered.

Fishing problems were encountered throughout the drilling of this well. At a drilled depth of 13,906 feet, the drill pipe became stuck, and after several days of unsuccessful fishing operations, the decision was made to plug the hole, kick off, and drill a new hole. Cementing difficulties and severe doglegs were encountered, and after several more days of plugging attempts, the well was kicked off below the 9 5/8-inch casing shoe. The entire operation took a total of 25 drilling days. At 16,272 feet, a bit cone and button inserts were lost in the hole. Milling operations took 3 days and drilling was resumed at 16,313 feet.

#### DRILLING MUD

Selected drilling mud properties taken from the mud log are shown in figure 6. Seawater was used to drill the first 1,536 feet, at which depth it was replaced with a saltwater and freshwater gel mud weighing 8.8 pounds per gallon (ppg) with a viscosity of 50 seconds. From 11,055 feet to total depth, a lignosulfonate drilling mud was used.

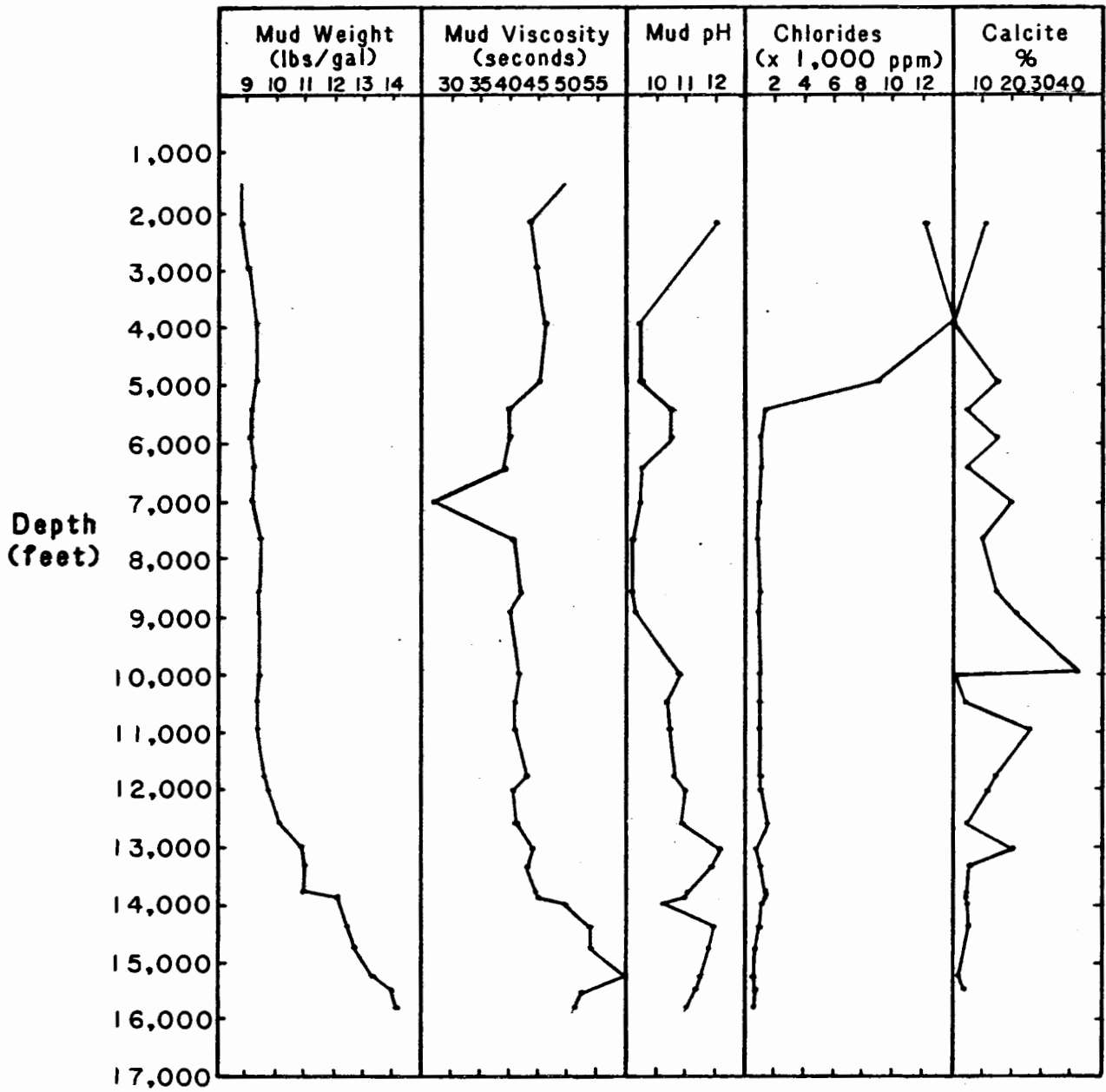


**FIGURE 6. CHANGES IN DRILLING MUD PROPERTIES WITH DEPTH, NAVARIN BASIN COST NO. 1 WELL.**

After the initial recorded mud weight of 8.8 ppg, the weight was increased gradually to 14.1 ppg at total depth. The viscosity of the mud ranged from 27 seconds at 7,000 feet to 60 seconds at 15,200 feet; viscosity was 51 seconds at total depth. The pH of the mud was 12 at the beginning of the well and 11 at total depth, a value of 11 being the norm throughout most of the drilling operation. Chloride concentrations began with a value of 12,000 ppm, increasing to 13,000 ppm where seawater was used heavily in the mud, decreasing to a range of 900 to 1,500 ppm from 5,000 feet to total depth. The percent of calcite found in the mud ranged from 0 to 20 percent throughout most of the well, but reached a high of 42 percent at 9,900 feet. Mud-logging services were provided by Exploration Logging (USA), Inc., from 1,500 feet to total depth.

#### SAMPLES AND TESTS

Drill cuttings were collected at various intervals for lithologic description and were analyzed for mineral composition and paleontological content. The information derived from these samples is discussed further in the applicable geological chapters of this report.

Twenty conventional cores were obtained and analyzed. Coring data are given in table 1.

Table 1. Conventional cores

Core No.	Interval (feet)	Recovered (feet)
1	3,627-3,657	30
2	4,184-4,214	27
3	5,100-5,130	21
4	5,572-5,592	7.7
5	6,370-6,400	23
6	7,160-7,166	5
7	7,600-7,626	26
8	8,639-8,669	10.5
9	9,400-9,430	30
10	9,656-9,686	30
11	9,948-9,987	39
12	10,979-11,019	36.9
13	11,707-11,737	29.5
14	12,709-12,749	39
15	12,850-12,880	30
16	13,141-13,159	18
17	13,876-13,906	27.9
18	14,575-14,605	30
19	15,500-15,510	9
20	16,313-16,342	29

Four series of sidewall cores were taken. At 5,048 feet, 180 cores were attempted and 133 recovered. At 11,060 feet, 305 cores were attempted and 269 recovered, with 13 misfires, two empty bullets, and 21 bullets left in the hole. At 12,880 feet, 69 cores were attempted and 61 recovered, with 8 bullets left in the hole. The last series of sidewall cores was run at 16,400 feet: 281 cores were attempted and 158 recovered, with 78 misfires and 45 empty or broken bullets.

The types of logs (Schlumberger nomenclature) and the intervals logged are as follows:

5,032 to 1,497 feet

Dual Laterolog/Micro-Spherically Focused Log  
Borehole Compensated Sonic Log  
Compensated Neutron/Formation Density Log  
Natural Gamma Ray Spectrometry Tool  
Long-Spaced Sonic Log  
Sonic Waveforms--8 foot  
High Resolution Dipmeter Tool  
Repeat Formation Tester  
Sidewall Sampler Tool

11,046 to 5,004 feet

Dual Induction Laterolog/Spherically Focused Log  
Borehole Compensated Sonic Log  
Compensated Neutron/Formation Density Log  
Natural Gamma Ray Spectrometry Tool  
Long-Spaced Sonic Log  
Sonic Waveforms--8 foot  
Proximity-Microlog  
High Resolution Dipmeter Tool  
Repeat Formation Tester  
Repeat Formation Tester Quicklook  
Sidewall Sampler Tool

12,834 to 5,004 feet

Dual Induction Laterolog/Spherically Focused Log  
Borehole Compensated Sonic Log  
Compensated Neutron/Formation Density Log  
Natural Gamma Ray Spectrometry Tool  
Long-Spaced Sonic Log  
Sonic Waveforms--8 foot  
Proximity-Microlog  
High Resolution Dipmeter Tool  
Profile Caliper  
Repeat Formation Tester  
Repeat Formation Tester Quicklook  
Sidewall Sampler Tool

15,341 to 12,815 feet

Dual Induction Laterolog/Spherically Focused Log  
Borehole Compensated Sonic Log  
Compensated Neutron/Formation Density Log  
Natural Gamma Ray Spectrometry Tool  
Long-Spaced Sonic Log  
Sonic Waveforms--8 foot  
Proximity-Microlog  
High Resolution Dipmeter Tool  
Repeat Formation Tester  
Sidewall Sampler Tool

16,385 to 12,815 feet

Dual Induction Laterolog/Spherically Focused Log  
Borehole Compensated Sonic Log  
Compensated Neutron/Formation Density Log  
Natural Gamma Ray Spectrometry Tool  
Long-Spaced Sonic Log  
Sonic Waveforms--8 foot  
Proximity-Microlog  
High Resolution Dipmeter Tool  
Repeat Formation Tester  
Sidewall Sampler Tool  
High Resolution Thermometer  
Cement Bond/Variable Density Log

Three drill stem tests were performed in the interval from 6,278 to 6,298 feet, which was perforated with four shots per foot and 90-degree phasing. Formation fluid samples and pressure buildup data were recovered for water resistivity calculations.

**WEATHER**

Weather conditions were monitored from late May through late October. During this period, maximum wind speeds of 46 knots and maximum wave heights of 38 feet were recorded. The lowest temperature recorded was 34° F and the highest, 50° F.

## SHALLOW GEOLOGY AND GEOHAZARDS

by

David A. Steffy

Shallow geologic characteristics and potential geohazards at the drill site were identified in a survey conducted by Nekton, Inc., in 1980. This site-clearance survey, part of the Application for Permit to Drill (APD), included a geotechnical study of the upper 5 feet of sediment and a high-resolution seismic reflection survey of the sea floor and its near-surface features. The regional description of the Navarin Basin and the Navarin oil and gas lease planning area is a synopsis of the work done by the U.S. Geological Survey, as summarized by Carlson and Karl (1981) and Karl and Carlson (1984). The summary is based on a composite of Government and university data. These data consisted of shallow geotechnical sampling and analog high-resolution and multichannel seismic reflection surveys. The location of the major physiographic and geologic features discussed in the following text is shown in figure 40 (Seismic Stratigraphy chapter).

### PHYSIOGRAPHY

The Navarin Basin sale planning area contains four physiographic features: continental shelf, continental slope, continental rise, and submarine canyons. The largest province, the shelf, covers most of the basin. Water depths range from less than 320 feet to 500 feet at the shelf break. This broad, flat surface has a very gentle slope of  $0.02^\circ$  to the southwest. About 35 miles to the east, the shelf rises to form St. Matthew Island.

The shelf grades into the continental slope, which lies in water depths of 500 to 9,200 feet. This province trends northwestward and slopes to the southwest. The continental slope ranges from 11 to 30 miles in width, and gradients range from  $3^\circ$  to  $8^\circ$ . The slope bathymetry is irregular because of slump blocks and channels.

Three large submarine canyons cut the shelf and slope. From south to north, they are the Zemchug, the Pervenets, and the Navarinsky Canyons. All three canyons begin as erosional channels in water depths of less than 500 feet and widen into vast canyons with large subsea fans. The toes of the fans extend into water depths greater than 9,800 feet. Dredge sampling indicates that the channels have eroded through the Cenozoic fill of the Navarin basin and into the Mesozoic basement rock. Navarinsky, the longest canyon (211 miles), has a relief of 2,300 feet and a width of 62 miles at the shelf break. Its two main channels have thalweg gradients

of  $0.33^\circ$  and  $0.50^\circ$ . Pervenets, the shortest canyon (78 miles), has a relief of 2,600 feet and a width of 19 miles at the shelf break. Its two main channels have a thalweg gradient of  $0.30^\circ$  and  $0.33^\circ$ . The Zemchug Canyon is 150 miles long and 62 miles wide at the shelf break. Its relief is 8,500 feet, and thalweg gradients range from  $1.2^\circ$  to  $2.2^\circ$ .

The continental rise comprises the remaining part of the planning area. It lies in water depths greater than 9,200 feet. The rise contains both submarine-canyon mouths and the toe deposits of subsea fans. Slopes range from  $0.5^\circ$  to  $1.8^\circ$ , with a generally southwestward gradient.

### SHALLOW GEOLOGY

The Navarin Basin is located on a broad, flat, stable continental shelf. During Pleistocene glaciations (and associated low stands of sea level), parts of the shelf were exposed to subaerial erosion. Sediment eroded from the exposed shelf and sediment carried by the ancestral Anadyr and Yukon Rivers were deposited across the basin and onto the continental slope and rise. Sea level low stands were also periods of active slumping along the slope. An irregular shelf edge and irregular bathymetry (fig. 47, Seismic Stratigraphy chapter) indicate this degradation. The interglacial periods and their associated high stands of sea level were intervals of little or no sediment accumulation on the shelf.

Quaternary sedimentation rates vary over the shelf, slope, and rise. Shelf rates range from 3.3 inches/1,000 years north of the shelf break, to 8.3 inches/1,000 years at the head of the submarine canyons, with a shelf average of 5.6 inches/1,000 years. Slope rates range from 2.0 inches/1,000 years at the upper slope, to 5.9 inches/1,000 years on the lower slope. This range reflects the effects of mass movement carrying large amounts of sediment down gradient. Rise sedimentation rates range from 2.8 to 8.3 inches/1,000 years, with an average of 5.9 inches/1,000 years. Areas of high sediment accumulation are characterized by turbidite fan deposits interbedded with hemipelagic muds.

The Holocene sedimentation rate on the shelf has been low, with an average accumulation of less than 3 feet. The lack of an immediate sediment source and the presence of weak bottom currents unable to carry much sediment load have resulted in sediment-starved depositional environments on the outer and middle shelf. Storm currents and tide-induced bottom currents dominate. These currents rework existing deposits but bring little or no new sediment into the basin. Bottom sampling indicates relict Pleistocene coarse-grained sand deposits along the shelf break and at the heads of

submarine canyons. Silts and sandy silts typify the rest of the shelf; muds and coarse-grained turbidites dominate the slope and rise.

Drop cores were collected at the well site. The upper 60 inches of sediment consisted of soft marine clay and clayey silt. This represents the thin veneer of unconsolidated Holocene mud that covers the inner and middle shelf of the region.

An isopach map of a probable Quaternary reflector by Carlson and others (1983) shows that this is a structurally controlled depositional environment. In the Pinnacle Island subbasin, a northwest-trending trough of Quaternary sediment parallels and is slightly offset to the northeast from a similar trough of Tertiary rock. Structural control of Quaternary sedimentation is also seen in the Navarinsky subbasin. High-resolution seismic data have detected faults that offset Quaternary reflections and parallel basement-controlled faults. These isopach trends and fault offsets indicate an actively subsiding basin.

#### GEOHAZARDS

Sea-floor instability, gas-charged sediments, and possible overpressuring are major geologic hazards in the Navarin Basin planning area. Limited public data have prohibited the lease-block-specific identification of geohazards. The available data did identify the types and general characteristics of potentially hazardous conditions.

Sea-floor instability hazards which may affect bottom-founded structures include faulting, seismicity, slides, and erosion. Apparently, both detached growth and basement-controlled faulting are presently active in the Navarin Basin. High-resolution seismic data reveal the fault offset of sediment as young as Pleistocene near the well site and throughout the margins of the individual subbasins. Fault offsets of Pliocene reflections near the well site were no more than 10 feet. Offsets of unspecified shallow reflections ranging from 33 to 67 feet were reported by Carlson and Karl (1981). Because few earthquakes have been observed in the planning area, most of the recent subsidence is probably in response to sediment compaction due to dewatering or grain reorientation. Meyers (1976) lists only seven reported earthquakes of unspecified magnitude in the area since 1786.

Submarine slides are a common hazard on the continental slope and in the dissecting submarine canyons. The USGS reconnaissance surveys have identified slides occurring in water depths of 500 to more than 3,900 feet, with one slide covering an area of over 480 square miles and composite slides affecting the upper 640 to 960 feet of sediment.

USGS gravity cores of the upper 16 feet of slide material reveal a mixture of pebbly mud to very soft mud. Slides were recognized as slumps, debris flows, and mud flows (Nardin and others, 1979) on the basis of seismic reflection characteristics. Rapidly deposited, unconsolidated, cohesionless, fine-grained material on the slope or shelf break is prone to sliding. Sliding may have been initiated either by cyclic wave loading induced by storms during low stands of sea level or by earthquakes. Lease blocks that exhibit the characteristics of active or potential submarine slides were identified in the Notice of Sale for the Navarin Sale 83 (fig. 7). The identifying characteristics include proclivities greater than 2 degrees, fault scarps, disrupted reflection sequences, hummocky bathymetry, and detached slump blocks. The lease blocks were classified on the basis of direct seismic evidence and inference. Where a hazard was inferred, the inference was justified by the block's bathymetric location and its proximity to blocks with direct seismic evidence of slides. Relict and recent movements could not be distinguished by seismic criteria.

Active erosion and redistribution of sediment could present hazards by reducing the support of bottom-founded structures. Such processes are expressed as sediment waves and sea-floor depressions. USGS surveys have identified relict large sediment waves formed at the heads of the three submarine canyons during low stands of sea level. At the Navarinsky Canyon, the waveforms cover an area of 230 to 270 square miles between the 700- and 1,475-foot isobaths. In some areas these sediment waves are covered by a thin veneer of recent sedimentation. Sea-floor depressions were surveyed on the down-slope sides of sediment waves. These depressions of unknown origin lie parallel to the bathymetric contours. The depressions are about 165 feet wide and 16 to 33 feet deep, and are located 330 to 6,500 feet apart. Bottom currents generated by surface waves have been proposed as a mechanism for fine-grained sediment transportation, although limited investigation has been conducted.

Gas-charged sediments are ubiquitous in the Navarin Basin. Shallow occurrences of gas-charged sediment can cause an increase in pore pressure and a decrease in shear strength which may result in unstable foundation conditions. These occurrences are identified on analog high-resolution seismic data as anomalous acoustic events recognized by polarity reversal, amplitude increase, reflector "wipe out," and reflector "pull down." Hydrocarbon gas was present in all USGS gravity cores. No significant shows of thermogenic gas were identified (Vogel and Kvenvolden, 1981). Shallow gas was also encountered at the well site (see Organic Geochemistry chapter). Most of the shallow gas is probably biogenic, although some thermogenic gas is possible. There

**Explanation:**

☐ Blocks with direct seismic evidence of submarine slides.

■ Blocks having an inferred potential for submarine slides.

-100- Bathymetric contour in meters.

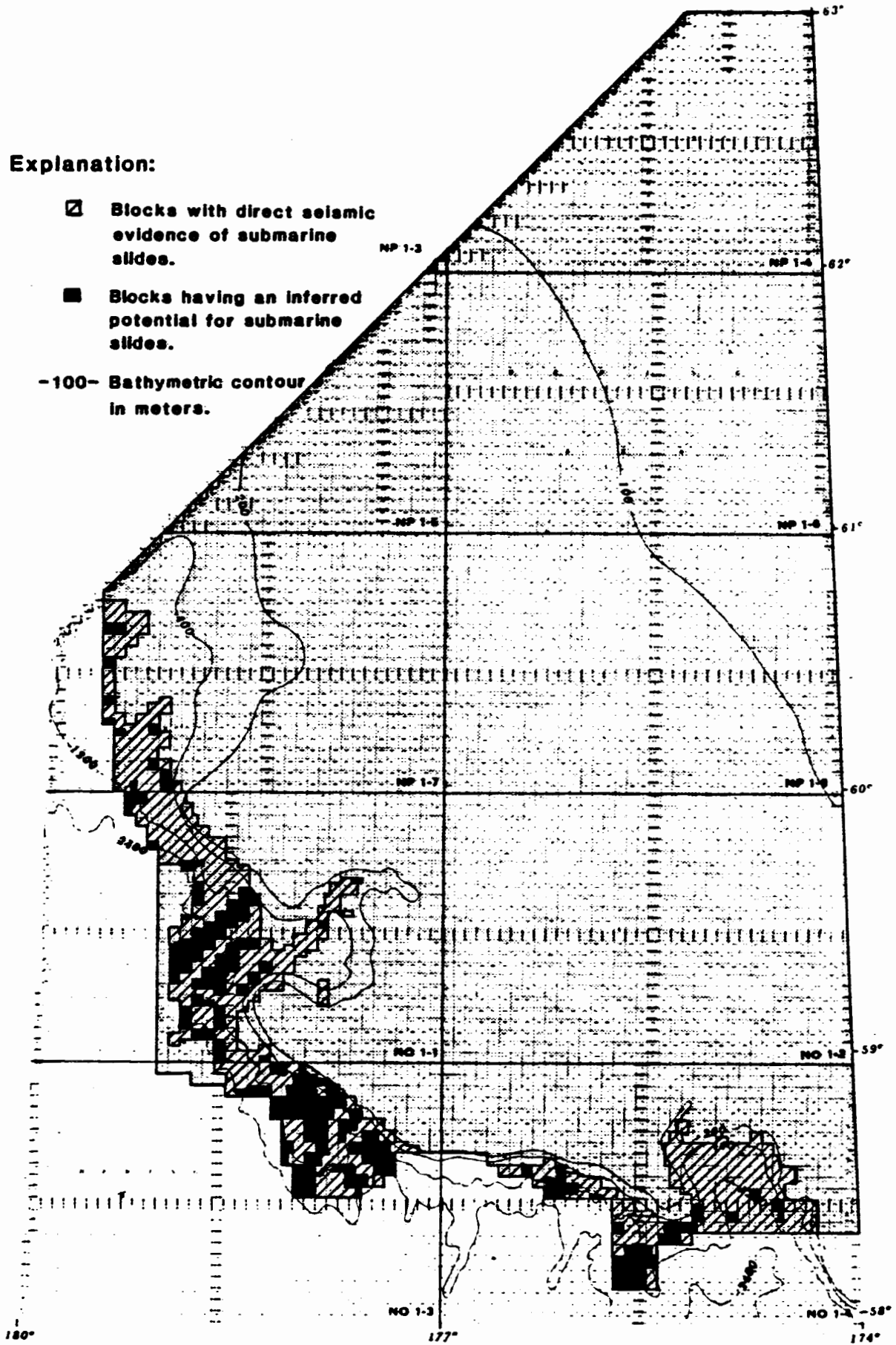


**FIGURE 7. LEASE BLOCKS OF NAVARIN LEASE SALE 83 THAT EXHIBIT CHARACTERISTICS OF ACTIVE OR POTENTIAL SUBMARINE SLIDES.**

is no obvious lithologic zone in which shallow gas accumulates. Anomalous seismic events that might be gas associated are found in the upper five lithologic Zones, A-1, A-2, B, C-1, and C-2 (see Well Log Interpretation chapter), of all three subbasins. Gas accumulations may be present in the form of a solid-phase mixture of water and gas in the continental slope and rise areas. This phenomenon is well documented in the Bering Sea (Kvenvolden and McMenamin, 1980; Marlow and others, 1981; Hammond and Gaither, 1983). The gas hydrate is identifiable because the acoustic impedance contrast produces a seismic reflection. Because the hydrate is temperature-pressure dependent, the reflection mimics the sea floor and appears to be a time-transgressive reflection in areas of structural relief.

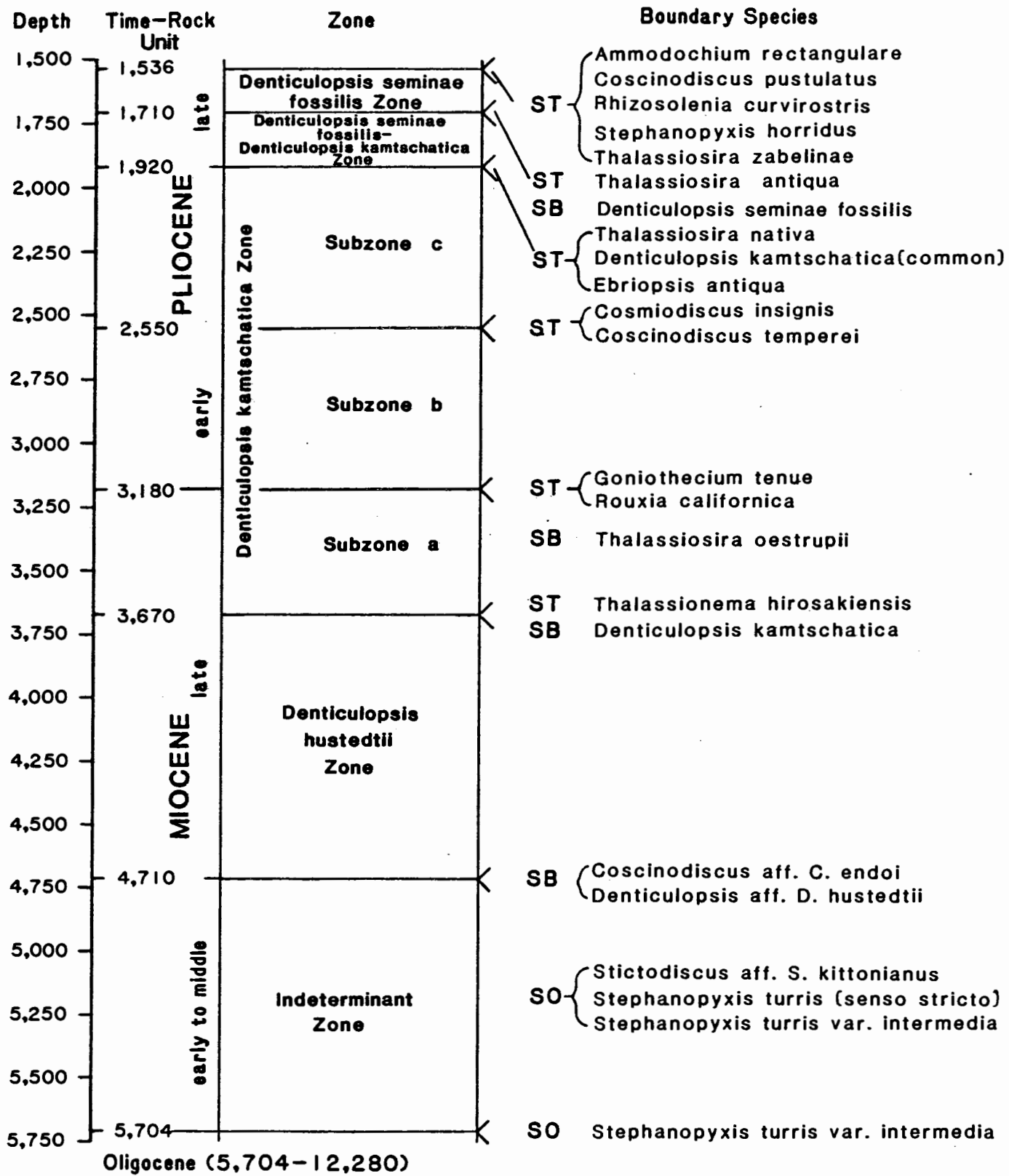
Unpredicted abnormal hydrostatic pressure can be hazardous during drilling. There is evidence from the Navarin Basin COST No. 1 well and from seismic reflection surveys for the presence of abnormal pressures in the Navarin Basin. The Abnormal Pressure chapter of this report discusses well log evidence for anomalous pressure in the well. In the Oligocene section, between 9,000 and 10,000 feet, hydrostatic pressure begins to deviate from the expected pressure gradient for the Bering Sea region. The deviation apparently continues down into the Cretaceous section. Abnormal pressures are also indicated in the Navarinsky subbasin by the presence of shale diapirs (fig. 45, Seismic Stratigraphy chapter). These diapirs are probably derived from Paleogene clays buried in a rapidly subsiding basin. The basinward divergence of continuous, coherent reflections, and their subsequent disappearance in the center of the basin, imply continuous, rapid deposition (fig. 41, Seismic Stratigraphy chapter). Rapid deposition increases the likelihood of overpressured shales by increasing the pressure on a porous medium having restricted flow (Gretener, 1981). Well data indicate that lithologic Zones E, F, and perhaps part of D-2 are within the oil window. Zones E and F contain appropriate types and amounts of kerogen for hydrocarbon generation. The time-equivalent sections of Zones E and F thicken considerably in the center of the northern subbasin. Thus, the source beds for the shale diapirs may be prone to hydrocarbon generation. Hedberg (1976) postulated that shales which produce gas under restricted-flow conditions enhance their diapiric capabilities. Therefore, at least in the Navarinsky subbasin, overpressured shales are likely and could pose a hazard to drilling operations.

## PALEONTOLOGY AND BIOSTRATIGRAPHY

by  
Ronald F. Turner

Paleoecologic and biostratigraphic determinations in the Navarin Basin COST No. 1 well are based on detailed analyses of microfossil assemblages containing Foraminifera, ostracodes, silicoflagellates and ebridians, diatoms, calcareous nannoplankton, Radiolaria, and marine and terrestrial palynomorphs. Rotary drill bit cuttings were processed and examined at 30-foot intervals from the first sample at 1,536 feet to the total depth of 16,400 feet. Data from conventional and sidewall cores were also examined and utilized. In addition, slides, processed samples, and reports prepared for the participants by consultants (BioStratigraphics, 1983; ERT biostrat, 1983) were examined, interpreted, and integrated into this report. Differences between consultant reports, principally the location of biostratigraphic tops, appear to be as much the result of philosophical differences concerning the taxonomy and biostratigraphic significance of certain microfossils as of variations due to different sample content or preparation techniques. The Minerals Management Service biostratigraphic interpretation also incorporated analyses of megafossils recovered from conventional cores (J. G. Marks, 1983; E. G. Kauffman, written commun., 1983), ostracode studies (Elizabeth Brouwers, written commun., 1984), and identifications of the rare planktonic Foraminifera in the well (Gerta Keller, written commun., 1984). Foraminiferal analysis and the synthesis of other data were done by the author. Siliceous microfossil analysis was done by Donald L. Olson.

Strata are discussed in the order in which they were penetrated. The integrated biostratigraphic units delineated were derived from various micropaleontological subdisciplines that do not agree in every biostratigraphic particular. Figure 8 is a siliceous microfossil zonation chart for the Neogene of the well. Figure 9 summarizes the MMS biostratigraphic and paleobathymetric interpretation. Figure 10 is a comparison of the MMS interpretation with those of the two consultants. Sample depths may disagree slightly with measured depths. Fossil occurrences are listed as highest and lowest rather than the potentially confusing first and last. Data obtained from conventional cores are given somewhat more weight than those from cuttings. Sidewall core data were not as reliable as usual because there was some trouble with uphole contamination from circulating drilling mud. The various lithologic zones and seismic sequences referred to in the text are discussed at length in the applicable chapters of this report. Regional correlation is discussed at the conclusion of this chapter.



ST-Stratigraphic Top; SB-Stratigraphic Base; SO-Significant Occurrence.

**FIGURE 8.** SILICEOUS BIOSTRATIGRAPHIC ZONAL SUMMARY.

MESOZOIC		CENOZOIC				ERA
Cretaceous		Neogene				PERIOD
LATE	CRETACEOUS	MIOCENE		PLIOGENE		EPOCH
? Campanian or older	Maastrichtian	middle to early	late	early	late	AGE

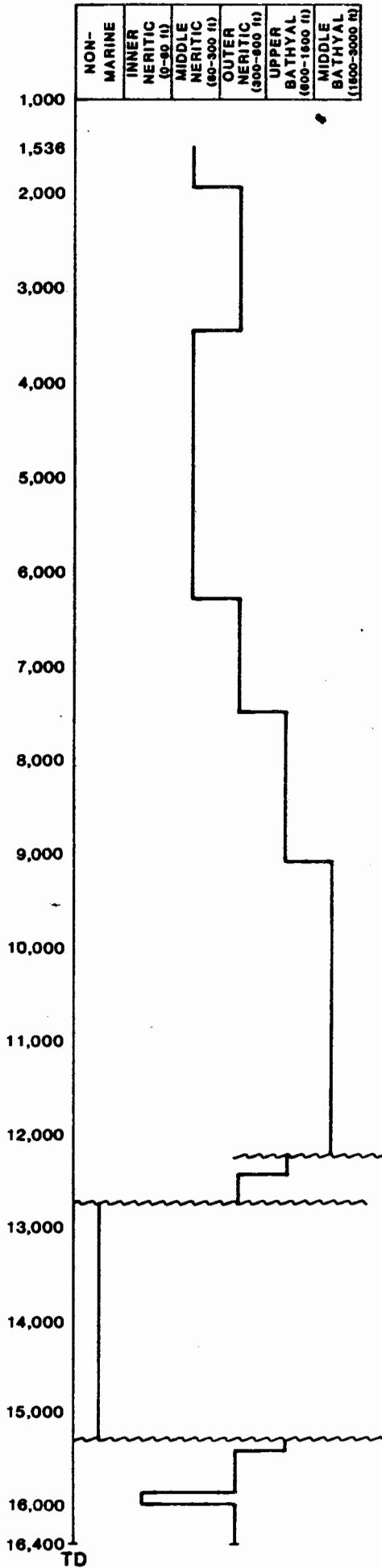


**FIGURE 9.**  
**BIOSTRATIGRAPHY**  
**AND**  
**PALEOBATHYMETRY**  
**OF THE**  
**NAVARIN BASIN**  
**COST NO. 1 WELL.**

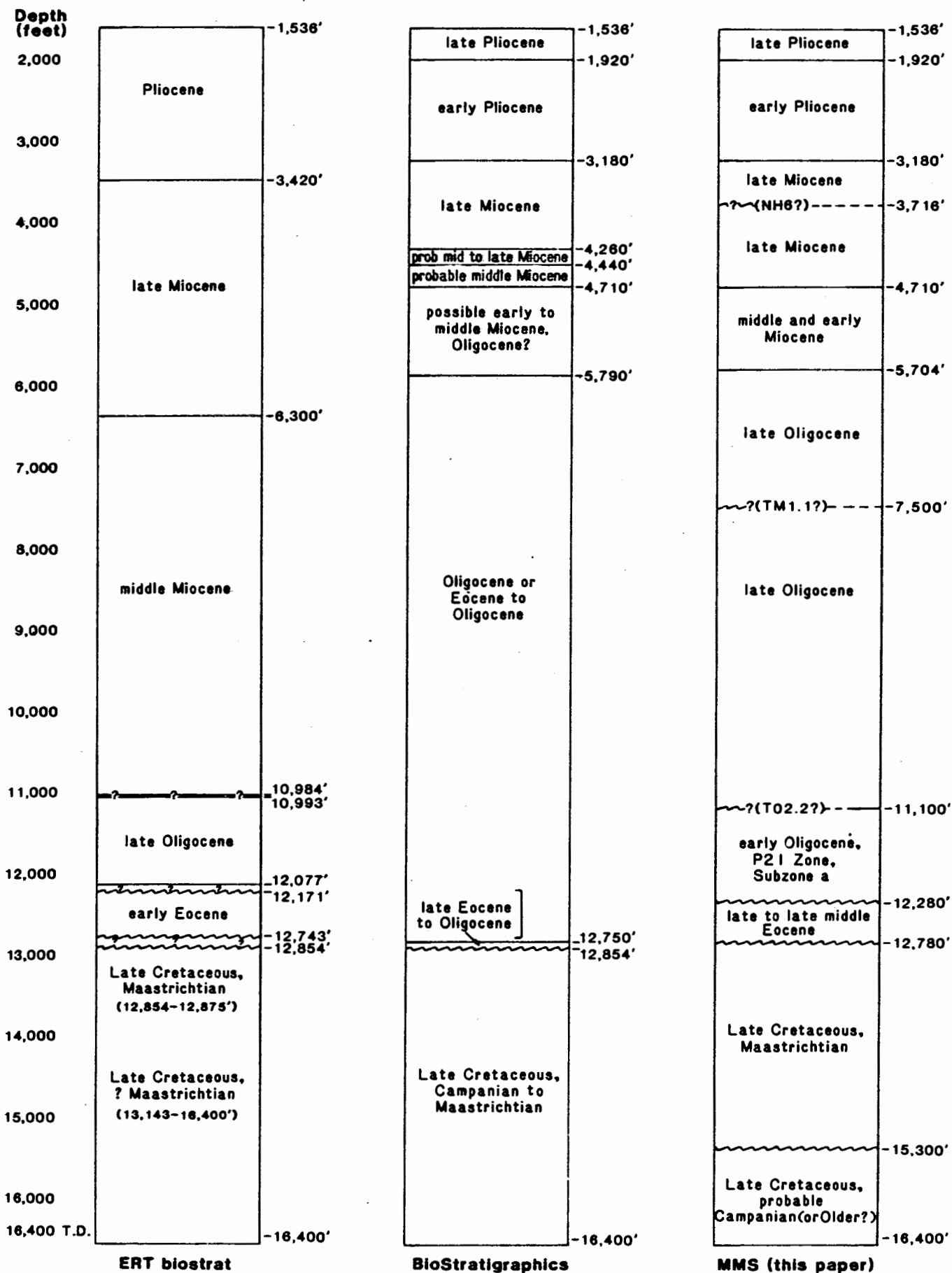


**FIGURE 10. COMPARISON OF BIOSTRATIGRAPHIC SUMMARIES OF ERT BIOSTRAT, BIOSTRATIGRAPHICS, AND MINERALS MANAGEMENT SERVICE**

Paleoenvironmental determinations are based on both microfossil and macrofossil suites. Paleoclimatological interpretations are based on spore and pollen assemblages and, to a lesser extent, on diatoms, silicoflagellates, Foraminifera, ostracodes, and molluscs. Fluvial, lacustrine, and paludal environments are classified as continental or nonmarine. Transitional environments include marshes, brackish estuaries, and hypersaline and hyposaline lagoons. For sediments deposited in marine environments, the paleoenvironment is expressed in terms of bathymetry (fig. 9) and is divided into inner neritic (0 to 60 feet), middle neritic (60 to 300 feet), outer neritic (300 to 600 feet), upper bathyal (600 to 1,500 feet), and middle bathyal (1,500 to 3,000 feet). Paleobathymetric determinations are primarily based on foraminiferal criteria, but dinoflagellates and other marine organisms such as bryozoans, molluscs, brachiopods, echinoids, ophiuroids, and cirripeds were taken into account. Lithological and sedimentological criteria were also utilized.

#### PLIOCENE

The Pliocene section of the well (1,536 to 3,180 feet) was subdivided into early and late ages primarily on the basis of diatom and silicoflagellate distributions. Although the siliceous microfloras were both abundant and diverse, the zonal subdivisions are somewhat tenuous. Even after factors such as reworking and up- and downhole contamination are taken into account, siliceous microfossil assemblages from the well are still characterized by unusual stratigraphic ranges and associations. Zonal equivalences were difficult to establish because "flagship taxa" were frequently either absent or out of place. That different taxonomic and zonal systems were utilized by the three siliceous microfossil investigators only compounded the problem. A provisional zonation was erected nevertheless.

The late Pliocene (1,536 to 1,920 feet) contains the middle and lower part of the Denticulopsis seminae var. fossilis Zone and the entire Denticulopsis seminae var. fossilis - Denticulopsis kamtschatica Zone. The former zone is characterized by the highest occurrences of Stephanopyxis horridus, Thalassiosira zabelinae, Coscinodiscus pustulatus, Rhizosolenia curvirostris inermis, and Ammodochium rectangulare; the latter zone (1,710 to 1,920 feet) is somewhat more problematical, and is defined here by the highest occurrence of Thalassiosira antiqua and the lowest occurrence of Denticulopsis seminae var. fossilis.

The late Pliocene siliceous microflora contains at least 70 species, many of which have long or uncertain stratigraphic ranges. Genera present include Actinocyclus, Ammodochium, Arachnoidiscus, Aulocodiscus, Bacteriosira, Biddulphia, Coscinodiscus, Chaetoceros, Cladogramma, Cosmiodiscus, Delphineis, Denticulopsis, Distephanus, Ebriopsis, Grammatophora, Goniothecium, Hyalodiscus, Melosira, Navicula, Nitzschia, Porosira, Pseudopodosira, Pseudopyxilla, Rhaponeis, Rhizosolenia, Stephanopyxis, Thalassionema, Thalassiosira, Thalassiothrix, and Xanthiopyxis.

The early Pliocene (1,920 to 3,180 feet) is subdivided into Subzones b and c of the Denticulopsis kantschatica Zone. Subzone c (1,920 to 2,550 feet) is defined by the highest stratigraphic occurrence of Thalassiosira nativa and the presence of common Denticulopsis kantschatica and Ebriopsis antiqua. The top of Subzone b (2,550 to 3,180 feet) is defined by the highest occurrences of Cosmiodiscus insignis and Coscinodiscus temperei; the base is defined by the lowest occurrence of Thalassiosira oestrupii and the top of the subjacent zone.

The generic composition of the diverse early Pliocene microflora is similar to that of the overlying late Pliocene. Additional genera include Actinoptychus, Cocconeis, Cymatosira, Dictyocha, Diploneis, Endictya, Mesocena, Rhabdonema, Rouxia, and Stephanogonia.

The moderately diverse, though quite sparse, ostracode assemblage present from 1,536 to 3,180 feet indicates a Pliocene age for the interval (Elizabeth Brouwers, written commun., 1984). The late Pliocene (1,536 to 1,920 feet) contains specimens of Normanicythere leioderma, Eucytheridea bradyi, Acanthocythereis dunelmensis, ?Rabilimis sp. B, "Rabilimis" sp. A, and Robertsonites tuberculata. The early Pliocene ostracode fauna is similar, but also contains a single specimen of Australimoosella sp. at 2,070 feet. Several of these taxa were previously recorded in the Pliocene section of the Norton Sound COST No. 1 and No. 2 wells (Turner, 1983a and 1983b).

The Pliocene foraminiferal faunas are typical of high-latitude cold-water shelf environments. There are no truly age-diagnostic species in the assemblage. The late Pliocene fauna is characterized by Elphidium clavatum, Elphidium bartletti, Protoelphidium orbiculare, Elphidiella sibirica, Elphidiella cf. E. gorbunovi, Buccella frigida, Buccella tenerrima, Dentalina baggi, Dentalina soluta, Pullenia sp., Poropullenia cf. P. bulloides, Cassidulina californica, Cassidulina laticamerata, Cassidulina teretis, Cassidulina norcrossi, Nonionella miocenica, Glandulina sp., Polymorphina sp., Quinqueloculina akneriana, and Epistominella cf. E.

bradyi. Molluscan shell shards, barnacle plates, fish teeth and bones, echinoid and ophiuroid plates, and bryozoan fragments are common.

The early Pliocene foraminiferal fauna is essentially the same as that of the late Pliocene, with the addition of Trifarina angulosa, Marginulina cf. M. adunca, Melonis cf. M. barleeanum, Melonis cf. M. pompilioides, and Uvigerina juncea. Thin-shelled terebratulid brachiopods and rare vinculariiform bryozoan zoaria are also present.

The palynological assemblages present from 1,536 to 3,180 feet indicate a Pliocene age for the interval. The pollen and spore assemblage is characterized by Alnipollenites spp., Tsugaepollenites spp., Ulmipollenites sp., Caryapollenites sp., Pterocaryapollenites sp., Piceapollenites spp., Betulaepollenites spp., Liquidambarpollenites sp., Juglanspollenites sp., Malvaceae, Ericaceae, Onagraceae, Compositae, Quercus sp., Pinus spp., Pediastrum sp. (fresh-water algae), Jussiaea sp., Diervilla echinata, Chenopodium leptophyllum, Deltoidospora spp., Lycopodiumsporites sp., Sphagnumsporites sp., Laevigatosporites spp., Stereisporites spp., Epilobium latifolium, and Cyathidites minor.

The dinoflagellate assemblage contains Tectatodinium pellitum, Spiniferites spp., Cymatiosphaera sp., Operculodinium sp., Kallosphaeridium sp., Lejeunia spp., Lejeunia fallax, Nematosphaeropsis labyrinthea, and Impagidinium pacificum. Reworked Cretaceous dinocysts are also present.

Judy Lentin, of ERT biostrat, recognized two unpublished palynological zones in the Pliocene section, the spore-pollen Laevigatosporites Zone of Norris (in preparation) and the dinoflagellate Impagidinium pacificum Zone of Bujak (in press). The former was developed by utilizing well data from the Beaufort-Mackenzie Basin, the latter from core hole data from Leg 19 of the Deep Sea Drilling Project (DSDP) in the Bering Sea. When published and integrated with diatom and foraminiferal data, these new zones may prove to be quite useful in high latitude biostratigraphy.

#### Environment

The Pliocene section reflects shelf deposition in relatively cold water. The late Pliocene environment ranged from cold temperate to subfrigid. The early Pliocene was predominantly cold temperate. Water depths in the late Pliocene were middle neritic. The early Pliocene section was deposited in outer neritic depths.

## MIOCENE

The interval from 3,180 to 5,704 feet is Miocene in age. This section is subdivided into several biostratigraphic zones, for the most part on the basis of diatom and palynomorph distributions. In addition to the biostratigraphic problems discussed in the Pliocene section, the zonation of the Miocene is further complicated by barren intervals. Seismic horizon A is unconformable on the flanks of the basin; at the well site this reflector corresponds to lithologic Zone A-2 and a paleontologically barren interval beginning at 3,716 feet. Seismic horizon A may correspond in part to the NH6 hiatus of Barron and Keller (1982). There are significant differences of opinion between the various consultants and between the various subdisciplines concerning the position of the Miocene-Oligocene boundary.

The interval from 3,180 to 4,710 feet is late Miocene in age and is subdivided into the Denticulopsis kamschatica Zone, Subzone a (3,180 to 3,670 feet), and the Denticulopsis hustedtii Zone (3,670 to 4,710 feet). The top of the Denticulopsis kamschatica Zone, Subzone a, is defined by the highest occurrences of Goniothecium tenue and Rouxia californica; the base is defined by the top of the subjacent zone. There are approximately 170 siliceous microfossil species in this interval. Additional genera not present in the overlying Pliocene section include Asteromphalus, Di cladia, Dictyo cha, Hemiaulus, Isthmia, Lithodesmium, Muelleriella, Rocella, Synedra, and Tetracyclus.

The top of the Denticulopsis hustedtii Zone is here defined by the highest occurrence of Thalassionema hirosakiensis and the lowest occurrence of Denticulopsis kamschatica. The base of the zone is placed at 4,710 feet on the basis of the lowest occurrences of Coscinodiscus aff. C. endoi and Denticulopsis aff. D. hustedtii. The siliceous microflora in this interval is relatively diverse and abundant but very poorly preserved. The zone of mineralogical phase change from opal-A to opal-CT appears to begin at approximately 3,565 feet; the change from opal-CT to quartz appears to begin below 4,440 feet. These changes were qualitatively observable optically, although exhaustive X-ray diffraction analysis (AGAT, 1983; James Hein, oral commun., 1984; Maurice Lynch, written commun., 1984) failed to disclose unequivocal evidence for the presence or location of these diagenetic boundaries. Definitive peaks are not generally discernible on X-ray diffractograms when opaline silica is present in amounts of 5 percent or less. However, some sidewall and conventional cores below 3,600 feet contained sediments composed of more than 50 percent diatoms. This is discussed further in the chapter on the bottom-simulating reflector (BSR).

The interval from 4,710 to 5,704 feet probably represents the middle and early Miocene. Most of the microfossils are too poorly preserved to be useful for detailed zonal biostratigraphy. The middle to early Miocene age determination is supported by the presence of Stictodiscus aff. S. kittonianus. Dean Milow, of BioStratigraphics, noted that in this interval, populations of Stephanopyxis turris sensu stricto are equal to or more abundant than those of Stephanopyxis turris var. intermedia. He suggests that this relationship is typical of Neogene populations, whereas populations dominated by Stephanopyxis turris var. intermedia are restricted to the Paleogene.

The ostracode fauna is sparse and poorly preserved. Many of the species also occur in the Pliocene section. New taxa indicative of a Miocene age include "Costa" sp., "Leguminocythereis" sp., and Elofsonella aff. E. concinna.

Palynological evidence also supports a Miocene age for the interval from 3,180 to 5,704 feet, although in the Miocene section the palynological consultants begin to differ significantly both in taxonomy and in the placement of stratigraphic tops. This interpretive divergence continued until Eocene strata were encountered and described. Species of Tsugaepollenites occur as high as 3,090 feet (early Pliocene) but became progressively more abundant downhole. The highest occurrence of Tsugaepollenites alexandriana (3,420 feet) marks the top of the unpublished Miocene Tsugaepollenites Zone of Norris (in preparation). In the Navarin Basin COST No. 1 well, this pollen zone appears to more or less coincide with the unpublished dinoflagellate Spiniferites ovatus Zone of Bujak (in press). Dinoflagellates became more abundant and stratigraphically useful below 3,800 feet. Taxa present include Spiniferites ovatus, Spiniferites spp., Cannosphaeropsis spp., Hystrichosphaeropsis sp. A (Williams, 1975), Tuberculodinium vancampoae, Tuberculodinium rossignoliae, Cordosphaeridium gracilis, Pentadinium laticinctum, Achomosphaera alaicornu, Paralecaniella indentata, Operculodinium centrocarpum, Nematosphaeropsis balcombiana, Oligosphaeridium sp., Lejeunia fallax, and Lejeunia globosa.

Calcareous nannoplankton were of limited value in the well. A single specimen of Cyclicargolithus floridanus was recovered from cuttings composited over the interval 5,520 to 5,610 feet. It indicated an age range of middle Eocene to early middle Miocene. The upper part of the range is consistent with the evidence from other fossil groups.

The foraminiferal faunas support a Miocene age for the interval 3,180 to 5,704 feet. Foraminifera are rare above 3,400 feet. The most significant foraminiferal markers are the highest occurrences of Porosorotalia clarki at 3,450 feet

and Ammonia japonica varianta (= Rotalia beccarii) at 5,280 feet. Other distinctive faunal elements are Elphidiella oregonensis, Elphidiella problematica, Elphidiella aff. E. discoidalis, Elphidiella cf. E. okhotica, Elphidiella cf. E. hannai, Criboelphidium cf. C. crassum, Elphidium clavatum, Elphidium bartletti, Haplophragmoides trullissata, Haplophragmoides deformes, Uvigerina juncea, Uvigerina cf. U. hootsi, Bolivina advena, Sigmomorphina sp., Cassidulina californica, Cassidulina taticamerata, Cassidulina norcrossi, and Sphaeroidina bulloides variabilis.

The fauna is similar to that described from the Norton Sound COST No. 1 and No. 2 wells, but may represent a somewhat deeper water depositional environment. The Navarin Basin Miocene foraminiferal fauna does not appear to have as close affinities with the Sakhalin Island and Kamchatka Peninsula assemblages as did those from the Norton Basin wells. Conflict between the published and unpublished biostratigraphic ranges of high-latitude Foraminifera is a problem that is compounded by the large amount of taxonomic synonymy in the American, Russian, and Japanese northern Pacific literature.

Molluscan fossils recovered from core 4 (5,572 to 5,580 feet) indicate a Miocene age. Bivalve taxa identified were Macoma?, Tellina?, and a cardiid.

#### Environment

The upper part of the Miocene section was deposited in outer neritic depths; below 3,450 feet the paleoenvironment was middle neritic. The climate was probably temperate to cold temperate.

#### OLIGOCENE

Oligocene strata (5,704 to 12,280 feet) represent the thickest sedimentary section in the No. 1 well. The top of the Oligocene is placed at the highest occurrence of diatom populations composed entirely of poorly preserved Stephanopyxis turris var. intermedia. Although this evidence alone does not warrant a firm age assignment, taken in conjunction with the palynological assemblage at 5,790 feet, it is quite defensible. The base of the Oligocene (12,280 feet) is placed at a lithologic boundary (Zone F) that marks an apparently unconformable contact with Eocene strata.

The section is paleontologically subdivided into late Oligocene (5,704 to 11,100 feet) and early Oligocene (11,100 to 12,280 feet). The boundary between lithologic Zones D-2 and E (10,800 feet), as well as the unconformity on the basin flanks that correlates with the reflector at 11,100 feet,

may both be related to a mid-Oligocene drop in sea level caused by a global cooling event 28 to 32 million years ago (Keigwin and Keller, 1984). This event is characterized by cooler oceanic water and is thought to be associated with an accumulation of continental ice in the Antarctic (Matthews and Poore, 1980; Kerr, 1984). The early Oligocene paleontologic top (11,100 feet) is correlative with the top of seismic sequence IV (seismic horizon C), which onlaps and truncates older strata and basement highs. Seismic sequence IV grades into apparent proximal turbidites on the southwestern flanks of the Pinnacle Island subsbasin. Lithologic Zone E is within the lower part of the Globorotalia opima Zone (P21 Zone, Subzone a) of Bolli (1957) and Blow (1969), as defined by Keller (1983). The early Oligocene age assignment is based primarily on planktonic foraminiferal data.

The abundant and diverse late Oligocene dinoflagellate assemblage is characterized by Paleocystodinium benjaminii, Paralecaniella indentata, Diphyes spp., Lejeunia fallax, Lejeunia hyalina, Lingulodinium pugiatum, Evittosphaerula paratabulata, Operculodinium centroporum, Hystrichokolpoma rigaudiae, Apteodinium australiense, Achomosphaera spp., Nematosphaeropsis balcombiana, Rottnestia borussica, Tuberculodinium vancampoae, Tuberculodinium rossignoliae, Membranilarnecia ursula, Polysphaeridium pastielsii, Areoligera senonensis, Spiniferites spp., Distatodinium craterum, Phthanoperidinium amoenum, and Cordosphaeridium multispinosum.

The range of Tuberculodinium vancampoae in Alaska has recently been questioned. There is one school of thought that considers it to be a Miocene marker, another that considers it to be more typical of the Oligocene. Williams and Bujak (1977) show it ranging from the "middle" Oligocene to the Pleistocene on the Labrador shelf of eastern Canada. Harland (1978) shows it ranging from the early Miocene into the Holocene on the northwestern European shelf. Wall and Dale (1971) have placed Holocene cysts assignable to Tuberculodinium vancampoae in the modern genus Pyrophacus, and Lentini and Williams (1977) list Tuberculodinium vancampoae as a Pleistocene species. In the St. George Basin COST No. 1 and No. 2 wells, Tuberculodinium vancampoae was present in strata dated as Oligocene on the basis of calcareous nannoplankton. In the Norton Sound COST No. 1 and No. 2 wells, this species was a common element of the Miocene marine microflora.

The spore and pollen assemblage is similar to the overlying Miocene Tsugaepollenites assemblage.

Foraminifera are relatively abundant, diverse, and well preserved in the Oligocene section. With the exception of the definitive early Oligocene planktonic assemblage, however, most of the species present are not strictly age diagnostic.

Although benthic Foraminifera were important for paleoenvironmental determinations, there are some ambiguities involving the paleobathymetric significance of Ammonia and Cyclammina. The late Oligocene (5,704 to 11,100 feet) contains both neritic and bathyal assemblages. Ammonia japonica (= Rotalia beccarii and several ecotypic varieties), generally considered a shallow-water species, is present in both environments. This suggests either a wider bathymetric range than commonly assumed or a depositional environment characterized by downslope mixing. The latter case is the most likely, although the relatively consistent presence of the species in deeper water deposits in other Bering Sea wells suggests that it may not have always been restricted to inner neritic and transitional environments. Ammonia japonica and Ammonia japonica varianta were both recorded from near the top of the section considered to be Oligocene in both Norton Sound COST wells, and were also present in the Oligocene of both St. George Basin COST wells. In the St. George Basin No. 1 well, the section was unequivocally dated as Oligocene on the basis of calcareous nannoplankton. In the Navarin Basin well, the highest occurrence of Ammonia japonica varianta is early Miocene. In most of the Bering Sea wells it has usually been encountered somewhat below the highest occurrence of Porosorotalia clarki.

Although Cyclammina is a dominantly bathyal genus in modern and ancient seas, Robinson (1970) showed that in the Gulf of Mexico it commonly ranged up into shelf depths as recently as late Miocene. In the Norton Sound COST No. 2 well, Cyclammina cf. C. pacifica was present in shelf sediments. The highest occurrence of the genus in the Navarin Basin COST No. 1 well (5,400 feet, early Miocene) is in sediments deposited in less than bathyal depths.

Other foraminiferal species present in the late Oligocene include Elphidiella oregonensis, Elphidiella cf. E. katangliensis, Elphidiella spp., Elphidium spp., Ammonia spp., Porosorotalia clarki, Porosorotalia cf. P. tumiensis, Psammosphaera carnata, Cassidulina cf. C. laevigata, Haplophragmoides trullisata, Haplophragmoides translucens, Cyclammina cf. C. cancellata, Cyclammina japonica, Cyclammina spp., Budashevella spp., Melonis pompilioides, Melonis cf. M. barleeianum, Gyroidina orbicularis planata, Gyroidina soldanii, Anomalina glabrata, Cassidulinoides bradyi, Sphaeroidina bulloides variabilis, Bathysiphon spp., Martinottiella pallida, Silicosigmollina sp., Pullenia sp., Pseudoglandulina inflata, Eponides spp., and Sigmomorpha schencki. The presence of Globigerina cf. G. ciperoensis at 8,100 feet suggests that at least the lower part of this section is within the P22 planktonic zone.

The early Oligocene section (11,100 to 12,280 feet) contains, in addition to most of the above species, Fissurina sp., Pyrgo sp., Gyroidina sp., Oridorsalis sp., and Cornuspira cf. C. byramensis. The most distinctive faunal elements are age-diagnostic planktonic species such as Globigerina linaperta, Globigerina angiporides, Globigerina cf. G. officinalis, Globigerina cf. G. senilis, Globigerina praebulloides, and Catapsydrax pera that are present from 11,110 to 11,850 feet. This interval is early Oligocene (P21 Zone, Subzone a) in age (Gerta Keller, written commun., 1984). A reworked specimen of the middle Eocene species Globorotalia bullbrooki was also present at 11,120 feet.

Ostracodes are rare but interesting in the late Oligocene section. With the exception of "Hemicythere" sp., the few specimens recovered above 9,090 feet are similar to those in the overlying Miocene. Below 9,090 feet, several additional genera with Paleogene affinities are present, including Krithe sp., ?Pectocythere sp., "Leguminocythereis" sp., "Robertsonites" sp., and Wichmanella sp. Of these, the latter genus is of particular interest. Wichmanella has heretofore been found in the Cretaceous of eastern South America and the Neogene of Japan. It probably migrated via straits bisecting the isthmus of Panama into the Pacific, then north and west, appearing first in the Alaskan Paleogene, then in the Japanese Neogene (Elizabeth Brouwers, written commun., 1984).

The early Oligocene ostracode fauna includes Wichmanella sp., Xestoleberis sp., Krithe sp., Eucytherura sp., ?Buntonia sp., ?Spinileberis sp., and "Patagonacythere" sp.

Calcareous nannoplankton are rare and nondiagnostic in the Oligocene section. A single specimen of the long-ranging (Late Cretaceous to early middle Miocene) species Braarudosphaera bigelowi was recovered from samples composited over the interval 6,240 to 6,330.

Isolated molluscan specimens were recovered from cores 9, 10, and 11 in the late Oligocene section. The best age determination was "post-Eocene". Taxa present include the bivalves Macoma? sp. and Lucinoma acutilineata, and an unidentified gastropod. Rare molluscan and arthropod fossils were recovered from core 13 in the early Oligocene section. Possible solenid and tellinid bivalves, Ostrea? sp., the gastropod "Buccinum?" sp., and a crab claw were identified between 11,707 and 11,711 feet. On the basis of this macrofossil data, Marks (1983) considered the depositional environment to have been outer neritic to bathyal in a temperate or warm sea with rather low bottom temperatures. This interpretation fits that derived from microfossils.

## Environment

The upper part of the Oligocene section (5,704 to 6,300 feet) was deposited in a middle neritic environment, possibly shallower. There is some calcareous nannoplankton evidence that suggests reduced salinity or a fresh-water influence in this interval. From 6,300 to 7,500 feet the depositional environment was probably outer neritic. The base of seismic sequence II (seismic horizon B, at approximately 7,400 feet) marks a regressive event that may represent the third order sea level drop TM1.1 of Vail and others (1977). The basal part of seismic sequence II represents the first marine transgression to extend substantially beyond the structurally defined margins of the basin. The interval from 7,500 to 9,100 feet was deposited in upper bathyal depths. The interval from 9,100 to 12,280 feet was probably deposited, for the most part, in middle bathyal depths. Paleontological evidence for the mid-Oligocene sea level drop (T02.2 of Vail and others, 1977) is subtle. There is a rather sharp reduction in faunal diversity between 11,100 and 11,300 feet that coincides with the top of the interval containing early Oligocene planktonic Foraminifera. This diversity decrease may mark the eustatic event more precisely than either the lithologic boundary between Zones D-2 and E or the top of seismic sequence IV (seismic horizon C). Given the different parameters being defined and differences in resolution, all of these "boundaries" may reflect the same suite of related events.

The overall Oligocene paleoclimate was probably temperate to warm temperate.

## EOCENE

A 500-foot-thick Eocene section is present from 12,280 to 12,780 feet. The upper contact appears to be unconformable on the basis of a combination of well log, lithological, geochemical, and paleontological criteria, but there is no geophysical evidence for an unconformity. The lower unconformable contact is defined by strong seismic evidence as well as the above criteria. Lithologic Zone F appears to represent the entire Eocene section present in the well. There is no compelling geochemical evidence for large amounts of missing section at either unconformity. There is some disagreement between foraminiferal and palynological ages. The Foraminifera present tend to suggest a late Eocene age; the dinoflagellates indicate a slightly earlier age. The interval is assigned a late to late middle Eocene age.

The marine palynomorph assemblage is characterized by Areosphaeridium diktyoplokus, Apectodinium homomorphum, Operculodinium centrocarpum, Micrhystridium sp., Paralecaniella

indentata, Lejeunia hyalina, and Impletosphaeridium insolitum. The overlapping ranges of Areosphaeridium diktyoplokus and Apectodinium homomorphum (as shown by Williams and Bujak, 1977) support a late middle Eocene age.

The foraminiferal fauna is similar to that seen in the overlying Oligocene. The fauna includes Globobulimina ilpinica, Bulimina cf. B. lirata, Bulimina cf. B. pupoides, Pullenia eocenica, Sigmomorphina undulata, Eponides spp., Cibicides sp., Nuttallites sp., Gyroldina sp., Melonis pompilioides, Bathysiphon spp., Rhabdammina sp., Martinottiella palida, Ammobaculites sp., Trochammina sp., Haplophragmoides spp., Cyclammina spp., Elphidiella cf. E. californica, Porosorotalia tumiensis, Ammonia japonica, Pyrgo sp., and Globocassidulina globosa.

No molluscs, ostracodes, siliceous microfossils, or calcareous nannoplankton were identified in the Eocene section.

#### Environment

The depositional environment was upper bathyal from 12,280 to 12,450 feet; outer neritic from 12,450 to 12,780 feet.

The paleoclimate was probably temperate or warmer.

#### CRETACEOUS

The interval from 12,780 to 16,400 feet is Late Cretaceous in age on the basis of both marine and nonmarine fossils. The rocks beneath the angular unconformity (seismic horizon D) that defines the top of the section are nonmarine from 12,780 to 15,300 feet (combined lithologic Zone G/H) and marine from 15,300 to 16,400 feet (lithologic Zone I). The contact between the marine and nonmarine sections appears to be unconformable on the basis of paleontological, lithological, and well log criteria. Diabase sills radiometrically dated (K-Ar) as early Miocene by Teledyne Isotopes (1983) are intercalated with the coal and siltstone beds of the nonmarine section.

The nonmarine section is Maastrichtian in age on the basis of the pollen Aquilapollenites parallelus and Manicorpus cf. M. trapeziforme.

The marine section (15,300 to 16,400 feet) is probably Maastrichtian or Campanian in age. Foraminifera present include Praebulimina kickapooensis, Praebulimina venusae, Praebulimina carseyae, Gavelinella whitei, Gyroldinoides nitidus, Gyroldinoides goudkoffi, Haplophragmoides excavatus,

Haplophragmoides incognatus, Nodosaria sp., Dentalina spp.,  
Pullenia cretacea, Saccammina sp., Silicosigmoidina californica,  
Saracenaria cf. S. triangularis, and Osangularia cordieriana.  
The foraminiferal fauna is similar to the ?Campanian to  
Maastrichtian assemblage identified from the Lower Cook  
Inlet COST No. 1 well (Wills and others, 1978).

A single specimen of the calcareous nannoplankton  
Zygodiscus cf. Z. acanthus is present in samples composited  
over the interval from 15,300 to 15,390 feet. This species  
indicates a Late Cretaceous age (Maastrichtian or Campanian).

Rare, poorly preserved pseudoaulophacid Radiolaria were  
recovered from core 19 (15,500 feet). These specimens suggest  
a Cretaceous age.

Rare Inoceramus prisms, both in situ and reworked, were  
present throughout the Cretaceous section. In addition, a  
single valve from an inoceramid bivalve was recovered from  
core 20 (16,316 feet). The specimen was identified by E. G.  
Kauffman (written commun., 1983) as a species of Platyceramus,  
a genus that ranges from the Coniacian to the Campanian. The  
specimen compared most closely with Coniacian to Santonian  
species. It is possible that the strata at the bottom of  
the well could be that old. Palynomorphs from the marine  
section below the unconformity at 15,300 feet have been  
thermally degraded and yield no definitive age older than  
?Campanian to Maastrichtian. There are nearby dredge sample  
data that indicate the presence of older Cretaceous rocks in  
the immediate area (see correlation section). Paleomagnetic  
data, however, tend to support an age of no older than  
Campanian at total depth.

#### Environment

The nonmarine section (12,780 to 15,300 feet) probably  
represents a fluvial-paludal floodplain system. The marine  
section (15,300 to 16,400 feet) was deposited in inner neritic  
to upper bathyal depths. Both faunal and geochemical evidence  
(kerogen profile) suggests several transgressive-regressive  
cycles in the Late Cretaceous marine section. The paleoenvironment  
of the interval from 15,300 to 15,400 feet was upper bathyal.  
From 15,400 to 15,840 feet the environment was dominantly  
outer neritic, perhaps occasionally shallower, with a  
considerable amount of terrigenous organic input. From 15,840  
to 15,960 feet the environment was probably inner neritic.  
From 15,690 to 16,400 feet the paleobathymetry was probably  
outer neritic.

The Late Cretaceous paleoclimate was probably warm  
temperate, possibly subtropical.

## CORRELATION

The Navarin Basin COST No. 1 well can be correlated with the other Bering Sea deep stratigraphic test wells in a very general way. The Neogene section, in particular, is similar to that seen in the Norton Sound and St. George Basin wells. In all of these, the Neogene biostratigraphy was based on zones primarily defined by siliceous microfossils. Foraminifera were of more use for paleoenvironmental determinations, although there were some age-diagnostic species present in the early Miocene sections. Ostracodes proved to be surprisingly useful for both paleoecology and biostratigraphy. Neogene palynological zonations are still in the developmental stage in the Bering Sea area, and calcareous nannoplankton have proven to be of very limited utility in this section. Nevertheless, the Neogene sections of these five deep stratigraphic test wells can be correlated with some degree of confidence.

Paleogene correlations are far more difficult to establish. In particular, there is disagreement among industry, academic, and government biostratigraphers as to the nature and extent of Oligocene strata in the Bering Sea area. Much of the confusion stems from correlation with Russian onshore sections on the Kamchatka Peninsula and Sakhalin Island that were initially described as Miocene but are now considered to be, in part, Oligocene (Gladenkov, 1980). The ages of Paleogene foraminiferal and palynological assemblages are often the subject of dispute. Siliceous microfossils are difficult to work with in the older sections because they have generally been diagenetically replaced by pyrite. Calcareous nannoplankton and planktonic foraminifera yield the best information, but neither group is consistently present.

The Oligocene foraminiferal assemblage of the Navarin Basin COST No. 1 well is somewhat similar to assemblages described from the Norton Sound and St. George Basin deep stratigraphic test wells, from the Kamchatka Peninsula and Sakhalin Island, and from the Poul Creek Formation (offshore) in the Gulf of Alaska. There are significant differences, however, such as the absence of the diverse shallow water assemblages seen in the Norton Sound COST No. 1 well (which were quite similar to Sakhalin Island assemblages), and the absence of the Caucasina assemblages seen in Eocene and Oligocene strata in other Bering Sea wells and in the Eocene of the Kamchatka and Ilpinsky peninsulas. Some of the correlation problems are facies related, others are attributable to the present imperfect knowledge of species ranges.

Palynological zonations are particularly tenuous in the late Oligocene because many key dinoflagellate species range into the early Miocene. It is also likely that the influence of facies on marine palynofloral assemblages is as significant as it is on foraminiferal assemblages. Oligocene ranges for some dinoflagellate species seen in the Navarin and Norton wells have been confirmed by calcareous nannoplankton data from the St. George Basin wells.

The Eocene section of the Navarin well may be in part correlative with the Eocene section in the St. George Basin COST No. 1 well, though it appears to be somewhat older; there are few similarities between the faunas or floras. The possibly equivalent Eocene sections in the St. George Basin No. 2 and Norton Sound No. 1 wells were dominantly nonmarine or contained no age-diagnostic microfossils. The Eocene section in the Norton Sound No. 2 well was deposited in transitional to continental environments and yielded no marine palynomorphs.

The Navarin Basin Eocene foraminiferal fauna contains some species found in Russia (Globobulimina ilpinica, Ammonia japonica, Porosorotalia tumiensis) and others characteristic of deep-water deposits around the north Pacific rim. The presence of Globocassidulina globosa indicates a somewhat younger age for the section (late Eocene) than do dinoflagellates (late middle Eocene).

The Cenozoic sedimentary section in the Navarin Basin COST No. 1 well can be considered a deeper water analog of the basin fill described in the Opukh-Pekulnei Trough, the Khatyrka Basin, and the southeastern part of the Anadyr Basin (McLean, 1979a; Gladenkov, 1980; Marlow and others, 1983a), although there may be a thicker and more complete Cenozoic section present in the Navarin Basin. Dredge sample and seismic reflection data suggest that there is more Eocene (and probable Paleocene) section in the deeper parts of the basin than was encountered in the Navarin Basin COST No. 1 well. Dredge sample L5-78-22-4, for instance, contained a dinoflagellate assemblage of Paleocene (Danian) age (Jones and others, 1981; Rosemary Jacobson, written commun., 1984).

There are no correlative Late Cretaceous strata in the St. George Basin or Norton Sound COST wells. Pollen from the nonmarine Maastrichtian section of the Navarin well (12,780 to 15,300 feet) are similar to those described by Jones and others (1981) from sample L5-78-27-1 dredged from the nearby Bering Sea continental margin, although the dredge sample was far more marine in aspect and contained a Late Cretaceous dinoflagellate assemblage. A reinvestigation of this dredge sample yielded a significant recycled assemblage

of Albian to Santonian age dinoflagellates (Rosemary Jacobson, written commun., 1984). This recycled component was also present in the nonmarine Maastrichtian section of the well. There is little doubt that the rocks dredged from the continental margin represent a marine facies of the Maastrichtian strata penetrated by the well.

Dredge sample L5-78-27-2, from the same general location as L5-78-27-1, contained volcanoclastic sandstone and tuff. Rosemary Jacobson (written commun., 1984) identified a poorly preserved ("corroded and mineral-scarred") assemblage of marine and nonmarine palynomorphs of ?Cenomanian to Turonian age mixed with recycled Albian elements. Thin lenses of very similar tuff are present in core 20 associated with a *Platyceramus* shell dated as possible Campanian to Coniacian. This "correlation" is far more tenuous than that with sample L5-78-27-1. Nevertheless, these data do lend support to the concept of a section of Late Cretaceous rocks below the unconformity at 15,300 feet that is older than Maastrichtian. The foraminiferal assemblages from 15,300 to 16,400 feet are similar to those described from the ?Campanian to Maastrichtian section of the Lower Cook Inlet COST No. 1 well (Wills and others, 1978).

The Late Cretaceous section is somewhat similar to equivalent marine and nonmarine rocks of the Impeneyen suite of the Koryak Highlands of eastern Siberia (Dundo, 1974; Korotkevich, 1974). Any such correlations, however, must await far more well data from the Navarin Basin and an unraveling of the movement histories of the several Mesozoic tectonostratigraphic terranes (Stone and others, 1982) that are juxtaposed in this area. Paleomagnetic data from conventional cores (Van Alstine, 1983) suggest that although the Cenozoic section was deposited within 5° of the present well site, the Late Cretaceous section may have been deposited as much as 50° south of the present location. The polarity data also suggest that the Late Cretaceous section was deposited during the Maastrichtian and Campanian. The presence of recycled carboniferous spores in Mesozoic well samples can be most easily explained by transport into the basin from eroding Paleozoic rocks in eastern Siberia or Alaska, although this might suggest far less movement than the paleomagnetic data from the well.

NOTE: We received Bujak, J. P., 1984, "Cenozoic dinoflagellate cysts and acritarchs from the Bering Sea and northern North Pacific, DSDP Leg 19," *Micropaleontology*, vol. 30, no. 2, pp. 180-212, pls. 1-4, too late for inclusion in this report, although certain aspects of his zonation were incorporated in Judy Lentin's (ERT biostrat, 1983) interpretation.

LITHOLOGY  
by  
Maurice B. Lynch

The following lithologic descriptions of rocks recovered from the Navarin Basin COST No. 1 well are based on an examination of 20 conventional cores, a detailed study of chips and thin sections from cores 1 through 20, and an examination of washed and unwashed rotary drill bit cuttings taken at 30-foot intervals from the first sample at 1,536 feet to the total depth of 16,400 feet. A detailed lithologic report was prepared by AGAT Consultants of Denver, Colorado (1983). The AGAT report described 345 core plugs taken from the 20 conventional cores, together with 191 sidewall cores and 4 junk basket samples. Geological analyses included detailed core descriptions (501.2 total feet), X-ray diffraction (343 samples), petrography (344 thin sections), scanning electron microscopy and energy-dispersive spectrometry (342 samples), and electron microprobe analysis (3 samples). Measured porosity and permeability values were determined by Core Laboratories, Inc. (1983), of Anchorage. Visible porosities were estimated by AGAT geologists. Vitrinite reflectance and total organic carbon content figures were derived by Robertson Research (U.S.) of Houston, Texas (Dow and Coleman, 1983). A lithology log prepared by ARCO well site geologists during drilling was also utilized.

Depths are measured in feet from the Kelly Bushing. The ARCO mud logger on the rig began collecting cuttings at 1,536 feet. The first sidewall core was taken at 2,500 feet and the first conventional core was started at 3,627 feet.

AGAT Consultants divided the subsurface section into nine zones, designated A through I, on the basis of lithology, depositional environment, diagenetic alteration, and well log characteristics. With minor modifications, these divisions are utilized in this report.

A number of figures and tables have been included to illustrate the lithology. Conventional cores are described in figures 11 through 30. Table 2 lists each sample analyzed, its depth, type, lithology, measured porosity, estimated visible porosity, and measured permeability. Tables 3 and 4 show percentages of several minerals present in the 20 conventional cores. Figure 31 is a summary chart of the X-ray diffraction data from conventional and sidewall cores. Figures 32 and 33 are ternary diagrams showing the range of quartz, feldspar, and lithic composition in conventional and sidewall core samples from the various lithologic zones. Figures 34 and 35 are ternary diagrams showing the range of volcanic, metamorphic, and sedimentary rock fragments in the

lithic fractions of samples from conventional and sidewall core samples. Tables 5 and 6 are summaries of petrographic data and reservoir characteristics.

The sedimentary section penetrated by the Navarin well is dominantly marine: the upper 12,780 and lower 1,100 feet of section were deposited in marine environments. Sediments between 12,780 and 15,300 feet were deposited in fluvial, floodplain, and deltaic environments. In the interval between 12,800 and 15,048 feet, Late Cretaceous age sediments are intruded by numerous basaltic and diabasic sills. The sills were radiometrically dated by Teledyne Isotopes Laboratory of Westwood, New Jersey, using potassium-argon (K-Ar) age determination methods. Samples from three depths were analyzed. A junk basket sample taken between 12,835 and 13,500 feet was determined to be  $18 \pm 0.9$  million years old. A sample from about 13,880 feet was dated at  $20.9 \pm 3.6$  million years. The third sample, taken from conventional core 18 at 14,599 feet, was found to be  $21.7 \pm 4.2$  million years old. Igneous sill emplacement probably occurred during early Miocene or late Oligocene time.

#### ZONE A-1 (1,536 to 3,565 feet)

##### PLIOCENE AND MIOCENE

This interval consists of poorly sorted, silty, sandy mudstone and diatomaceous ooze deposited in a mid-shelf environment. Primary sedimentary structures were destroyed by extensive bioturbation. Concentrations of granule-sized rock and shell fragments are associated with scour surfaces. Coarser grained material may represent basal lag deposits on erosional surfaces created by storm-generated currents. The framework grains are mainly volcanic lithic fragments, angular quartz, and feldspars. Diatom and clay matrix content ranges from 50 to 80 percent. Most of the diatom fragments are broken and angular. Lithic components are dominated by basaltic and intermediate volcanic fragments, glauconite, metamorphic rock fragments, mica, chert, and clay. Accessory minerals include hornblende, epidote, apatite, and pyroxene. Diagenetic changes included compaction, weak alteration and dissolution of lithic fragments, and the development of authigenic pyrite, clinoptilolite or heulandite, and chlorite.

Porosity and permeability have not been significantly altered by diagenesis at these shallow depths. Although measured porosities are very high in this zone (35 to 50 percent), estimated visible porosities are very low because of poor sorting and an abundance of very fine grained matrix material. Near the bottom of this zone, the silica minerals of the diatoms are progressively replaced by framboidal pyrite.

## ZONE A-2 (3,565 to 3,860 feet)

### MIOCENE

There is little lithologic difference between Zones A-1 and A-2. Diatomaceous sediments in this interval have been subjected to diagenesis that changed the dominant silica phase (opal-A) to clinoptilolite and clay. The sediments in Zone A-2 are overpressured and more compact, hard, brittle, and dense than similar sediments in Zone A-1 (see Well Log Interpretation and Bottom-Simulating Reflector chapters).

## ZONE B (3,860 to 5,010 feet)

### MIOCENE

Zone B consists of bioturbated, muddy, very fine and fine-grained sandstone interbedded with sandy mudstone. The depositional environment was probably middle neritic. The grains are poorly to well sorted and locally cemented with calcite. The only primary sedimentary structures still visible are a few wavy, discontinuous laminations. The isolated lithic granules and pebbles present were probably transported and deposited by storm activity. Whole and broken gastropod and bivalve shells are present. Below 3,850 feet opaline silica that originally made up the diatoms has apparently been diagenetically altered to clinoptilolite or heulandite. Opal-CT (cristobalite-tridymite) was not identified by scanning electron microscopy but has been identified in trace amounts by X-ray diffraction analysis.

The framework grains are monocrystalline and polycrystalline quartz, plagioclase and potassium feldspar, and abundant, varied lithic fragments that include volcanic, metamorphic, and sedimentary rock fragments, hornblende, chert, mica, clay clasts, glauconite, and molluscan shell fragments.

Detrital matrix is rare in the well-sorted sandstones and abundant in muddy sandstones. Authigenic minerals present include framboidal pyrite, siderite, smectitic clay, clinoptilolite or heulandite, analcite, and calcite cement. The measured porosity is high (25 to 35 percent), but most of this is intercrystalline microporosity in the intergranular matrix of detrital and authigenic clays and cements. The original porosity and permeability were probably good in the well-sorted sandstones, but smectite and zeolite precipitation reduced both considerably. Secondary porosity generated by the dissolution of framework grains did not increase the overall porosity significantly. The hydrocarbon reservoir potential for this zone is low.

## ZONE C-1 (5,010 to 5,360 feet)

### MIOCENE

This interval consists of thin-bedded fine and very fine grained muddy sandstone and siltstone interbedded with mudstone and claystone. The sandstone is poorly sorted, bioturbated, and locally cemented by calcite. Bioturbation has resulted in mottling of sand and clay. Lithic pebbles and broken and intact, thin molluscan shells are present. The sediments in this zone were probably deposited in a middle to outer neritic environment. Well logs indicate that most of the sandstones are 10 feet thick or less.

The framework grain size ranges from silt to fine sand. The grains include chert, monocrystalline and polycrystalline quartz (22 to 30 percent), lithic fragments (32 to 44 percent), and feldspar (31 to 38 percent). Plagioclase is the predominant feldspar. Most of the lithic fragments appear to be volcanic in origin, but some are sedimentary, plutonic, and metamorphic. Glauconite is common. Minor constituents include chert, hornblende, pyroxene, fossil fragments, epidote, zircon, garnet, and rare tourmaline. Diagenetic alterations include compaction, alteration of some feldspar, alteration of volcanic rock fragments, and precipitation of clinoptilolite and authigenic pyrite. Reservoir potential is nil in the claystone and poor in the sandstone. Measured porosity (28 to 32 percent) in the sandstone is high, but permeability is low because of the abundance of detrital and authigenic clay. Measured permeability in analyzed sandstone samples ranges from 2 to 23 millidarcies. Alteration of framework grains and precipitation of authigenic zeolites have also degraded reservoir quality.

## ZONE C-2 (5,360 to 7,130 feet)

### MIOCENE TO OLIGOCENE

This interval consists of fine and very fine grained, relatively clean to muddy sandstone and siltstone interbedded with mudstone and claystone. The sandstone is poorly to well sorted. The sediments are bioturbated and locally cemented by calcite. There are some wavy interbeds and laminations of sandstone and claystone. Bioturbation has resulted in horizontal and oblique burrows. Lithic pebbles and broken and intact, thin molluscan shells are present. The sediments in this zone were probably deposited in a middle to outer neritic environment. Well logs indicate that some of the sandstones are up to 100 feet thick.

The framework grain size ranges from silt to fine sand. The grains include chert, monocrystalline and polycrystalline quartz (20 to 70 percent), lithic fragments (4 to 60 percent), and feldspar (10 to 26 percent). Plagioclase is the predominant feldspar. Most of the lithic fragments appear to be volcanic in origin, but some are metamorphic. Glauconite is common. Minor constituents include chert, hornblende, pyroxene, fossil fragments, epidote, zircon, garnet, and rare tourmaline. Diagenetic alterations include compaction, alteration of some feldspar, alteration of volcanic rock fragments, and precipitation of clinoptilolite and authigenic pyrite. Reservoir potential is nil in the claystone and poor to good in the sandstone. Measured porosity (28 to 33 percent) in the sandstone is high, but permeability is low because of the presence of detrital clay. Measured permeability in analyzed sandstone samples ranges from 5 to 233 millidarcies. Alteration of framework grains and precipitation of authigenic zeolites have also degraded reservoir quality.

Although most of these sandstones are only poor to fair reservoir rocks, a few would make good reservoir rock and are the best seen in the well. In a high energy depositional setting, perhaps closer to the source, equivalent strata might have better reservoir characteristics.

#### ZONE D-1 (7,130 to 9,450 feet)

##### OLIGOCENE

This interval is characterized by sandy mudstone, fine-grained muddy sandstone, and claystone with rare lenses of siltstone and sandy carbonate. Isolated coarse-sand-sized to pebble-sized volcanic rock fragments are present. The sediments have been bioturbated. Whole and broken molluscan shells and microfossils are present. The only primary sedimentary structures seen in the cores are wavy laminations. This interval was probably deposited in marine outer shelf and upper slope environments.

The framework grains are subrounded and subangular quartz, feldspar, and lithic fragments. The average abundances of framework constituents are 47 percent quartz, 19 percent feldspar, and 34 percent lithic fragments. The lithic fragments are about 53 percent volcanic, 30 percent metamorphic, and 15 percent sedimentary. Accessory minerals include glauconite, micas, clay, chert, chlorite, and hornblende. Fossil fragments and organic matter are also present. Authigenic minerals include smectite, mixed-layer illite and smectite, calcite, siderite, pyrite, zeolites, gypsum, chlorite, quartz, and feldspar.

The reservoir potential of this zone is very poor. Because of poor sorting, extremely fine grain size, and precipitation of many authigenic minerals, porosity and permeability values are very low.

#### ZONE D-2 (9,450 to 10,800 feet)

##### OLIGOCENE

There is little lithologic difference between Zones D-1 and D-2. The smectite clays which predominate in Zone D-1 have been diagenetically altered to illite, mixed-layer illite-smectite and chlorite (fig. 31). Associated with the clay diagenesis is overpressuring which occurs in and below this zone (see Abnormal Formation Pressure chapter).

#### ZONE E (10,800 to 12,280 feet)

##### OLIGOCENE

This zone consists of poorly sorted gray claystone, mudstone, and sandy mudstone with abundant detrital clay matrix. The sediments exhibit wavy lamination and have been moderately burrowed. Calcite concretions are present. The rocks in this zone are slightly finer grained than those of Zones D-1 and D-2. The section was probably deposited in a bathyal environment.

The framework grains are subangular and subrounded. Silt-sized monocrystalline quartz, plagioclase, micas, chert, and volcanic rock fragments are all present as framework clasts. Other minerals present in small amounts are pyroxene, glauconite, hornblende, gypsum, and clays. Clays constitute about 40 to 70 percent of the rock and include chlorite, kaolinite, illite, and mixed-layer illite and smectite. Organic material and molluscan shell fragments are present. Authigenic minerals include chert, siderite, calcite, laumontite, leonhardite, mixed-layer clay, pyrite, zeolites, quartz, potassium feldspar, and ankerite. The provenance was probably a mixed volcanic and metamorphic terrane.

The reservoir potential of this interval is very poor. The rocks are characterized by very low mesoporosities and permeabilities. This is a function of small grain size, poor sorting, abundant clay matrix, and the precipitation of authigenic minerals.

## ZONE F (12,280 to 12,780 feet)

### EOCENE

This section consists of dark-gray calcareous claystone and sandy mudstone. No primary sedimentary structures are apparent. The environment of deposition was probably outer shelf to upper slope. Framework grains range in size from clay to coarse sand. The grains are composed of quartz, feldspar, volcanic and altered rock fragments, hornblende, chert, mica, glauconite, and carbonaceous shale fragments. Intergranular authigenic constituents include pyrite, siderite, calcite, chert, chlorite, kaolinite, illite, and smectite. Some of the plagioclase has been replaced by calcite, and some has been altered to clay. Porosity and permeability are very poor in the claystone because of the extremely fine grain size. Effective porosity and permeability in the sandy mudstone are negligible because of poor depositional sorting, fine grain size, and precipitated calcite that has filled much of the space between grains. The dark-colored carbonaceous claystone in this interval has the best hydrocarbon source rock potential encountered in the well.

## ZONE G/H (12,780 to 15,300 feet)

### LATE CRETACEOUS

An angular unconformity is present at approximately 12,780 feet. Below this depth, rocks dip 25 to 30 degrees and have been intruded by diabase and basalt sills. The intrusives are hard, dark greenish gray (5 G 4/1 on the Geological Society of America color chart) with intergranular and intersertal textures. Interstices between plagioclase crystals are filled with clinopyroxene or alteration products such as clay, calcite, and minor quartz. Small amounts of pyrite, siderite, chlorite, leucoxene, anatase, hornblende, and potassium feldspar are also present, as well as trace amounts of clinoptilolite and laumontite or leonhardite. Diabase and basalt sills were intruded into the sediments after burial. Distinguishing igneous from sedimentary rock by using only wireline logs is difficult in this section because bulk density values are lower than is typical of diabase and basalt. This may be a result of weathering effects beneath the unconformity.

This interval contains siltstone, very fine grained sandstone, mudstone, claystone, and coal. Depositional environments probably included stream and distributary channels and possibly tidally influenced deltaic distributary systems. Core 16 (13,141 to 13,158 feet; fig. 26) may have been

deposited in an intertidal zone. No marine microfossils were recovered. Sedimentary features include flaser structure and wavy and lenticular interbeds of sandstone and mudstone. Truncated ripple sets and herringbone crossbedding are present within sandstone units. Minor soft-sediment deformation, attributable to the slumping of semiconsolidated sediments on unstable surfaces, is also present. From bottom to top, core 17 (13,876 to 13,904 feet; fig. 27) consists of about 12 feet of crossbedded, medium-grained sandstone; 2 feet of light-gray claystone; approximately 2 feet of coal; and 11 feet of greenish-gray, altered diabase. The sedimentary part of the core probably represents abandoned stream or distributary channel deposits.

Core 18 (14,575 to 14,607 feet; fig. 28) contains two diabase sills 3.5 feet and 11.5 feet thick, with tops at 14,590.5 and 14,595.5 feet, respectively. The remaining 17 feet of core consists of finely laminated mudstone, siltstone, claystone, and sandstone that contain carbonized plant fragments. Sediments were probably deposited in an interdistributary pond or bay that was gradually infilled and invaded by plants. A sandstone bed near the top may be an ancient distributary channel deposit. The lenticular bedding and ripple laminations in this sandstone bed may be due to reworking by tidal currents near a delta front.

The framework grains include abundant monocrystalline and polycrystalline quartz, chert, plagioclase feldspar, volcanic and rare metamorphic rock fragments, mica, and hornblende. Many rock fragments were altered in the source area. Authigenic minerals include minor amounts of pyrite, clinoptilolite, siderite, locally abundant calcite, kaolinite, chlorite, mixed-layer illite and smectite, and traces of chert. Densely packed kaolinite and chlorite are present as alteration products of unstable grains and as pore-filling clays. The mixed-layer illite and smectite is an alteration product of labile grains as well as a regenerated detrital clay. Effective mesoporosity in the siltstone is negligible because of fine grain size and poor depositional sorting. Total porosity in some of the sandstone is moderate (10 to 15 percent), but mesoporosity is low because of poor sorting, and has been further reduced by pore-filling calcite cement and ductile deformation of altered framework grains during compaction. Alteration of grains to kaolinite, chlorite, and mixed-layer illite and smectite produced intercrystalline microporosity, but decreased effective mesoporosity and permeability. The hydrocarbon reservoir potential of this zone is very low.

## ZONE I (15,300 to 16,400 feet)

### LATE CRETACEOUS

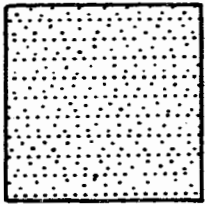
This interval is composed of claystone, siltstone, tuff, and mudstone. Deposition was in a marine environment. Bioturbation, rare leaf fossils, Inoceramus fragments, discontinuous wavy laminations, and isolated tuff layers are present in cores 19 and 20. Core 19 (15,500 to 15,509 feet; fig. 29) has been tentatively interpreted as a prodelta mud deposit. Core 20 (16,313 to 16,343 feet; fig. 30) was deposited in a marine shelf environment.

Rocks in this zone are composed of 70 to 80 percent clay minerals. Chlorite accounts for about 40 percent of the clay present. Illite and mixed-layer illite and smectite together compose about 50 percent of the clay. The remaining clay fraction is kaolinite. The nonclay part of the rock is made up of volcanic rock fragments, quartz, plagioclase and potassium feldspar, pyrite, siderite, calcite, clinopyroxene, clinoptilolite, heulandite, hornblende, and mica. Quartz is the dominant nonclay mineral. Organic material is common.

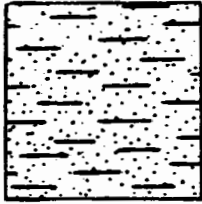
Authigenic minerals include pyrite, calcite, and mixed-layer illite and smectite. Calcite has replaced both detrital silt grains and clay matrix and has thereby reduced porosity and permeability locally. Small pyrite framboids associated with organic fragments define weak laminations. Thin isolated layers of tuff near the bottom of this zone indicate local volcanic activity. The hydrocarbon reservoir potential of this interval is negligible.

# EXPLANATION

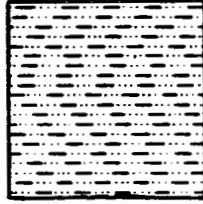
## FIGURES 11 THROUGH 30



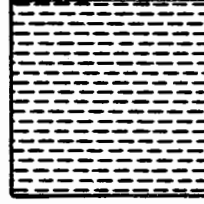
SANDSTONE



MUDDY  
SANDSTONE



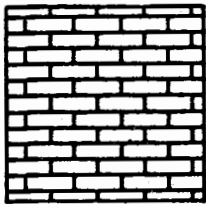
SILTSTONE



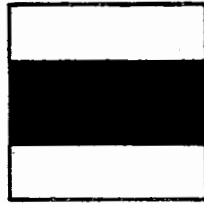
CLAYSTONE



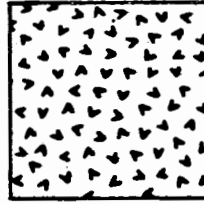
MUDSTONE



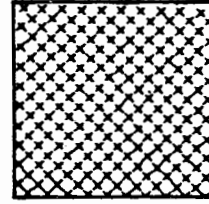
LIMESTONE



COAL



VOLCANIC  
DIABASE,  
BASALT



TUFF

⊗ FORAMINIFERA

⌒ MOLLUSC SHELL

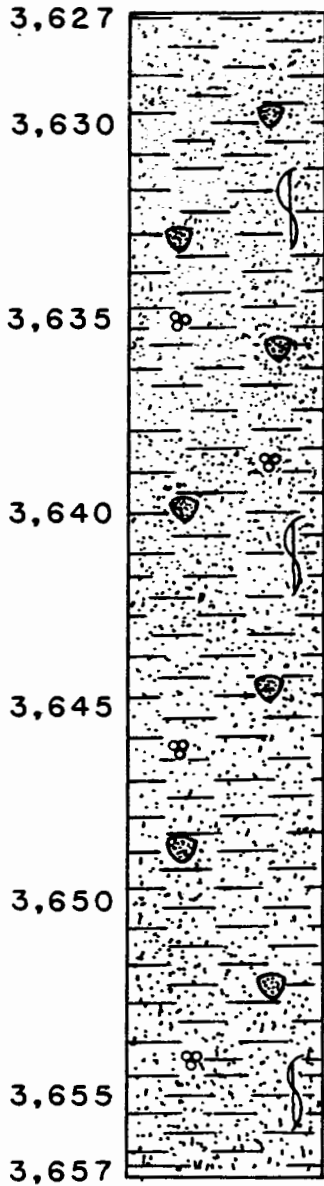
⊕ DIATOM

⌋ BIOTURBATION

*Color codes from the Rock Color Chart,  
published by the Geological Society of America.*

POROSITY AND PERMEABILITY DATA FROM CORE LABORATORIES, INC.

RANDOM VITRINITE REFLECTANCE AND TOTAL ORGANIC CARBON DATA  
FROM ROBERTSON RESEARCH (U.S.), INC.

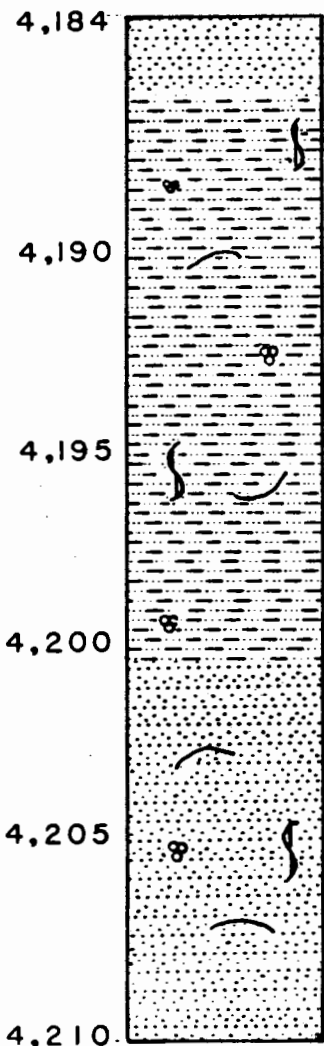


Core 1 consists of light-gray (N7), poorly sorted, fine- to very fine-grained, bioturbated, glauconitic, diatomaceous, muddy sandstone. The framework clasts (grains) are mainly quartz, feldspar, and lithic fragments. Most of the feldspar is plagioclase. Quartz makes up 35 to 50 percent of the core, plagioclase feldspar 8 to 14 percent, and pyrite 10 to 14 percent; there are lesser amounts of potassium feldspar, siderite, calcite, hornblende, chlorite, kaolinite, mixed-layer illite-smectite clay, and mica. The lithic fragments are almost entirely of volcanic origin and are in various stages of alteration. Pebble-sized clasts occur throughout the core. The primary sedimentary structures have been destroyed by extensive bioturbation. A few Foraminifera are present. Some siliceous diatoms have been replaced by framboidal pyrite. The depositional environment was middle neritic.

AGE: late Miocene

	POROSITY (%)	PERMEABILITY (mD)	% ORGANIC CARBON	% VITRINITE REFLECTANCE
3,627 - 3,630	48.8	3.88	0.52	0.32
3,630 - 3,635				
3,635 - 3,640	50.6	2.69		
3,640 - 3,645			0.51	0.35
3,645 - 3,650				
3,650 - 3,655	50.7	6.15		
3,655 - 3,657				

**FIGURE 11. DESCRIPTION OF CONVENTIONAL CORE 1, NAVARIN BASIN COST NO. 1 WELL**

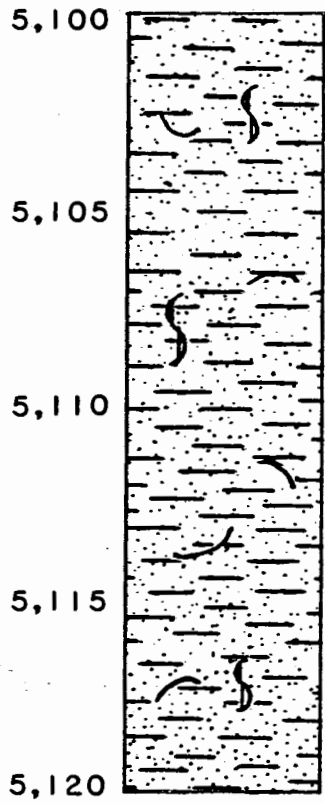


Core 2 is light-gray (N7) to medium-gray (N5), fine- and very fine-grained, bioturbated sandstone and siltstone. The lower 9 feet is coarser grained than the top. The cement is calcite and clay. Minerals present are quartz (26 to 42 percent), plagioclase feldspar (9 to 39 percent), potassium feldspar (0 to 6 percent), pyrite (2 to 8 percent), siderite (2 to 3 percent), with minor amounts of mica, hornblende, analcite, clinoptilolite, and ankerite. Clays constitute 5 to 38 percent of the core. The most abundant clays are smectite and mixed-layer illite-smectite. Many siliceous spicules and a few diatoms are present. Foraminifera and fragments of molluscs are also present. The depositional environment was middle neritic.

AGE: late Miocene

	POROSITY(%)	PERMEABILITY(mD)	%ORGANIC CARBON	% VITRINITE REFLECTANCE
4,184	7.7	0.02		
4,190	35.5	2.07		
4,195	37.3	0.80		
4,200	29.7	3.99	0.29	0.34
4,205	32.4	27.0		
	33.8	51.0		
	9.6	0.05		
4,210	35.2	118.0		

FIGURE 12. DESCRIPTION OF CONVENTIONAL CORE 2, NAVARIN BASIN COST NO. 1 WELL

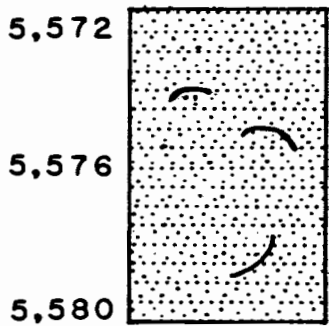


Core 3 is poorly sorted, fine- and very fine-grained sandstone containing some silt and clay. The colors are medium light gray (N6), medium gray (N5), and dark gray (N3). Bioturbation is evident and molluscan shell fragments are present. Lithic fragments include volcanic, metamorphic, and sedimentary rocks, most in various stages of alteration. There are large volcanic clasts at 5,105.8, 5,109.8, and 5,110.3 feet. The rock consists of 38 to 51 percent subangular quartz grains, 14 to 28 percent plagioclase feldspar, and 14 to 24 percent clay. There are minor amounts of potassium feldspar, mica, pyrite, hornblende, glauconite, pyroxene, and siderite. Diagenetic clay, zeolites, and pyrite have reduced porosity and permeability. The depositional environment was middle neritic.

AGE: middle to early Miocene

	POROSITY(%)	PERMEABILITY(mD)	%ORGANIC CARBON	%VITRINITE REFLECTANCE
	30.1	4.96		
	30.6	8.18	0.45	0.35
	28.2	4.19		

**FIGURE 13. DESCRIPTION OF CONVENTIONAL CORE 3, NAVARIN BASIN COST NO. 1 WELL**



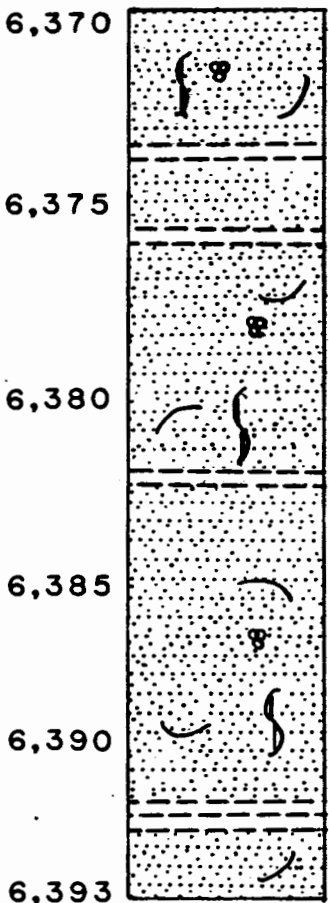
Core 4 is composed of well-sorted, fine-grained, hard, dark-gray (N3) to light-gray (N7) sandstone. The rock is 25 to 30 percent quartz, 10 to 18 percent plagioclase feldspar, less than 10 percent clay, and up to 50 percent calcite cement. There are minor amounts of hornblende, pyrite, ankerite, mica, and siderite present. There are rare molluscan shell fragments. Visible porosity and permeability are both near zero. The depositional environment was middle neritic.

AGE: middle to early Miocene

POROSITY(%)  
PERMEABILITY(mD)  
%ORGANIC CARBON  
% VITRINITE REFLECTANCE

6.6	0.05		
6.0	0.02		
6.1	0.02		

**FIGURE 14. DESCRIPTION OF CONVENTIONAL CORE 4, NAVARIN BASIN COST NO. 1 WELL**

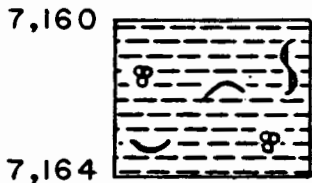


Core 5 is fine- and very fine-grained sandstone, extensively bioturbated, with horizontal, wavy interbeds of claystone at irregular intervals. The colors are medium light gray (N6), light brown (5 YR 5/6), and brownish gray (5 YR 6/1). The framework is composed of angular quartz and feldspar grains, and volcanic, metamorphic, and sedimentary lithic fragments. Most of the feldspar is plagioclase. Authigenic clay makes up about 10 percent of the rock. Other minerals present are pyrite, mica, hornblende, siderite, and calcite. Diatoms replaced by framboidal pyrite are locally abundant. Calcareous concretions, Foraminifera, molluscan shell fragments, and calcite cement are also present. The depositional environment was middle to outer neritic.

AGE: late Oligocene

28.4	4.85		
29.2	7.87		
34.0	117.0		
33.3	30.0		
32.1	6.16		
29.7	2.42		
		0.28	0.45
32.5	3.74		

**FIGURE 15. DESCRIPTION OF CONVENTIONAL CORE 5, NAVARIN BASIN COST NO. 1 WELL**



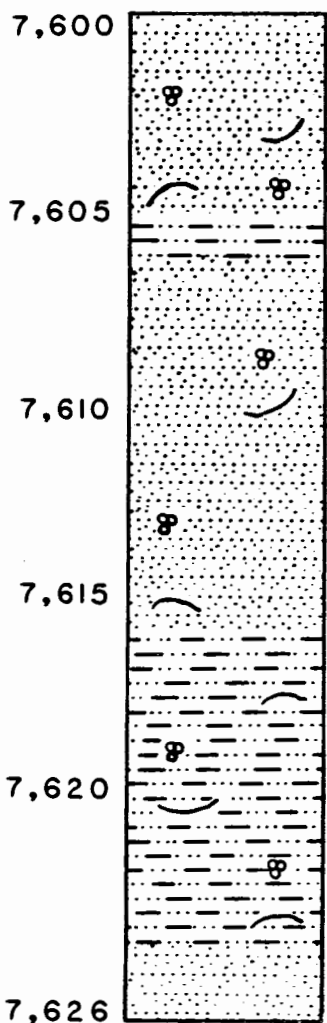
Core 6 is composed of medium-gray (N5) claystone. About 70 percent of the rock is clay (mostly smectite) and about 20 percent is quartz, with minor amounts of potassium feldspar, mica, siderite, ankerite, and calcite. Discontinuous laminations and faint burrows can be seen. Molluscan shell fragments, Foraminifera, and pyritized diatoms are present. The depositional environment was outer neritic.

AGE: late Oligocene

POROSITY(%)  
 PERMEABILITY(mD)  
 %ORGANIC CARBON  
 % VITRINITE REFLECTANCE

19.1	0.23	0.69	0.45
18.6	0.41	0.66	0.47

**FIGURE 16. DESCRIPTION OF CONVENTIONAL CORE 6, NAVARIN BASIN COST NO. 1 WELL**

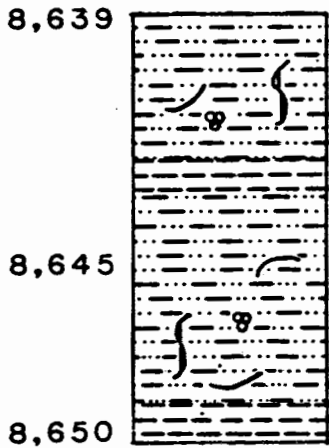


Core 7 consists of medium-light-gray (N6), well-sorted, very fine grained sandstone, siltstone, claystone, and mudstone. There are wavy, discontinuous horizontal bedding planes, with Foraminifera and molluscan shells parallel to the bedding. There are some small stringers of fine-grained sandstone. The framework grains are quartz, feldspar, and lithic fragments of volcanic, metamorphic, and sedimentary origin. Minerals present include quartz (18 to 25 percent), plagioclase feldspar (4 to 16 percent), pyrite (5 to 8 percent), and minor amounts of mica, siderite, and calcite. Smectite is the most abundant clay. Pyritized diatoms are rare to common. The depositional environment was upper bathyal.

AGE: late Oligocene

21.5	0.43		
21.6	0.21		
21.1	0.46		
23.1	0.08		
19.6	0.49		
21.6	0.09		
19.3	1.14		
20.5	0.11	0.57	0.49
21.6	0.13	0.79	
21.4	0.30		
21.8	1.78		

**FIGURE 17. DESCRIPTION OF CONVENTIONAL CORE 7, NAVARIN BASIN COST NO. 1 WELL**

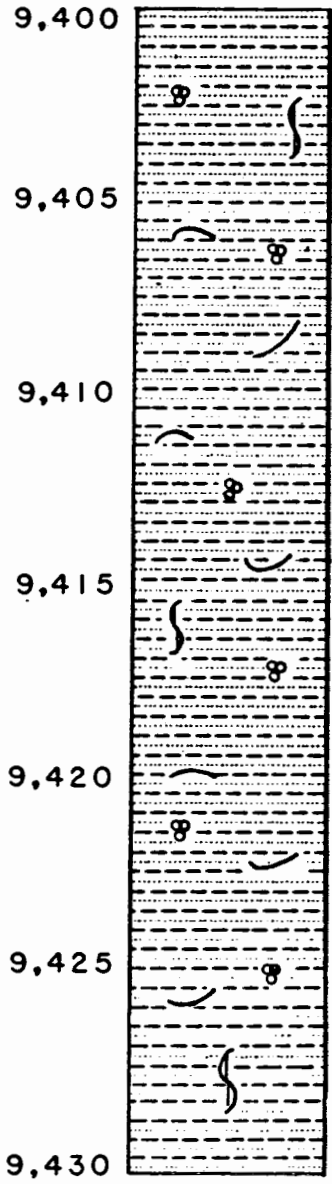


Core 8 consists of siltstone, claystone, and mudstone, medium gray (N5) in color, with minor amounts of fine- and very fine-grained sand. The sand appears to be concentrated in burrows. There are wavy, discontinuous laminations. Minerals present include quartz, plagioclase feldspar, pyrite, mica, siderite, glauconite, smectite, chlorite, and calcite as cement and in nodules. Unabraded volcanic clasts and fossil material suggest a low energy, upper bathyal depositional environment.

AGE: late Oligocene

	POROSITY(%)	PERMEABILITY(mD)	%ORGANIC CARBON	%VITRINITE REFLECTANCE
21.6	0.05			
21.5	0.05			
20.2	0.05			
21.4	0.09			
18.8	0.03	0.58	0.56	

**FIGURE 18. DESCRIPTION OF CONVENTIONAL CORE 8, NAVARIN BASIN COST NO. 1 WELL**

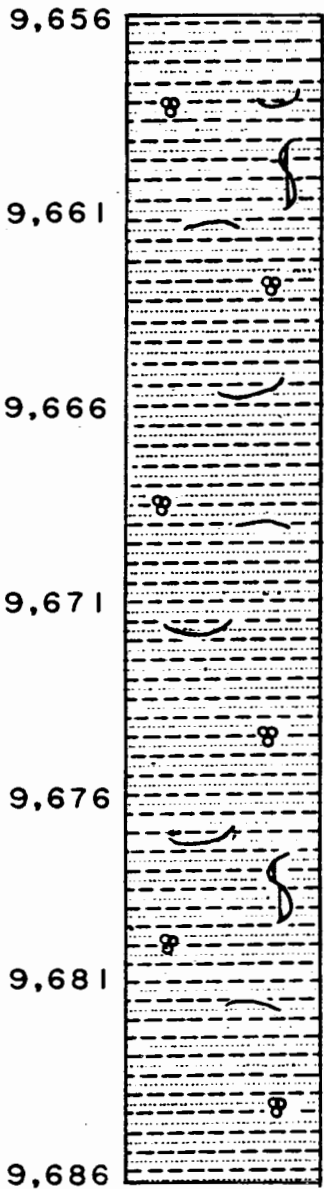


Core 9 contains well to moderately sorted mudstone and siltstone, with lenses of fine and very fine sandstone, and continuous and discontinuous horizontal clay laminations. Some sand lenses may be burrows filled with very fine sand. The color is medium gray (N5). Chlorite, smectite, illite, and kaolinite clays make up about 24 to 53 percent of the core; the remainder is quartz, plagioclase feldspar, potassium feldspar, pyrite, siderite, ankerite, calcite, hornblende, mica, and minor glauconite. Minor amounts of coaly organic matter, Foraminifera, and molluscan shell fragments are present. Calcite concretions and calcite cement are present. The depositional environment was middle bathyal.

AGE: late Oligocene

	POROSITY(%)	PERMEABILITY(mD)	%ORGANIC CARBON	%VITRINITE REFLECTANCE
9,400	15.2	0.02		
9,405	14.9	5.93		
9,410	14.6	0.22		
9,415	14.2	0.05		
9,420	14.3	0.05		
9,425	13.2	0.01		
9,430	14.4	12.0	0.64	0.56
	11.7	0.37		
	13.9	8.49		
	15.1	1.57		
	13.7	1.04		
	13.5	0.13		
	12.5	25.0		
	14.8	0.59		
	14.6	0.19	0.63	

FIGURE 19. DESCRIPTION OF CONVENTIONAL CORE 9, NAVARIN BASIN COST NO. 1 WELL

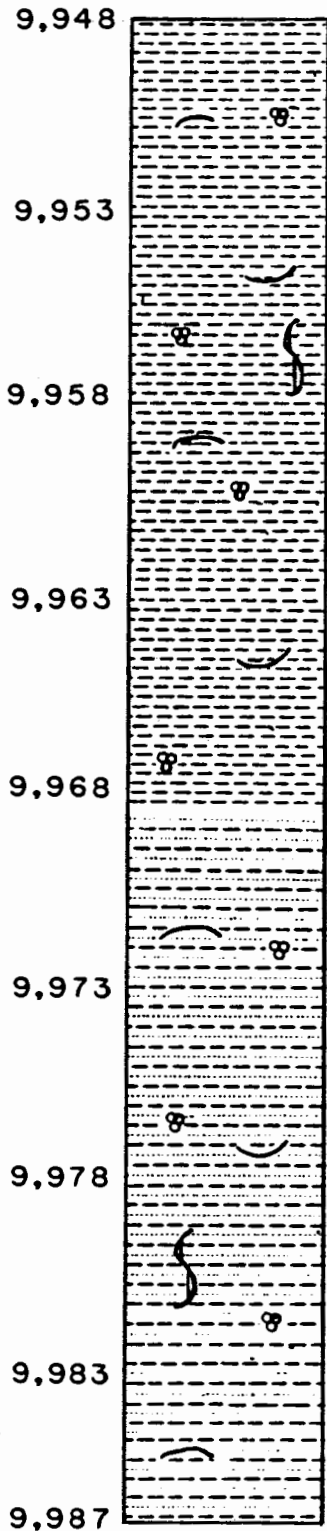


Core 10 is composed of poorly sorted mudstone, siltstone, and claystone, with wavy, discontinuous, very fine sandstone laminations. The compacted laminations drape over and around pebble-sized volcanic rock fragments and brown calcite concretions. The colors are medium light gray (N6) and medium gray (N5). The rock is composed of 51 to 61 percent clay (smectite, chlorite, kaolinite, and illite), 1 to 34 percent quartz, 6 to 33 percent plagioclase feldspar, 2 to 7 percent authigenic pyrite, and up to 33 percent calcite, with minor amounts of potassium feldspar, siderite, mica, and hornblende. Glauconite is rare. Foraminifera, molluscan shells, pyritized diatoms, and bits of coaly plant material are present. Faint elliptical burrows are present from 9,656 to 9,659 feet. There are some microfaults at 9,662 feet. This section was deposited under anaerobic conditions in a middle bathyal environment.

AGE: late Oligocene

	POROSITY(%)	PERMEABILITY(mD)	%ORGANIC CARBON	%VITRINITE REFLECTANCE
	14.3	0.02		
	14.5	0.02		
	15.8	0.02	0.65	0.59
	15.8	0.02		
	14.6	0.14		
			0.92	0.57
	14.0	0.02		
	14.5	0.08		
	14.4	0.12		
	8.8	0.02		

FIGURE 20. DESCRIPTION OF CONVENTIONAL CORE 10, NAVARIN BASIN COST NO. 1 WELL

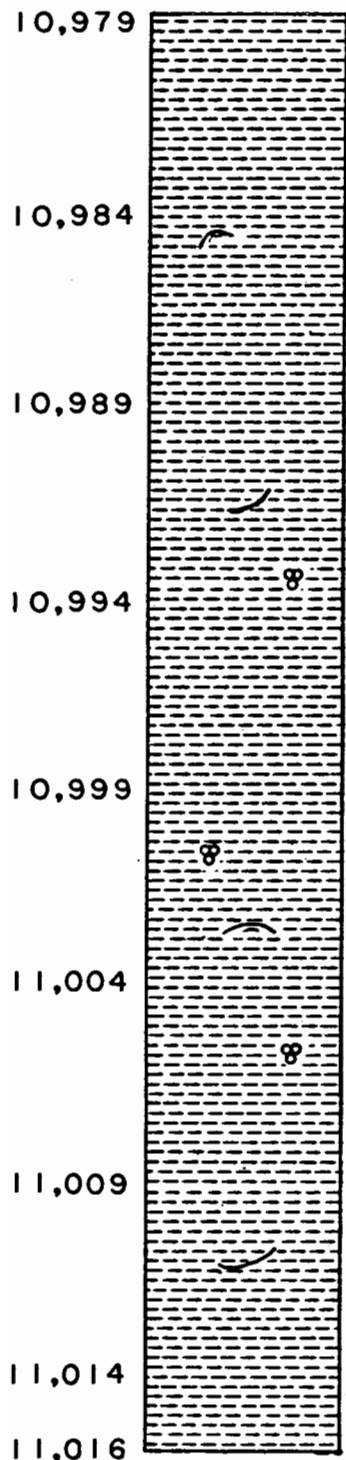


Core 11 consists of mudstone, claystone, and siltstone, with lenticular to thin wavy beds of fine- and very fine-grained sandstone. The color is medium gray (N5) and medium light gray (N6). The core is 37 to 64 percent clay (mixed-layer illite-smectite, chlorite, illite, and kaolinite); the remainder is 8 to 32 percent quartz, 5 to 25 percent plagioclase feldspar, and 5 to 28 percent pyrite. There are minor amounts of potassium feldspar, siderite, calcite, mica, glauconite, and hornblende. Thirty percent of the core is composed of lithic fragments (about half volcanic and half metamorphic). Calcite concretions and volcanic pebbles are present. Compaction and diagenesis have greatly reduced porosity and permeability. The depositional environment was middle bathyal.

AGE: late Oligocene

	POROSITY(%)	PERMEABILITY(mD)	%ORGANIC CARBON	%VITRINITE REFLECTANCE
9,948	15.1	0.02	0.80	0.60
9,953				
9,958	14.7	0.01		
9,963				
9,968				
9,973	12.6	0.02		
9,978				
9,983	14.4	0.01		
9,987			0.93	0.60

FIGURE 21. DESCRIPTION OF CONVENTIONAL CORE II, NAVARIN BASIN COST NO. 1 WELL

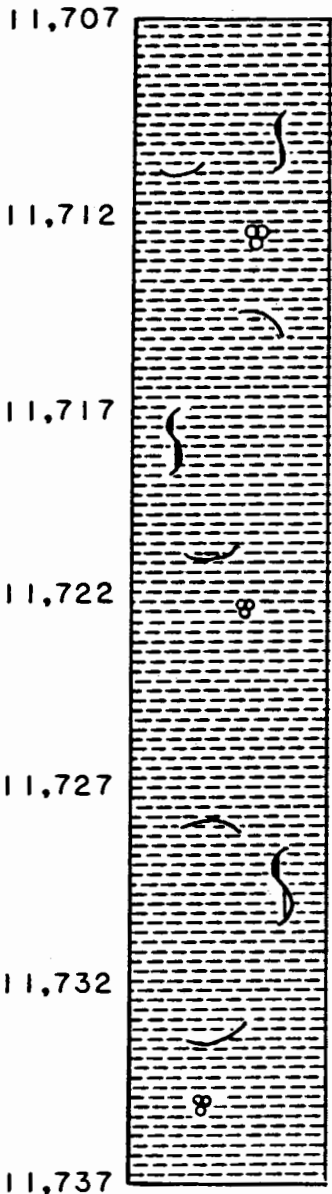


Core 12 is composed of medium-gray (N5) and medium-light-gray (N6) claystone, with wavy, discontinuous laminations of silty clay and volcanic clasts. The rock is up to 68 percent clay (chlorite, illite, kaolinite, and mixed-layer illite-smectite); the remainder is 11 to 21 percent quartz, 4 to 5 percent plagioclase feldspar, with small amounts of pyrite, potassium feldspar, mica, siderite, hornblende, and calcite cement. Very coarse sand grains, calcite concretions, and claystone clasts are present. Molluscan shell fragments, Foraminifera, pyritized diatoms, and fish scales are also present. Effective porosity and permeability are very poor because of the poor sorting and fine grained texture. The depositional environment was middle bathyal.

AGE: early Oligocene

	POROSITY(%)	PERMEABILITY(mD)	% ORGANIC CARBON	% VITRINITE REFLECTANCE
10,979 - 10,984	16.9	0.04	0.73	0.71
10,984 - 10,989				
10,989 - 10,994				
10,994 - 10,999	15.8	0.02		
10,999 - 11,004			0.76	0.70
11,004 - 11,009				
11,009 - 11,014	15.2	0.02		
11,014 - 11,016				

**FIGURE 22. DESCRIPTION OF CONVENTIONAL CORE 12, NAVARIN BASIN COST NO. 1 WELL**



Core 13 is composed of medium-gray (N5) claystone, with minor amounts of silt and pebbles. Slightly wavy bedding laminations and moderate burrowing are present. A large altered volcanic rock fragment is present at 11,726.5 feet. The core is 55 to 68 percent clay (chlorite, kaolinite, smectite, and mixed-layer illite-smectite); the remainder consists of 20 to 30 percent quartz, 4 to 5 percent pyrite, 5 to 7 percent plagioclase feldspar, and minor amounts of potassium feldspar, siderite, mica, calcite, and hornblende. Foraminifera, fish scales, molluscan shell fragments, coaly plant material, and pyritized diatoms are present. The depositional environment was upper bathyal.

AGE: early Oligocene

	POROSITY (%)	PERMEABILITY (mD)	% ORGANIC CARBON	% VITRINITE REFLECTANCE
11,707	11.4	0.02	0.92	0.79
11,712				
11,717	11.4	0.02		
11,722				
11,727	4.4	0.33		
11,732	11.8	0.26		
11,737			1.03	0.74

FIGURE 23. DESCRIPTION OF CONVENTIONAL CORE 13, NAVARIN BASIN COST NO. 1 WELL



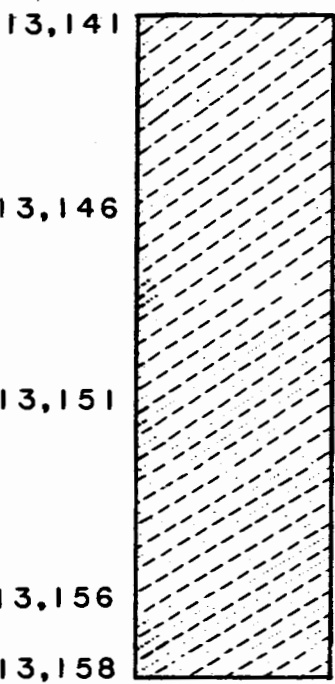


Core 15 is composed of very fine grained sandstone, siltstone, mudstone, and coaly, laminated claystone. The colors are medium light gray (N6), medium gray (N5), and black (N1). The rock is made up of 56 to 81 percent clay, 14 to 28 percent quartz, 3 to 9 percent plagioclase feldspar, and minor amounts of potassium feldspar, pyrite, siderite, mica, and hornblende, with local concentrations of up to 8 percent calcite. There is abundant carbonaceous material in the sediments and some calcitic, mottled root zones. The lower 5 feet is laminated sandstone with carbonaceous and claystone partings. The core is fractured throughout. The depositional environment was fluvial to paludal.

AGE: Late Cretaceous (Maastrichtian)

	POROSITY(%)	PERMEABILITY(mD)	%ORGANIC CARBON	%VITRINITE REFLECTANCE
			0.98	0.78
13.2	1.97			
12.6	0.05		0.80	0.89
14.1	0.26			
11.8	54.0			
13.4	0.08			

FIGURE 25. DESCRIPTION OF CONVENTIONAL CORE 15, NAVARIN BASIN COST NO. 1 WELL



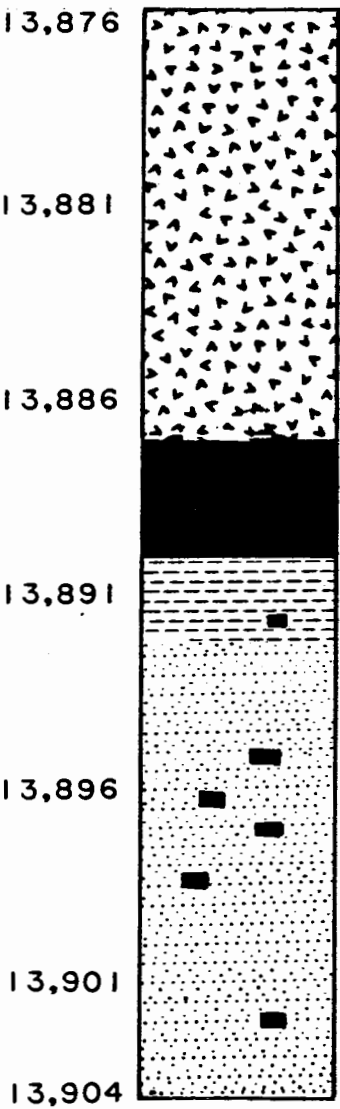
Core 16 consists of mudstone and ripple-laminated sandstone. The mudstone is wavy and lenticular and contains flaser structures. The colors range from black (N1) to medium gray (N5). Sixty-one to 69 percent of the core is clay, mostly chlorite and mixed-layer illite-smectite. Other minerals present are plagioclase feldspar (21 to 25 percent), quartz (5 to 8 percent), and small amounts of potassium feldspar, pyrite, and mica. The bedding dips 25 to 30 degrees. The depositional environment was nonmarine.

AGE: Late Cretaceous (Maastrichtian)

POROSITY(%)  
 PERMEABILITY(mD)  
 %ORGANIC CARBON  
 %VITRINITE REFLECTANCE

	POROSITY(%)	PERMEABILITY(mD)	%ORGANIC CARBON	%VITRINITE REFLECTANCE
13.8	0.02	1.09	2.33	
14.4	0.02			
13.3	0.02			
13.8	0.02	1.19	2.15	
15.5	0.04			

**FIGURE 26.** DESCRIPTION OF CONVENTIONAL CORE 16, NAVARIN BASIN COST NO. 1 WELL

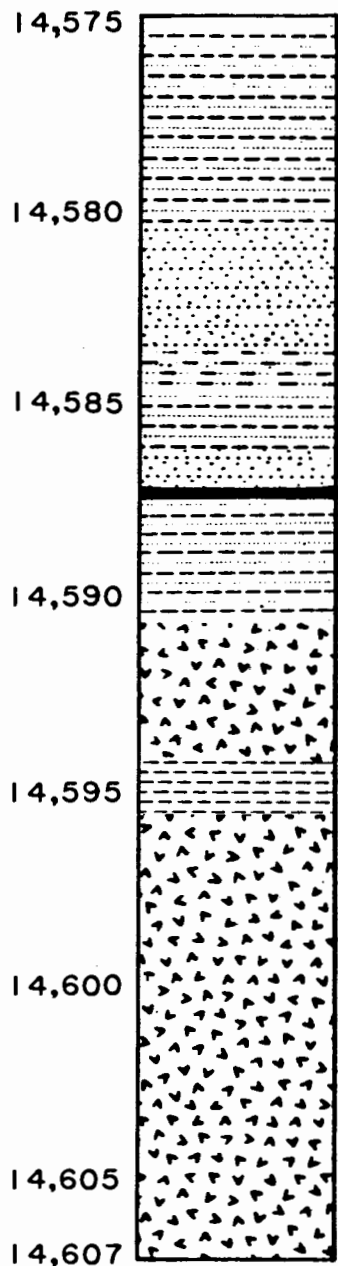


Core 17 is composed of diabase, coal, claystone, and sandstone. The colors, in the same order, are greenish-gray (5B 7/1), black (N1), dark gray (N3), and medium light gray (N6). The diabase appears to be an igneous sill with a fine-grained chilled margin. Fractures in the coal are filled with calcite, pyrite, and chalcopryite that may be related to hydrothermal fluids from the diabase. The claystone beneath the coal may be an abandoned stream or distributary channel deposit. The sandstone at the base of the core is a medium-grained, moderately sorted litharenite. The framework clasts are mainly volcanic fragments, quartz, and plagioclase feldspar. There are some coal and clay clast inclusions. The depositional environment was nonmarine.

AGE: Late Cretaceous (Maastrichtian)

	POROSITY(%)	PERMEABILITY(mD)	%ORGANIC CARBON	%VITRINITE REFLECTANCE
13,876-13,881	2.40	0.01		
13,881-13,886			32.67	4.20
13,886-13,891			0.15	2.66
13,891-13,896	4.7	0.01		
13,896-13,901	9.9	0.04		
	9.5	0.02		
	10.2	0.02		
13,901-13,904	7.6	0.02		

FIGURE 27. DESCRIPTION OF CONVENTIONAL CORE 17, NAVARIN BASIN COST NO. 1 WELL



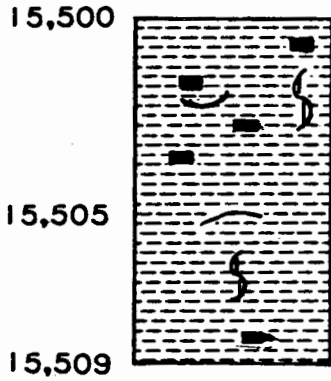
Core 18 contains mudstone, sandstone, siltstone, coal, claystone, and diabase. The colors are varying shades of gray, black, and light olive gray. The mudstones are bioturbated and intervals contain silt laminae, carbonized plant fragments, small burrows, parallel wavy laminations, and ripple marks. The sandstones contain discontinuous clay laminae, clay clasts, and pebbles. The siltstone has discontinuous, wavy, and parallel clay laminae. The coal has slickensided surfaces. The claystone has varves that were disrupted by the igneous intrusions. Clays are the most abundant minerals in the sediments, followed by quartz, plagioclase feldspar, potassium feldspar, pyrite, calcite, hornblende, siderite, mica, and clinoptilolite. The igneous intrusives are composed of plagioclase feldspar, clinopyroxene, and alteration products. The intrusives have chilled margins next to the sediments, and there are baked zones in the sediments. The nonmarine depositional environments included marsh, delta front, abandoned distributary channel, and pond deposits.

AGE: Late Cretaceous (Maastrichtian)

POROSITY (%)  
 PERMEABILITY (mD)  
 % ORGANIC CARBON  
 % VITRINITE REFLECTANCE

12.2	0.07	0.72	3.74
12.1	0.05		
13.4	0.02		
13.2	0.02		
11.5	0.02		
11.3	0.02		
8.9	0.02		
5.5	0.02		
7.8	0.02		
4.0	0.19		
4.9	0.05		
7.4	0.02		
8.0	0.02		
7.1	0.02		

**FIGURE 28. DESCRIPTION OF CONVENTIONAL CORE 18, NAVARIN BASIN COST NO. 1 WELL**

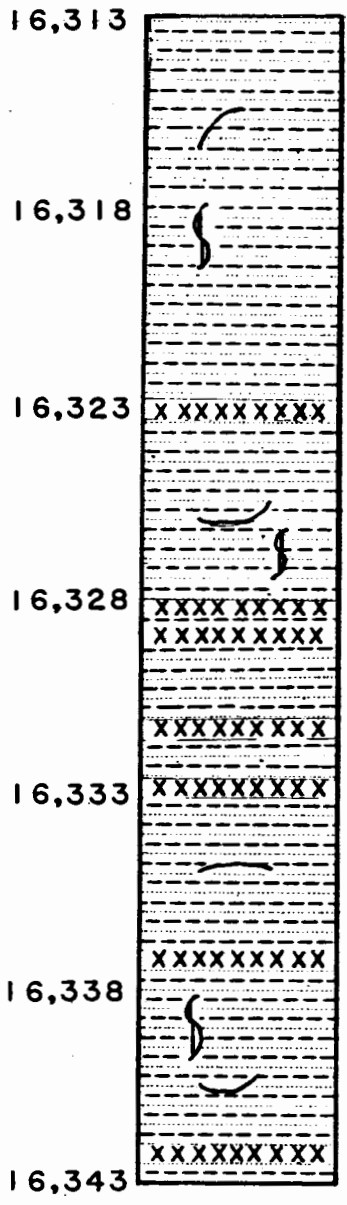


Core 19 is composed of dark-gray (N3) claystone. It is poorly sorted, bioturbated, sparsely fossiliferous, faintly laminated, and contains scattered plant debris. The rock contains 21 to 73 percent clay (mostly chlorite), quartz, plagioclase feldspar, and very small amounts of potassium feldspar, siderite, pyrite, hornblende, clinopyroxene, and mica. The source terrane was volcanic. The depositional environment was outer neritic.

AGE: Late Cretaceous (?Campanian or older)

	POROSITY(%)	PERMEABILITY(mD)	%ORGANIC CARBON
	7.8	0.10	0.47
	7.8	0.29	0.57
	7.8	0.04	

**FIGURE 29. DESCRIPTION OF CONVENTIONAL CORE 19, NAVARIN BASIN COST NO. 1 WELL**



Core 20 consists of mudstone, claystone, and muddy siltstone, with ash and crystal tuff layers 1/2 to 3 inches thick. The color ranges from near black in some of the siltstone to near white in some of the tuff layers. The pyroclastic layers fine upward (from medium-sand-sized plagioclase crystal tuff to fine altered ash). The mudstone and siltstone are highly indurated and contain clay, quartz, plagioclase feldspar, potassium feldspar, pyrite, mica, siderite, and calcite. Vertical fractures have been filled with calcite and zeolites. Pyritic and carbonaceous wisps are common in the bioturbated mudstone. Inoceramus fragments are present. The depositional environment was outer neritic.

AGE: Late Cretaceous (?Campanian or older)

	POROSITY(%)	PERMEABILITY(mD)	%ORGANIC CARBON
16,313	3.3	0.02	
16,318			0.41
16,323	3.8	0.10	
16,328			
16,333	2.4	0.05	
16,338			
16,343	9.8	0.05	
	3.7	0.12	

**FIGURE 30. DESCRIPTION OF CONVENTIONAL CORE 20, NAVARIN BASIN COST NO. 1 WELL**

**BULK ROCK**

**CLAY FRACTION**

**Average % of Total Rock**

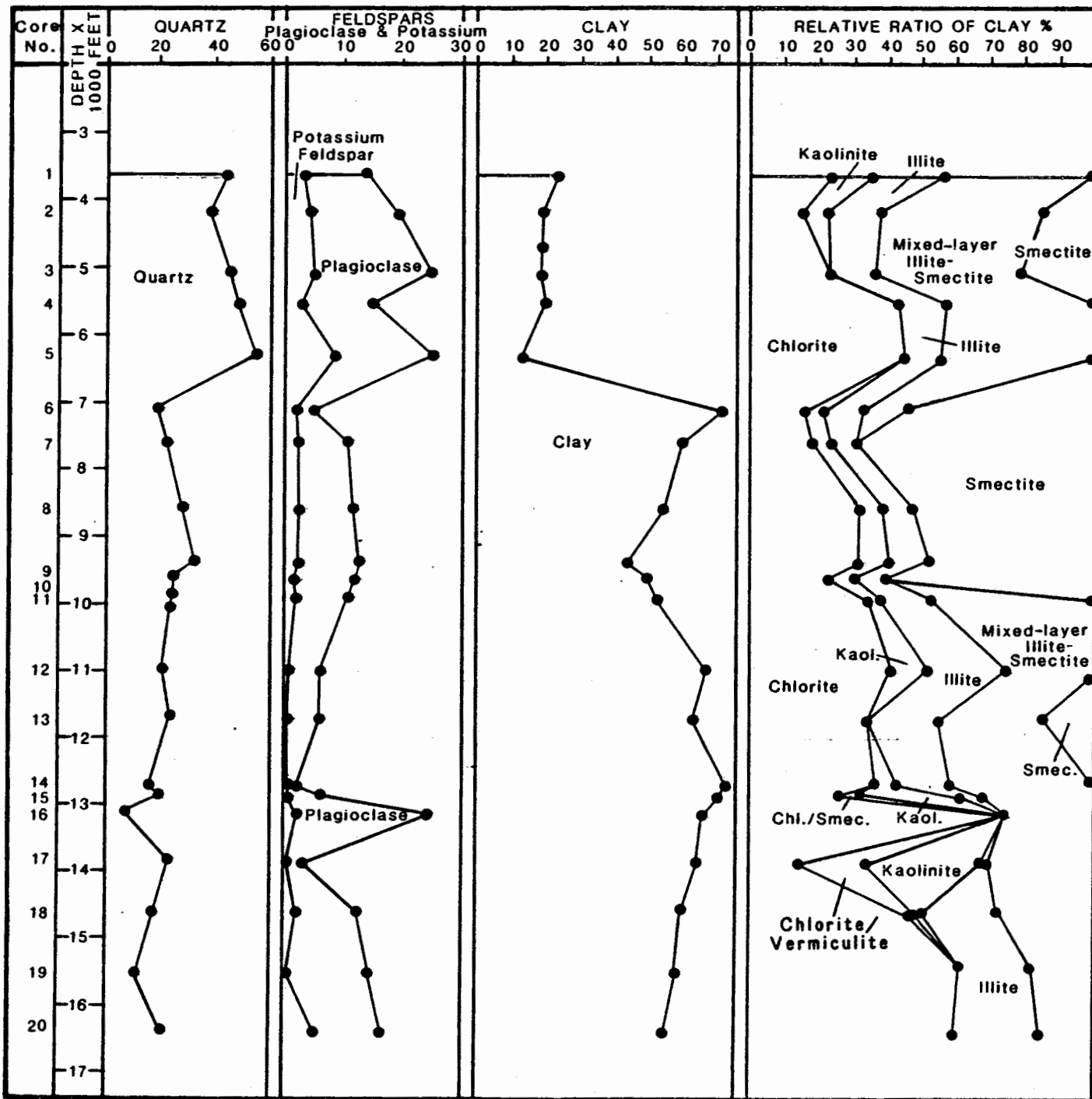


**FIGURE 31. SUMMARY CHART OF X-RAY DIFFRACTION DATA.**  
(From AGAT Consultants, Inc.)

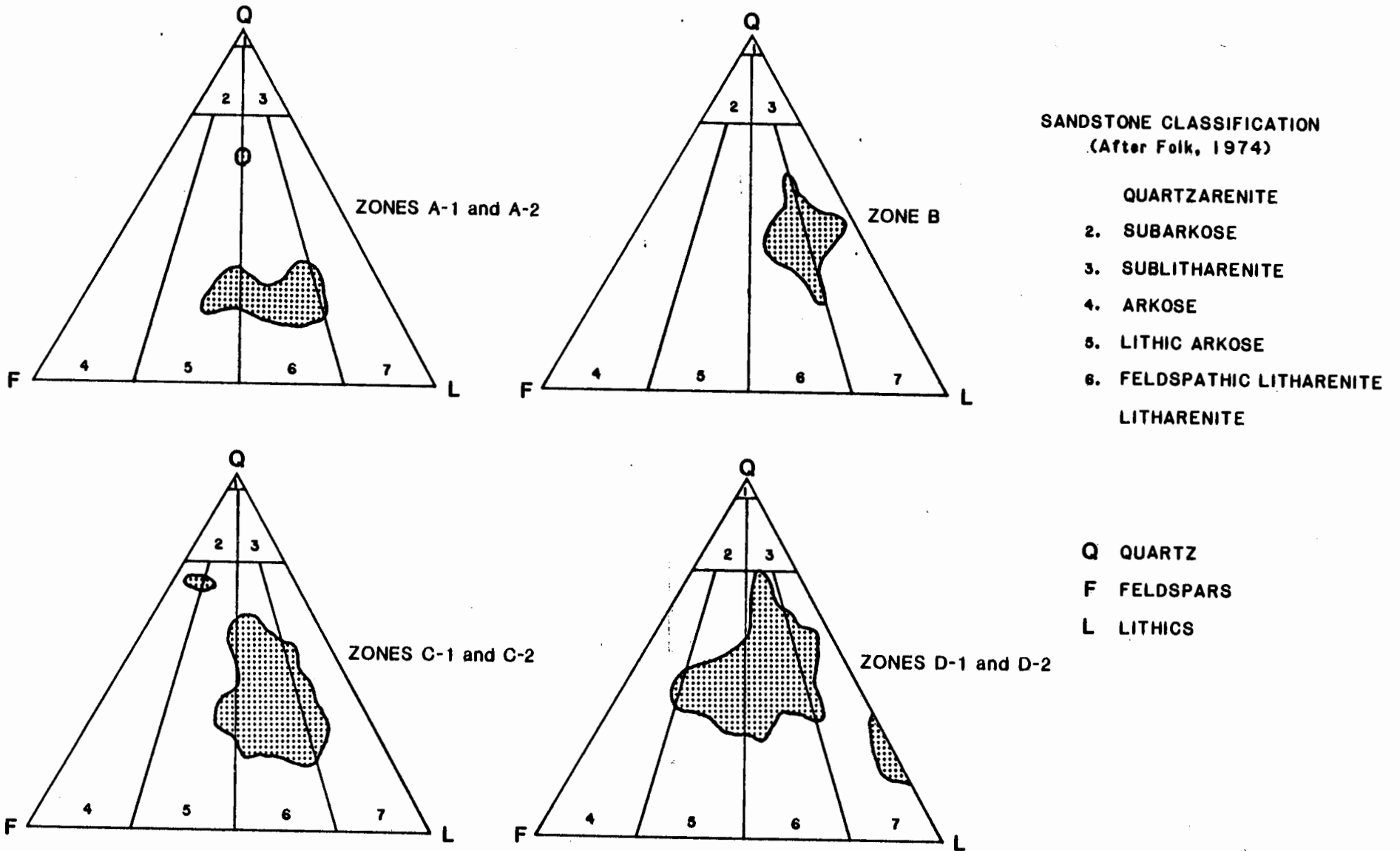
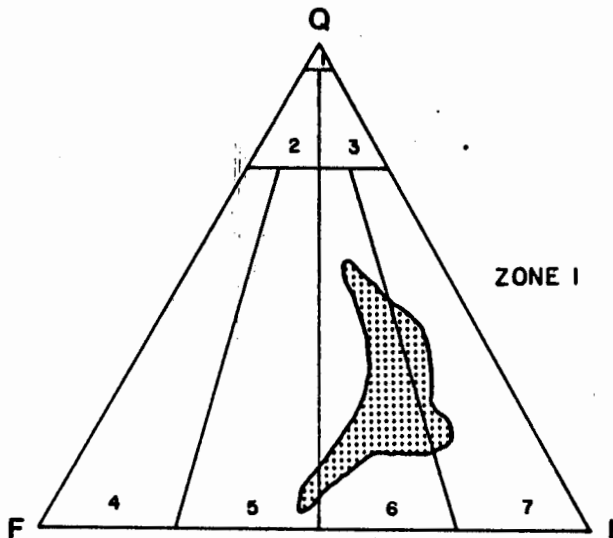
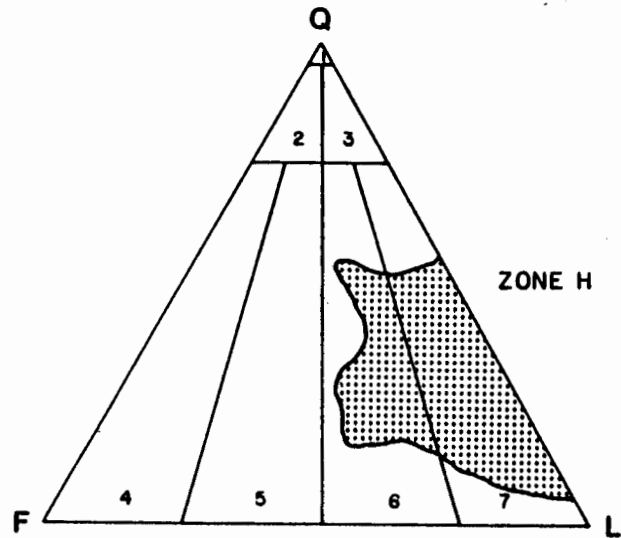
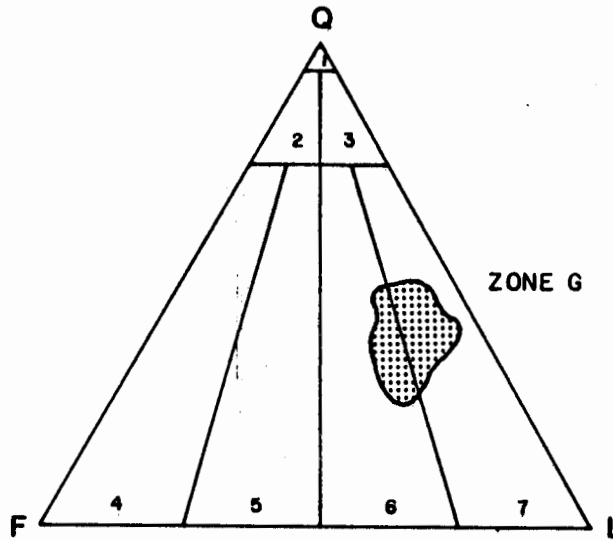
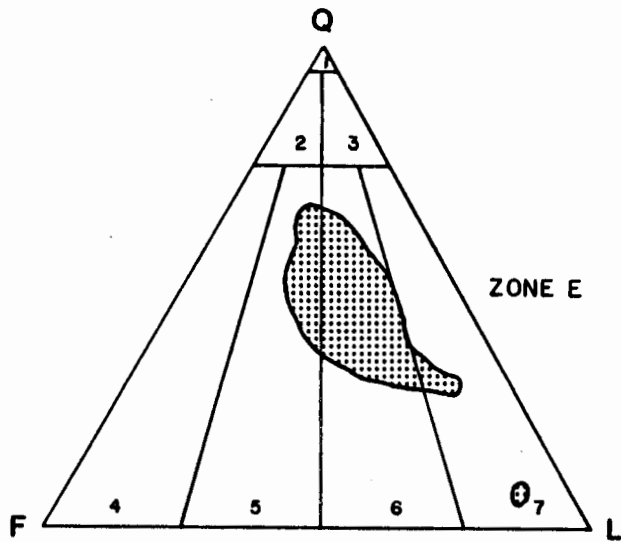


**FIGURE 32.** TERNARY DIAGRAMS SHOWING THE RANGE OF QUARTZ, FELDSPAR, AND LITHIC VALUES FOUND IN CONVENTIONAL AND SIDEWALL CORE SAMPLES FROM ZONES A-1 TO D-2 IN THE NAVARIN BASIN COST NO. 1 WELL. (From AGAT Consultants, Inc.)



**SANDSTONE CLASSIFICATION  
(After Folk, 1974)**

1. QUARTZARENITE
2. SUBARKOSE
3. SUBLITHARENITE
4. ARKOSE
5. LITHIC ARKOSE
6. FELDSPATHIC LITHARENITE
7. LITHARENITE

Q QUARTZ  
F FELDSPARS  
L LITHICS

INSUFFICIENT DATA FOR ZONE F

**FIGURE 33.** TERNARY DIAGRAMS SHOWING THE RANGE OF QUARTZ, FELDSPAR, AND LITHIC VALUES FOUND IN CONVENTIONAL AND SIDEWALL CORE SAMPLES FROM ZONES E, G, H, AND I IN THE NAVARIN BASIN COST NO. 1 WELL. (From AGAT Consultants, Inc.)

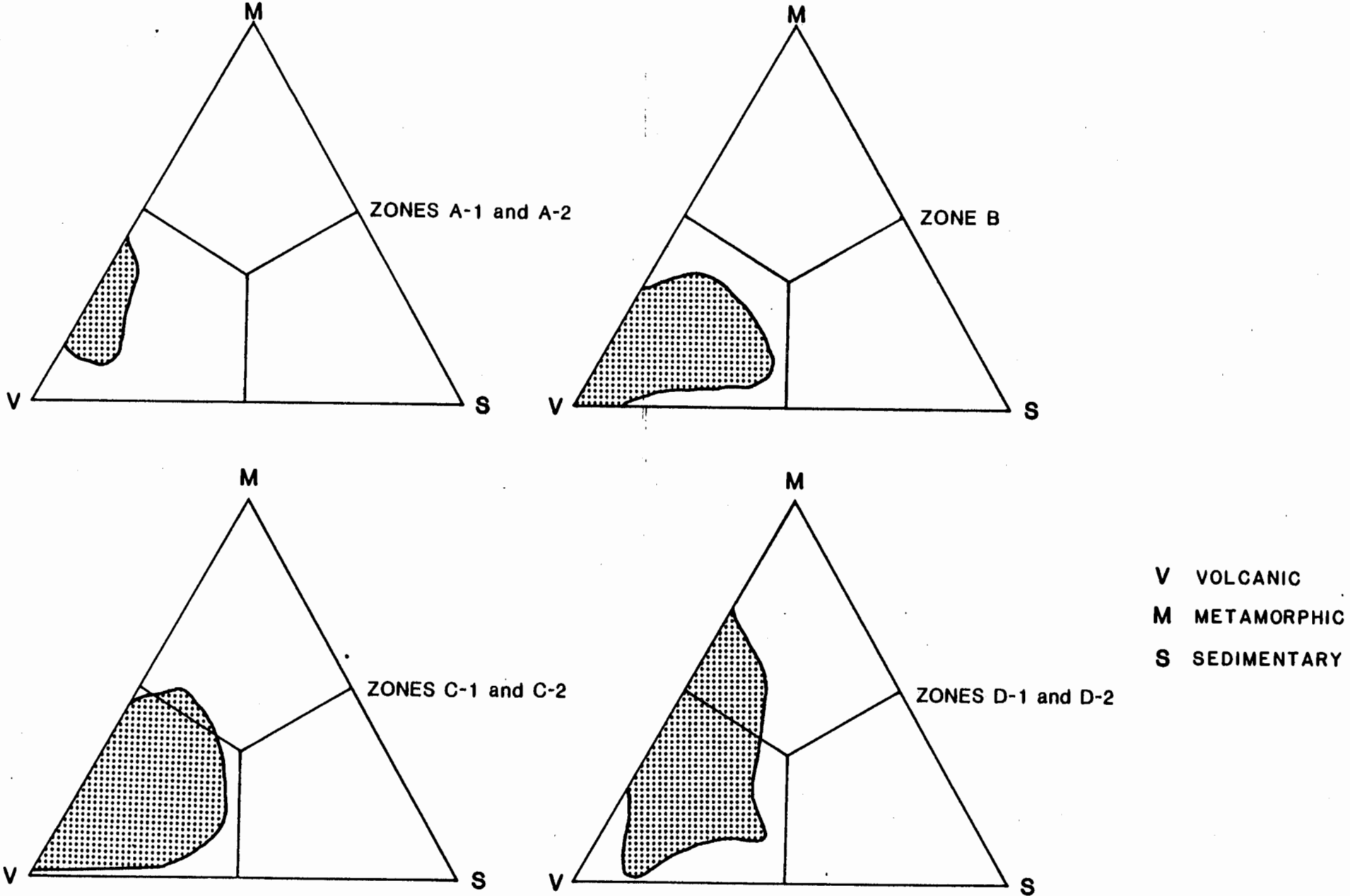
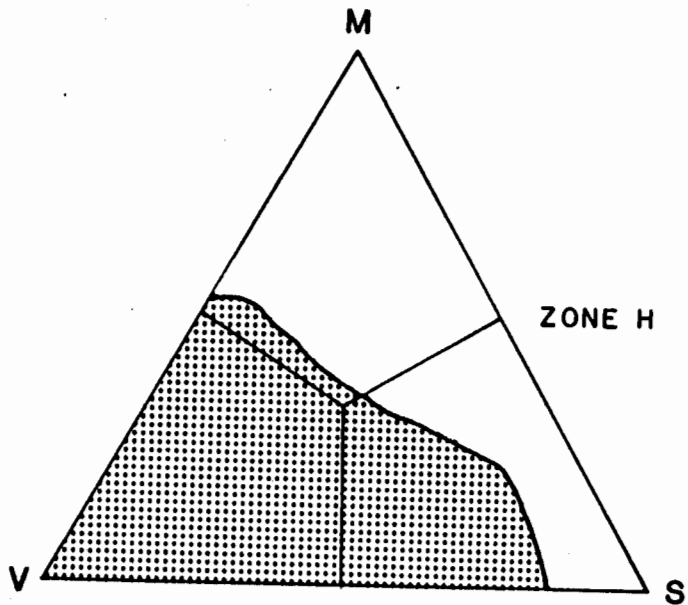
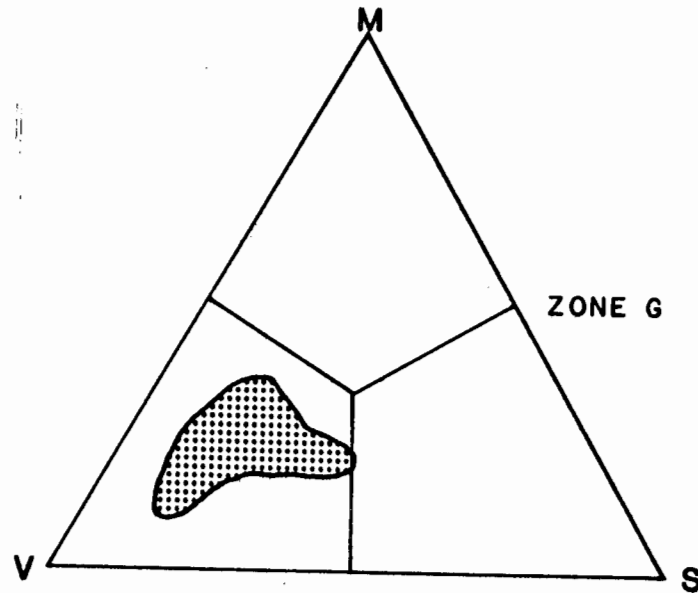
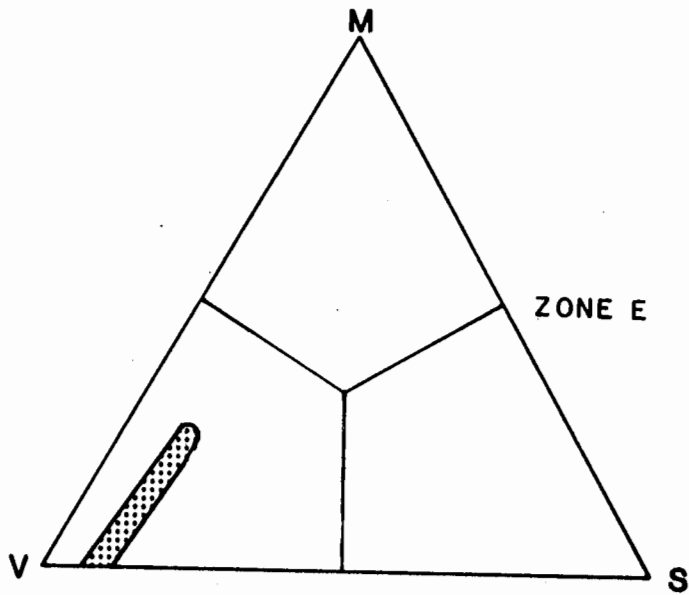


**FIGURE 34.** TERNARY DIAGRAMS SHOWING THE RANGE OF VOLCANIC, METAMORPHIC, AND SEDIMENTARY VALUES FOUND IN CONVENTIONAL AND SIDEWALL CORE SAMPLES FROM ZONES A-1 TO D-2 IN THE NAVARIN BASIN COST NO. 1 WELL. (From AGAT Consultants, Inc.)



V VOLCANIC  
 M METAMORPHIC  
 S SEDIMENTARY

INSUFFICIENT DATA FOR ZONES F AND I

**FIGURE 35.** TERNARY DIAGRAMS SHOWING THE RANGE OF VOLCANIC, METAMORPHIC, AND SEDIMENTARY VALUES FOUND IN CONVENTIONAL AND SIDEWALL CORE SAMPLES FROM ZONES E, G, AND H IN THE NAVARIN BASIN COST NO. 1 WELL. (From AGAT Consultants, Inc.)

Table 2. Lithology, measured porosity, estimated visible porosity, and measured permeability of samples from sidewall and conventional cores. Lithology and estimated visible porosities were determined from thin sections by geologists at AGAT Consultants in Denver. Measured porosity and permeability were derived by Core Laboratories in Anchorage. SWC -- sidewall core. Conv - - conventional centerline core.

Sample Depth (Feet)	Sample Type	Lithology	Measured Porosity (Percent)	Estimated Visible Porosity (Percent)	Measured Permeability (Millidarcies)
2,500	SWC	Silty diatomaceous ooze	-	2.0	-
2,904	SWC	Sandy diatomaceous ooze	38.6	3.2	16.0
3,030	SWC	Sandy diatomaceous mudstone	-	2.0	-
3,300	SWC	Silty diatomaceous ooze	35.1	4.4	21.0
3,454	SWC	Sandy diatomaceous ooze	-	2.8	-
3,590	SWC	Sandy diatomaceous ooze	-	-	-
3,633.6	Conv	Diatomaceous sandy mudstone	48.8	8.0	3.88
3,651.7	Conv	Diatomaceous sandy mudstone	50.7	4.4	6.15
3,671	SWC	Sandy diatomaceous ooze	-	5.6	-
3,774	SWC	Sandy diatomaceous ooze	-	2.8	-
3,836	SWC	Sandy diatomaceous ooze	-	7.6	-
3,980	SWC	Very fine sandstone	34.6	13.1	73.0
4,012	SWC	Very fine sandstone	-	11.3	-
4,087	SWC	Muddy very fine sandstone	-	10.3	-

Table 2 (cont.)

Sample Depth (Feet)	Sample Type	Lithology	Measured Porosity (Percent)	Estimated Visible Porosity (Percent)	Measured Permeability (Millidarcies)
4,114	SWC	Muddy very fine sandstone	-	19.1	-
4,161	SWC	Calcitic, muddy very fine sandstone	-	1.3	-
4,184.8	Conv	Calcareous very fine sandstone	7.7	0	0.02
4,190.4	Conv	Muddy very fine sandstone	35.5	6.0	2.07
4,196.4	Conv	Sandy mudstone	37.3	1.2	0.80
4,200.6	Conv	Muddy very fine- fine sandstone	29.7	4.4	3.99
4,202	SWC	Muddy very fine sandstone	-	-	-
4,202.4	Conv	Muddy very fine sandstone	32.4	11.6	27.0
4,205.5	Conv	Muddy very fine sandstone	33.8	11.2	51.0
4,206.6	Conv	Calcareous very fine sandstone	9.6	-	0.05
4,209.1	Conv	Very fine sandstone	35.2	16.0	118.0
4,295	SWC	Fine sandstone	23.8	9.7	30.0
4,374	SWC	Muddy very fine sandstone	-	13.2	-
4,432	SWC	Muddy very fine sandstone	26.0	7.5	62.0
4,456	SWC	Fine sandstone	33.7	9.3	248.0
4,556	SWC	Fine sandstone	27.4	7.6	115.0
4,697	SWC	Calcitic fine sandstone	-	2.8	-

Table 2 (cont.)

Sample Depth (Feet)	Sample Type	Lithology	Measured Porosity (Percent)	Estimated Visible Porosity (Percent)	Measured Permeability (Millidarcies)
4,746	SWC	Fine sandstone	28.8	13.6	325.0
4,777	SWC	Fine sandstone	30.3	7.2	590.0
4,861	SWC	Very fine sandstone	-	15.8	-
4,944	SWC	Muddy very fine sandstone	25.6	7.3	47.0
4,989	SWC	Muddy very fine sandstone	-	4.0	-
5,012	SWC	Muddy very fine sandstone	-	8.1	-
5,078	SWC	Sandy claystone	30.3	2.0	6.49
5,102.2	Conv	Fine sandstone	30.1	4.8	4.96
5,115.9	Conv	Muddy very fine sandstone	30.6	6.0	8.18
5,118.8	Conv	Muddy very fine sandstone	28.2	7.2	4.19
5,156	SWC	Very fine sandstone	30.8	7.0	23.0
5,188	SWC	Mudstone	-	2.0	-
5,224	SWC	Mudstone	32.2	5.2	12.0
5,309	SWC	Claystone	-	-	-
5,360	SWC	Muddy very fine sandstone	28.9	8.0	2.50
5,408	SWC	Very fine sandstone	31.8	20.0	59.0
5,454	SWC	Slightly muddy very fine sandstone	31.2	22	63.0
5,553	SWC	Very fine sandstone	28.8	13.5	18.0
5,572.2	Conv	Calcareous very fine sandstone	6.6	0	0.05

Table 2 (cont.)

Sample Depth (Feet)	Sample Type	Lithology	Measured Porosity (Percent)	Estimated Visible Porosity (Percent)	Measured Permeability (Millidarcies)
5,575.6	Conv	Calcareous very fine sandstone	6.0	0	0.02
5,576.6	Conv	Calcareous very fine sandstone	6.1	0	0.02
5,577.7	Conv	Very fine sandstone	-	17.6	-
5,578.5	Conv	Muddy very fine sandstone	-	12.8	-
5,579.2	Conv	Muddy very fine sandstone	-	18.4	-
5,586	SWC	Very fine sandstone	34.0	5.0	156.0
5,715	SWC	Muddy very fine sandstone	30.8	3.0	64.0
5,745	SWC	Very fine sandstone	34.3	14.0	127.0
5,788	SWC	Very fine sandstone	32.3	11.0	86.0
5,842	SWC	Muddy fine sandstone	32.1	7.0	67.0
5,955	SWC	Muddy very fine sandstone	-	3.2	-
6,027	SWC	Very fine sandstone	-	6.4	-
6,057	SWC	Muddy fine sandstone	26.1	6.4	5.82
6,106	SWC	Very fine sandstone	35.3	16.0	1.53
6,154	SWC	Mudstone	-	2.0	-
6,218	SWC	Fine sandstone	34.3	16.0	233.0
6,279	SWC	Very fine sandstone	31.9	18.0	56.0
6,289	SWC	Very fine sandstone	29.6	15.0	23.0
6,370.8	Conv	Fine sandstone	28.4	10.4	4.85
6,374.6	Conv	Fine sandstone	29.2	11.2	7.87

Table 2 (cont.)

Sample Depth (Feet)	Sample Type	Lithology	Measured Porosity (Percent)	Estimated Visible Porosity (Percent)	Measured Permeability (Millidarcies)
6,376.2	Conv	Fine sandstone	34.0	18.4	117.0
6,378.9	Conv	Muddy very fine sandstone	33.3	9.6	30.0
6,385	SWC	Very fine sandstone	28.9	9.6	19.0
6,385.4	Conv	Very fine sandstone	32.1	13.6	6.16
6,387.4	Conv	Very fine sandstone	29.7	8.8	2.42
6,392.3	Conv	Very fine sandstone	32.5	9.6	3.74
6,443	SWC	Muddy very fine sandstone	27.8	5.6	13.0
6,494	SWC	Sandy micrite	-	-	-
6,534	SWC	Very fine sandstone	-	12.4	-
6,538	SWC	Muddy very fine sandstone	31.0	14.0	19.0
6,617	SWC	Mudstone	-	-	-
6,690	SWC	Muddy very fine sandstone	24.4	13.6	23.0
6,813	SWC	Muddy very fine sandstone	31.6	16.8	39.0
6,880	SWC	Muddy very fine sandstone	31.5	14.8	58.0
6,938	SWC	Calcareous very fine sandstone	-	-	-
7,080	SWC	Sandy mudstone	-	-	-
7,129	SWC	Mudstone	-	-	-
7,162.6	Conv	Claystone	18.6	-	0.41
7,254	SWC	Claystone	-	-	-

Table 2 (cont.)

Sample Depth (Feet)	Sample Type	Lithology	Measured Porosity (Percent)	Estimated Visible Porosity (Percent)	Measured Permeability (Millidarcies)
7,366	SWC	Mudstone	22.5	2.0	0.81
7,375	SWC	Sandy mudstone	-	-	-
7,466	SWC	Mudstone	-	-	-
7,530	SWC	Claystone	-	-	-
7,540	SWC	Muddy very fine sandstone	-	-	-
7,600.4	Conv	Fossiliferous muddy very fine sandstone	21.5	4.4	0.43
7,602.3	Conv	Sandy mudstone	21.6	1.6	0.21
7,604.8	Conv	Claystone	21.1	-	0.46
7,607.6	Conv	Mudstone	23.1	0	0.08
7,608.9	Conv	Slightly fossiliferous mudstone	19.6	4.0	0.49
7,611.2	Conv	Claystone	21.6	-	0.09
7,614.4	Conv	Claystone	19.3	0	1.14
7,616.3	Conv	Slightly fossiliferous mudstone	20.5	0	0.11
7,619.8	Conv	Slightly fossiliferous claystone	21.6	-	0.13
7,625.3	Conv	Mudstone	21.4	1.2	0.30
7,626.0	Conv	Sandy mudstone	21.8	4.4	1.78
7,648	SWC	Sandy mudstone	-	-	-
7,714	SWC	Claystone	19.6	1.0	0.29
7,827	SWC	Sandy mudstone	-	-	-
7,988	SWC	Sandy mudstone	-	-	-

Table 2 (cont.)

Sample Depth (Feet)	Sample Type	Lithology	Measured Porosity (Percent)	Estimated Visible Porosity (Percent)	Measured Permeability (Millidarcies)
8,024	SWC	Calclitic sandy mudstone	22.1	0	-
8,136	SWC	Silty mudstone	-	-	-
8,220	SWC	Pyritic mudstone	-	-	-
8,236	SWC	Pyritic mudstone	-	-	-
8,306	SWC	Pyritic mudstone	-	-	-
8,390	SWC	Sandy mudstone	-	-	-
8,433	SWC	Pyritic sandy mudstone	21.4	1.2	-
8,517	SWC	Muddy very fine sandstone	22.8	0.4	1.40
8,566	SWC	Muddy fine sandstone	22.8	3.2	4.55
8,639.3	Conv	Calclitic sandy mudstone	21.6	0	0.05
8,641.5	Conv	Siltstone	21.5	0	0.05
8,644.3	Conv	Siltstone	20.2	0	0.05
8,645.8	Conv	Siltstone	21.4	0	0.09
8,649.3	Conv	Sandy mudstone	18.8	0	0.03
8,654	SWC	Muddy very fine sandstone	-	-	-
8,740	SWC	Muddy very fine sandstone	-	-	-
8,760	SWC	Muddy very fine sandstone	-	-	-
8,856	SWC	Very fine sandstone	24.3	9.6	7.70
8,874	SWC	Muddy very fine sandstone	22.0	0.4	-

Table 2 (cont.)

Sample Depth (Feet)	Sample Type	Lithology	Measured Porosity (Percent)	Estimated Visible Porosity (Percent)	Measured Permeability (Millidarcies)
8,934	SWC	Muddy very fine sandstone	-	-	-
8,963	SWC	Muddy very fine sandstone	24.2	2.0	6.48
9,105	SWC	Calcitic, muddy very fine sandstone	-	-	-
9,185	SWC	Muddy very fine sandstone	-	-	-
9,204	SWC	Calcitic, muddy very fine sandstone	20.9	4.4	9.26
9,253	SWC	Muddy very fine sandstone	-	-	-
9,280	SWC	Mudstone	-	-	-
9,333	SWC	Muddy very fine sandstone	-	-	-
9,380	SWC	Silty carbonate	-	-	-
9,401.6	Conv	Claystone	15.2	0	0.02
9,404.4	Conv	Mudstone	14.9	0	5.93
9,405.9	Conv	Mudstone/siltstone	14.6	0	0.22
9,408.7	Conv	Very fine sandstone/mudstone	14.2	0	0.05
9,411.2	Conv	Very fine sandstone/mudstone	14.3	0	0.05
9,413.4	Conv	Mudstone	13.2	0	0.01
9,414.6	Conv	Very fine sandstone/mudstone	14.4	0	12.0
9,418.3	Conv	Very fine sandstone/mudstone	11.7	1.2	0.37

Table 2 (cont.)

Sample Depth (Feet)	Sample Type	Lithology	Measured Porosity (Percent)	Estimated Visible Porosity (Percent)	Measured Permeability (Millidarcies)
9,420.7	Conv	Mudstone	13.9	0	8.49
9,422.5	Conv	Very fine sandy mudstone	15.1	0	1.57
9,424.7	Conv	Mudstone	13.7	0	1.04
9,425.5	Conv	Mudstone/ very fine sandstone	13.5	0	0.13
9,427.8	Conv	Mudstone	12.5	0	25.0
9,428.5	Conv	Mudstone/ very fine sandstone	14.8	0	0.59
9,429.8	Conv	Sandy mudstone	14.6	0	0.19
9,514	SWC	Sandy mudstone	-	-	-
9,544	SWC	Mudstone	-	-	-
9,566	SWC	Slightly silty fossiliferous carbonate	-	-	-
9,599	SWC	Mudstone	-	-	-
9,649	SWC	Mudstone	-	-	-
9,656.3	Conv	Sandy mudstone	14.3	0	0.02
9,657.9	Conv	Sandy mudstone	14.5	0	0.02
9,662.4	Conv	Quartz andesite Siltstone	-	-	-
9,665.8	Conv	Mudstone	15.8	0	0.02
9,666.7	Conv	Slightly fossiliferous lime mudstone	-	-	-
9,672.6	Conv	Sandy mudstone	14.6	0	0.14
9,678.7	Conv	Andesite/basalt? Mudstone	-	-	-

Table 2 (cont.)

Sample Depth (feet)	Sample Type	Lithology	Measured Porosity (Percent)	Estimated Visible Porosity (Percent)	Measured Permeability (Millidarcies)
9,681.6	Conv	Mudstone	14.0	0	0.02
9,683.7	Conv	Mudstone	14.5	0	0.08
9,684.8	Conv	Mudstone	14.4	0	0.12
9,685.4	Conv	Lithic lapilli tuff	-	-	-
9,685.5	Conv	Andesite	-	-	-
9,685.7	Conv	Andesite	-	-	-
9,685.8	Conv	Mudstone	8.8	0	0.02
9,704	SWC	Mudstone	19.0	0	-
9,734	SWC	Mudstone	-	1.6	-
9,826	SWC	Sandy mudstone	-	-	-
9,882	SWC	Sandy carbonate	-	-	-
9,938	SWC	Mudstone	-	-	-
9,949.2	Conv	Claystone	15.1	0	0.02
9,960.4	Conv	Mudstone	14.7	0	0.01
9,970.5	Conv	Mudstone/claystone Calcite concretion	-	-	-
9,970.7	Conv	Sandy mudstone	-	-	-
9,972.3	Conv	Mudstone/ very fine sandstone	12.6	0	0.02
9,974.1	Conv	Sandy mudstone Volcanic pebble Plutonic pebble	-	-	-
9,975.9	Conv	Mudstone Volcanic pebble	-	-	-
9,980.4	Conv	Mudstone Plutonic pebble	-	-	-

Table 2 (cont.)

Sample Depth (Feet)	Sample Type	Lithology	Measured Porosity (Percent)	Estimated Visible Porosity (Percent)	Measured Permeability (Millidarcies)
9,983.6	Conv	Mudstone/ very fine sandstone	14.4	0	0.01
9,984.4	Conv	Mudstone/ very fine sandstone Calcite concretion	-	-	-
10,011	SWC	Sandy mudstone	22.3	0.4	-
10,110	SWC	Claystone	-	-	-
10,127	SWC	Sandy mudstone	-	-	-
10,189	SWC	Silty claystone	-	-	-
10,253	SWC	Mudstone	-	-	-
10,328	SWC	Sandy mudstone	-	-	-
10,440	SWC	Silty claystone	-	-	-
10,540	SWC	Mudstone	17.9	0.4	-
10,603	SWC	Silty claystone	-	-	-
10,717	SWC	Claystone	-	-	-
10,796	SWC	Mudstone	-	-	-
10,906	SWC	Claystone	20.5	0.4	-
10,984.5	Conv	Claystone	16.9	0	0.04
10,984.9	Conv	Volcanic rock fragment/claystone	-	-	-
10,990	SWC	Mudstone	-	-	-
11,000.7	Conv	Claystone	15.8	0	0.02
11,012.4	Conv	Claystone	15.2	0	0.02
11,014.9	Conv	Calcite concretion	-	-	-
11,232	SWC	Claystone	-	-	-

Table 2 (cont.)

Sample Depth (Feet)	Sample Type	Lithology	Measured Porosity (Percent)	Estimated Visible Porosity (Percent)	Measured Permeability (Millidarcies)
11,298	SWC	Claystone	-	-	-
11,590	SWC	Sandy mudstone	-	-	-
11,707.2	Conv	Muddy very fine sandstone	-	-	-
11,709.6	Conv	Claystone	11.4	0	0.02
11,717.1	Conv	Claystone	11.4	0	0.02
11,717.5	Conv	Claystone	-	-	-
11,726.5	Conv	Calclitic volcanic rock fragment	4.4	0	0.33
11,729.7	Conv	Claystone	11.8	0	0.26
11,740	SWC	Claystone	-	-	-
11,819	SWC	Claystone	-	-	-
11,993	SWC	Claystone	-	-	-
12,137	SWC	Sandy claystone	-	-	-
12,270	SWC	Claystone	-	-	-
12,313	SWC	Sandy mudstone	-	-	-
12,461	SWC	Claystone	-	-	-
12,580	SWC	Claystone	-	-	-
12,710.3	Conv	Limestone	-	-	-
12,711.4	Conv	Limestone	2.1	0	0.02
12,716.5	Conv	Claystone	-	-	-
12,723	SWC	Claystone	-	-	-
12,729.5	Conv	Claystone	12.5	0	-
12,734.1	Conv	Claystone	-	-	-

Table 2 (cont.)

Sample Depth (Feet)	Sample Type	Lithology	Measured Porosity (Percent)	Estimated Visible Porosity (Percent)	Measured Permeability (Millidarcies)
12,737.8	Conv	Claystone	12.9	0	-
12,756	SWC	Pyritic muddy medium sandstone	26.1	0	-
12,783	SWC	Carbonaceous mudstone	-	-	-
12,792	SWC	Mudstone	19.4	0	21.0
12,805	SWC	Basalt	-	-	-
12,830	SWC	Calclitic mudstone	20.2	0	41.0
12,851.0	Conv	Silty mudstone/ very fine sandstone	-	-	-
12,856.1	Conv	Sandy mudstone	-	-	-
12,860.6	Conv	Muddy very fine sandstone	13.2	0	1.97
12,865.1	Conv	Calcareous muddy siltstone	-	-	-
12,865.7	Conv	Muddy siltstone	12.6	0.4	0.05
12,874.1	Conv	Muddy siltstone	-	-	-
12,876.4	Conv	Muddy very fine sandstone	14.1	3.2	0.26
12,878.7	Conv	Carbonaceous muddy very fine sandstone	11.8	0.4	54.0
12,879.5	Conv	Muddy very fine sandstone	13.4	4.4	0.08
12,886	SWC	Basalt	-	-	-
12,982	SWC	Calcite	-	-	-
13,014	SWC	Diabase	20.9	0	1.83
13,088	SWC	Basalt	-	-	-

Table 2 (cont.)

Sample Depth (feet)	Sample Type	Lithology	Measured Porosity (Percent)	Estimated Visible Porosity (Percent)	Measured Permeability (Millidarcies)
13,143.7	Conv	Laminated carbonaceous mudstone	13.8	0	0.02
13,144.3	Conv	Laminated carbonaceous sandy mudstone	-	-	-
13,147.5	Conv	Laminated carbonaceous mudstone	14.4	0	0.02
13,150.5	Conv	Laminated carbonaceous muddy very fine sandstone	13.3	0	0.02
13,153.3	Conv	Laminated muddy very fine sandstone	13.8	0	0.02
13,156.7	Conv	Laminated carbonaceous sandy mudstone	15.5	0	0.04
13,242	SWC	Basalt	-	-	-
13,266	SWC	Basalt	-	-	-
13,410	SWC	Diabase	-	-	-
13,460	SWC	Diabase	-	-	-
13,478	SWC	Diabase	-	-	-
13,518	SWC	Diabase	-	-	-
13,536	SWC	Diabase	-	-	-
13,544	SWC	Diabase	23.5	0	88.0
13,548	SWC	Basalt	17.6	0	13.0
13,602	SWC	Basalt	-	-	-
13,634	SWC	Basalt	-	-	-
13,670	SWC	Diabase	-	-	-
13,710	SWC	Diabase	-	-	-

Table 2 (cont.)

Sample Depth (Feet)	Sample Type	Lithology	Measured Porosity (Percent)	Estimated Visible Porosity (Percent)	Measured Permeability (Millidarcies)
13,715	SWC	Diabase	-	-	-
13,760	SWC	Claystone	-	-	-
13,866	SWC	Diabase	-	-	-
13,874	SWC	Diabase	-	-	-
13,876.6	Conv	Altered diabase	-	-	-
13,879.5	Conv	Altered diabase	-	-	-
13,885.3	Conv	Altered diabase	-	-	-
13,886.8	Conv	Altered diabase	-	1.6	-
13,890.6	Conv	Claystone	-	-	-
13,892.6	Conv	Medium sandstone	4.7	0	0.01
13,896.3	Conv	Medium sandstone	9.9	0	0.04
13,897.6	Conv	Medium sandstone	9.5	0	0.02
13,898.6	Conv	Medium sandstone	10.2	0	0.02
13,903.6	Conv	Medium sandstone	7.6	0	0.02
13,915	SWC	Calcitic coarse sandstone	-	-	-
14,106	SWC	Calcitic medium sandstone	-	-	-
14,110	SWC	Medium sandstone	-	-	-
14,145	SWC	Diabase	-	-	-
14,177	SWC	Calcitic medium sandstone	-	-	-
14,188	SWC	Medium sandstone	-	-	-
14,206	SWC	Basalt	-	-	-

Table 2 (cont.)

Sample Depth (Feet)	Sample Type	Lithology	Measured Porosity (Percent)	Estimated Visible Porosity (Percent)	Measured Permeability (Millidarcies)
14,288	SWC	Medium sandstone	-	-	-
14,326	SWC	Diabase	-	-	-
14,413	SWC	Clayey medium sandstone	-	-	-
14,480	SWC	Clayey medium sandstone	-	-	-
14,501	SWC	Clayey medium sandstone	19.0	0	111.0
14,546	SWC	Clayey fine sandstone	-	-	-
14,575.4	Conv	Mudstone	12.2	0	0.07
14,577.6	Conv	Mudstone	12.1	0	0.05
14,578	SWC	Claystone	-	-	-
14,580.1	Conv	Laminated sandy mudstone	13.4	0	0.02
14,581.4	Conv	Muddy fine sandstone	13.2	0	0.02
14,582.8	Conv	Muddy fine sandstone	11.5	0	0.02
14,584.8	Conv	Sandy mudstone	11.3	0.4	0.02
14,586.4	Conv	Calcitic fine sandstone	8.9	0	0.02
14,590.5	Conv	Claystone/diabase	5.5	0	0.02
14,592.1	Conv	Diabase	7.8	0	0.02
14,593.8	Conv	Diabase	4.0	0	0.19
14,595.3	Conv	Cherty claystone	4.9	0	0.05
14,595.8	Conv	Diabase	7.4	0	0.02
14,599.6	Conv	Diabase	8.0	0	0.02

Table 2 (cont.)

Sample Depth (Feet)	Sample Type	Lithology	Measured Porosity (Percent)	Estimated Visible Porosity (Percent)	Measured Permeability (Millidarcies)
14,601.3	Conv	Diabase	7.1	0	0.02
14,622	SWC	Diabase	-	-	-
14,630	SWC	Diabase	-	-	-
14,637	SWC	Diabase	-	-	-
14,660	SWC	Diabase	-	-	-
14,695	SWC	Diabase	-	-	-
14,794	SWC	Diabase	-	-	-
14,805	SWC	Diabase	-	-	-
14,848	SWC	Diabase	-	-	-
14,862	SWC	Diabase	-	-	-
14,890	SWC	Diabase	-	-	-
14,914	SWC	Diabase	-	-	-
14,983	SWC	Diabase	-	-	-
14,988	SWC	Clayey medium sandstone	-	-	-
15,005	SWC	Feldspathic medium sandstone	-	-	-
15,018	SWC	Medium sandstone	-	-	-
15,048	SWC	Diabase	-	-	-
15,072	SWC	Clayey feldspathic fine sandstone	17.0	0	51.0
15,090	SWC	Clayey fine sandstone	-	-	-
15,501.5	Conv	Mudstone/ calcitic siltstone	-	-	-

Table 2 (cont.)

Sample Depth (Feet)	Sample Type	Lithology	Measured Porosity (Percent)	Estimated Visible Porosity (Percent)	Measured Permeability (Millidarcies)
15,502.3	Conv	Mudstone	7.8	0	0.10
15,503.5	Conv	Mudstone	7.8	0	0.29
15,506.9	Conv	Sandy mudstone	7.8	0	0.04
15,477	SWC	Silty claystone	-	-	-
15,728	SWC	Silty claystone	-	-	-
15,834	SWC	Silty claystone	-	-	-
15,981	SWC	Silty claystone	-	-	-
16,094	SWC	Silty claystone	-	-	-
16,315.2	Conv	Mudstone	3.3	0	0.02
16,317.8	Conv	Crystal lithic tuff/ calcitic claystone	3.8	0	0.10
16,328.5	Conv	Crystal lithic tuff	2.4	0	0.05
16,328.9	Conv	Crystal tuff	-	-	-
16,335.0	Conv	Laumontite/leonhardite fracture-filling	-	-	-
16,337.4	Conv	Tuff	9.8	0	0.05
16,341.9	Conv	Mudstone	3.7	0	0.12
12,834-13,590	Junk basket A <sub>1</sub>	Basalt	-	-	-
12,834-13,590	Junk basket A <sub>2</sub>	Basalt	-	-	-
12,834-13,590	Junk basket A <sub>3</sub>	Basalt	-	-	-
12,834-13,590	Junk basket A <sub>4</sub>	Basalt	-	-	-

Table 3. X-ray diffraction data from conventional cores, ranges of values for whole rock, Navarin Basin COST No. 1 well. From AGAT Consultants, Inc.

Core No.	Depth (feet)	Whole Rock (Percent)													
		Qtz	Plag	K-Spar	Sid	Pyr	Cal	Hbl	Clino	Anlc	L/L	Ill-mica	Other	Clay	
1	3,627-3,657	35/50	8/14	1/3	4/5	10/14	1/1	1/2	0/0	0/0	0/1	1/1	-	0/0	22/26
2	4,184-4,210	26/42	9/39	0/6	2/3	2/8	0/33	0/8	0/7	0/2	0/0	1/2	Ank	0/1	5/38
3	5,100-5,121	38/51	14/28	3/4	1/1	5/6	0/0	1/3	2/3	0/0	0/0	1/1	-	0/0	14/24
4	5,572-5,580	25/30	10/18	0/2	0/1	0/1	40/52	1/3	0/0	0/0	0/0	0/1	Ank	0/1	7/9
5	6,370-6,393.3	49/59	12/27	4/13	0/5	0/1	0/6	0/1	0/0	0/0	0/0	1/2	-	0/0	8/17
6	7,160-7,164.2	-/18	-/3	-/1	-/1	-/5	-/1	-/0	-/0	-/0	-/0	-/1	Ank	-/1	-/71
7	7,600-7,626.3	18/25	4/16	1/2	0/1	5/8	0/1	0/1	0/1	0/0	0/1	1/1	Ank	0/1	53/68
8	8,639.3-8,649.8	23/29	8/11	1/2	tr/1	3/6	0/1	0/1	0/0	0/0	0/0	2/3	-	0/0	51/57
9	9,400-9,430.4	25/51	7/17	0/4	0/1	4/10	0/7	0/1	0/1	0/0	0/0	1/3	Ank	0/1	24/53
10	9,656-9,686.2	1/34	6/33	0/3	0/2	2/7	0/33	0/1	0/1	0/0	0/0	<1/2	Hem	0/<1	51/61
11	9,948-9,987	8/32	5/25	0/3	tr/1	5/28	0/9	0/<1	0/1	0/0	0/1	0/1	-	0/0	37/64
12	10,979-11,016	11/21	4/5	0/<1	0/1	2/5	<1/80	0/<1	0/0	0/0	0/0	1/2	Ank	0/1	1/68
13	11,707-11,737	20/30	5/7	<1/1	<1/<1	4/5	0/1	<1/<1	0/0	0/0	0/0	1/1	-	0/0	55/68
14	12,709-12,748	0/19	0/2	0/<1	0/<1	0/9	<1/100	0/<1	0/0	0/0	0/0	0/<1	-	0/0	0/76
15	12,850-12,880	14/28	3/9	0/<1	<1/1	0/2	0/8	0/<1	0/1	0/1	0/0	1/1	-	0/0	56/81
16	13,141-13,158	5/8	21/26	1/3	0/0	0/1	0/0	0/<1	0/0	0/0	0/0	0/1	-	0/0	61/69
17S	13,876-13,904	18/28	2/14	0/<1	<1/1	0/1	1/14	0/<1	0/0	0/<1	0/0	0/<1	Heul	0/<1	54/77
17I	13,876-13,904	6/12	2/19	0/<1	0/3	1/6	8/30	0/<1	0/0	0/<1	0/0	0/<1	Heul	0/1	55/60
18S	14,575-14,607	13/28	4/27	0/5	0/2	0/2	0/17	0/1	0/2	0/0	0/2	<1/2	Hem	0/<1	41/78
18I	14,575-14,607	0/3	31/69	1/4	0/1	0/2	0/19	0/2	0/2	0/0	0/2	0/2	Hem	0/<1	19/59
19	15,500-15,509	9/15	9/29	0/<1	1/1	2/3	1/37	0/<1	0/<1	0/0	0/0	0/1	-	0/0	21/73
20S	16,313-16,343	20/22	12/12	6/7	1/1	2/5	0/0	1/1	0/0	0/0	0/0	1/1	Fa	0/0	54/56
20I	16,313-16,343	4/21	11/28	5/23	0/3	0/1	0/11	0/0	0/0	0/0	0/100	0/1	Fa	0/14	24/55

Abbreviations: Qtz, quartz; Plag, plagioclase feldspar; K-spar, potassium feldspar; Sid, siderite; Pyr, pyrite; Cal, calcite; Hbl, hornblende; Clino, clinoptilolite; Anlc, analcite; L/L, laumontite/leonhardite; Ill, illite; Ank, ankerite; Hem, hematite; heul, heulandite; Fa, fluorapatite; S, sedimentary; I, igneous; tr, trace (detectable but not measurable).

Table 4. X-ray diffraction data from conventional cores, ranges of values for the fraction finer than 5 microns. From AGAT Consultants, Inc.

Core No.	Depth (Feet)	Less than 5 Micron Grain-Size Fraction (Percent)						
		Chl	Kaol	Ill	ML	Smec	C-S	C-V
1	3,627-3,657	22/24	12/13	19/23	43/44	0/0	0/0	0/0
2	4,184-4,210	12/21	6/10	6/21	0/72	0/76	0/0	0/0
3	5,100-5,121	20/29	0/0	11/13	0/68	0/67	0/0	0/0
4	5,572-5,580	21/31	0/0	20/27	47/52	0/0	0/0	0/0
5	6,370-6,393.3	27/62	0/0	8/13	30/60	0/0	0/0	0/0
6	7,160-7,164.2	-/16	-/5	-/12	-/0	-/67	-/0	0/0
7	7,600-7,626.3	10/25	3/9	5/10	0/0	59/76	0/0	0/0
8	8,639.3-8,649.8	25/40	0/13	6/11	0/0	50/56	0/0	0/0
9	9,400-9,430.4	27/36	6/10	10/14	0/0	43/55	0/0	0/0
10	9,656-9,686.2	7/34	0/13	0/14	0/0	45/88	0/tr	0/0
11	9,948-9,987	27/42	0/14	7/19	34/54	0/0	0/0	0/0
12	10,979-11,016	28/51	0/20	23/27	25/25	0/0	0/0	0/0
13	11,707-11,737	22/42	6/26	0/0	0/39	0/72	0/0	0/0
14	12,709-12,748	0/48	0/12	13/18	37/85	0/0	0/0	0/0
15	12,850-12,880	10/56	13/58	1/12	12/61	0/0	0/18	0/0
16	13,141-13,158	64/84	0/tr	tr/2	16/36	0/0	0/tr	0/0
17S	13,876-13,904	12/22	10/44	0/3	19/74	0/0	0/29	0/0
17I	13,876-13,904	7/15	51/65	tr/1	9/42	0/0	tr/16	0/0
18S	14,575-14,607	19/65	0/9	11/61	0/40	0/0	0/0	0/15
18I	14,575-14,607	40/91	0/0	0/3	0/0	0/0	0/0	9/60
19	15,500-15,509	53/81	0/0	5/25	14/22	0/0	0/0	0/0
20S	16,313-16,343	49/60	0/0	24/41	10/16	0/0	0/0	0/0
20I	16,313-16,343	62/78	0/0	17/26	5/14	0/0	0/0	0/0

Abbreviations: Chl, chlorite; Kaol, kaolinite; Ill, illite; ML, mixed-layer clays (commonly illite and smectite); Smec, smectite; C-S, mixed-layer chlorite and smectite; C-V, mixed-layer chlorite and vermiculite; S, sedimentary; I, igneous; tr, trace (detectable but not measurable).

Table 5. Summary of petrographic data. Modified from AGAT Consultants, Inc.

Zone	Zone Depth (feet)	Number of Samples	Major Lithologies	Average Q/F/L of Framework Fraction	Average V/M/S and Major Lithic Components
A-1 and A-2	1,536-3,860	11	Sandy diatomaceous mudstone and diatomaceous ooze	28/29/43	75/23/2 V-RF M-Mica; RF S-chert (silicified volcanic); R.F.
B	3,860-5,010	25	Poorly to well sorted, very fine sandstone, muddy sandstone, and calcitic sandstone	45/15/40	68/16/16 Components as above
C-1 and C-2	5,010-7,130	51	Poorly to well sorted, very fine to fine sandstone, muddy sandstone and calcitic sandstone; mudstone	37/22/38	62/20/18 Components as above
D-1 and D-2	7,130-10,800	103	Mudstone, sandy mudstone, and claystone; siltstone	47/19/34	53/30/15 Components as above
E	10,800-12,280	22	Claystone	44/18/37	63/23/13 Components as above
F	12,280-12,780	11	Claystone	14/56/30	-
G	12,780-13,000	12	Poorly sorted, muddy, very fine sandstone; siltstone, mudstone	32/19/49	62/24/14 Components as above
H	13,000-15,300	38	Moderately sorted fine to coarse sandstone; mudstone; claystone; coal	30/12/58	51/11/38 Components as above
I	15,300-16,400	11	Mudstone; sandy mudstone	17/27/56	

Abbreviations: Q, quartz; F, feldspar; L, lithic fragments; V, volcanic; M, metamorphic; S, sedimentary; RF, rock fragments

Table 6. Summary of reservoir characteristics. Modified from AGAT Consultants, Inc.

Zone	Zone Depth (feet)	Number of Samples	Visible Porosity (percent)	Total Pore Fillers (percent)	Measured Porosity* (percent)	Measured Permeability* (mD)	Reservoir Potential	Major Mechanism of Porosity Reduction
A-1 and A-2	1,536-3,860	11	2.0-8.0	56.0-84.4	48.8-50.7	3.88-6.15	Very poor to poor	Abundant detrital matrix
B	3,860-5,010	25	1.2-19.1	18.4-65.2	7.7-35.5	0.02-118.0	Nonreservoir to good	Abundant detrital matrix; local calcite cement
C-1 and C-2	5,010-7,130	51	0-22.0	6.8-85.2	6.0-34.0	0.02-117.0	Nonreservoir to good	Detrital matrix; local calcite cement; authigenic clay and zeolites
D-1 and D-2	7,130-10,800	103	0-9.6	25.2-95.0	8.8-23.1	0.01-25	Nonreservoir to very poor	Abundant detrital matrix; authigenic chert and local calcite cement
E	10,800-12,280	22	0-0.4	56.4-95.0	11.4-16.9	0.02-0.33	Nonreservoir to extremely poor	Abundant detrital matrix; authigenic chert and local calcite
F	12,280-12,780	11	0	78.0-96.8	2.2-12.9	0.02	Nonreservoir	Abundant detrital matrix; authigenic chert and local calcite
G	12,780-13,000	12	0-4.4	38.8-82.8	11.8-14.1	0.03-1.97	Nonreservoir to very poor	Abundant detrital clay; pseudomatrix; authigenic chert, clay, and local calcite
H	13,000-15,300	38	0-1.6	13.6-100.0	4.0-17.4	0.01-0.19	Nonreservoir	Abundant detrital clay; pseudomatrix; authigenic clay, chert, and calcite
I	15,300-16,400	11	0	63.2-96.4	2.4-9.8	0.02-0.29	Nonreservoir	Abundant detrital clay; authigenic chert and local calcite

\* Values are from conventional cores only.

VELOCITY ANALYSIS IN  
RELATION TO TIME-DEPTH CONVERSION  
by  
David A. Steffy

Velocity characteristics of the Navarin Basin COST No. 1 well were identified and analyzed to obtain the proper time-depth conversion for seismic reflection data and to aid in the evaluation of mappable seismic sequences. The analysis was performed using Long-Spaced Sonic (LSS) well logs and stacking velocity spectra displays generated from nearby seismic reflection data. The results of the velocity analysis were integrated throughout the COST well report in sections dealing with seismic stratigraphy, paleontology, and lithology. All depths given in this chapter are measured from sea level. Well log and other subsurface depths which were measured from the Kelly Bushing can be adjusted to sea level by subtracting 85 feet.

WELL SITE VELOCITY

Proper conversion of two-way travel time to depth depends on accurate velocity information. Velocities derived from seismic spectra displays are influenced by geologic and nongeologic influences. Geologic influences are the heterogeneous nature of the geologic medium and the local structural setting (dip). Nongeologic influences include quality of seismic data, accuracy of subjective stacking-velocity picks, inherent inaccuracy of assumptions in the Dix equation, and instrument configuration. Well site velocity data provide an objective check for root mean square (RMS) velocities derived from seismic reflection techniques.

RMS velocity, average velocity, interval velocity, and a time-depth curve were calculated by using the LSS log (2 inch) from the well. These velocities and a time-depth curve were also calculated from seismic reflection data from nearby lines using the Dix equations (Dix, 1955). Both direct and indirect quantitative comparisons were made between similar velocity functions. The indirect comparisons included calculating subsurface heterogeneity and velocity anisotropy factors.

Figure 36 displays the time-depth curves calculated from integrated LSS log and seismic reflection data. The curves indicate that a steeper velocity gradient is calculated from

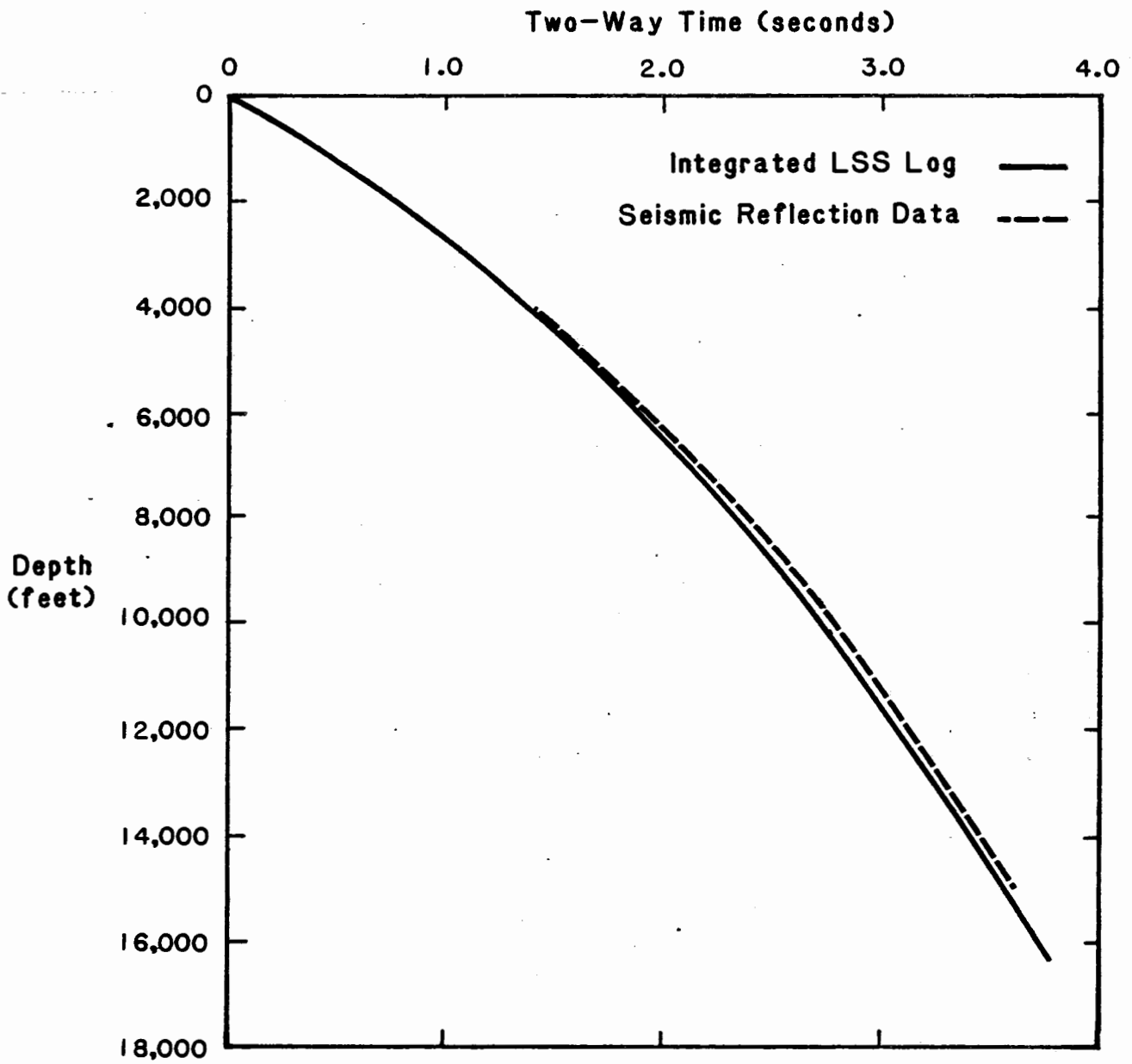


**FIGURE 36.** COMPARISON BETWEEN TIME-DEPTH CURVES GENERATED FROM AN INTEGRATED LONG-SPACED SONIC (LSS) LOG AND FROM SEISMIC REFLECTION DATA.

LSS log data. From sea bottom to 11,050 feet, the curves diverge to a maximum cumulative difference of 120 milliseconds. From 11,050 to 14,950 feet (base of usable seismic reflection data), the curves gradually converge. The 120-millisecond difference between the two methods represents a 4 percent error with respect to the LSS log curve. RMS and interval velocities were evaluated to determine the source of this deviation.

The maximum coherency stacking (MCS) velocities as defined by Al-Chalabi (1979) were picked from 22 velocity spectra displays along a 1978 Western Geophysical Company (WGC) line that profiles within 10 miles of the well site. These MCS velocities were picked at mappable seismic sequence boundaries, major internal reflectors, and major velocity changes. For each display, a linear interpolation was made every 10 milliseconds between the picked MCS velocities. An average interpolated value was then calculated for all 22 displays. Because of dispute over its proprietary term, the check-shot survey was not released. Instead, the integrated sonic log was used. Well log RMS velocities (fig. 37) were calculated from the integrated sonic data by using Dix's equation.

The well log RMS velocities are comparable to stacking velocities from the WGC line. Overall, the velocities calculated by these two methods are in agreement. However, from sea level to 3,800 feet and from 4,800 to 14,950 feet (base of usable stacking data), well log RMS velocities are greater than interpolated stacking velocities (fig. 37). The upper divergence reaches a maximum of 200 feet/second at 1,850 feet. The lower divergence is cumulative to a maximum of 240 feet/second at 7,000 feet. Thereafter, the difference is constant to the acoustic basement at 12,850 feet. Below the acoustic basement, the difference diminishes with depth. The velocity differences represent a 4 percent error with respect to the well log RMS velocities. The diverging trends could reflect either geological variations at the well site or minor inaccuracies in the assumptions that equate stacking velocities to true RMS values.

Many of the geometric and nongeometric differences between stacking velocities and check-shot velocities discussed by Anstey (1977) are relevant. These survey differences may have generated the velocity discrepancies described earlier. The integrated sonic log measures an essentially short vertical path at the well with little absorption, scattering, spherical divergence, or dip and refraction effects. On the other hand, stacking velocity is a function of a long two-dimensional raypath that is influenced by lateral variations in velocity, refraction,

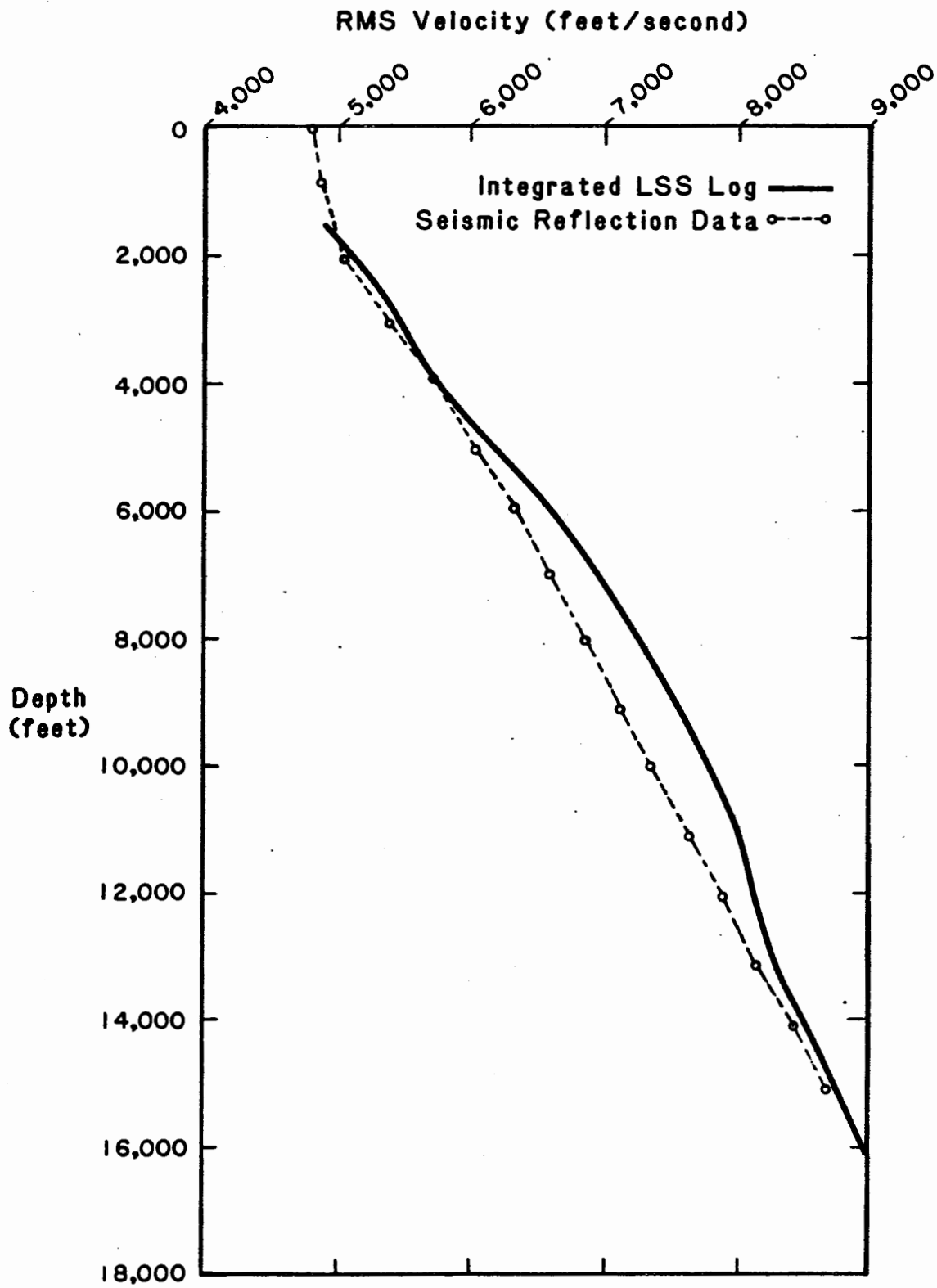


**FIGURE 37.** COMPARISON BETWEEN RMS VELOCITIES CALCULATED FROM AN INTEGRATED LONG-SPACED SONIC (LSS) LOG AND FROM SEISMIC REFLECTION DATA.

and the loss of higher frequencies. The velocity discrepancies found at the well site, however, exhibit trends that are discontinuous with depth, implying more than one cause for error.

In order to delineate the buildup of error in the stacking velocities, a quantitative evaluation was made of the RMS, average, and interval velocities. MCS velocities approximate seismic reflection RMS velocities in an isotropic, one-layered case. The approximation becomes less reliable in complex geologic settings. Al-Chalabi (1974) proposed a heterogeneity factor that reflects the two-dimensional variation of velocity. This factor relates the RMS velocity ( $V_{RMS}$ ) to the average velocity ( $V_A$ ), which is calculated from RMS velocity by using the Dix equation (Dix, 1955). The heterogeneity factor,  $g$ , is defined as:

$$g = (V_{RMS}^2 - V_A^2)/V_A^2$$

In a homogeneous earth  $g$  will equal zero, otherwise it has a positive value and is independent of the order of layering. Figure 38 is a plot of  $g$  versus RMS velocity. Heterogeneity increases nearly linearly with increasing RMS velocity, that is, with increasing depth. At an RMS velocity of 8,700 feet/second (or a depth of 14,950 feet), the heterogeneity factor reaches a maximum of 0.098. The discrepancy between stacking velocity and seismic-reflection-derived RMS velocity is directly proportional to this heterogeneity factor (Al-Chalabi, 1974).

To explain the heterogenetic nature of the rock, Banik (1983) modeled a similar heterogeneous medium (shale) as an anisotropic medium. In the Navarin basin, however, this anisotropy model must be treated as quasi-anisotropy because of the stratification of the basin fill which causes refraction at layer interfaces. Banik's model assumes that a semicircular wavefront traveling through an anisotropic medium is distorted to an elliptical wavefront. The amount of anisotropy is directly proportional to the ratio between the velocity parallel to bedding and the velocity normal to bedding. This ratio also defines the axes of the elliptical wavefront. Levin (1978), Banik (1983), and Byun (1983) estimated the horizontal axis from the interval velocities derived from seismic reflection data ( $V_H$ ), and the vertical axis from the interval velocities derived from the sonic logs ( $V_V$ ). The velocity anisotropy,  $A$ , of a lithologic unit is defined as:

$$A = 100 (V_H - V_V)/V_V$$

By use of this model an anisotropic factor was calculated for nine (A through F) of the eleven lithologic zones discussed in the Well Log Interpretation chapter. These nine sedimentary zones compose the Cenozoic basin fill, most of which is

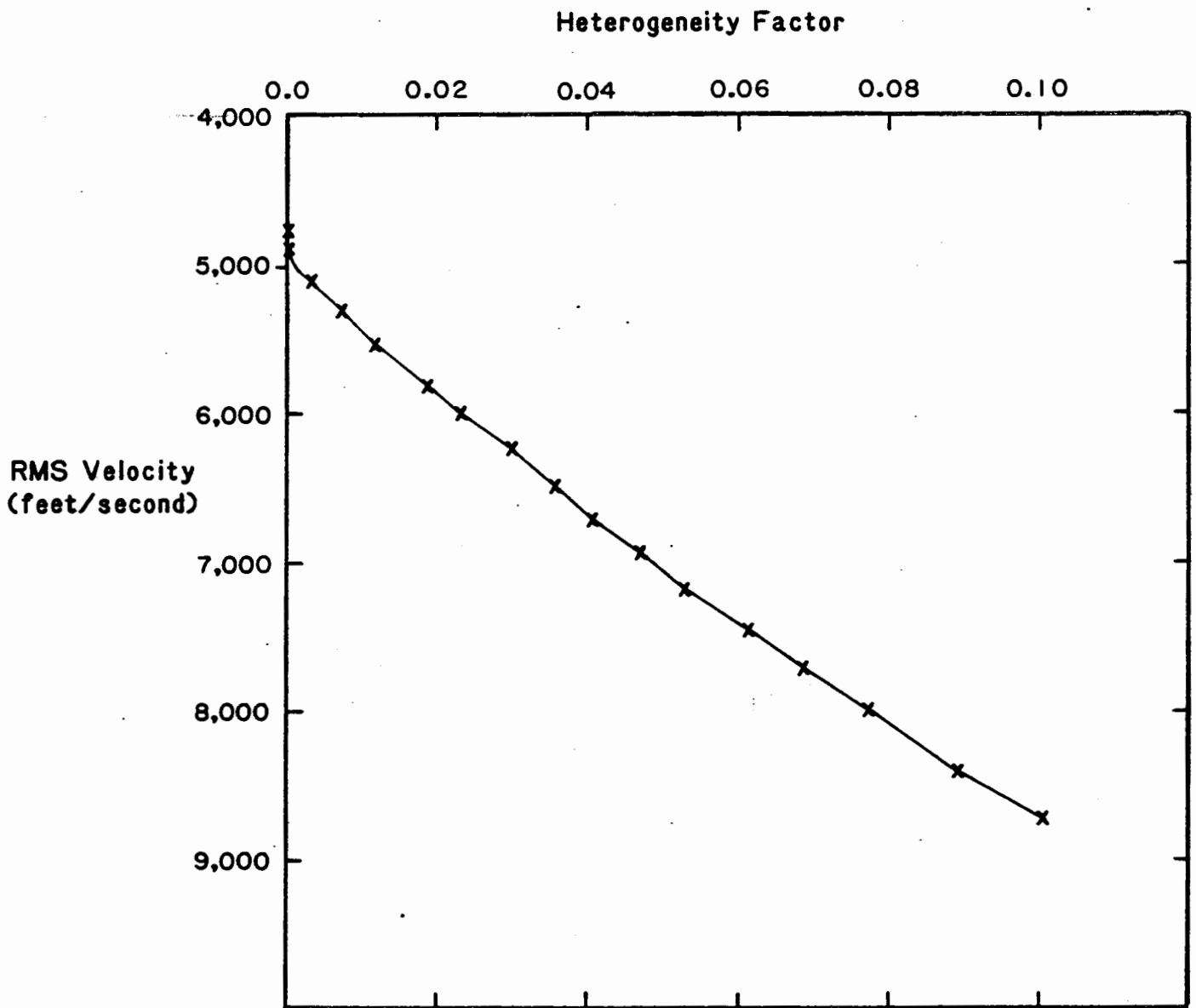


**FIGURE 38. HETEROGENEITY FACTOR VERSUS RMS VELOCITY.**

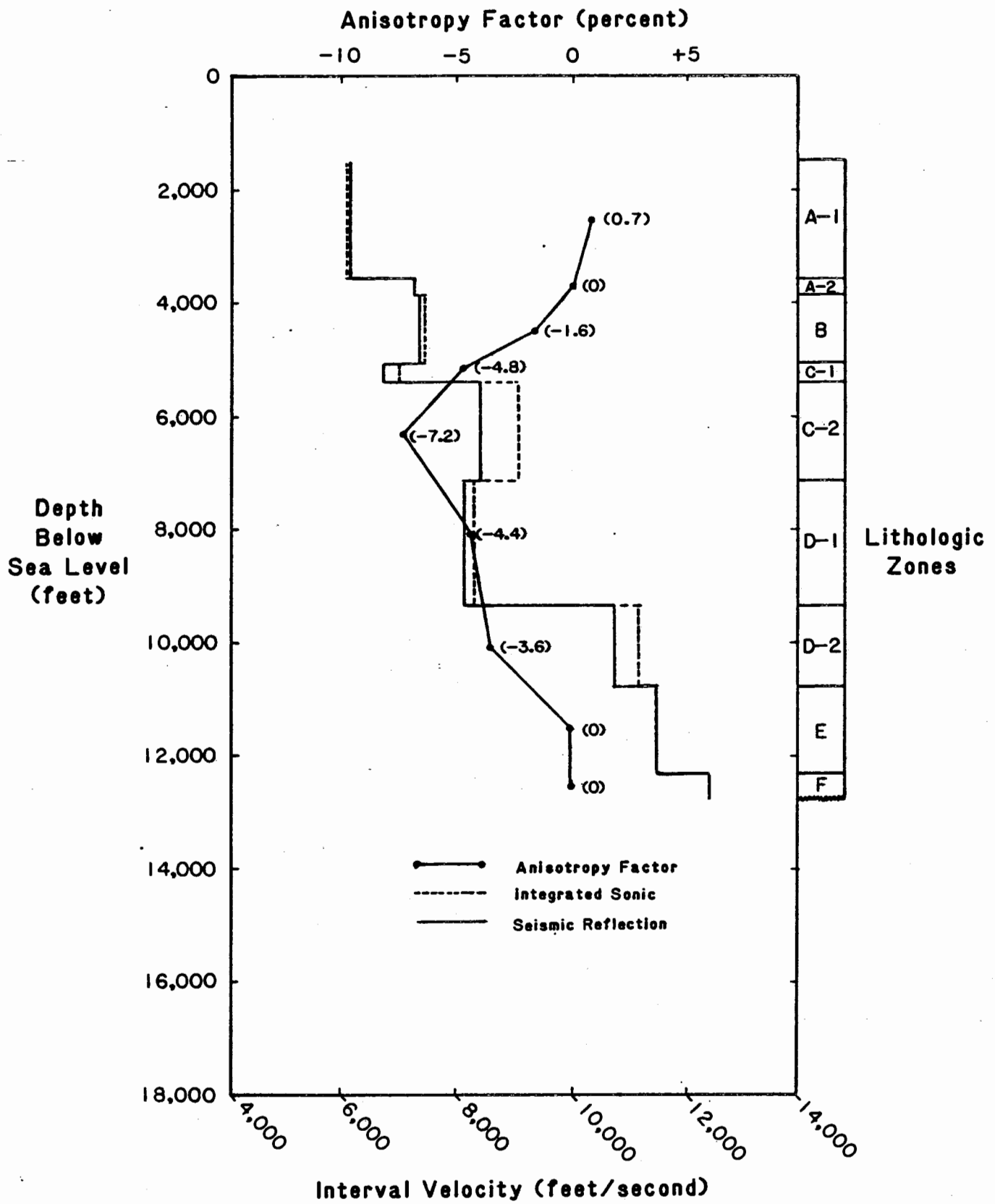


**FIGURE 39. INTERVAL VELOCITIES, ANISOTROPY FACTOR, AND CENOZOIC LITHOLOGIC ZONES.**

thin-bedded mudstone and muddy sandstone. Because the two deepest lithologic zones (G/H and I; Late Cretaceous) lie below the Cenozoic fill and are structurally more complex, the simple anisotropy model used for the Cenozoic is not adequate for this part of the stratigraphic section. Figure 39 displays the lithologic zones, the interval velocities calculated from both seismic reflection and sonic log data, and the calculated anisotropy factor expressed as a percentage. The anisotropy factor is plotted at the midpoint of the corresponding lithologic unit. Throughout the Cenozoic section the anisotropy is near zero or slightly negative. A negative anisotropy indicates an apparent higher vertical interval velocity than horizontal interval velocity.

Al-Chalabi (1979) states that the horizontal velocity may be up to 1.4 times greater than the vertical velocity in flat-lying strata. Banik (1983) found that flat-lying shale beds in the North Sea have a 5 to 40 percent higher horizontal than vertical velocity. In both instances, a positive anisotropic factor would be calculated. The Cenozoic strata in the Navarin well, on the other hand, exhibit an apparent higher vertical velocity (negative anisotropy factor). This conclusion is consistent with the observed difference between well log RMS velocities and stacking velocities, and indicates that the anisotropic model does not explain the velocity discrepancies illustrated in figures 37 and 38. The 4 percent discrepancy between well log and seismic reflection velocities cannot be resolved without further investigation of the effect of nongeologic influences, such as the fundamental assumptions of the Dix equations used to estimate  $V_A$  or the great differences in raypaths between LSS log and seismic reflection techniques.

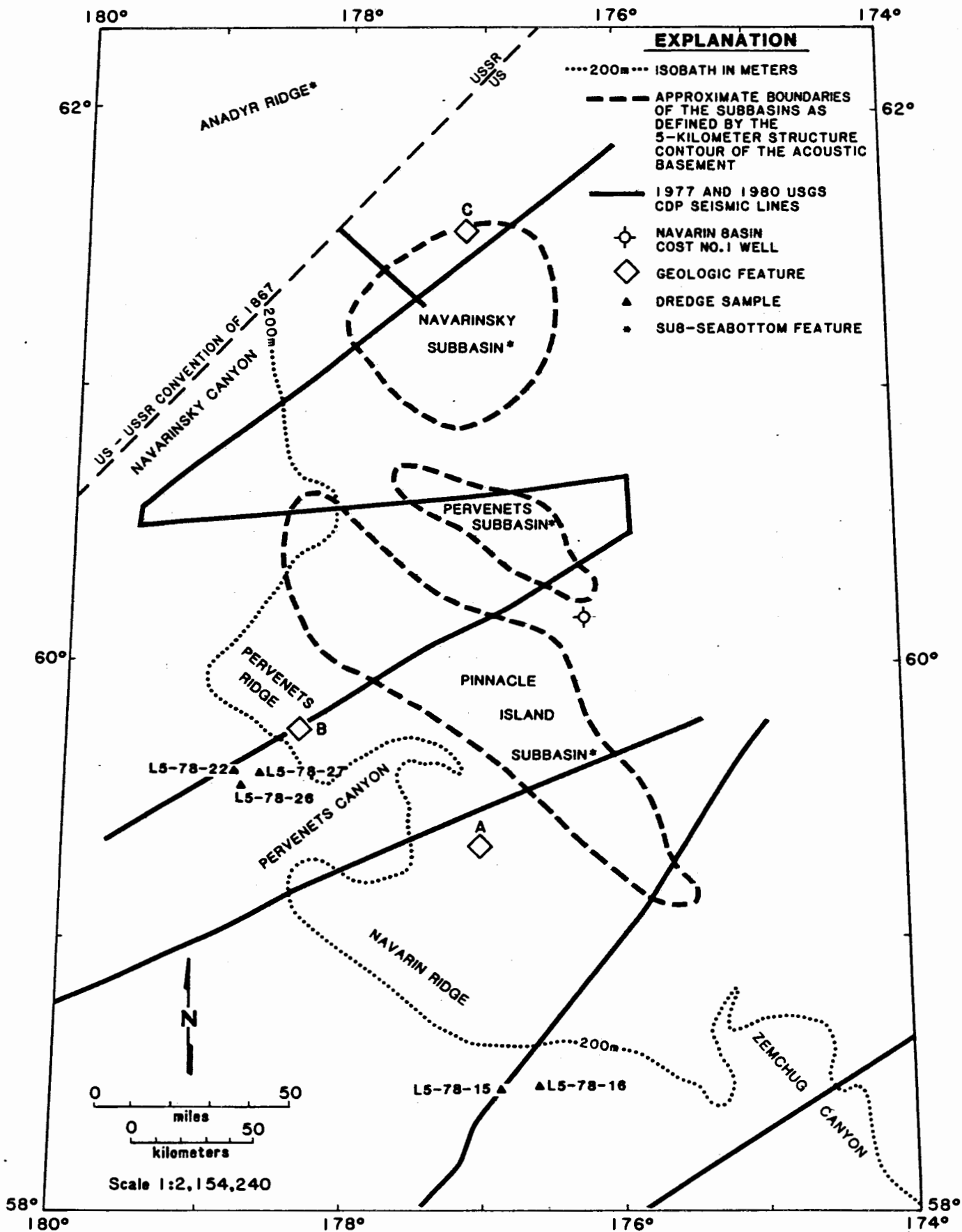


**FIGURE 40.** LOCATION MAP OF THE NAVARIN BASIN, COST NO. 1 WELL, SEISMIC DATA COVERAGE, DREDGE SAMPLES, AND FEATURES OF GEOLOGIC INTEREST. MODIFIED FROM CARLSON AND OTHERS (1983).

## SEISMIC STRATIGRAPHY

by

David A. Steffy

Geologic significance was assigned to individual reflections and seismic sequences seen on common-depth-point (CDP) seismic reflection survey lines that profile the Navarin Basin COST No. 1 well site. These geologic characteristics were then extrapolated from the well to establish a regional, basin-wide geologic setting. Structure-contour maps of three major seismic sequence boundaries were made to depict the configuration of the Navarin Basin, to represent the growth of the basin through time, and to locate potential hydrocarbon source beds and reservoir rocks. Integrating this analysis with information from dredge samples from the nearby continental slope and comparing this to published Navarin Basin-Bering Sea evolutionary models allows a more complete geologic history of the area to be developed.

The Navarin Basin is composed of three structurally distinct subbasins that are here informally named the Navarinsky, Pervenets, and Pinnacle Island subbasins (fig. 40). All depths discussed in this chapter are measured from sea level unless otherwise noted. The Kelly Bushing was 85 feet above sea level, and water depth was 432 feet.

### DATA BASE

Correlation of well information to the CDP seismic reflection survey lines was made in part by using a synthetic seismogram. The seismogram was generated from the Long-Spaced Sonic log (LSS) of the No. 1 well and then correlated to the 1978 Western Geophysical (WG) seismic line NB-11, which profiles the well location. Geological correlations were extrapolated from the well into the basin by tying the WG line to the 1977 and 1980 U.S. Geological Survey (USGS) regional CDP surveys of the Navarin and adjacent Anadyr Basins. The 1976 and 1982 USGS CDP surveys of the area were not incorporated because, although public data, they still have not been released by the USGS. In addition to WG NB-11, Western Geophysical gave the author permission to release part of the 1978 line NB-43 that profiles the continental-shelf-break area (area A, fig. 40). Petty-Ray Geophysical, Inc. (PR), granted permission to release parts of four CDP lines (7410a, 7411, 7415, and 7418), as well as their accompanying magnetic and gravity profiles, collected by a 1974 regional CDP survey of the Navarin Basin. PR 7410a and 7411 profile the shelf break and a diapir field, respectively (areas B and C, fig. 40). PR 7415 and 7418 profile the well site (figs. 41 and 42). Selected dredge samples from the 1977, 1978, 1980, and 1981 USGS surveys of the continental slope were also used. Published analyses of these samples and analyses made by MMS personnel and consulting geoscientists were incorporated.

## SEISMIC REFLECTION CORRELATION

A synthetic seismogram was produced by use of a LSS log of the No. 1 well. The sonic log was visually averaged while being stream-digitized and was measured to the nearest foot in depth and to the nearest microseconds/foot in transit time. This resulted in log samples being taken at irregular intervals. However, the sampling was frequent enough to prevent aliasing in the seismogram. The digitized data were then entered into a computer program that produced a synthetic seismogram without multiples. Constant density is assumed; therefore, density was not incorporated into the calculation of the reflection coefficients. This assumption apparently does not adversely affect the validity of synthetic seismograms from simple geologic settings (Sheriff, 1978). The computer program also assumes that the strata are horizontal and have a constant elastic modulus. The incident waves are assumed to be normal to the reflecting surface and have planar wavefronts. The calculated reflection coefficients were then convolved with a standard Ricker wavelet having a frequency range of 8 to 55 Hertz. This convolution results in a seismogram that is displayed with both normal and reverse polarity.

Figure 43 displays the LSS logs, the calculated reflection coefficients, the resulting synthetic seismograms, and WG CDP seismic line NB-11. To illustrate the correlation, figure 44 displays the seismic line, a geologic column (see Well Log Interpretation chapter), and a time-stratigraphic column (see Paleontology and Biostratigraphy chapter). A comparison of the seismogram having normal polarity with the seismic reflection profile reveals a moderately good correlation of reflections. Between 0.6 and 1.0 seconds, several continuous reflections appear on the CDP profile that do not appear on the synthetic seismogram. These continuous reflections are probably sea-floor multiples or interbed multiples which the seismogram did not generate. The internal reflections of seismic sequence II and its bounding reflections (horizons A and B) correlate well with the synthetic seismogram. The large impedance contrasts and resulting reflections of the individual sandy layers in sequence II are discernible events recognized on the seismogram. The correlation between the seismogram and the seismic profile is generally poorer from horizon B down to the base of the Tertiary fill (horizon D). Seismic sequences III and IV in this section are dominantly mudstones. On CDP seismic profiles, reflections from a thick sequence of mudstone are discontinuous and variable in amplitude. Their generation could be due to constructive interference and subtle acoustic changes that would not be recognized by this simple synthetic seismogram program. The Late Cretaceous section below horizon D produces unmappable, discontinuous, large-amplitude reflections that are somewhat correlative with the synthetic seismogram.

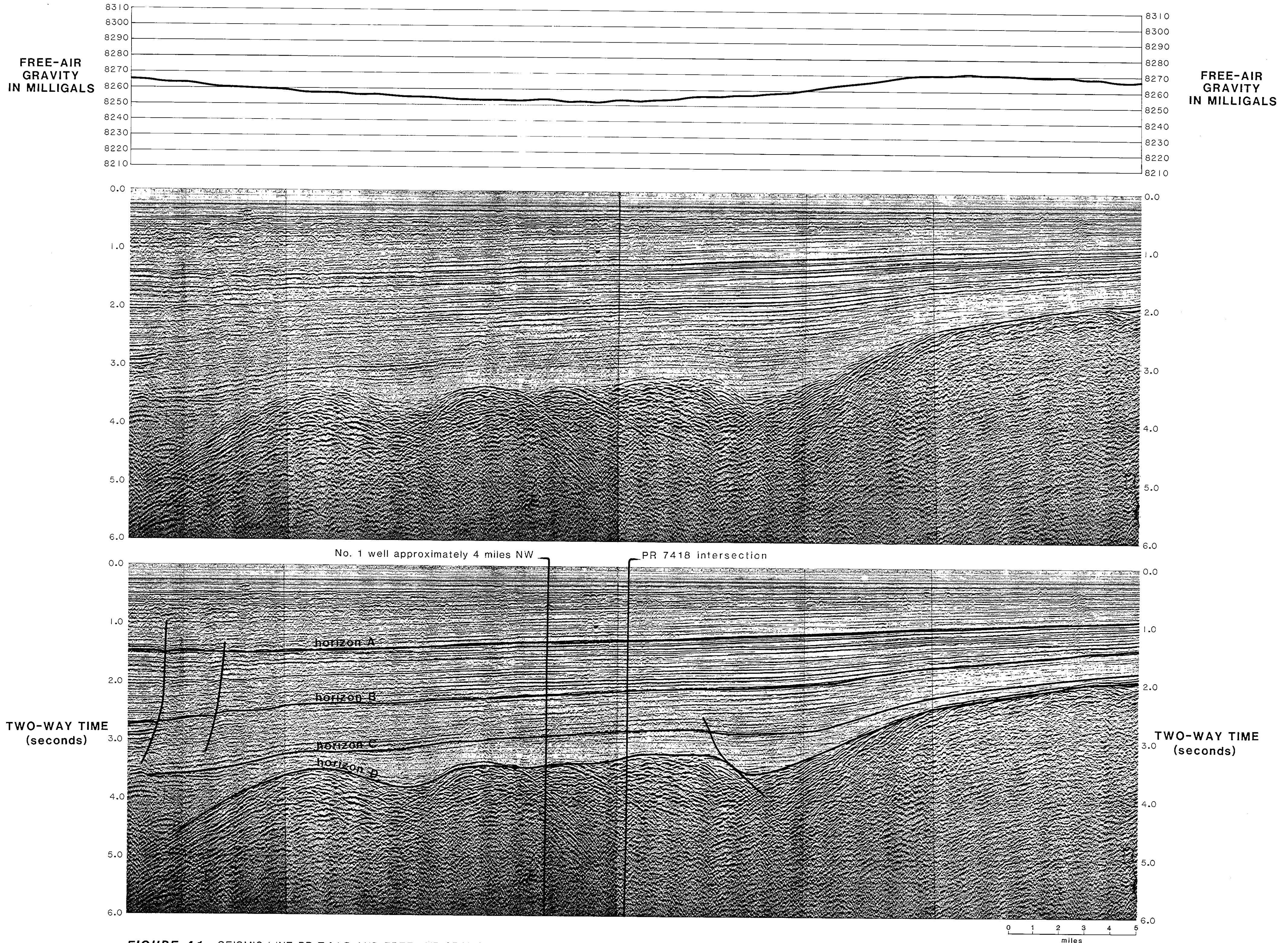
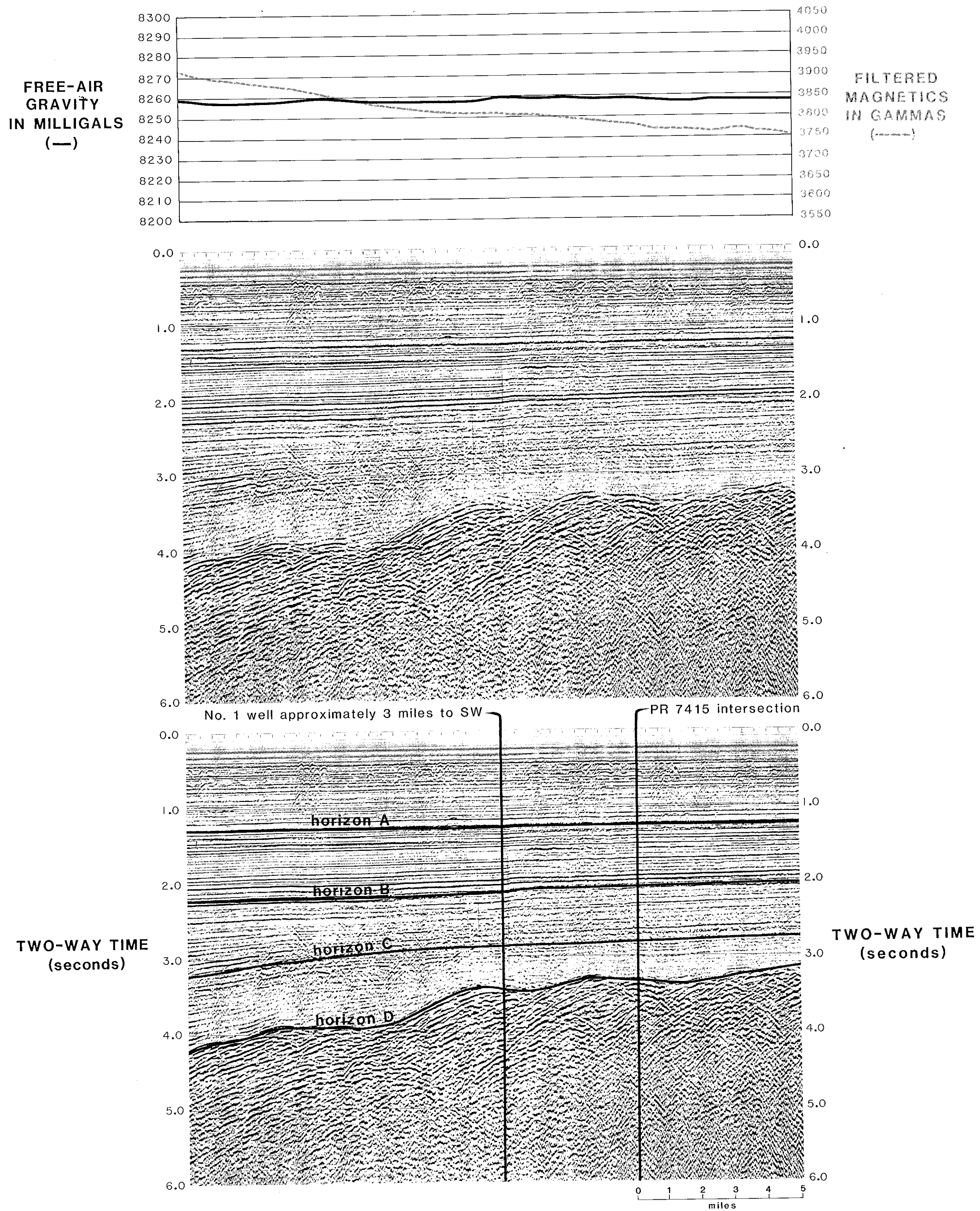


FIGURE 41. SEISMIC LINE PR 7415 AND FREE-AIR GRAVITY PROFILE.



**FIGURE 42.** SEISMIC LINE PR 7418, FREE-AIR GRAVITY PROFILE, AND FILTERED MAGNETICS PROFILE.

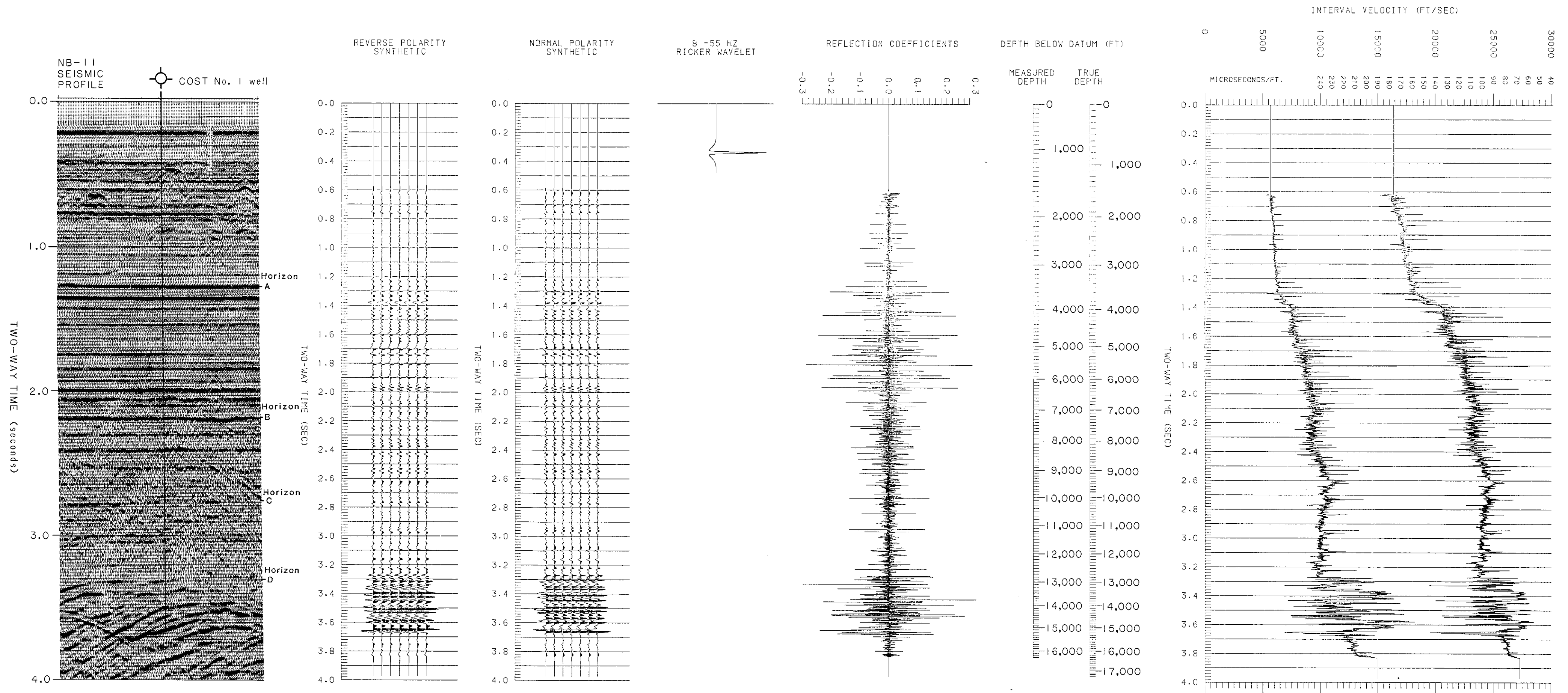


FIGURE 43. SYNTHETIC SEISMOGRAM OF THE NAVARIN BASIN COST NO. 1 WELL AND SEISMIC REFLECTION PROFILE.

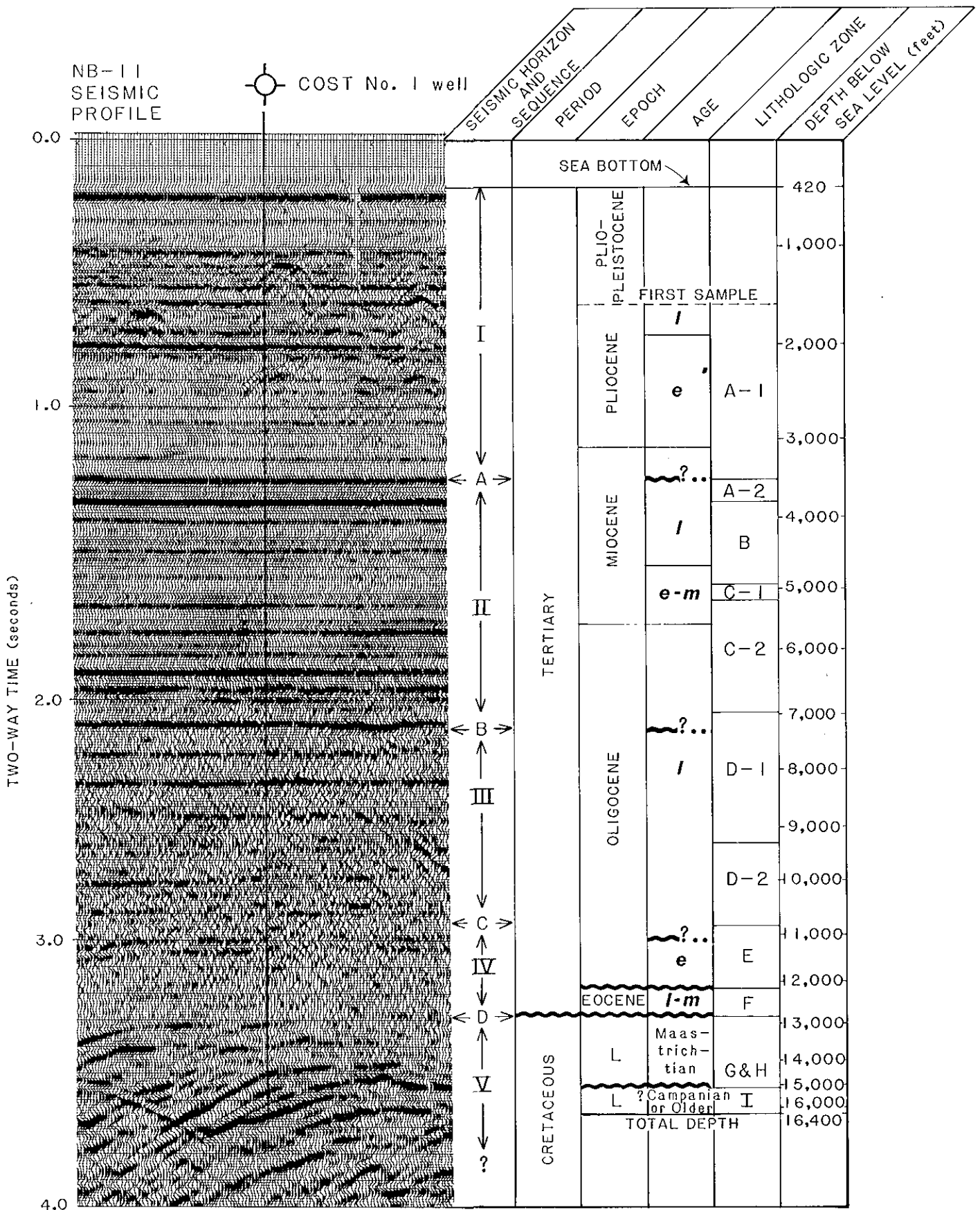


FIGURE 44. SEISMIC SEQUENCES AND HORIZONS, TIME-STRATIGRAPHIC COLUMN, LITHOLOGIC COLUMN, AND SEISMIC REFLECTION PROFILE OF THE NAVARIN BASIN COST NO. 1 WELL. (BASIN FLANK UNCONFORMITIES ARE INDICATED BY QUESTION MARKS).

## SEISMIC SEQUENCE ANALYSIS

Seismic sequence analysis of the CDP seismic reflection data reveals at least five regional depositional sequences (I through V). The upper four Tertiary sequences are composed of genetically related facies or depositional systems bounded by unconformities or by their correlative conformities (horizons A through D). Sequence V, the acoustic basement, is a structurally complex series of marine and nonmarine Mesozoic rocks. Figure 44 displays these sequences on a CDP seismic profile of the No. 1 well adjacent to time-stratigraphic divisions and lithologic zones. Other depositional sequences were identified locally, but limited nonproprietary seismic coverage prevented the mapping of their lateral extent or the determination of their stratigraphic significance.

### Seismic Sequence I

Sequence I is characterized by a zone of flat-lying, parallel, continuous reflections that are found throughout the basin (fig. 44). These reflections exhibit subtle divergences toward subbasin centers and onlap the continental sides. Sequence I is bounded by the sea bottom and horizon A. Horizon A occurs at 1.28 seconds (or about 3,560 feet below sea level) at the No. 1 well site. This horizon is defined by a continuous, large-amplitude, positive reflection that becomes discontinuous and variable in amplitude as the reflector becomes shallower toward the basin flanks. At the well, the reflections above and below horizon A are concordant, and they remain concordant throughout much of the basin. In the northwest area of the basin, however, horizon A becomes an angular unconformity between the overlying concordant reflections and the underlying truncated reflections of seismic sequence II (fig. 45). This erosional truncation is caused by the intrusion of shale diapirs and the associated uplift and erosion of sequence II strata.

Horizon A coincides with the boundary between lithologic Zones A-1 and A-2 and with a possible late Miocene unconformity. At the well, horizon A probably results from constructive interference between a chronostratigraphic surface and a diagenetic boundary. The absence of a lithologic break or any of the well log characteristics normally indicative of a disconformity suggests that at the well the reflection represents, at most, a depositional hiatus.

Diffractions are common in sequence I between 0.4 to 1.0 seconds (or about 950 to 2,700 feet below sea level). These diffractions are more prevalent in the southern two subbasins than in the northernmost subbasin. Probable sources for these diffractions are segments along the continuous reflections

that have increased in amplitude. Thin (usually less than 10 feet), highly indurated lenses of secondary carbonate minerals in the mudstone probably caused the diffractions. Reflections that lie between the diffractions and above horizon A are disrupted or disappear.

Seismic sequence I brackets lithologic Zone A-1 and the unsampled material above 1,500 feet. Lithologic Zone A-1 is composed of diatomaceous mudstone and diatomite. It is distinct from Zone A-2, which has undergone diagenesis and cementation. Dredge samples from the Navarin continental slope indicate that the time-stratigraphic equivalents of lithologic Zone A-1 are early to late Pliocene diatomaceous mudstone and volcanic sandstone, and late Miocene diatomaceous mudstone and diatomaceous limestone. The unsampled section above 1,500 feet contains Plio-Pleistocene and Holocene material. Dredge hauls from the lower part of the Navarin continental slope collected sandy and muddy limestone, conglomeratic sandstone, and muds of Pleistocene and Holocene age. The similarities between well and dredge samples indicate relatively uniform, regional deposition.

A structure-contour map of horizon A (fig. 46) was made with available Government and industry CDP seismic reflection data. Because of the paucity of data, only a general surface trend is depicted. The sedimentary accumulation represented by seismic sequence I appears to have been uniform in that the effects of subsidence and deposition in the Navarinsky and Pervenets subbasins are not distinct. The average thickness is 3,200 feet (1 kilometer) throughout the Navarin Basin, with a maximum thickness of more than 4,900 feet (1.5 kilometers) in the center of the Pinnacle Island subbasin. Although Mesozoic basement highs along the continental shelf break apparently remained as positive tectonic features throughout most of Tertiary time, sequence I extends beyond these structurally controlled subbasins. This probably indicates a regional subsidence in response to crustal cooling during Neogene time.

#### Seismic Sequence II

Sequence II is bounded by horizons A and B (fig. 44). At the well, horizon A occurs at 1.28 seconds (or about 3,560 feet below sea level) and horizon B occurs at 2.20 seconds (or about 7,400 feet below sea level). The characteristics of horizon A are described above. At the well, and throughout most of the Navarin Basin, horizon B is a continuous, large-amplitude reflection that separates the concordant, parallel, continuous, large-amplitude reflections of seismic sequence II from the concordant, parallel, discontinuous, variable-amplitude reflections of seismic sequence III. Along the shelf break, horizon B represents a late Oligocene lowering of sea

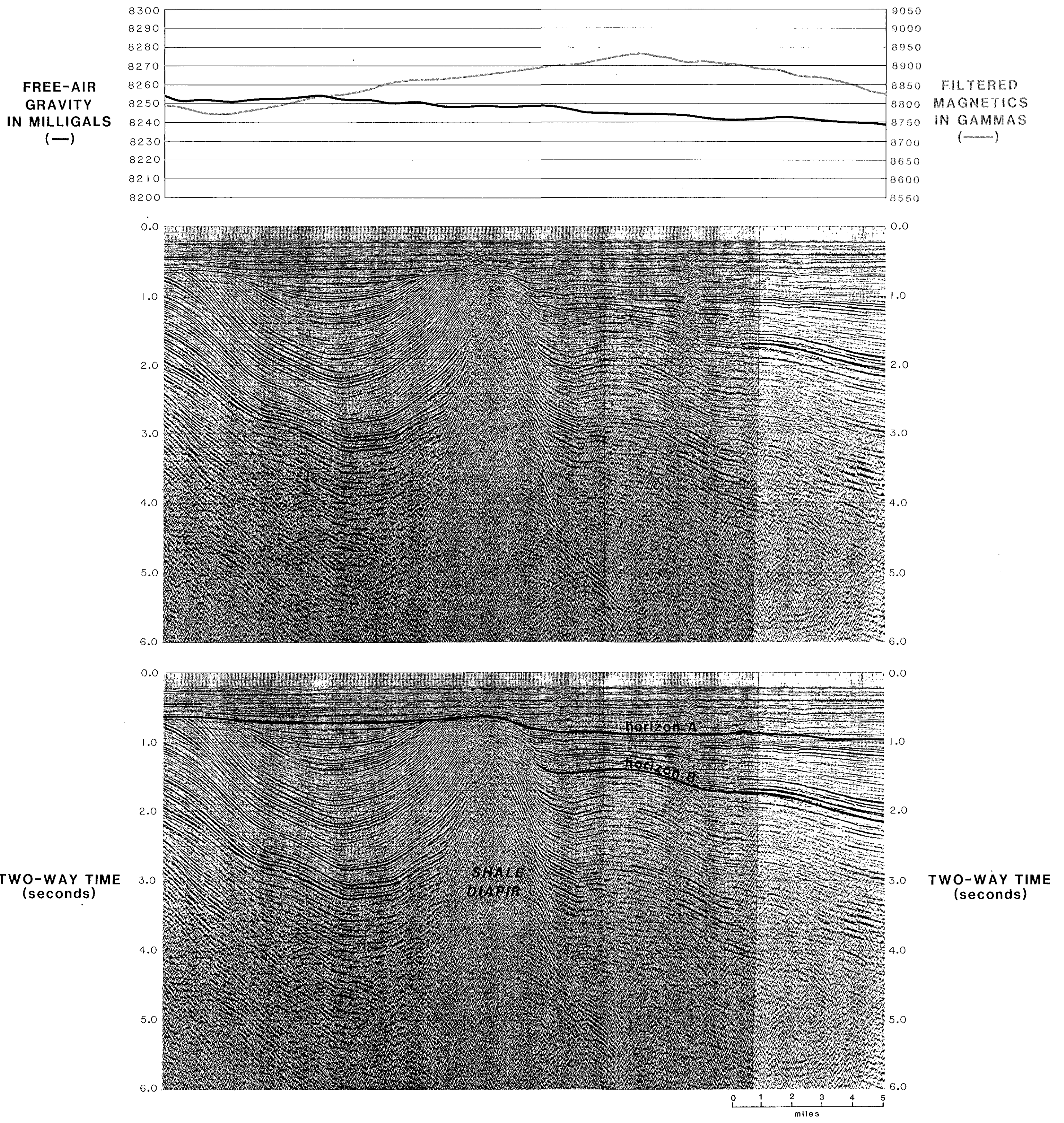
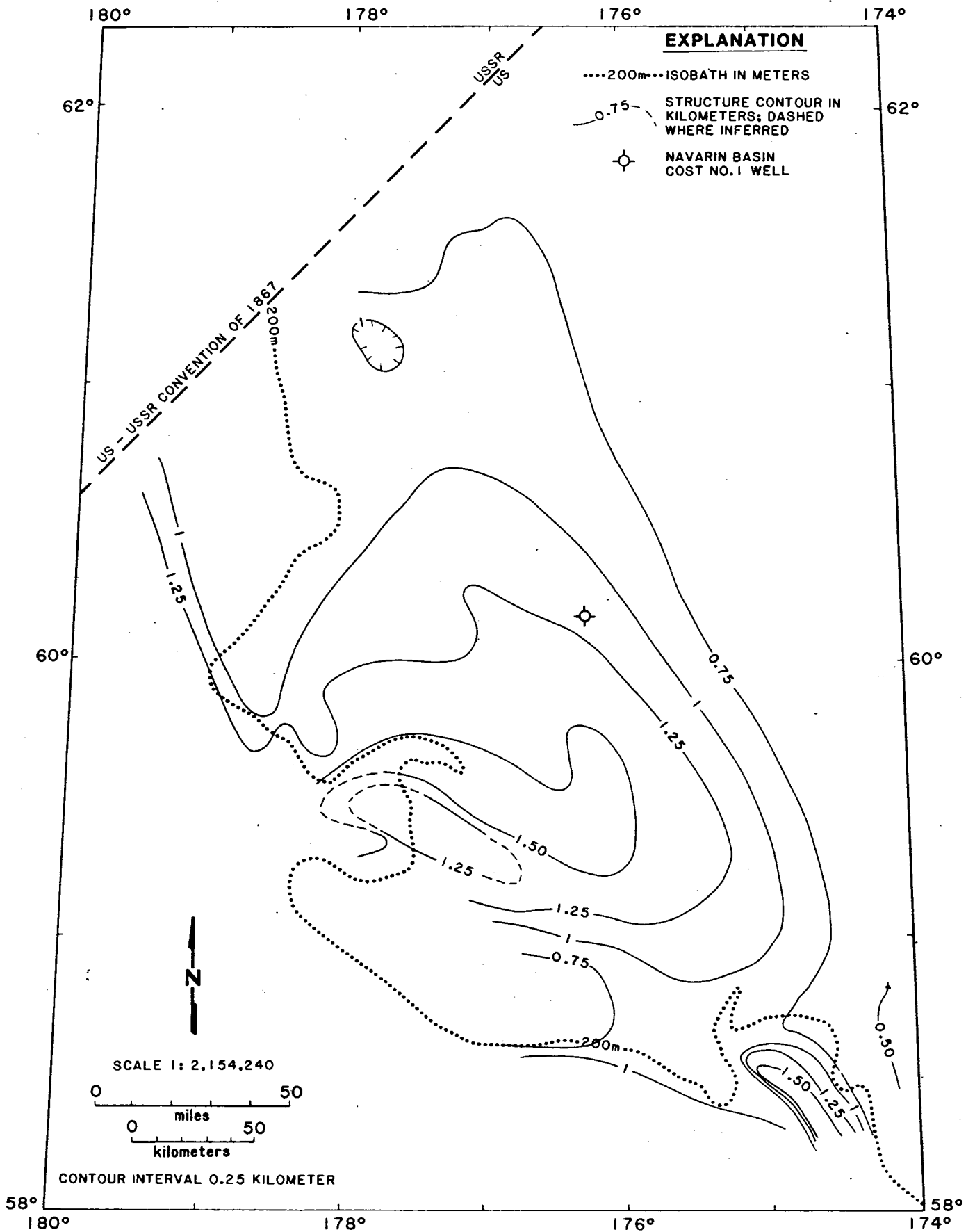


FIGURE 45. SEISMIC LINE PR 7410a, FREE-AIR GRAVITY PROFILE, AND FILTERED MAGNETICS PROFILE.



**FIGURE 46.** STRUCTURE-CONTOUR MAP OF A LATE MIOCENE UNCONFORMITY (HORIZON A) IN THE NAVARIN BASIN.

level (a regressive event) that subjected older Tertiary strata and Mesozoic basement rock to wave-base erosion; but in the subbasins, it represents, at most, a depositional hiatus.

Stratal surfaces of sequence II onlap the Mesozoic basement ridges of the Navarin Basin (fig. 47). In the northern Navarinsky subbasin these stratal surfaces were uplifted and intruded by shale diapirs (fig. 45). The uplifted stratal surfaces were also truncated by the late Miocene unconformity, horizon A. Where sequence II is not affected by postdepositional tectonism, its stratal surfaces exhibit a subtle divergence toward the subbasin centers, which suggests uninterrupted sedimentation.

At the No. 1 well, seismic sequence II is correlated to lithologic Zones A-2, B, C-1, and C-2. Zone A-2 represents a thin transitional layer of increasing diagenesis and cementation of Zone A-1 type rock. Zones B, C-1, and C-2 are muddy sandstones that represent continuous deposition from late Oligocene to late Miocene time. Horizon B separates the inner to middle shelf deposits of sequence II from the upper bathyal mudstones and siltstones of sequence III. Dredge samples from the Navarin continental slope indicate that the time-stratigraphic equivalents of the undifferentiated lithologic Zones B, C-1, and C-2 are middle Miocene diatomaceous, tuffaceous mudstones, clayey limestones, and diatomaceous sandstone; early Miocene calcareous diatomites, sandstones, and tuffaceous mudstones; and late Oligocene tuffaceous sandstones and mudstones.

CDP seismic reflection data indicate laterally continuous bedding and vertically continuous deposition within seismic sequence II. Sequence II sedimentary deposits were the first to extend beyond the structurally controlled limits of all of the subbasins, and probably linked the marine depositional environments of the area. A structure-contour map of horizon B displays the general trends (fig. 48). The figure also shows the erosional truncation of Mesozoic basement highs by horizon B to a common base level. The geometry of horizon B as deep as the 2.0-kilometer (6,560-foot) structure contour indicates regional subsidence in response to crustal cooling. The Pinnacle Island and Pervenets subbasins were the sites of local sediment accumulation. The Pinnacle Island subbasin deepens to more than 11,500 feet (3.5 kilometers), and the Pervenets subbasin deepens to slightly more than 8,000 feet (2.5 kilometers). Sequence II is transitional from local accumulation in subbasins controlled by tectonic movement to regional subsidence and uniform deposition between subbasins.

### Seismic Sequence III

Sequence III is bounded by horizons B and C (fig. 44). At the well, horizon B occurs at 2.20 seconds (or about 7,400 feet below sea level), and horizon C occurs at 2.94 seconds (or about 11,000 feet below sea level). The characteristics of horizon B are described above. At the well and on most of the basin flanks, horizon C is an indistinct, discontinuous, variable-amplitude reflection. In the deeper part of the subbasins, however, horizon C is a distinct seismic sequence boundary recognized as a continuous, large-amplitude reflection. Along the shelf break, horizon C represents a regressive event that truncated older Tertiary and Mesozoic rocks. In the center of the subbasins and at the No. 1 well, it represents at most a depositional hiatus. Sequence III is a zone of discontinuous, parallel, variable-amplitude reflections at the well (and in the shallower parts of the basin) that become larger in amplitude and more continuous in the deeper parts of the basin. The stratal surfaces of sequence III are concordant with horizon C except along the Navarin Basin flanks where they onlap older rocks. These surfaces may represent flank deposits derived from Mesozoic basement highs along the continental shelf break that were eventually truncated by the regressive horizon B event (fig. 47). In addition, they were uplifted and intruded by the late Miocene shale diapirs in the northern Navarinsky subbasin. The stratal surfaces exhibit an obvious divergence toward the subbasin centers, indicating rapid, constant sedimentation. No structural or isopach map of sequence III was generated, but the sediment accumulation is probably greater than 10,000 feet.

At the No. 1 well, seismic sequence III is correlated to the late Oligocene lithologic Zones D-1 and D-2. Zone D-1 is composed of outer neritic to upper bathyal mudstones and siltstones. Zone D-2 contains middle bathyal mudstones with sandstone interlamination. Dredge samples from the Navarin continental slope indicate that the time-stratigraphic equivalents of the late Oligocene lithologic zones are tuffaceous sandstones and mudstones.

CDP seismic reflection data indicate that the deposition of sequence III was laterally and vertically continuous. However, the sequence grades into what appear to be proximal turbidite deposits flanking local basement highs along the continental shelf break (fig. 47). This inference is based on three observations: (1) the onlapping of sequence III stratal surfaces over local structural highs; (2) the presence of coarse-grained material in dredge samples of rocks that are time equivalent to sequence III; and (3) the exposure of early Oligocene sequence IV and Mesozoic basement rocks to wave-base erosion in the late Oligocene, which could have provided a local sediment source adjacent to deep-water basins.

## Seismic Sequence IV

Sequence IV is bounded by horizons C and D (fig. 44). At the No. 1 well, horizon C occurs at 2.94 seconds (or about 11,000 feet below sea level), and horizon D occurs at 3.30 seconds (or about 12,700 feet below sea level). The characteristics of horizon C are described above. Throughout the basin, horizon D represents a distinct angular unconformity between sequences IV and V. Horizon D is the contact where the discontinuous, variable-amplitude reflections of sequence IV overlies and onlap the discordant, dipping, large-amplitude reflections and diffractions that characterize the acoustic basement, sequence V. The stratal surfaces of sequence IV diverge as they deepen in the centers of the subbasins, indicating continuous sedimentation during structural subsidence.

At the well, sequence IV correlates to lithologic Zones E and F. There is some well log, geochemical, and paleontological evidence for an unconformity between Zones E and F, although the geochemical data indicate that there is little missing section at the well site. Zone E consists of early Oligocene, middle bathyal mudstones containing calcite concretions. Zone F consists of late to late middle Eocene, upper bathyal to outer neritic, calcareous and sandy mudstones. Dredge samples from the Navarin continental slope indicate that the time-stratigraphic equivalents of Zone E are mudstones containing limestone nodules. The equivalents of Zone F are mudstone and volcanic sandstone. Dredge samples from the nearby continental slope contain early Eocene and Paleocene rocks that are missing from the Tertiary section at the well site. These samples consist of probable Paleocene volcanic sandstone and limestone; Paleocene to Eocene brecciated mudstone and conglomerate; and early Eocene basalt. Although no direct evidence is available, this section is assumed to be part of sequence IV; therefore, it is bounded at the bottom by horizon D. The extent and thickness of these early Paleogene rocks are unknown.

CDP seismic reflection data indicate laterally discontinuous bedding but vertically continuous deposition of sequence IV. Along the continental shelf break, sequence IV, like sequence III, grades into what are inferred to be proximal turbidite deposits flanking local basement highs (fig. 47).

Sequence IV is believed to be the source for the shale diapirs in the northern Navarinsky subbasin. The lateral continuity of seismic sequence IV outward from the well indicates that the sequence is made up of fine-grained material throughout the subbasin. These fine-grained materials are believed to be overpressured in the well (see Abnormal Formation Pressure chapter). Lithologic Zone F, in sequence IV,

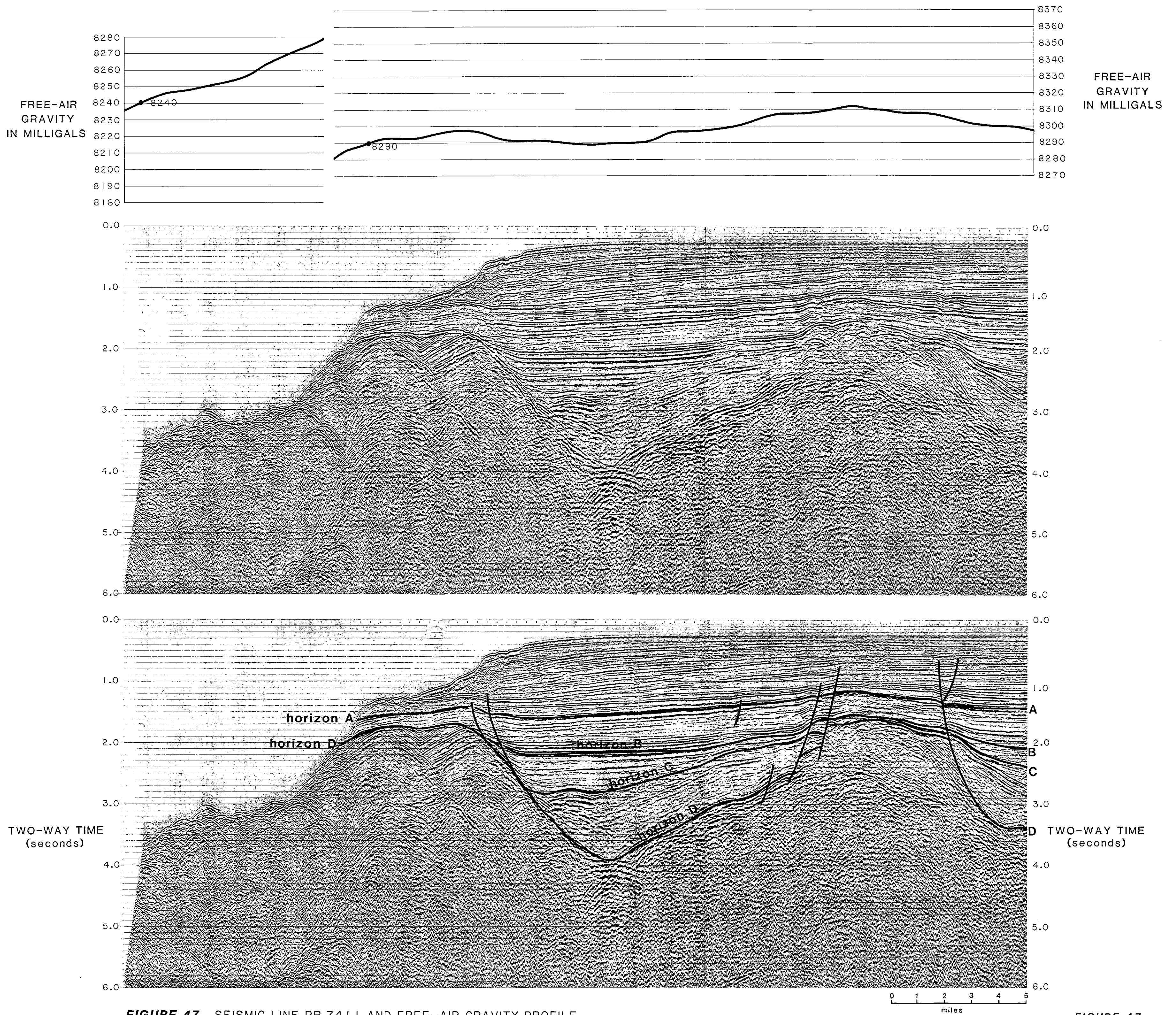


FIGURE 47. SEISMIC LINE PR 741 I AND FREE-AIR GRAVITY PROFILE.

FIGURE 47. Seismic Stratigraphy, 121

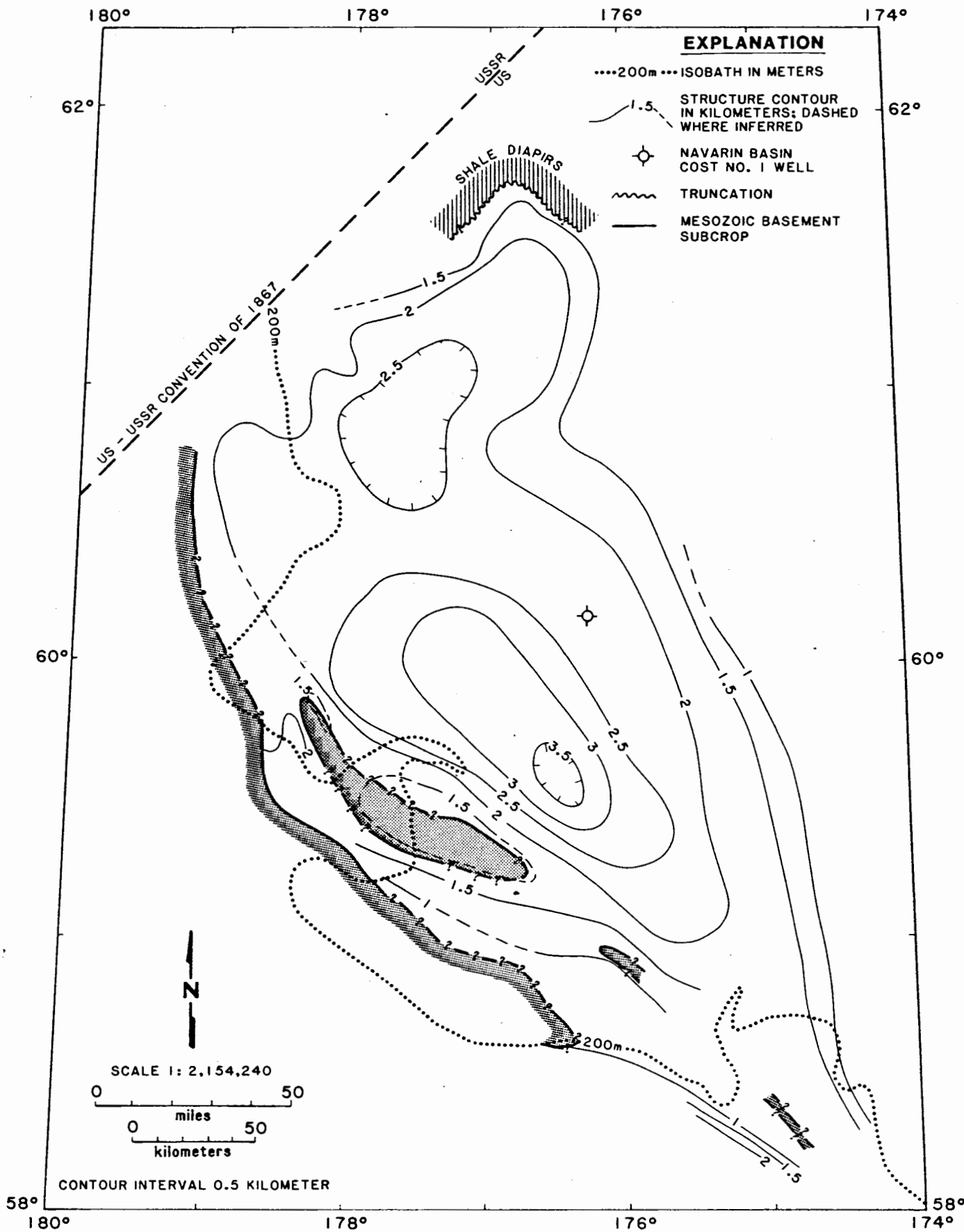


FIGURE 48. STRUCTURE-CONTOUR MAP OF THE OLIGOCENE B HORIZON IN THE NAVARIN BASIN.

lies within the oil window and contains kerogen suitable for wet-gas generation. Hedberg (1974) suggested that methane formation in organic-rich shales might enhance their instability. The presence of an unsampled gas plume over the flank of a shale diapir in the Navarinsky subbasin (Carlson and Marlow, 1984) may corroborate Hedberg's contention. The diverging stratal surfaces of sequence IV indicate continuous, rapid sedimentation. Rapid sedimentation increases the likelihood of maturation of trapped organic matter by enhancing anoxic conditions near the sea floor and later decreasing geothermal heat loss at depth (Anstey, 1977). Diapir movement occurred as recently as late Miocene, piercing and disrupting the stratal surfaces of sequences II and III. Eventually the diapirs were truncated by an erosional surface, horizon A. Emplacement of the diapirs seems to have been controlled by the structural relief of the basement rock, sequence VI. A free-air gravity profile of the diapir area (fig. 45) reflects the gradual deepening of the basement rock toward the center of the subbasin. Uneven sediment loading appears to have forced the diapir to rise near the northern flank of the subbasin near the Anadyr Ridge.

A structure-contour map of horizon D (fig. 49) depicts Mesozoic basement highs separating three structurally distinct subbasins. All three subbasins deepen to greater than 26,000 feet below sea level. The Pinnacle Island and Pervenets subbasins are elongated depressions that parallel the northwest-trending Navarin continental shelf break. The more circular Navarinsky subbasin is bordered by the Anadyr Ridge on the west and lies farthest from the present shelf break.

#### Seismic Sequence V

Sequence V (acoustic basement) is recognized by its variable-amplitude, discordant reflections, diffractions, and incoherent noise (fig. 44). At the No. 1 well, the top of sequence V occurs at 3.30 seconds (about 12,700 feet below sea level). Throughout the Navarin Basin, there is an erosional surface separating the Mesozoic sequence V from the overlying Tertiary section. Horizon D represents the area-wide degradation of the Bering Sea outer continental shelf before the formation of the Navarin subbasins. Subsequent erosional events, such as those represented by horizons B and C, eroded the local basement highs that flank the individual subbasins.

Sequence V contains lithologic Zones G/H and I at the No. 1 well. Lithologic Zone G/H consists of Maastrichtian mudstone, sandstone, and coal deposited in a nonmarine environment. Lithologic Zone I is probably Campanian or

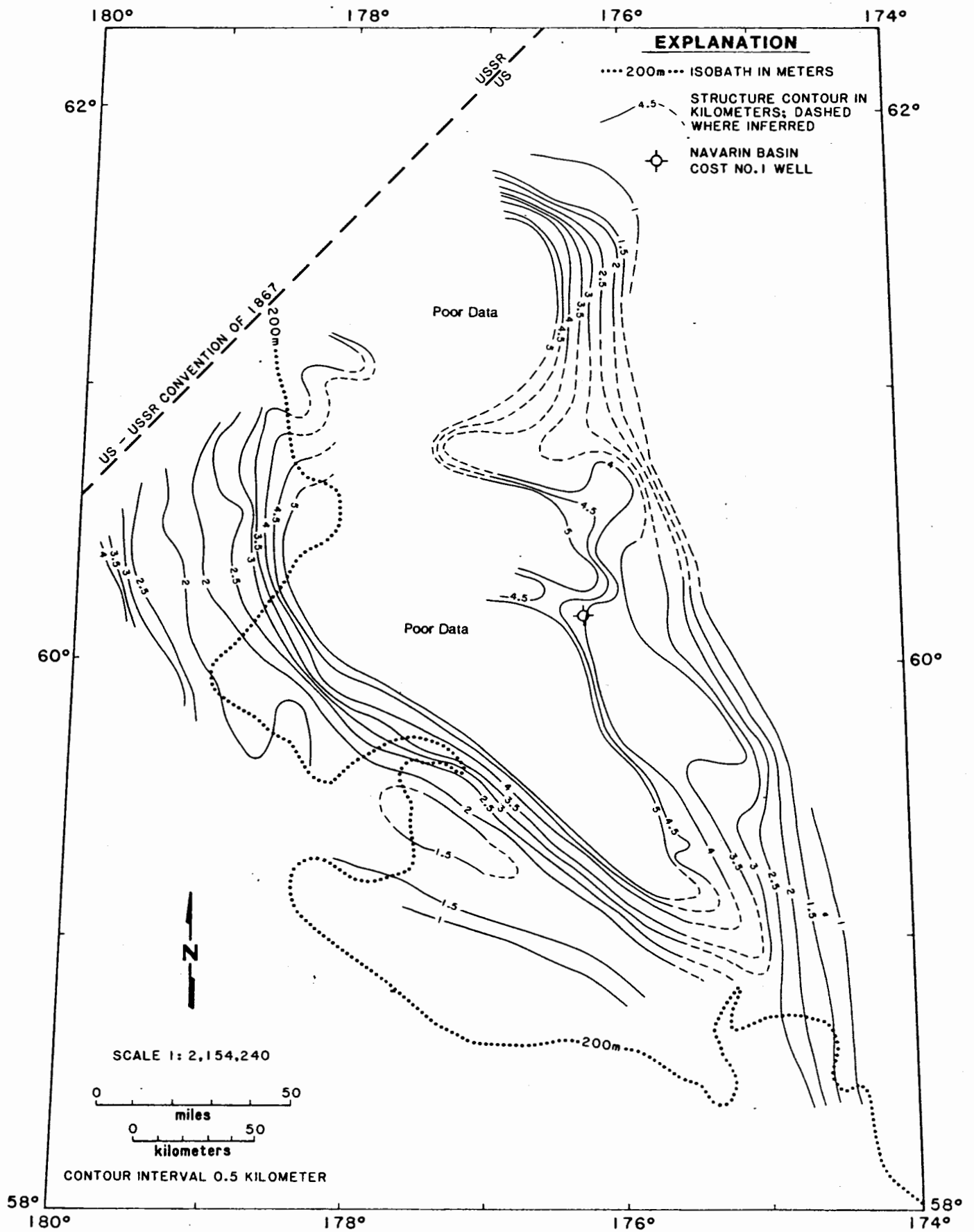


**FIGURE 49.** STRUCTURE-CONTOUR MAP OF AN EOCENE-CRETACEOUS UNCONFORMITY (HORIZON D) IN THE NAVARIN BASIN.

older mudstone deposited in inner neritic to upper bathyal environments. The lower part of the zone contains thin volcanic tuff layers. Dredge samples from the Navarin continental slope that are time-stratigraphic equivalents to sequence V are listed in table 7.

Table 7. Lithology and age of dredge samples

Sample No.	Lithology	Age	
		This Report	USGS (Jones & others, 1981)
L5-78-(27-1)	sandy siltstone	Late Cretaceous (Maastrichtian and reworked Albian)	Late Cretaceous (Campanian or Maastrichtian)
L5-78-(27-2)	sandstone	Late Cretaceous (Cenomanian to Turonian)	not evaluated
L5-78-(5-5)	volcanic sandstone	Late to Middle Jurassic (Calloviaian?)	Late Jurassic (Kimmeridgian)
L5-78-(22-4)	siltstone	Paleocene (probable Danian)	Late Cretaceous (Campanian or Maastrichtian)

The locations of the sampling sites are plotted on figure 40, except for sample 5-5, which lies east of the map area at lat 56°51.1' N. and long 173°32.7' W. Biostratigraphic similarities between the Maastrichtian rocks found at the well site and the dredge samples indicate a continuous Late Cretaceous depositional environment throughout the Navarin continental shelf (see Paleontology and Biostratigraphy chapter). McLean (1979a) and Vallier and others (1980) indicated that the Late Jurassic (Kimmeridgian) Naknek Formation extends from the Alaska Peninsula to the Pribilof Islands. Sample L-5-78-(5-5) is a Late to Middle Jurassic volcanic sandstone dredged from the Zemchug Canyon of the Navarin continental slope. This suggests that the Naknek Formation (or a time-stratigraphic equivalent) extends into the Navarin shelf. This supports the contention of Marlow and others (1983a) that the basement rock in the Navarin shelf is an extension of the Alaskan Mesozoic terrane and suggests that the outer Beringian shelf is a single, continuous terrane. This terrane is bordered by the Anadyr Ridge (fig. 40) to the northwest and the Okhotsk-Chukotsk volcanic belt to the north. The acoustic basement rises to form St. Matthew Island, which lies approximately 115 miles east of the No. 1 well site. Patton and others (1975) found that Late Cretaceous age (65 to 77 million years), high-alumina basalt to rhyolite cover most of the island. These rocks are part of the Okhotsk-Chukotsk volcanic belt.

Figure 49 is a structure-contour map of the top of the acoustic basement (horizon D). The map depicts three en echelon subbasins parallel to the continental shelf break, each having more than 26,000 feet of layered Tertiary fill. The evolutionary model proposed by Marlow and others (1983a) indicates that this structural configuration is the result of Late Cretaceous to early Tertiary oblique subduction or strike-slip motion between the Kula and North American Plates. This model postulates that the basin formed in a forearc setting. The Kula Plate progressed northward past the Beringian continental shelf and eventually underthrust Siberia. As the Kula Plate was subducted beneath Siberia, a melange sequence was obducted, forming part of the Koryak Range. Marlow and others (1983a) believe that this melange sequence extends offshore to form the Anadyr Ridge (fig. 40). The Beringian shelf plate motion may have formed the Okhotsk-Chukotsk volcanic belt, which lies north of the Navarin Basin and parallel to the shelf break. This belt extends from eastern Siberia to at least St. Matthew Island. When the subduction zone shifted to its present position along the Aleutian Arc in the late Eocene (Whitney and Wallace, 1984), the Kula Plate was isolated. This isolation rendered the Kula Plate passive by the late Oligocene (?), which relaxed the shear stress along the Beringian margin. The shear-stress-associated tectonism was eventually replaced by regional collapse in response to crustal cooling, allowing a more uniform basin-wide sediment deposition. Basement-controlled normal faults in the Navarin Basin offset strata as young as Pleistocene (Carlson and others, 1983), indicating that the continued subsidence was caused by sediment loading. Figure 47 shows that structures within these Mesozoic rocks formed before erosional truncation by horizon D.

#### SUMMARY

The Navarin Basin consists of three en echelon subbasins filled with more than 26,000 feet of layered Tertiary sedimentary rock. The subbasins formed as a result of extensional deformation associated with strike-slip motion between the Kula and the North American Plates in Late Cretaceous to early Tertiary time. By the late Eocene, movement of the Kula Plate was isolated by subduction at the Aleutian Arc. Subbasin subsidence in response to structural downdropping probably remained active until the late Oligocene. Regional subsidence in response to crustal cooling eventually led to sedimentation beyond the structurally defined subbasins. Beginning in the late Eocene, the three subbasins were filled with marine mudstones. Sea level lowerings in the "middle" and late Oligocene, however, exposed older Tertiary and Mesozoic basement highs to wave-base erosion, which resulted

in the deposition of coarser grained material along the subbasin flanks. Paleocene and early to middle Eocene marine mudstones and sandstones with good source and reservoir potential may be present in the deeper parts of the subbasins.

## BOTTOM-SIMULATING REFLECTOR

by

Ronald F. Turner  
David A. Steffy  
Gary C. Martin  
Tabé O. Flett

Anomalous seismic reflections that mimic sea-floor topography and exhibit a discordant relationship with coherent reflections from chronostratigraphic surfaces have been termed bottom-simulating reflectors or BSRs (Scholl and Creager, 1973; Hein and others, 1978; Hammond and Gaither, 1983). The time-transgressive characteristics of these reflections are most apparent on seismic profiles that display dipping beds. BSRs are generally attributed to the presence of gas hydrates (solid ice-like water-methane clathrates that may contain other hydrocarbons) or buried diagenetic surfaces (Stoll and others, 1971; Scholl and Creager, 1973; Hein and others, 1978; Kvenvolden and McMenamin, 1980; Marlow and others, 1981). The presence of a BSR in the Bering Sea related to a possible siliceous diagenetic front has been the subject of numerous studies (Scholl and Creager, 1973; Fullam and others, 1973; Hein and others, 1978; Marlow and others, 1981; Hammond and Gaither, 1983).

On the Bering Sea shelf, a BSR is often apparent on seismic sections between 1.0 and 2.0 seconds two-way time (Hammond and Gaither, 1983). Figure 50 is a Western Geophysical Company common-depth-point (CDP) seismic reflection section located at point A on figure 40 (Seismic Stratigraphy chapter). The line is located near the continental shelf break approximately 80 miles southwest of the Navarin Basin COST No. 1 well in average water depths of 460 feet. The section displays Tertiary reflections dipping away from an acoustic basement high. An obvious BSR at 1.3 seconds two-way time (or 3,855 feet below sea level) is present as a large amplitude, discontinuous, discordant reflection. Constructive interference between the BSR and dipping Tertiary reflectors caused some of the BSR segments to display apparent dip (left of point B, fig. 50). This interference also caused a coherency loss in the underlying reflections at point A and a decrease in amplitude at point B (fig. 50).

Hammond and Gaither (1983) observed that a BSR is generally associated with a positive inflection point (velocity increase) on stacking velocity spectra displays, a character which allows it to be discriminated from sea-floor multiples. Stacking velocities were picked for three prominent reflections that define seismic sequences X and Y (fig. 50). Interval velocities for these sequences were then calculated from these RMS velocities by using the Dix equation (Dix, 1955).

Sequence Y, which lies below the BSR, shows a gradual downdip or basinward increase in interval velocity related to increased compaction of the sediments, whereas sequence X, which is cut by the BSR, shows a sharp increase (8 percent or more) in interval velocities.

Figure 41 shows a Petty-Ray Geophysical Company seismic line that profiled the Navarin Basin COST No. 1 well site. The site is characterized by a flat sea floor and flat-lying, parallel, continuous Cenozoic reflectors. There is no distinct BSR on the seismic reflection profile because there are no dipping reflectors. Any reflector generated by the physical properties that cause BSRs would be flat lying and undistinguishable at the well. However, at 1.27 seconds two-way time (3,560 feet below sea level) there is a large amplitude, positive, continuous reflection (seismic horizon A) which may be in part due to an impedance contrast caused by diagenetic changes in the sediment. This reflector is at the appropriate depth to correlate with the BSR identified southwest of the well site. Because of its discontinuous nature, the BSR cannot be traced laterally into the well. Although seismic horizon A and the BSR apparently coincide at the well, they do not coincide elsewhere in the basin. The CDP profile through the Navarin well places this reflector (horizon A and the possibly coincident BSR, hereafter termed the "BSR") approximately 75 feet lower than a narrow interval characterized by abruptly changing physical properties identified on well logs. This apparent disparity is within the vertical resolution of the dominant frequency of the CDP data at this depth. A calculated reflection coefficient of 0.20 for this reflector is low when compared to the various siliceous diagenetic boundaries analyzed by Pisciotto (1981), but is relatively high with respect to coefficients for other reflectors calculated from the sonic log for the synthetic seismogram (see Seismic Stratigraphy chapter).

Seismic horizon A (and the "BSR") coincides with the top of a paleontologically barren zone in the well apparently caused by the dissolution of most siliceous and calcareous microfossils. This interval corresponds in time to the late Miocene NH6 hiatus of Barron and Keller (1982). Seismic horizon A traces into an angular unconformity on the basin flanks.

Although relatively large amounts of CH<sub>4</sub> are present from the surface to about 6,000 feet, gas hydrates do not appear to be responsible for the "BSR" in the well or the BSR shown in figure 50 because the pressure and temperature are too high at these depths. An RFT test (Repeat Formation Tester) was performed at 4,016 feet (measured depth) which yielded a formation fluid pressure of 1,762 pounds per square

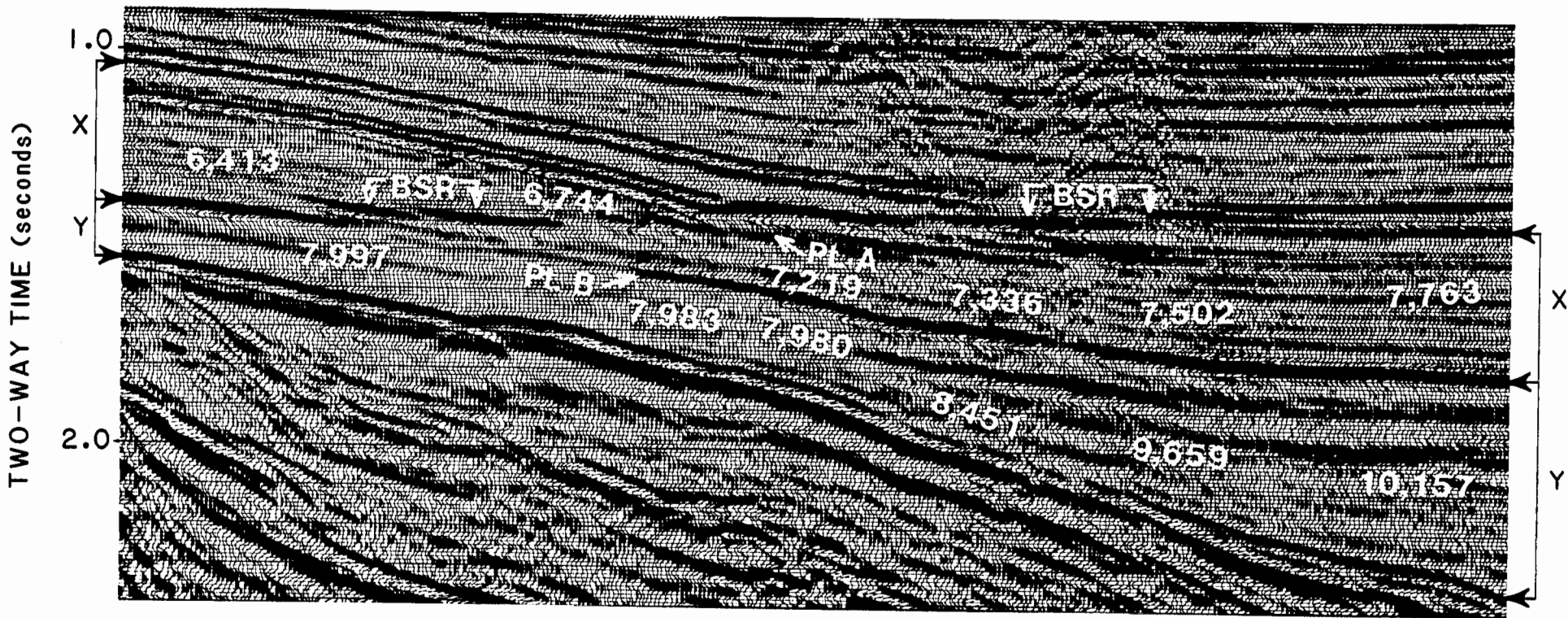


**FIGURE 50.** SEISMIC REFLECTION PROFILE OF A BSR AND ITS INFLUENCE ON THE INTERVAL VELOCITIES (FEET/SECOND) OF TWO SEISMIC SEQUENCES (X AND Y).



inch (psi) at 130° F. The pressure and temperature at 3,700 feet were calculated by assuming a pressure gradient of 0.448 psi per foot and a thermal gradient of 1.78° F per 100 feet. Pressure and temperature conditions at 3,700 feet (124° F and 1,620 psi calculated; 123° F measured from an incomplete RFT at 3,680 feet) are not within the stability field for methane hydrate, water, and gas (Kvenvolden and McMenamin, 1980). Temperatures below about 63° F would be required to produce these phases at the fluid pressure observed in the well. The presence of CO<sub>2</sub>, H<sub>2</sub>S, C<sub>2</sub>H<sub>6</sub>, and C<sub>3</sub>H<sub>8</sub> would all produce a shift in the phase boundary to higher temperatures; the presence of NaCl would reduce the temperature of the phase change. C<sub>2</sub>H<sub>6</sub> and C<sub>3</sub>H<sub>8</sub> are present in only minute amounts. H<sub>2</sub>S was not present. There were no analyses for CO<sub>2</sub> or NaCl.

The BSR identified in the basin and the correlative horizon in the well appear to represent a diagenetic surface related to the dissolution of diatoms (composed of opal-A silica). Diatoms constitute from 50 to 80 percent of the sediment recovered from sidewall and conventional cores down to a depth of about 3,700 feet. Because the diagenetic dissolution of biogenic opal-A is temperature controlled, Scholl and Creager (1973), Fullam and others (1973), and Hein and others (1978), suggested that the ubiquitous, time-transgressive BSR in the Bering Sea represented an isothermal surface related both to the depth of burial of diatomaceous sediments and to local geothermal gradients. In the Bering Sea area, a burial depth of at least 1,640 feet and a temperature range of 95° to 125° F are required to initiate large scale, relatively rapid conversion of opal-A to opal-CT (Hein and others, 1978). Both of these conditions are met in the Navarin Basin COST No. 1 well in the interval between 3,565 and 3,860 feet. Similar depth-temperature relations were observed for diagenesis in the Miocene Monterey Formation of California (Murata and others, 1977).

With increasing burial depth and temperature, the normal sequence of diatomite diagenesis is from opal-A to opal-CT (an opal phase with characteristics of alpha-tridymite and alpha-cristobalite) and eventually to quartz. The transformation of opal-A to opal-CT has been the subject of many studies, notably those of Murata and others (1977), Hein and others (1978), Hein and Scholl (1978), and Isaacs and others (1983). This "normal" silica diagenetic sequence appears to be present at the appropriate depths in the Navarin well. Microscopic observations of diatoms by Donald L. Olson qualitatively documented these transformations (see Paleontology and Biostratigraphy chapter). However, these visual observations were not supported by initial X-ray analyses (AGAT, 1983). Further X-ray analysis by MMS and USGS personnel determined that in some samples opal-CT was present in amounts of five percent or less (Hein, oral commun., 1984; Lynch, written commun., 1984). No diagenetic quartz was identified.

Thus, although the BSR in the Bering Sea is clearly associated with the dissolution of diatoms, the "BSR" in the Navarin well does not mark a diagenetic surface separating abundant opal-A from abundant opal-CT. An analysis of scanning electron microscopy and X-ray diffraction data suggests that most of the unstable biogenic opaline silica was used in the formation of silica-rich zeolites (AGAT, 1983) or clays (Hein, oral commun., 1984). Hein and others (1978) observed that clinoptilolite and opal-CT both form in conjunction with the diagenesis of diatoms and that areas of abundant clinoptilolite coincide precisely with areas of opal-CT formation. Iijima (1980) and Iijima and Utada (1983) noted that the opal-CT Zone was equivalent to Zone II (clinoptilolite and/or mordenite, and low cristobalite) of the zeolite-burial metamorphism zonation, and that under similar conditions opal-CT formed in biogenic siliceous rocks while clinoptilolite formed in silicic volcanoclastic rocks. Although the association of clinoptilolite with the breakdown of volcanoclastic material has been documented by Deffeyes (1959), Mason and Sand (1960), and Murata and Whiteley (1973), Von Rad and Rosch (1972) reported the formation of clinoptilolite in biogenic rocks that contained no volcanoclastics.

The sediments in lithologic Zone A-1 (1,536 to 3,565 feet) contain both abundant diatoms and volcanoclastic material. The fact that trace amounts of opal-CT and abundant clinoptilolite occur together in lithologic Zone A-2 (below the zone of abundant opal-A diatoms) suggests that much of the silica liberated by the dissolution of diatoms went into the formation of clinoptilolite. Only a small fraction of the diatoms remaining in Zone A-2 altered to opal-CT. The diagenetic alteration of clay minerals and volcanoclastic debris in these diatomaceous sediments probably provided the aluminum and potassium cations necessary to form clinoptilolite, although some of the aluminum may have come from the dissolution of diatom frustules (Van Bennekom and Van Der Gaast, 1976; Hein and others, 1978). It is also possible that some of the diatoms altered to smectitic clay (Badaut and Risacher, 1982).

The interval from 1,536 to 3,860 feet consists of poorly consolidated and poorly sorted silty, sandy, diatomaceous mudstone and diatomite (see Lithology and Well Log Interpretation chapters). The lithic components include basaltic and intermediate volcanic fragments, clay, mica, glauconite, and chert. Lithologic Zone A-2 (3,565 to 3,860 feet) represents the transitional diagenetic zone in the well and is almost certainly responsible for the BSR. Changes in diatomaceous sediments that accompany the transformation of opal-A include marked increases in cementation, bulk density, hardness, cohesion, and brittleness, and a marked decrease in porosity (Isaacs and other, 1983).

These are the same changes recorded by wireline log responses through lithologic Zone A-2. Figure 51 shows the decrease in interval transit time over the diagenetic zone, and figure 52 shows the porosity reduction and increase in bulk density (see Well Log Interpretation chapter). Isaacs and others (1983) suggested that most porosity reduction in diatomaceous sediments is due to compaction during the opal-A to opal-CT transformation, probably because of a loss in framework strength under load during solution-precipitation. Porosity loss apparently occurs rapidly in individual beds, with those containing the greatest number of diatoms undergoing the greatest porosity reduction. The physical changes associated with biogenic silica diagenesis occur abruptly over a small stratigraphic interval in homogeneous sediments, or across a broader transitional zone in interbedded heterogeneous sediments (Isaacs and others, 1983). The latter condition best describes lithologic Zone A-2 in the Navarin well.

Secondary carbonates are quite common through this interval in carbonate-cemented "hard streaks" and account for some of the physical changes seen on the logs. X-ray diffraction studies of highly indurated, glauconitic, diatomaceous mudstones from Zone A-2 identified high-magnesium calcite, protodolomite, and rhodochrosite (Hein, oral commun., 1984; Lynch, written commun., 1984). Barite and volcanic ash were also present. The genesis of secondary carbonate minerals in diatomaceous and ash-rich Bering Sea sediments is discussed in detail by Hein and others (1979).

A number of striking physical changes occur in or near lithologic Zone A-2, seismic horizon A, and the "BSR" in the well. Some of these may be fortuitous, such as the association of the transition zone with seismic horizon A (which correlates with an angular unconformity on the basin flanks). Other changes are obviously related, among them the dissolution of opal-A, the anomalous paucity of opal-CT, the presence of abundant clinoptilolite and smectitic clays, the precipitation of secondary carbonate minerals, increases in bulk density, decreases in porosity and interval transit time, and the presence of an abnormally pressured zone above 3,860 feet (see Abnormal Formation Pressure chapter). All of these are related to the diagenesis of opal-A and all of these contributed to the physical character of the "BSR" interval in the well and probably to the character of the actual BSR in the basin.

The wholesale dissolution of opal-A and concomitant collapse of the sediment framework generates ionically active, abnormally pressured pore waters that precipitate different mineral suites depending on the local mineralogical composition of the sediment. Thus, although the nearby BSR identified in the Navarin Basin may represent an opal-A to opal-CT

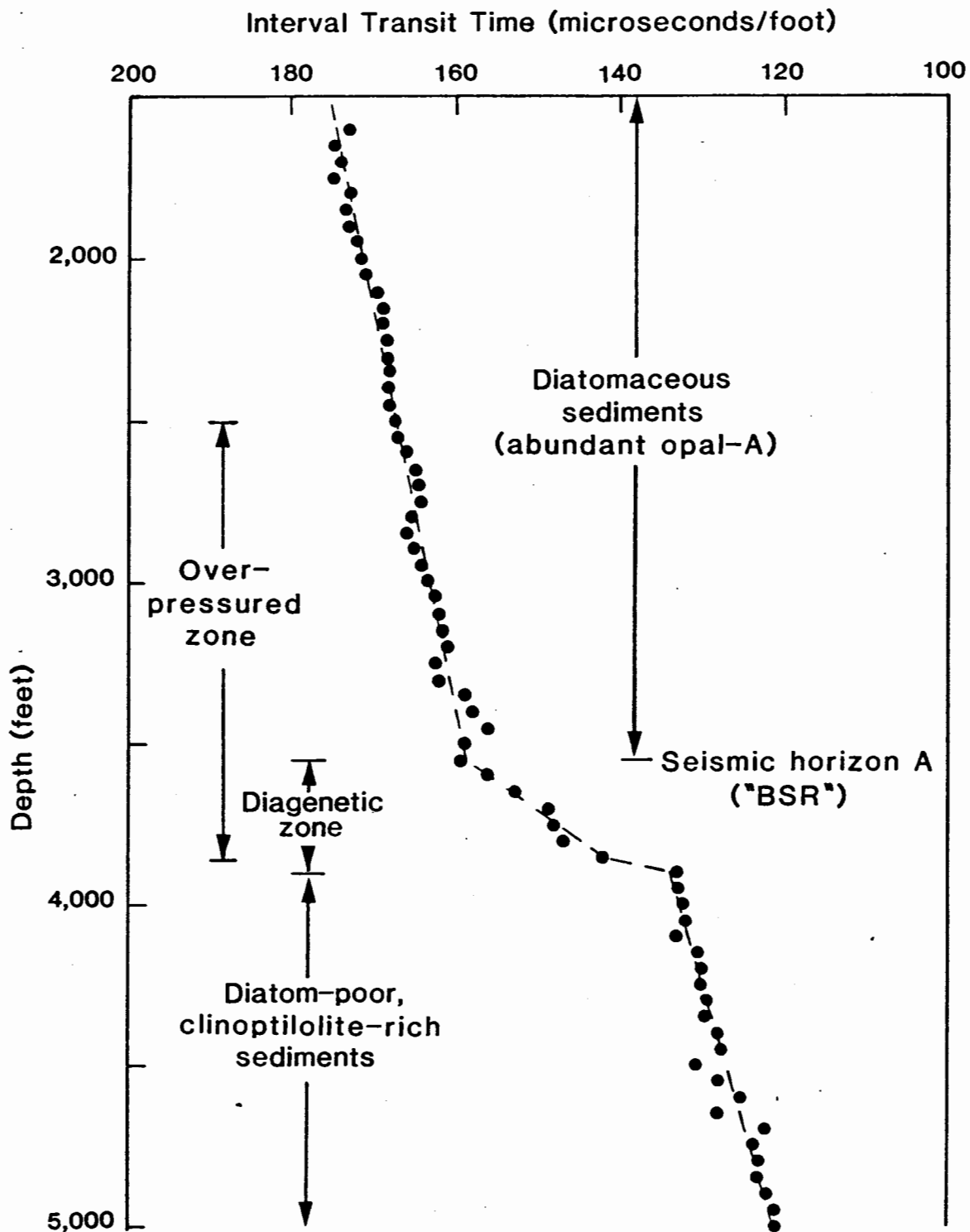


**FIGURE 51.** PATTERN OF DECREASE IN INTERVAL TRANSIT TIME FOR HIGHLY DIATOMACEOUS ROCKS AND THEIR DIAGENETIC EQUIVALENTS, NAVARIN BASIN COST NO. 1 WELL.

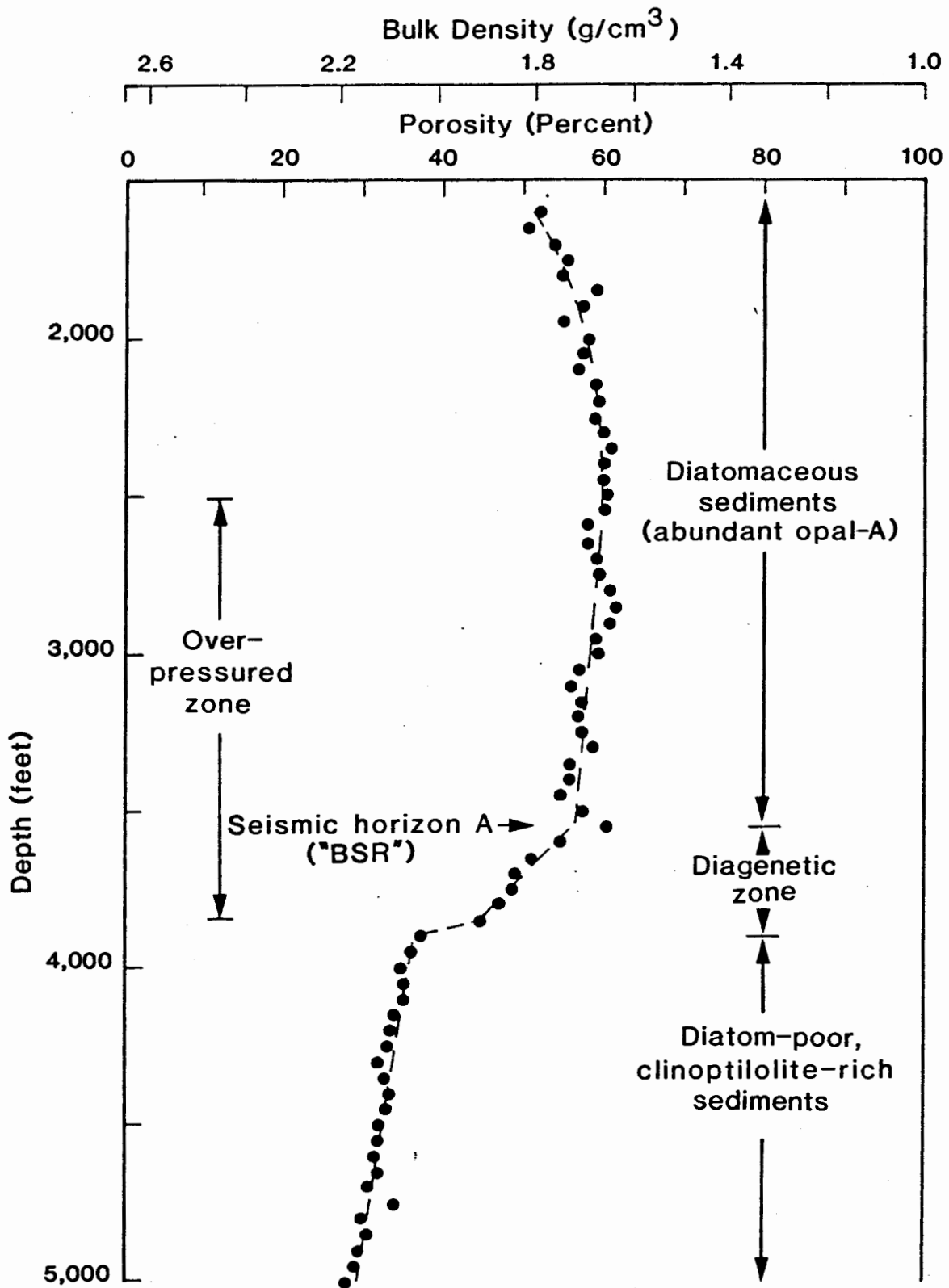


**FIGURE 52.** PATTERN OF POROSITY REDUCTION AND BULK DENSITY INCREASE FOR HIGHLY DIATOMACEOUS ROCKS AND THEIR DIAGENETIC EQUIVALENTS, NAVARIN BASIN COST NO. 1 WELL.

transition, it is more likely that it represents some other type of lithology-controlled change, probably the opal-A to clinoptilolite and clay transition identified in lithologic Zone A-2 (the "BSR") in the Navarin Basin COST No. 1 well.

Aside from its scientific interest, the diagenetically altered part of the Miocene diatomite sequence in the Navarin Basin (the BSR and "BSR") is important for at least three reasons: (1) it may seismically identify the base of a potentially hazardous, abnormally pressured zone; (2) the tight diagenetic zone could act as a seal in a structural or hydrodynamic trap; (3) it could easily lead to a number of seismic interpretation problems, such as being mistaken for a "bright spot", "flat spot", or seismic sequence boundary.

## WELL LOG INTERPRETATION

by  
Gary C. Martin

### INTRODUCTION

A suite of wireline well logs (listed below) run in the Navarin Basin COST No. 1 well by Schlumberger Ltd. were interpreted to provide data on lithology and reservoir characteristics of the strata penetrated. The petrophysical information from the wireline logs was supplemented by sidewall and conventional core data, descriptions of rock cuttings and hydrocarbon shows from lithology and formation evaluation (mud) logs, and the petrographic report by AGAT Consultants, Inc. (1983).

<u>Log</u>	<u>Depth (feet) below Kelly Bushing</u>
Dual Laterolog with Microspherically Focused Log (DLL-MSFL) -----	1,497 - 5,042
Dual Induction Laterolog with Spherically Focused Log (DIL-SFL)-----	5,004 - 16,376
Compensated Formation Density Log (FDC) -----	1,497 - 16,385
Compensated Neutron - Formation Density Log (CNL-FDC)-----	1,497 - 16,385
Borehole Compensated Sonic Log (BHC)-----	1,497 - 16,375
Long-Spaced Sonic (LSS)-----	1,497 - 16,385
Natural Gamma Ray Spectroscopy Tool (NGT)-----	1,497 - 16,385
High Resolution Dipmeter Tool (HDT) and Arrow plot from CLUSTER program -----	1,497 - 16,384

The well can be divided into two major zones separated by an angular unconformity at 12,780 feet. The upper zone consists of Tertiary marine clastics, and the lower zone (12,780 to 16,400 feet) consists of Late Cretaceous nonmarine to marine clastics and younger igneous intrusives. These two zones were further subdivided on the basis of lithology and log characteristics.

Potential reservoirs occur almost exclusively in the upper zone in Tertiary sandstones in the interval from 3,855 to 7,130 feet. Much of this sandstone is shaley and contains abundant detrital and authigenic clay and clay-rich lithic grains which degrade reservoir quality. However, some of the sandstone has significant reservoir potential. Well log evaluation (based on a correlation of wireline log data with core and petrographic data) indicates that these Tertiary sandstones probably include about 200 feet (aggregate) of

relatively good reservoir rock with porosities of 15 to 20 percent and permeabilities of greater than 70 millidarcies. Late Cretaceous sandstones below the major unconformity at 12,780 feet have lost almost all reservoir potential because of a complex history of burial, compaction, and diagenesis.

#### BOREHOLE CONDITION AND LOG QUALITY

Log quality is good throughout most of the hole with a few exceptions. The caliper curve recorded with the BHC, FDC, and CNL-FDC logs jammed on the bottom of the hole at the start of logging run 1 and is invalid from 1,497 to 5,042 feet. The caliper curve recorded with the FDC and CNL-FDC logs during run 4 (12,815 to 15,318 feet) is also invalid because the caliper was bent in the hole. The SP curve recorded with the BHC log had a bad ground and is invalid for run 3 from 5,004 to 12,834 feet.

Washouts and very irregular hole sizes occurred from 7,360 to about 8,800 feet, and were particularly severe from 7,650 to 8,150 feet. These washouts probably caused much of the erratic response of the density and neutron curves of the FDC and CNL-FDC logs in this interval.

The resistivity curves of the DIL tool between 12,800 and 15,300 feet also record a few zones of erratic tool response. These are probably due to the high resistivity contrasts between the complex lithologies in this interval.

Sandstone identification on the logs from the first run is difficult. The gamma-ray curve throughout the Tertiary section displays little or no deflection from a shale base line. This is due to the high content of detrital mud, clay matrix, glauconite, feldspar, and lithic grains in the sandstones. As a result, the gamma-ray curve is essentially useless in identifying sandstones in this section. The resistivity of the mud filtrate in the first log run was low because of the saltwater-base mud and showed little contrast with the formation water resistivity. In combination with the high mud content of the sands, this resulted in very little SP deflection across sandstone intervals. These same factors also depressed the resistivity curve responses. The net result was little difference in log response between sandstone and finer grained lithologies. Below the first log run (5,004 feet), mud filtrate resistivities were higher because of the lower salinity of the mud base, and SP curve deflections are adequate to define permeable sandstones.

#### LOG ANALYSIS METHODS

The matrix density values used in calculating porosity from the FDC bulk density curve were obtained from the grain

density data from analyses of conventional cores. Grain density values were averaged from the core or cores taken within each stratigraphic zone and used as the matrix density value for porosity analysis. Grain densities from highly cemented calcareous zones were excluded from the averages. The grain density calculated from these zones is generally anomalously high because of the high-density calcium carbonate cement. Excessively high porosity values would be obtained for sandstones with no calcareous cement if these values were included. These calcareous zones have little or no permeability and were excluded from net sand porosity calculations. Porosity calculated from the FDC data, when averaged over the cored interval, closely matched average core porosity. Log-derived porosity generally varied by less than 1 percent from core porosity.

Matrix travel times used to calculate porosity from the BHC tool are 55.5 microseconds/foot in Tertiary sandstones and 52.5 microseconds/foot in the more compacted and lithified Late Cretaceous sandstones below 12,780 feet. Sonic porosities for Tertiary sandstones were corrected for undercompaction by a compaction factor derived from travel times in adjacent shales.

Sonic and neutron porosities, when averaged over cored intervals, are consistently higher than core porosity by about 5 to 15 porosity percentage points. This is due to the high mud and clay content of the sandstones, to which these tools respond in the same manner as to porosity.

Porosity, and the log data from which it was derived, are shown for stratigraphic zones B, C-1, and C-2 in tables 8, 10 and 12. Shale volumes, net sandstone, effective porosity, and porosity-feet were evaluated from the data in these tables and are shown in tables 9, 11, and 13.

Net sandstone was derived primarily from the SP curve. Sandstone intervals that had SP deflections of at least -10 millivolts (mv) were assumed to have some permeability. Shale or mudstone interbeds and highly cemented streaks of sandstone were excluded in the calculation of net sandstone.

The effective porosity of net sandstone was obtained by subtracting the porosity component of shale or mudstone from the total porosity. Two different techniques were used to calculate shale volume ( $V_{sh}$ ).

One technique used the gamma-ray curve to determine  $V_{sh}$ . This procedure uses shale ( $GR_{sh}$ ) and clean sandstone ( $GR_{ss}$ ) values from the curve to determine the gamma-ray index (IGR) from the formula:

$$\text{IGR} = \frac{\text{GR}_{\text{log}} - \text{GR}_{\text{ss}}}{\text{GR}_{\text{sh}} - \text{GR}_{\text{ss}}}$$

The Vsh is then calculated from the IGR by the following formulas (Asquith, 1982, p. 103):

Tertiary rocks (unconsolidated):

$$\text{Vsh} = 0.083 (2^{3.7\text{IGR}} - 1.0)$$

Cretaceous rocks (consolidated):

$$\text{Vsh} = 0.33 (2^{2\text{IGR}} - 1.0)$$

The problem with this technique is the difficulty in determining a value for clean sandstone in this well. No clean quartz sandstones are present in the Tertiary section. A relatively thick coal bed at 15,153 feet in the Cretaceous section was used for the clean sandstone value. However, the difference in borehole environment (hole size, mud weight, compaction, etc.) between the Tertiary sandstones and the coal bed probably affected the gamma-ray curve response. Because of this, the clean sandstone value is uncertain, as is the shale volume determined by this technique for Tertiary sandstones.

The other technique employed a neutron-density crossplot to graphically determine Vsh and effective porosity (fig. 53) (Schlumberger, 1972, p. 96; Schlumberger, 1974, p. 40-42). Neutron and density porosities were determined in shale intervals within the Tertiary sandstone sequence from 3,900 to 7,300 feet, and these data were then crossplotted. Clean sandstone and shale lines were determined, and Vsh and effective-porosity lines were constructed within these base lines. Averaged neutron and density porosities from net sandstone intervals were then plotted to determine Vsh and effective porosity. This technique yielded more accurate porosity and Vsh for this well than did the gamma-ray technique. Vsh from the crossplot is based on the simultaneous solution of two different log curves from a large number of sample points. This is in contrast to Vsh from the gamma-ray index, which is derived from a single log curve that is dependent on the presence of thick, relatively pure lithologic end members.

Effective porosity was calculated from the neutron-density crossplot and from sonic porosity by using Vsh from the IGR. The two effective porosity values calculated from two different logs by using two different techniques were averaged for each sandstone.

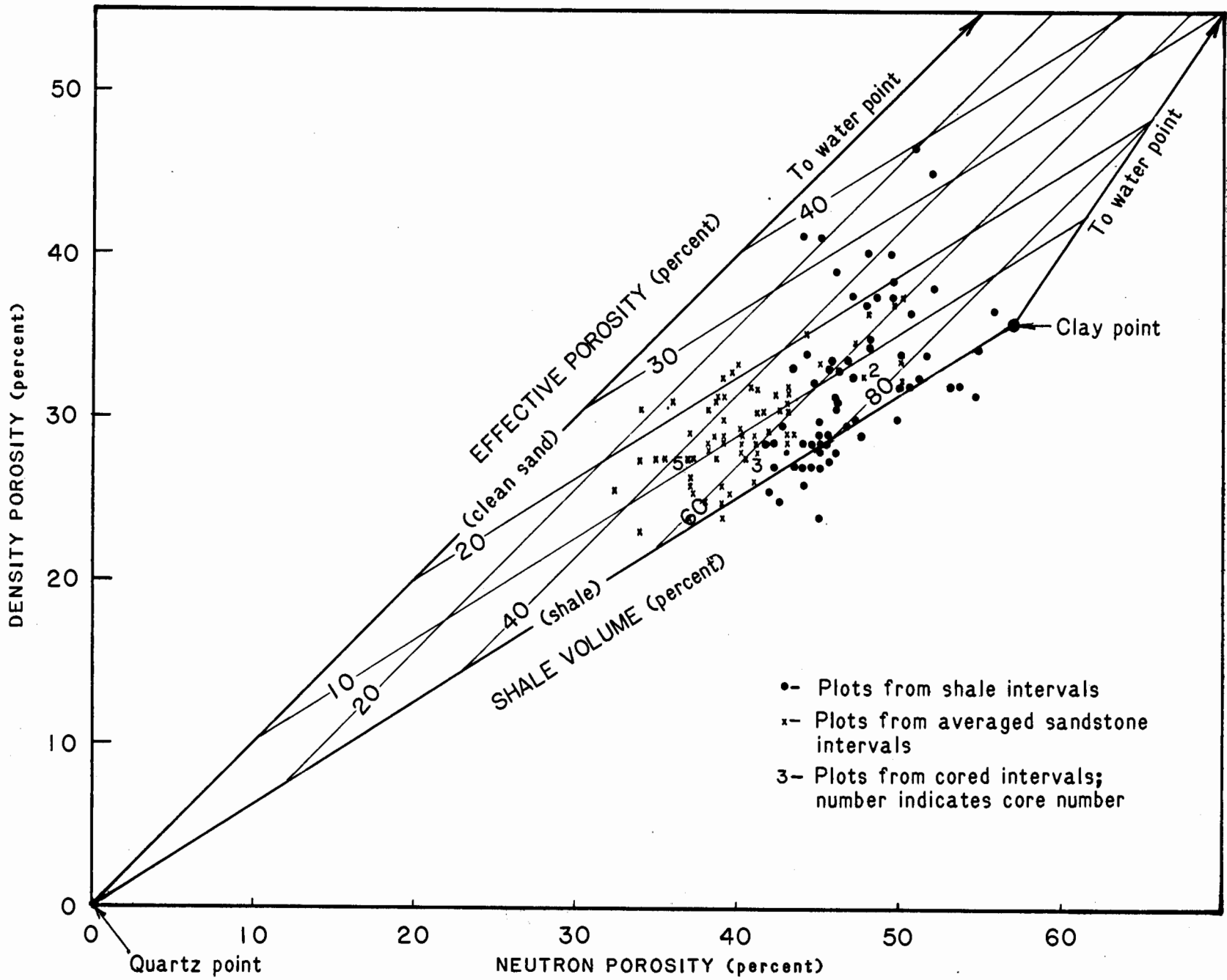


**FIGURE 53.** NEUTRON-DENSITY CROSSPLOT OF TERTIARY SANDSTONE INTERVALS, NAVARIN BASIN COST NO. 1 WELL.



A comparison of effective porosity (calculated from the wireline logs or modal analyses of thin sections) and measured core porosities from Tertiary sandstones shows that the core porosities are generally 20 to 25 porosity percentage points higher (fig. 54). Density porosity, uncorrected for shale content, more closely matches the core porosity than does the calculated effective porosity. Despite this disparity, the effective porosity calculated from the logs probably more accurately reflects true effective porosity than either the core porosity or the closely matching uncorrected density porosity. Petrographic analysis of thin sections made from conventional cores (AGAT, 1983) showed large amounts of total porosity to be in the form of ineffective microporosity in the intergranular detrital matrix and in the authigenic matrix of clays and cement. Intergranular or dispersed clay or shale, which is subjected only to hydrostatic rather than overburden pressure, can be expected to contain more bound water than structural or laminar shales. If during core analysis the loosely bound water of the dispersed shale is removed by the drying process, it results in an increased porosity measurement (Schlumberger, 1972, p. 91). This effect probably affected core measurements in this well. However, this effect alone is probably not large enough to account for the observed core-versus-effective-porosity differences. The microporosity of the intergranular shale component of the sands is apparently permeable to the helium employed in the core analysis and is detected as part of the total porosity (fig. 54). Modal analyses of the effective mesoporosities from thin sections match effective porosities calculated from the neutron-density crossplot to within 1 or 2 percent when both are averaged over the intervals of conventional cores. Effective porosity from the neutron-density crossplot and modal analysis from thin sections made from sidewall cores do not match nearly as well. This is probably because of the disruptive effects of the percussion sidewall coring process on rock fabric and the improbability of exactly matching the sidewall core depths with equivalent log depths.

Effective porosities calculated from the sonic log do not match visual estimates from the conventional-core thin sections nearly as well as effective porosities from the neutron-density crossplot do. This is because the poorly consolidated Tertiary sands are a poor medium for the transmission of acoustic waves and because  $V_{sh}$  employed in the sonic calculation was determined by the IGR method, which is less reliable than the crossplot technique for the reasons outlined above.

Petrographic analysis also revealed that a significant portion of the framework grains of these Tertiary sandstones are in the form of clay-rich lithic fragments. These lithic grains, along with the intergranular clay and shale matrix, are

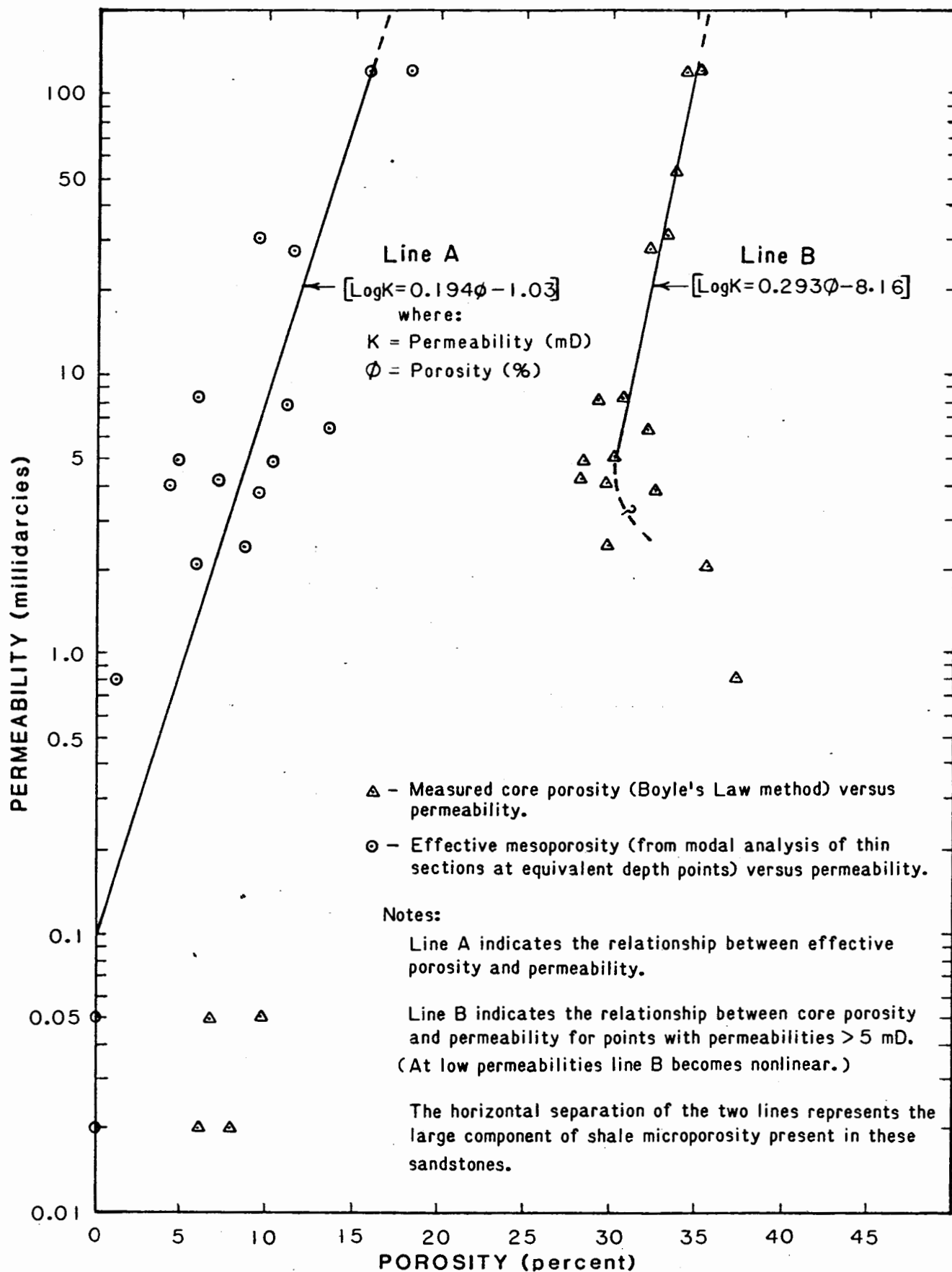


**FIGURE 54.** PLOT OF POROSITY VERSUS PERMEABILITY FOR TERTIARY SANDSTONES (CONVENTIONAL CORES 2 THROUGH 5), NAVARIN BASIN COST NO. 1 WELL.

read by the logs as shale. This accounts for the very high Vsh values calculated from the logs. A comparison of Vsh values from the logs and petrographic analyses of thin sections of conventional cores 3 through 5 indicates that clay-rich lithic grains or structural shale accounts for 30 to 70 percent of the Vsh calculated from logs. This explains the presence of effective porosity in sandstones that have apparent shale volumes of 50 percent or more.

#### DESCRIPTION OF STRATIGRAPHIC ZONES

The Navarin Basin COST No. 1 well is divided into 11 zones (pl. 1) based on lithologic, diagenetic, and petrophysical log characteristics. The nomenclature and zone boundaries used by AGAT (1983) to subdivide the well are generally followed here to facilitate comparison between the different reports.

The Navarin well is divided into two major sections by an angular unconformity at 12,780 feet which separates Tertiary and Late Cretaceous rocks. The Tertiary rocks are subdivided into zones labeled A through F, and the Cretaceous rocks into zones labeled G/H and I. Some of the zones are further subdivided where significant differences within them exist. Detailed descriptions of each zone are given below.

##### Zone A-1 (1,497 to 3,565 feet)

Rotary drill bit cuttings and sidewall cores from this interval consist of poorly consolidated and poorly sorted diatomaceous, sandy mudstone and sandy diatomaceous ooze. The SP and gamma-ray curves record few deflections from base line responses over much of this zone and indicate relatively constant lithology. However, from the top of this interval to a depth of 1,860 feet the gamma-ray curve does record several coarsening-upward sequences of bedding. The sequences range in thickness from 40 to 60 feet.

The DLL curves show little deflection over most of Zone A-1. The curves record a general downward decrease in resistivity because of increasing temperature and pore pressure gradients with depth. The relatively featureless character of the DLL curves is due to the relatively constant lithology of the sediments and the low resistivity contrast between the saltwater-base mud and formation water.

Comparison of the BHC and LSS logs indicates that the BHC log is invalid from 1,497 to 1,800 feet and from 1,900 to 2,165 feet because of cycle skipping. Elsewhere in this zone, the BHC log records interval transit times which gradually decrease downward from about 175 microseconds/foot near

1,800 feet to about 160 microseconds/foot at the base of the zone. The decrease is attributed to increasing overburden pressure and compaction with depth.

The bulk density recorded on the FDC log generally ranges from about 1.60 to 1.80 grams per cubic centimeter ( $\text{g/cm}^3$ ). In the upper part of this zone, where the coarsening-upward beds occur, the bulk density is more variable, ranging from 1.65 to 1.95  $\text{g/cm}^3$ . The CNL-FDC log records density and neutron porosities generally ranging from 53 to 63 percent. These porosities are also more variable in the upper coarsening-upward sequences, where they range from 45 to 63 percent.

The logs throughout Zone A-1 record local deflections or spikes of short interval transit times, high bulk density, low porosity, and high resistivity. These are interpreted to be hard, highly cemented zones of carbonate cement.

Arrow plots of dips from the HDT log show widely scattered measurements of random dip directions and variable dip angles. Because seismic sections indicate the strata are flat lying at this depth, many of these dip measurements are probably invalid. The randomness and scatter of the recorded dips are probably due to borehole rugosity, poor resistivity contrasts, and the inherent difficulty in obtaining measurements from the bioturbated, unconsolidated sediments.

No hydrocarbon shows were reported in tests of rock cuttings samples. However, the Formation Evaluation Log (mud log) recorded high background methane gas contents ranging from about 40 to 120 gas units.

The abundant diatoms, shell fragments, and relatively fine grained sediments present indicate deposition in a marine shelf environment. The coarsening-upward sequences and generally sandier sediments of the upper part of this zone may indicate progradational deposition in a slightly higher energy environment.

#### Zone A-2 (3,565 to 3,860 feet)

Cuttings and sidewall and conventional cores indicate little significant difference in lithology between this zone and Zone A-1. However, wireline-log shifts record marked alterations in physical properties of the sediments. These alterations are interpreted to be the result of diagenetic processes and related pore pressure changes from Zones A-1 to A-2. Changes in the physical properties of diatomaceous sediments have been shown to accompany the diagenetic transformation of biogenic opal-A of diatom tests to other forms of silica. These changes include marked increases in

cementation, bulk density, hardness, cohesion, brittleness, and a marked decrease in porosity (Isaacs and others, 1983). These are the same types of physical changes indicated by the wireline-log responses, which increase progressively downward in Zone A-2 (see Bottom-Simulating Reflector chapter).

The increase in hardness and cohesion is reflected by the sonic log, which records a rapid decrease in interval transit time from 160 to 145 microseconds/foot followed by an abrupt decrease to 130 to 135 microseconds/foot at the base of the zone. The increase in hardness and cohesion is also reflected on the drilling-time log which recorded harder and slower drilling at the lower boundary of this zone. The increase in bulk density is recorded on the FDC log, which shows a gradual increase from 1.70 to 1.90 g/cm<sup>3</sup>, followed by a sudden increase to 2.10 g/cm<sup>3</sup> in the basal 10 feet of the zone. Density porosity recorded on the CNL-FDC log decreases rapidly from 60 to 45 percent, with an abrupt decrease to about 35 percent in the bottom 10 feet of the interval.

The porosity loss due to the expulsion of excess pore fluids and increased cementation is reflected on the DLL curves, which record increasing resistivity through this zone. This reverses the trend of decreasing resistivity downhole observed in the overlying Zone A-1. The permeability decrease associated with the large porosity loss resulted in a slight positive shift of the base line of the SP curve. A similar base line shift of the gamma-ray curve toward higher radioactivity through Zone A-2 is probably caused by water loss in mudstones and claystones and the consequent relative increase in bulk clay content associated with increased compaction.

No hydrocarbon shows were reported in tests on cuttings samples, but the mud log recorded high background methane gas content throughout the zone.

The Dipmeter log also recorded a change. The pooled arrow plot shows a shift from widely scattered random dips at the top of the zone, to a higher frequency of measurements that are more densely grouped with respect to dip angle (generally less than 10 degrees) and less random in direction as the base of the section is approached. This is partially the result of the increasing consolidation and development of resistivity contrasts between laminae, and facilitates signature correlation and dip measurement by the HDT.

#### Zone B (3,860 to 5,010 feet)

Conventional and sidewall cores and cuttings indicate that this zone consists of very fine to fine-grained sandstone and muddy sandstone, which is poorly sorted (to locally well

sorted) and bioturbated. The sandstone is interbedded with siltstone and silty mudstone. The abundant diatoms characteristic of the A Zones are rare to absent in Zone B. The chief sandstone grain types include quartz, feldspar (mainly plagioclase), and lithic fragments (mainly volcanic). The quartz content is 30 to 40 percent. The clay matrix consists primarily of illite and smectite (mainly in mixed-layer form) with minor amounts of chlorite.

As discussed previously in the section on borehole condition and log quality, sandstones are difficult to delineate on logs from this zone. The SP, resistivity, and gamma-ray curve responses are all poor, and as a consequence, the sand/shale ratio is difficult to estimate. Conventional and sidewall cores recovered primarily muddy, very fine grained sandstone, but the cuttings lithology log indicates that mudstone and siltstone are more abundant than sandstone.

Sandstones that had negative SP deflections of at least -10 millivolts (mv) were evaluated for porosity and effective porosity. Thirteen such sandstones, ranging in thickness from 5 to 25 feet and totaling 193 feet (aggregate), were identified. Porosity, uncorrected for shale content, and other significant log data from Zone B are shown in table 8. Density porosity in table 8 was calculated by using a matrix density of  $2.67 \text{ g/cm}^3$ . This was derived from the average sandstone grain density in conventional core 2 (4,184 to 4,210 feet). The average core porosity of 34.0 percent (excluding two measurements from tight calcareous streaks) compares favorably to the average porosity of 34.7 percent calculated from the density log of this core interval. Density porosity values from the 13 sandstones range from 32 to 41 percent. Neutron and sonic porosities are generally 5 to 10 porosity percentage points higher because of the high clay content of these sandstones. These porosities corrected for shale or clay content are shown in table 9.

Neutron-density effective porosities of these sandstones range from 3.5 to 20 percent and have a weighted mean of 12.5 percent. The aggregate sand value for this zone is 193 feet. Modal analyses of effective porosity in thin sections from the permeable portion of core 2 were compared with effective porosity from the logs. The average value of 8.4 percent for thin-section porosity closely matches the 8.3 percent average porosity obtained from the neutron-density crossplot.

In these sandstones, shale volumes calculated from logs are high. Shale volumes vary from 32 to 78 percent, depending on which method is used. The shale volume derived by the gamma-ray technique is often 10 to 20 percent lower than that derived by the neutron-density method. Both methods

Table 8. Sandstone interval log data and porosity averages, Zone B: 3,860 to 5,010 feet

Interval (feet)	Bulk Density (g/cm <sup>3</sup> )	Interval Transit Time (microseconds/foot)	Porosity			Gamma-Ray Index (percent)
			Density (percent)	Neutron (percent)	Sonic (percent)	
4,010-4,025	2.07	133	38	44	44	71
4,110-4,123	2.05	132.5	39.5	48	43.5	67
4,156-4,166	2.09	130	37	44	42.5	73
4,200-4,220	2.08	128	37.5	47	41.5	73
4,294-4,300	2.17	111	32	43	32	69
4,433-4,438	2.10	121	36.5	50	38	79
4,453-4,478	2.09	126	37	46	41	67
4,550-4,560	2.14	124	34	43	40	79
4,585-4,610	2.11	123	35.5	47.5	39.5	69
4,680-4,695	2.16	116	32.5	45	35.5	75
4,712-4,728	2.12	121	35	46	38.5	71
4,735-4,760	2.04	123	40	49.5	39.5	62
4,770-4,780	2.03	122.5	41	50	39	62

Table 9. Net sandstone, shale volume, effective porosity, and porosity-feet, Zone B: 3,868 to 5,010 feet

Interval (feet)	Net Sandstone Thickness <sup>1</sup> (feet)	Shale Volume Gamma-Ray Index (percent)	Shale Volume Neutron- Density (percent)	Effective Porosity			Porosity <sup>2</sup> x Feet
				Sonic (percent)	Neutron- Density (percent)	Average (percent)	
4,010-4,025	15	43	42	19	20	19.5	300
4,110-4,123	13	38	54	23	17	20	221
4,156-4,166	8	46	47	18	17.5	18	140
4,200-4,220	20	46	58	17	13.5	15	270
4,294-4,300	6	41	66	11	5.5	8	33
4,433-4,438	5	54	78	10	6	8	30
4,453-4,478	25	39	57	19	13.5	16	337.5
4,550-4,560	10	65	56	12	11	11.5	110
4,585-4,610	25	41	71	20	7.5	14	187.5
4,680-4,695	15	49	73	13	3.5	8	52.5
4,712-4,728	16	43	66	20	8.5	14	136
4,735-4,760	25	32	59	27	16	21.5	400
4,770-4,780	10	32	59	27	16.5	22	165

1. Net sandstone is defined as sandstone with an SP deflection of at least -10 millivolts

2. Neutron-density porosity

yield high shale volumes, however. Petrographic analysis of thin sections from core 2 indicates that the Vsh consists of about 70 percent intergranular shale matrix (dispersed shale) and 30 percent clay-rich lithic grains (structural shale). It also indicates that the Vsh from the log crossplot (70 percent) is high relative to visual estimates from thin sections (50 percent).

Dip angles are generally less than 10 degrees, with a few dips of 20 to 35 degrees. Because seismic sections do not show significant dips in reflectors above 12,800 feet, dips steeper than about 4 degrees are interpreted as crossbedding or miscorrelations. Rose diagrams of the dip directions are generally polymodal and vary considerably from plot to plot. The absence of consistent direction indicators suggests a depositional environment characterized by variable current directions.

No hydrocarbon shows were reported in tests of the rock cuttings samples from Zone B. The high background methane gas contents recorded by the mud log in Zones A-1 and A-2 decrease across Zone B from 100 gas units at the top to about 40 units at the base.

Bioturbation and the presence of marine fossils indicate deposition in a marine shelf environment. The increase in sandstone in this interval relative to that of the A Zones indicates higher depositional energy and suggests a mid-shelf environment.

#### Zone C-1 (5,010 to 5,360 feet)

This zone is characterized by thinly bedded sandstones with secondary interbeds of mudstone or claystone. The resistivity curves indicate that individual sandstone beds are generally 10 feet thick or less. There appears to be a significant increase in the sand/shale ratio in this zone (2.3) relative to Zone B (0.8). Lithologic data from core 3, sidewall cores, and cuttings indicate that the sandstone is friable, poorly sorted, very fine to fine grained, bioturbated, and muddy. In core 3, sandstone clasts (grains) are composed of about 25 percent quartz, with the remainder consisting of about equal parts feldspar and lithic fragments. The intergranular clay matrix consists of mixed-layer illite-smectite, smectite, chlorite, and minor amounts of illite.

The resistivity of the mud filtrate used in drilling this zone (and most of the remainder of the well) was about twice that used in drilling the upper 5,000 feet. Consequently, SP and resistivity curve deflections through sandstone intervals are amplified because of the greater resistivity contrast between the mud filtrate and the formation

water. The resistivity of sandstone in this zone is generally 1.5 to 2.0 ohm-meters (ohm-m). SP deflections are -10 to -25 mv. The gamma-ray log recorded little or no contrast in radioactivity between the sandstones and mudstones, which suggests a high clay content in the sandstones.

Sandstones with some permeability (indicated by SP deflections of at least -10 mv) were evaluated for reservoir potential. Aggregate sandstone determined in this way totals 127 feet in this zone. The data are shown in tables 10 and 11.

Density porosity in table 10 was calculated by using a matrix density of 2.67 g/cm<sup>3</sup> derived from the average sandstone grain density in core 3 (5,100 to 5,121 feet). The average density-log porosity matched the average core porosity within 1 percentage point. Average sandstone density porosities, uncorrected for shale content, vary from 30 to 32 percent in Zone C-2. Neutron-density effective porosities (table 11) range from 4.5 to 9 percent and average 6.5 percent. Shale volumes derived from the two different log techniques vary from 28 to 71 percent, but as in the overlying zone, about 30 percent of the Vsh consists of clay-rich lithic fragments (structural shale). Average effective porosity calculated from the neutron-density crossplot over the interval of core 3 and the effective porosity from thin sections of core 3 compare well; both average 6 percent.

No hydrocarbon shows were reported in tests on cuttings samples.

The Dipmeter arrow plot in this zone yields results similar to those obtained in Zone B, with most dips less than 10 degrees and variable in direction.

Marine fossils and the extensive bioturbation of the sandstone in core 3 indicate a marine shelf depositional environment. The high sand/shale ratio and thin-bedded character of the sands are attributed to low sand influx, episodic current transport (possible storm currents), and long residence times.

#### Zone C-2 (5,360 to 7,130 feet)

This interval is characterized by cycles of thick coarsening-upward sandstone beds. The beds range in thickness from 10 to over 100 feet, but most are in the 30- to 70-foot range. The sand/shale ratio is about 2.0 for this zone, with a total aggregate sand count of 1,180 feet. Net sand (defined by SP deflections of at least -10 millivolts) totals 945 aggregate feet. Lithologic data from conventional and sidewall cores and cuttings indicate poorly to well-sorted, bioturbated, very fine to fine-grained sandstone and muddy

Table 10. Sandstone interval log data and porosity averages, Zone C-1: 5,010 to 5,360 feet

Interval (feet)	Bulk Density (g/cm <sup>3</sup> )	Interval Transit Time (microseconds/foot)	Porosity			Gamma-Ray Index (percent)
			Density (percent)	Neutron (percent)	Sonic (percent)	
5,010-5,020	2.16	122	31.5	45	39	58
5,080-5,113	2.18	116	30	41	35	71
5,122-5,143	2.17	119	31	41.5	37	74
5,149-5,161	2.15	118	32	43	36.5	65
5,190-5,212	2.18	117	30	42.5	35	78
5,228-5,233	2.18	111	30	42	32.5	77
5,260-5,280	2.17	115	31	43.5	35	71
5,325-5,332	2.16	115	31.5	44	35	71

Table 11. Net sandstone, shale volume, effective porosity, and porosity-feet, Zone C-1: 5,010 to 5,360 feet

Interval (feet)	Net Sandstone Thickness <sup>1</sup> (feet)	Shale Volume Gamma-Ray Index (percent)	Shale Volume Neutron- Density (percent)	Effective Porosity			Porosity <sup>2</sup> x Feet
				Sonic (percent)	Neutron- Density (percent)	Average (percent)	
5,010-5,020	10	28	71	23	4.5	14	45
5,080-5,113	33	43	59	11	7.5	9	247.5
5,122-5,143	21	47	58	10.5	8.5	9.5	178.5
5,149-5,161	12	36	59	16	9	12.5	108
5,190-5,212	22	53	66	6	5	5.5	110
5,228-5,233	5	51	63	3	6	4.5	30
5,260-5,280	17	43	68	10.5	5	8	85
5,325-5,332	7	43	68	11	5.5	8.5	38.5

1. Net sandstone is defined as sandstone with an SP deflection of at least -10 millivolts

2. Neutron-density porosity

sandstone, interbedded with siltstone and silty mudstone. Sand grain and intergranular matrix compositions are similar to those of Zones B and C-1.

The gamma-ray curve, as in the overlying zones, displays little or no deflection through sandstone intervals. The SP curve, however, exhibits the largest deflections observed in the well, generally -25 to -30 mv. Although the magnitude of these SP deflections cannot be directly related to permeability, they do indicate that the best potential reservoirs in the well are within this zone. The sandstones are well defined by the resistivity curve as well, with resistivities of 1.5 to 2.5 ohm-meters against a shale background of 0.9 ohm-meters.

Density porosity (table 12) was calculated using a matrix density of 2.69 g/cm<sup>3</sup> derived from the average sandstone grain density data from core 5 (6,370 to 6,393.3 feet). Data from core 4 (also in this zone) were not used because this core sampled a high-density calcite-cemented interval, and the grain density values are not representative. Average density porosity calculated for the interval of core 5 was within 1 percentage point of the average core porosity. Average sandstone porosities calculated from the density log and uncorrected for shale content (table 12) range from 24.5 to 33.5 percent.

Sandstone porosities corrected for shale content are shown in table 13. Average values for neutron-density effective porosity range from 0 to 18.5 percent and have a mean value of 10.8 percent.

Effective mesoporosity determined by modal analysis of thin sections from core 5 averages 11.7 percent. Effective porosity calculated by the neutron-density crossplot method for the same interval averages 11.8 percent. The Vsh calculated from the neutron-density crossplot also matches the visual estimate quite closely. Both methods indicate a Vsh of 41 to 42 percent. The petrographic analysis indicates the Vsh consists of about 30 percent dispersed and 70 percent structural shale. This marks a notable decrease in the ratio of dispersed to structural shale from that in sandstones in Zones B and C-1, and indicates that sandstones in this zone are cleaner and better sorted.

Reservoir potential tends to be better in the upper parts of the sandstone beds in this zone. The SP and resistivity curves diverge upward and indicate that these sandstones grade upward from mudstone and siltstone near the base to relatively clean sandstone at the top. The upper contacts of these beds with overlying strata tend to be sharp, in contrast to the gradational lower contacts.

Table 12. Sandstone interval log data and porosity averages, Zone C-2:  
5,360 to 7,130 feet

Interval (feet)	Bulk Density (g/cm <sup>3</sup> )	Interval Transit Time (microseconds/foot)	Porosity			Gamma-Ray Index (percent)
			Density (percent)	Neutron (percent)	Sonic (percent)	
5,360-5,371	2.29	95	24.5	36	23.5	73
5,382-5,410	2.23	116	28	41	36	78
5,430-5,457	2.20	117	30	40	36.6	71
5,485-5,600	2.15	116	33	39	36	74
5,625-5,657	2.17	110	31.5	35.5	33	71
5,664-5,695	2.17	115	31.5	40	36.5	71
5,708-5,800	2.14	116	33.5	42.5	37	72
5,818-5,850	2.19	113	30.5	41	35.5	77
5,875-5,900	2.14	116	33.5	40	38	66
5,942-5,970	2.16	114	32.5	39	36.5	69
5,979-5,992	2.19	113	30.5	37	36	73
6,013-6,043	2.16	114	32.5	38	37	75
6,057-6,067	2.20	111	30	35.5	35	71
6,080-6,145	2.17	114	31.5	38	37	77
6,172-6,219	2.18	110	31	38.5	34.5	73
6,240-6,251	2.17	114	31.5	41	37	71
6,265-6,310	2.17	111	31.5	40	35.5	75
6,344-6,400	2.18	110	31	37	35	71
6,429-6,458	2.24	101	27.5	36.5	29.5	68
6,478-6,498	2.22	108	28.5	37	34	74
6,529-6,550	2.17	111	31.5	37.5	36.5	69
6,582-6,602	2.22	106	28.5	38	32.5	71
6,637-6,703	2.18	108	31	42	35	68
6,710-6,750	2.21	106	29	38.5	33	74
6,780-6,837	2.21	106	29	39.5	33.5	73
6,879-6,900	2.18	113	31	41.5	38.5	71
6,930-6,953	2.18	105	31	40.5	33.5	71
7,010-7,020	2.27	91	25.5	34	24	67

Table 13. Net sandstone, shale volume, effective porosity, and porosity-feet,  
Zone C-2: 5,360 to 7,130 feet

Interval (feet)	Net Sandstone Thickness <sup>1</sup> (feet)	Shale Volume Gamma-Ray Index (percent)	Shale Volume Neutron- Density (percent)	Effective Porosity			Porosity <sup>2</sup> x Feet
				Sonic (percent)	Neutron- Density (percent)	Average (percent)	
5,360-5,371	11	46	68	2.5	0	1	0
5,382-5,410	28	51	73	13	0	6.5	0
5,430-5,457	27	43	57	12.5	6	9	162
5,485-5,600	100	47	40	13	16	14.5	1,600
5,625-5,657	32	44	29	11	18.5	15	592
5,664-5,695	31	43	50	15	11	13	341
5,708-5,800	92	44	55	15	12	13.5	1,104
5,818-5,850	32	51	59	10	6	8	192
5,875-5,900	23	38	42	18.5	15.5	17	356.5
5,942-5,970	24	42	40	16	14.5	15	348
5,979-5,992	13	46	42	13.5	12.5	13	162.5
6,013-6,043	26	48	38	13	15.5	14	403
6,057-6,067	10	43	36	13	14	13.5	140
6,080-6,145	57	50	40	12	14.5	13	826.5
6,172-6,219	57	46	46	11.5	12	12	684
6,240-6,251	11	43	54	16	9.5	13	104.5
6,265-6,310	40	49	49	13	11	12	440
6,344-6,400	51	43	40	14.5	14.5	14.5	739.5
6,429-6,458	22	39	53	11	5	8	110
6,478-6,498	16	47	51	11.5	8	10	128
6,529-6,550	21	41	37	18.5	15	17	315
6,582-6,602	20	43	55	12	6	9	120
6,637-6,703	66	40	62	15.5	6	11	396
6,710-6,750	34	53	54	10.5	7	9	238
6,780-6,837	57	46	58	14	5	9.5	285
6,879-6,900	17	43	61	19.5	7	13	119
6,930-6,953	17	45	54	14	8.5	11	144.5
7,010-7,020	10	38	50	8	4.5	6	45

1. Net sandstone is defined as sandstone with an SP deflection of at least -10 millivolts

2. Neutron-density porosity

This type of vertical sequence suggests a progradational cycle of gradually increasing depositional energy and proximity to wave base during the deposition of each sandstone bed.

A few sandstone beds have blocky or fining-upward configurations on the SP and resistivity curves and probably represent a different sedimentary environment from that of the prograding sand bodies. Such profiles are characteristic of sandstones deposited in channels. These depositional sequence patterns, and the presence of bioturbated sediments, abundant marine fossils, and glauconite, all indicate deposition in a middle shelf setting. If these sands represent the distal facies members of a deltaic sequence, the clastic wedge with which they may be associated has not been identified within the basin.

Most dips recorded by the Dipmeter arrow plot are 10 degrees or less. Dip directions are quite variable. Aggregate dips and dips in mudstone and siltstone intervals have a small preferred northeast to southeast direction. Dips within sandstones are variable because of crossbedding. Consistent dip directions over small intervals of individual beds occur in many of the sandstones. A comparison of these directions suggests a small tendency toward a bimodal distribution with modes to the northwest-west and southeast.

The lithology log noted several intervals where samples yielded weak hydrocarbon shows in fluorescence tests of solvent cuts from cuttings samples. The fluorescence was an extremely pale to very pale milky-white cut with an extremely pale, yellow-white residue cut. This type of show was observed throughout most of the zone. No significant mud gas shows were associated with the intervals of sample fluorescence, and no gas effects were observed on the CNL-FDC log, although a small increase of about 10 units in background mud gas was registered from 5,965 feet to the base of the zone at 7,130 feet.

#### Zone D-1 (7,130 to 9,450 feet)

Zone D-1 is predominantly mudstone and claystone. Conventional and sidewall cores and cuttings indicate moderately bioturbated mudstone, sandy mudstone and claystone, and very muddy siltstone and sandstone. X-ray diffraction data indicate that the clay fraction is largely smectite with secondary amounts of chlorite and minor kaolinite and illite.

The SP and gamma-ray curves show very little or no deflection from the shale base line in this interval. The resistivity curves record small deflections from the top of

the zone to about 7,850 feet, possibly indicating thinner bedding of different lithologies in the upper third of the zone. Overall, the resistivity gradually increases from about 1 ohm-meter at the top of the zone to about 2 ohm-meters at the base. This gradual increase is a function of increasing compaction with depth and, possibly, a gradual downward increase in the quartz/clay ratio (indicated by X-ray diffraction data of bulk sediment contents from cores 6 through 9). An increase in the sand/mud ratio with depth is also indicated by the sidewall cores. In the lower third of the zone, the sidewall core samples are identified as very muddy, very fine grained sandstone.

The BHC log records a gradual decrease in average interval transit time from 110 to 100 microseconds/foot from the top of the zone to 9,050 feet. Below this (from about 9,050 to 9,450 feet), the sonic curve steepens and transit times decrease another 10 microseconds/foot in only 350 to 400 feet, a five-fold increase in the rate of change. The sonic curve is variable, with larger, more frequent deflections in the upper two-thirds of the zone. This is attributed to the thin, distinct bedding style in the upper third of the zone (also indicated by the resistivity curves).

The CNL-FDC logs were run 18 days later than the BHC log in this zone. Hole washouts and overall borehole size (recorded on the caliper curves) both increased considerably during this time, and the density and neutron curves were adversely affected. Washouts and hole enlargements were particularly severe from 7,460 to 8,160 feet. Here the density and neutron curves fluctuate wildly and are probably invalid. The high content of smectite, an expanding clay, in the mudstones of the upper part of the zone was probably a major factor in the severe washouts. Below 8,490 feet, the borehole size was generally within 1 inch of the bit size, and these two log curves are relatively stable.

In the basal 350 feet of this zone (9,050 to 9,400 feet) there is a noticeable increase in the rate of porosity loss with depth on the CNL-FDC logs. This is also indicated by measured porosities from conventional and sidewall cores, which show a loss of at least 5 percentage points across the basal zone. Core and density porosities above the interval are generally over 20 percent; below the interval they are generally less than 15 percent. This highly consolidated interval may be a "caprock" at the top of the major zone of abnormal pore pressure below 9,450 feet (see Abnormal Formation Pressure chapter).

Marine fossils, moderate bioturbation, poor sorting, and the predominantly mud and silt particle size indicate that

the depositional environment was probably outer shelf to upper slope. The upper half of the interval may represent a more distal, fine-grained facies of the sandstones of Zone C-2.

The Dipmeter arrow plot records dips of 10 degrees or less, probably structural in origin, that exhibit a strong north to northeasterly trend from the top of the zone to about 7,350 feet. From 7,350 to about 7,800 feet, the dip direction is variable, but has a general south to southeasterly trend, with local secondary trends to the northeast. From 7,800 to 9,000 feet, the dips steepen, with a considerable number between 10 and 35 degrees. High-angle dip measurements are scattered and probably spurious. Direction in this interval is even more variable, but two slight trends are apparent--one to the northeast and one to the northwest. From 9,000 to 9,450 feet, dips become shallower and have stronger directional trends to the northeast and northwest.

The lithology log records a few very poor oil shows (similar to those in Zone C-2 from 7,500 to 7,800 feet and from 8,300 to 8,500 feet). The shows are described as "poor to very poor, faint, milky yellow-white fluorescence cuts."

#### Zone D-2 (9,450 to 10,800 feet)

This zone is very similar to Zone D-1 and is distinguished mainly by the diagenetic alteration of the clays. The clays in this predominantly mudstone interval are mainly illite, mixed-layer illite-smectite, and chlorite, in contrast to mainly smectite in Zone D-1. The relative percentage of chlorite and illite increases with depth until chlorite and illite are the dominant clays at the base of the zone (AGAT, 1983).

Associated with the diagenetic alteration of smectite is the conversion of interlayer bound water in the clay into free pore water. Because the pore water requires 40 to 50 percent more space than the bound water, overpressuring of shale is frequently associated with this diagenetic change (McClure, 1977). A reversal in trend recorded by the resistivity, sonic, and density curves suggests overpressuring in this zone. From about 9,450 to 9,600 feet, the logs show decreasing resistivity, bulk density, and sonic velocity. Throughout the rest of the zone, these logs record little or no increase in bulk density or sonic velocity. Shale interval transit time, bulk density, and porosity are relatively constant at about 100 microseconds/foot, 2.60 to 2.63 g/cm<sup>3</sup>, and 13 to 16 percent, respectively.

The SP curve tracks the shale base line throughout the zone. The lithology log indicates the presence of limestone

and calcite concretions. Most of the local thin spikes on the resistivity, sonic, and density curves are a result of these thin carbonate beds and concretions.

The depositional environment is interpreted to be the same as that of D-1 because of similar lithology and fossil content. Zone D-2 may have been deposited slightly farther offshore as suggested by the lower sand and higher carbonate content of the sediments. The Dipmeter arrow plot records dips generally of 10 degrees or less. The principal dip direction is west with variation from the southwest to the northwest.

Traces of milky-white cut and residue fluorescence in cuttings samples were noted sporadically throughout this zone on the lithology log. From 10,070 to 10,080 feet, a strong milky fluorescent residue cut was noted.

#### Zone E (10,800 to 12,280 feet)

This zone is characterized by slightly silty claystone that is locally moderately burrowed. It contains marine microfossils and shell material. It is distinguished from the mudstone and claystone sequences of Zones D-1 and D-2 by its lower sand-silt fraction and a small change in the Dipmeter arrow plot. Dip measurements are more sporadic and slightly more variable in angle and direction in Zone E. This may be due to the less well stratified character of Zone E sediments relative to Zones D-1 and D-2.

Log responses in the upper half of Zone E are very similar to Zone D-2. The SP curve tracks the shale base line and the resistivity, sonic, and density curves record relatively constant shale responses of about 2 ohm-meters, 100 microseconds/foot, and 2.60 g/cm<sup>3</sup>, respectively. There is no gradual downward shift of these curves due to compaction, which may suggest the presence of overpressured conditions.

In the lower half of Zone E, below about 11,500 feet, two or three relatively long cycle shifts from 100 to 300 feet in thickness are recorded on the logs. The gamma-ray curve shows a shift with depth in the shale base line toward lower radioactivity. The SP curve records three long "fining upward" cycles. Within each of these SP cycles, the sonic curve exhibits a gradual downward increase in velocity followed by an abrupt shift to lower velocity near the base of the cycle. Resistivity in each cycle increases gradually downward, followed by an abrupt shift to lower resistivity near the base. The density curve records subtle though similar shifts through each cycle.

Associated with these log shifts, an increase in background gas and two gas peaks at or near the base of each of the lower two cycles were recorded on the mud log. These log shifts do not correspond to identifiable lithologic changes. Core 13 sampled the base of the highest "fining upward" cycle where the SP deflection was greatest, and a sidewall core sampled the equivalent section of the lowest "fining upward" cycle. Neither core showed any significant change from a claystone lithology. The apparent lack of lithologic change, the character of the log shifts, and the presence of gas peaks (characteristic of overpressured zones) suggest that the logs are responding to variations in free pore water of the overpressured shale.

The depositional environment for Zone E is interpreted to be outer shelf to upper slope because of the low sand and silt content of the claystone, moderate bioturbation, the type of marine fossil material, and the absence of high energy sedimentary structures.

#### Zone F (12,280 to 12,780 feet)

This zone is characterized by dark-gray, organic rich claystone with local limestone beds and calcite-filled fractures. The SP curve shows little deflection from the shale base line. The resistivity, density, and sonic curves record only minor deflections except across local thin limestone beds. The gamma-ray curve records the largest deflections (as much as 75 API units) observed within the Tertiary section. This is due to the large natural radioactivity contrast between relatively clean, clay-free limestones and organic-rich claystones (which are typically more radioactive than other sediments). The Natural Gamma Ray Spectroscopy Tool (NGT) indicates higher than usual proportions of uranium in the radioactive minerals in this zone. High radioactivity and uranium enrichment are often characteristic of organic-rich rocks (Meyer and Nederlof, 1984).

The Dipmeter arrow plot over the interval from 12,280 to 12,580 feet records dip angles chiefly of 10 degrees or less, ranging from southeast to northeast. From 12,580 to 12,780 feet, the dip angles are steeper, ranging from 6 to 26 degrees, with a more southerly direction, generally from southeast to south.

Oil shows in solvent cuts were reported on the mud log from 12,440 feet to near the base of the zone. The shows were described as "dull brown to gold fluorescence with slow to moderate, dull to strong yellow cuts." Relatively high background gas is recorded throughout the zone, with the highest levels from the base of the zone to a strong gas peak at about 12,570 feet.

The oil and gas shows and geochemistry (see Geochemistry chapter) indicate that the claystones of this zone contain the richest source rocks observed in the Navarin Basin COST No. 1 well. The dark color and high organic content of the claystones suggest that the sediments were deposited in an anaerobic environment. The fossil material indicates that the depositional environment was probably outer shelf to upper slope.

#### Zone G/H (12,780 to 15,300 feet)

This interval is characterized by very fine grained sandstone, siltstone, mudstone, and coal of Late Cretaceous age, intercalated with Miocene diabase and basalt sills. These rocks unconformably underlie the Eocene rocks of Zone F. The igneous sills range in thickness from less than 2 feet to 240 feet and compose about 40 percent of this interval. In the sedimentary intervals, coal beds are common and range in thickness from less than 1 foot to 28 feet.

This interval was divided into two different zones by AGAT (1983), chiefly because of the presence of secondary porosity in Zone G. However, because the logs, cores, and cuttings indicate that the two intervals are otherwise essentially identical, they are treated here as one combined zone.

The contact of this zone with Zone F is an angular unconformity which separates Cretaceous and Tertiary rocks. The Dipmeter arrow plot records a shift from dip measurements averaging 15 degrees to the southwest in the lower part of Zone F, to dips averaging about 30 degrees north-northwest in Zone G/H. The change occurs between 12,760 and 12,780 feet. No dips were recorded within this interval, so the exact contact cannot be determined. The contact is placed at the top of the resistivity break at 12,780 feet, which also marks the top of the first coal bed in the well.

Diabase and basalt intervals were identified by their characteristic responses on the sonic, density, and gamma-ray curves. The gamma-ray curve records blocky deflections of low radioactivity, generally of about 10 API units. Interval transit times generally average about 65 microseconds/foot, and bulk density is typically 2.60 to 2.80 g/cm<sup>3</sup>. The DIL tool response in igneous intervals was more variable. Resistivities range from 2 to 140 ohm-meters, but more commonly vary from 10 to 20 ohm-meters. The SP response tends to mirror the resistivity curves, with small negative SP deflections opposite zones of high resistivity.

Two zones of anomalously low bulk density (1.98 to 2.28 g/cm<sup>3</sup>) occur in diabase intervals from 12,980 to 13,020 feet and from 13,435 to 13,485 feet. The interval transit

time opposite these zones does not show a corresponding increase. This may indicate the presence of porosity (in vugs or fractures), which the BHC tool probably would not detect. A drilling break recorded in this interval also indicates the presence of some form of porosity. The CNL-FDC tool records a gas anomaly in the interval from 12,986 to 13,002 feet. The apparent porosity for this gas-bearing interval, calculated by subtracting the sonic porosity from the density porosity, is 25 percent. This large computed value is probably much larger than the actual porosity, however, because of the gas effect and the adverse borehole conditions indicated by the delta rho (DRHO) curve. The absence of significant SP deflections indicates that the porosity present is largely ineffective.

The numerous coal beds are identified by sharp, high resistivity peaks on the DIL curve, sharp peaks of long interval transit time (generally 115 to 150 microseconds/foot) on the BHC curve, sharp peaks of low bulk density (generally 1.60 to 2.0 g/cm<sup>3</sup>) on the FDC curve, and low values on the gamma-ray curve. The SP curve does not typically display a consistent response to coal, although the largest SP deflection recorded in the well occurs opposite the 28-foot-thick coal bed at 15,150 feet. This large deflection (50 mv) is attributed to permeability along fractures and cleats in the coal.

The sandstones are generally thin and tight; deformation and diagenesis have destroyed most of the original porosity. A few sandstones appear to have minor porosity and permeability, as indicated by small SP deflections and drilling breaks on the drilling-time log.

Porosity was calculated for two of the best sandstones (14,168 to 14,190 feet and 14,980 to 15,000 feet). Both exhibited drilling breaks, gas peaks, and small SP deflections of 10 to 15 mv. The sandstone at 14,168 feet was described on the mud log as unconsolidated, fine to coarse grained, with a white clay matrix. The sandstone at 14,980 feet was described as igneous, hard, fine to medium grained, moderately sorted, with abundant calcite cement and poor visible porosity. Porosity from the sonic and density logs corrected for shale content (as indicated by the gamma-ray log) averaged about 6 percent for the upper sandstone and about 13.5 percent for the lower sandstone.

The mud log recorded numerous gas kicks associated with the coal beds. All of this gas was probably generated from coal.

The presence of coal, the fining-upward sandstones observed in the cores and logs, and the type of sedimentary structures observed in the cores indicate that the sedimentary rocks in Zone G/H were deposited in a nonmarine environment.

### Zone I (15,300 to 16,400 feet)

This interval consists of fractured dark-gray silty claystone and siltstone. The sediments are bioturbated and contain isolated, thin tuff layers. The fractures are commonly filled with calcite. The Dipmeter arrow plot indicates these rocks are dipping 20 to 30 degrees to the north.

The SP curve tracks the shale base line throughout Zone I. The DIL curve records a gradual increase in average resistivity with depth from about 3 to 5 ohm-m at the top to about 20 to 40 ohm-m at the base. The increase in average resistivity with depth is related to compaction, as indicated by the sonic curve of the BHC tool and the density curve of the FDC tool. Both sonic velocity and bulk density gradually increase with depth. Average interval transit time decreases from about 82 to 66 microseconds/foot, and average bulk density increases from about 2.60 to 2.65 g/cm<sup>3</sup>.

The depositional environment for this zone is interpreted to be marine shelf or slope because of the dominantly silt to clay grain size and the bioturbation of the sediments. Marine macrofossils are also present.

### SUMMARY OF RESERVOIR QUALITY

The best potential reservoirs in the Navarin Basin COST No. 1 well are in the Tertiary (Miocene to Oligocene) sandstone sequence from 3,860 to 7,130 feet. The Late Cretaceous sandstones below 12,800 feet have lost almost all effective porosity because of a complex history of burial, compaction, deformation, and diagenesis.

Figure 54 shows the relationship between porosity and permeability for Tertiary sandstones in this well. The graph was constructed by using data from conventional cores 2 through 5. Modal analyses of effective mesoporosity from thin sections and core porosity measurements were plotted against corresponding permeability measurements. Although the resulting plots are scattered, there is a significant correlation between porosity and permeability. A linear regression (least squares) of effective porosity versus the logarithm of permeability (fig. 54, line A) suggests the following general relationship between effective porosity, permeability, and sandstone reservoir quality:

<u>Porosity (Percent)</u>	<u>Permeability (Millidarcies)</u>	<u>Reservoir Quality</u>
15-20	>70	Good
10-15	10-70	Fair
<10	<10	Poor

Because the neutron-density effective porosities closely match the thin-section effective porosities, the Tertiary sandstones can be evaluated for general reservoir quality by using neutron-density effective porosities and the criteria in the above table. The relationship between measured core porosity and permeability (fig. 54, line B) was not used because of the large shale porosity component in these measurements and the poor relationship at low permeabilities. The reservoir quality of the lithologic zones is summarized as follows:

Zone B - The reservoir quality ranges from poor to good, with roughly equal amounts of the total 193 feet of sandstone in each category. These sandstones are thin with generally high dispersed-shale contents, however. The shallow burial depths and low compaction account for most of the good reservoir characteristics.

Zone C-1 - The reservoir quality is poor because the sandstones are thin, dirty, and tight.

Zone C-2 - The reservoir quality ranges from good to poor. This zone contains the best potential reservoir rocks observed in the well. Five sandstones, ranging from 21 to 100 feet in thickness (202 feet aggregate), are rated as having good reservoir quality; nine sandstones, ranging from 10 to 92 feet in thickness (375 feet aggregate), may be considered fair reservoirs; and fourteen sandstones, ranging in thickness from 10 to 66 feet (368 feet aggregate), fall into the poor category.

## ABNORMAL FORMATION PRESSURE

by

Kirk W. Sherwood

### INTRODUCTION

The possible existence of abnormal pore pressures in the Navarin Basin COST No. 1 well was first suggested by operational problems encountered while drilling the well. These problems included sloughing shale, increased background gas, high connection/trip gases, and stuck pipe at 13,906 feet. The stuck pipe necessitated a sidetrack and redrill. Velocity profiling (acoustic log analysis) documented the presence in the lower parts of the well of a significant velocity inversion, thought to be a manifestation of abnormal formation pressure. Because of the potential effect of a large sequence of overpressured rock on seismic interpretation throughout the basin and because of the potential hazards that excess formation pressures present to drilling operations, the Minerals Management Service undertook a study of the overpressuring phenomenon.

### DOCUMENTATION OF ABNORMAL PRESSURE GRADIENTS

The preferred way to identify the interval and magnitude of abnormal pressure in a well is to measure formation pressures directly through conventional drill stem production tests or wireline devices such as the Schlumberger Repeat Formation Tester (RFT). Graphical displays of such pressure data plotted versus burial depth ("pressure profile plots") characterize abnormal pressure zones as intervals in which pressure increases more rapidly with burial depth than in the overlying (or underlying) parts of the sedimentary section. In such intervals, the share of the weight of the overlying rock-fluid mass borne by the pore fluids (as opposed to the enclosing rock fabric) exceeds the pressure exerted only by the fluid column. The point of change in slope (inflection point) in the pressure curve represents the top of the overpressured interval and is thought to mark a seal or barrier to the normal upward expulsion or migration of pore fluids. A typical pressure profile is illustrated in figure 55. Note that at least two valid pressure measurements on opposite sides of the seal are needed to define the top of the overpressured zone.

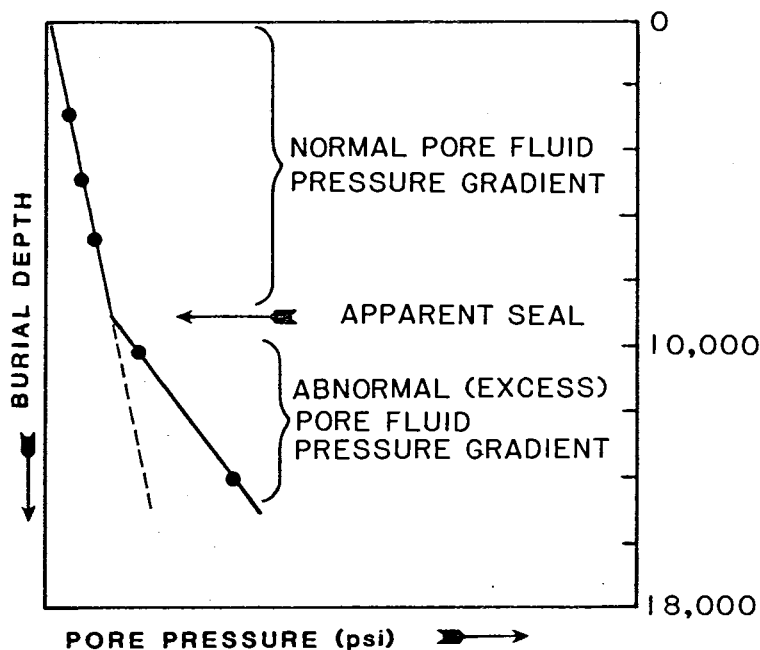


**FIGURE 55.**

SCHEMATIC DIAGRAM ILLUSTRATING TYPICAL PORE PRESSURE PROFILE ACROSS TRANSITION FROM NORMALLY PRESSURED SEQUENCE INTO UNDERLYING OVERPRESSURED INTERVAL. Inflection point marks apparent seal at top of overpressured interval.

Only a limited number of direct pressure measurements are available in the Navarin Basin COST well. A drill stem test (DST) was conducted through perforations over the interval from 6,278 to 6,298 feet. (All depths referred to in this chapter are measured from the Kelly Bushing unless otherwise indicated.) In addition, 61 open-hole RFT tests were attempted over the interval from 1,828 to 12,809 feet. Of these 61 tests, only 17 (or 28 percent) were successful. The successful tests span the interval from 1,828 to 10,248 feet. The remaining 44 attempts failed because of lost seal (mud test) or impermeable formation. The results of the DST and RFT tests are summarized in the pressure plot of figure 56. Only a single pressure measurement, an RFT test at 10,248 feet, was successfully obtained within the apparent

overpressured interval. This test obtained a pressure of 5,320 pounds per square inch (psi) at 10,163 feet subsea depth (SSD), yielding a pressure gradient of 0.524 psi/foot or 10.09 pounds per gallon (ppg) mud equivalent. This pressure value clearly deviates from the "normal" gradient of 0.452 psi/foot (8.71 ppg) obtained as an arithmetic average of the 16 tests in the interval from 1,828 to 6,944 feet. This gradient is identical to that found in the North Sea (McClure, 1977, p. AP-2), but is somewhat less than the 0.468 psi/foot gradient in the Gulf of Mexico. The RFT test at 10,248 feet measured a static mud column pressure underbalance of 100 psi relative to formation pore pressure at the time of the test.

In the absence of direct pressure data, wireline well logs which measure formation properties such as resistivity, conductivity, acoustic transmission velocity, and density may be employed to obtain an estimate of formation pore pressure. Regional studies have shown that the formation resistivity, sonic velocity, and density of sediments rise progressively and systematically with burial load. These changes in physical properties are attributed to tighter particle packing, greater interparticle bonding, and the introduction of occluding chemical cements. Collectively, these processes result in a decrease in bulk porosity and the expulsion of pore fluids. In zones of abnormal pore pressure, these normal processes are reversed or nullified because of pore fluid retention, resulting in increased total porosities and fluid content and in reduced shear strength and rigidity of the rock bulk.

The alteration of rock properties and pore fluids within overpressured zones is reflected in the measurements obtained from wireline logs. In log profiles of rock resistivity, velocity, and density, an overpressured zone is manifested as a reversal or deviation from the compaction trends seen in the normally compacted, overlying sequence. Thus, within zones of abnormal pore pressure, values for density, velocity, and resistivity are less than those typically found in "normal" sediments at that depth, and occasionally less than like values for sediment at shallower depths in the same well. Resistivity values in overpressured zones may depart radically from normal compaction trends, because in addition to the effect of higher pore fluid content, the retained fluids in overpressured zones may be more saline than those in the overlying, normally compacted sequence (McClure, 1977, p. I-18). These changes affect all lithologies, but are most consistent

## MEASURED PORE PRESSURES

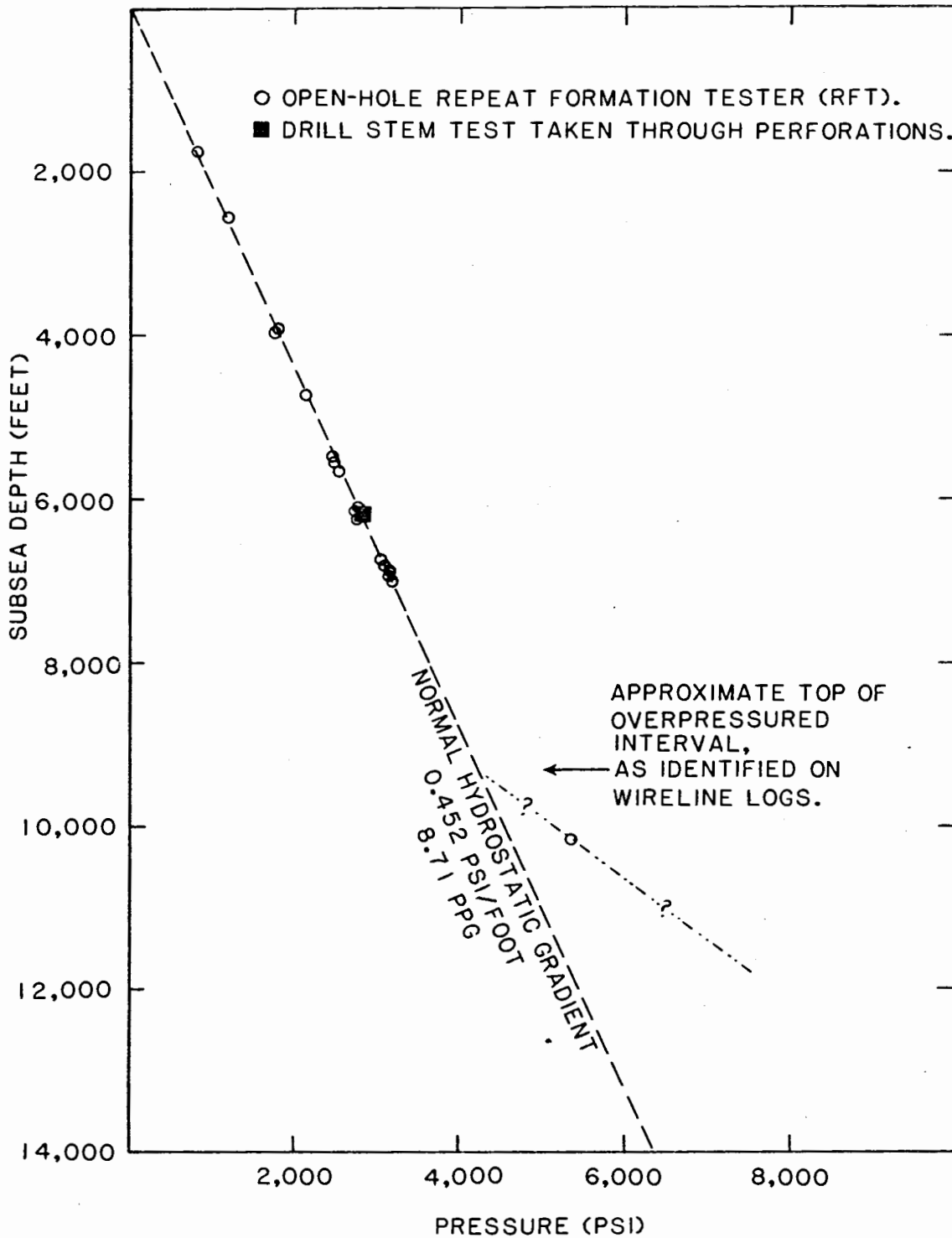


**FIGURE 56.** PLOT OF FORMATION PORE PRESSURES VERSUS SUBSEA DEPTH FOR NAVARIN BASIN COST NO. 1 WELL. The pressure measurements above 8,000 feet collectively define an average "normal" hydrostatic gradient of 0.452 psi/foot, shown as a dashed line. Only one valid measurement was obtained within the zone of suspected abnormal pressure, where an RFT test at 10,163 feet (subsea depth) yielded 5,320 psi on pressure buildup, or 726 psi greater than that anticipated (4,594 psi) if normally pressured. A second measurement elsewhere within the zone of abnormal pressure would be required to independently define its pore pressure gradient.

and easily compared in shales. A schematic illustration of the effect of abnormal pore pressure on shale properties as measured on wireline logs is presented in figure 57.

Empirical studies, such as the pioneering paper by Hottmann and Johnson (1965), have shown that the anomaly (or amount of departure from normal values of shale resistivity, density, or velocity) can be quantitatively related to actual pore pressure. The proper evaluation of formation pressures through analysis of log data hinges on three factors: (1) the proper identification of "pure" shales through simultaneous analysis of the SP, gamma-ray, and CNL-FDC logs so as to eliminate the component of log response related to compositional changes; (2) the availability of sufficient data from a column of normally pressured sediments to allow the delineation of a normal compaction trend for the local basin; and (3) the availability of sufficient direct pressure measurements from overpressured formations to allow the establishment of a relationship between the shale anomaly and shale pore pressure.

Empirical curves for the second and third factors above have been generated by Hottmann and Johnson (1965, p. 720, fig. 5; p. 721, fig. 6) and MacGregor (1965) for the Oligocene-Miocene of the Gulf Coast. Studies of wider scope (Wallace, 1965) have generated world composite curves that are applicable to most sedimentary basins characterized by more or less continuous deposition. The world composite curves are valuable in frontier basins where data are insufficient to establish local evaluation curves. Useful general curves have been published by Pennebaker, Jr. (1968a, 1968b; and in McClure, 1977, p. IV-7, 8, and Appendixes) and by Drilling Well Control, Inc., of Lafayette, Louisiana (Stewart, 1983, p. 40).

#### COMPOSITE BERING SHELF SHALE VELOCITY COMPACTION CURVE

Prior to analysis of the apparent overpressured interval in the Navarin Basin COST No. 1 well, an attempt was made to establish a normal compaction curve for the basin by following the guidelines of Stewart (1983). On the Gulf Coast, the logarithm of shale velocity was shown to vary linearly with burial depth to depths of at least 14,000 feet (Hottmann and Johnson, 1965, p. 719, fig. 2), while the logarithm of shale resistivity was shown to vary nonlinearly with burial depth (Hottmann and Johnson, 1965, fig. 6). The shale velocity data set was thus selected for study because it seemed more amenable to simple statistical analysis. A composite Bering shelf curve was obtained by crossplotting acoustic velocity and burial depth for the following data sets:

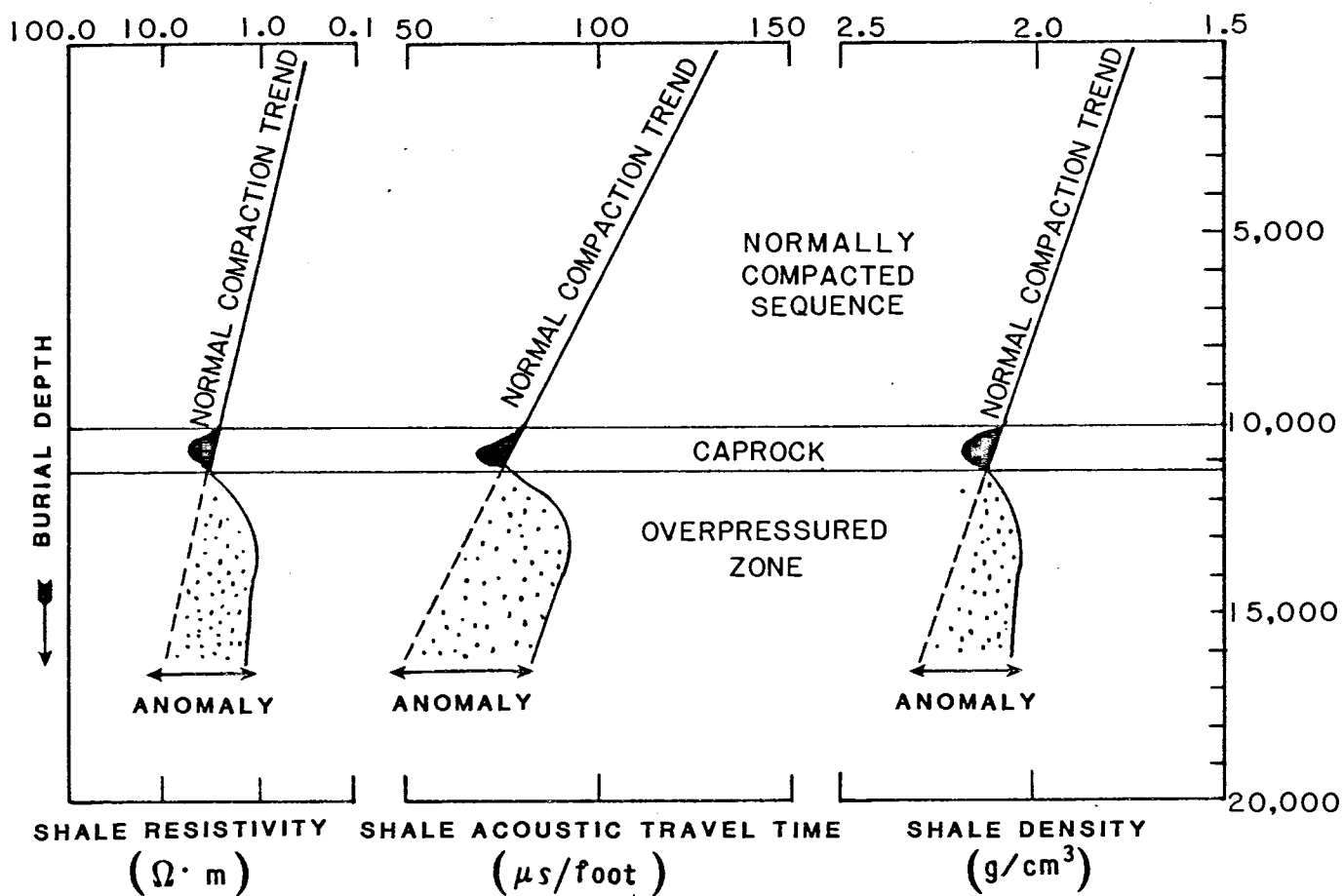


**FIGURE 57.** SCHEMATIC DIAGRAM ILLUSTRATING TYPICAL EFFECT OF ABNORMAL FORMATION PRESSURES ON SHALE RESISTIVITY, SHALE ACOUSTIC VELOCITY, AND SHALE DENSITY. If sufficient empirical data are available, the amount of departure from a normal compaction trend ("anomaly") can yield a quantitative estimate of formation pressure. Modified after Fertl (1976, p. 226, fig. 5.44).

(1) The interval from 1,800 to 9,430 feet (Pliocene to late Oligocene age sediments) in the Navarin Basin COST No. 1 well. This interval appeared to be normally compacted, and direct pressure measurements (fig. 56) confirmed the presence of normal pore pressures.

(2) The interval from 1,800 to 10,368 feet (Pliocene to Eocene age sediments) in the St. George Basin COST No. 1 well (Turner and others, 1984a). Shales within the Tertiary volcanic sequence below 10,380 feet were not included in the analysis because they were considered to be nonrepresentative.

(3) The interval from 1,980 to 12,510 feet (Pliocene to Oligocene age sediments) in the St. George Basin COST No. 2 well (Turner and others, 1984b). Cretaceous sediments below the unconformity at 12,540 feet were not included in the analysis.

All three data sets were posted on semilog paper and analyzed to see whether sufficient coherence existed to permit definition of a single "type" compaction trend for Bering Sea wells. This data is presented in plate 2. Visual inspection suggests fairly close agreement among shale velocity data for the three wells. Simultaneous linear regression of all three data sets in the natural logarithm mode yields a line defined by the function:

$$\text{LN (travel time)} = 5.267 - (\text{subsea depth (feet)}/12,061 \text{ feet})$$

The visual coherence of the data is confirmed by a correlation coefficient of 0.9731 for the line.

Although it differs in detail, the shale velocity compaction curve is comparable to that established for the Miocene-Oligocene of the Gulf Coast by Hottmann and Johnson (1965), as illustrated in figure 58. Any depth-versus-travel-time shale point which plots a significant distance to the right of this Bering Sea curve is considered to be overpressured. Intermediate sonic-log runs which identify shale exhibiting travel times higher than those predicted by this curve should be analyzed for pore pressure estimates, and mud weights should be modified accordingly before the resumption of drilling. Methods of analyzing travel-time anomalies to derive pressure estimates are discussed in a separate section below.

The Bering shelf shale velocity curve displayed in plate 2 intersects the theoretical compaction limit of 62 microseconds/foot for pure shale at a subsea depth of 13,750 feet. Therefore, at depths below 13,000 feet, the compaction function probably becomes nonlinear (in semilog space) and asymptotically approaches the theoretical limit of 62 micro-

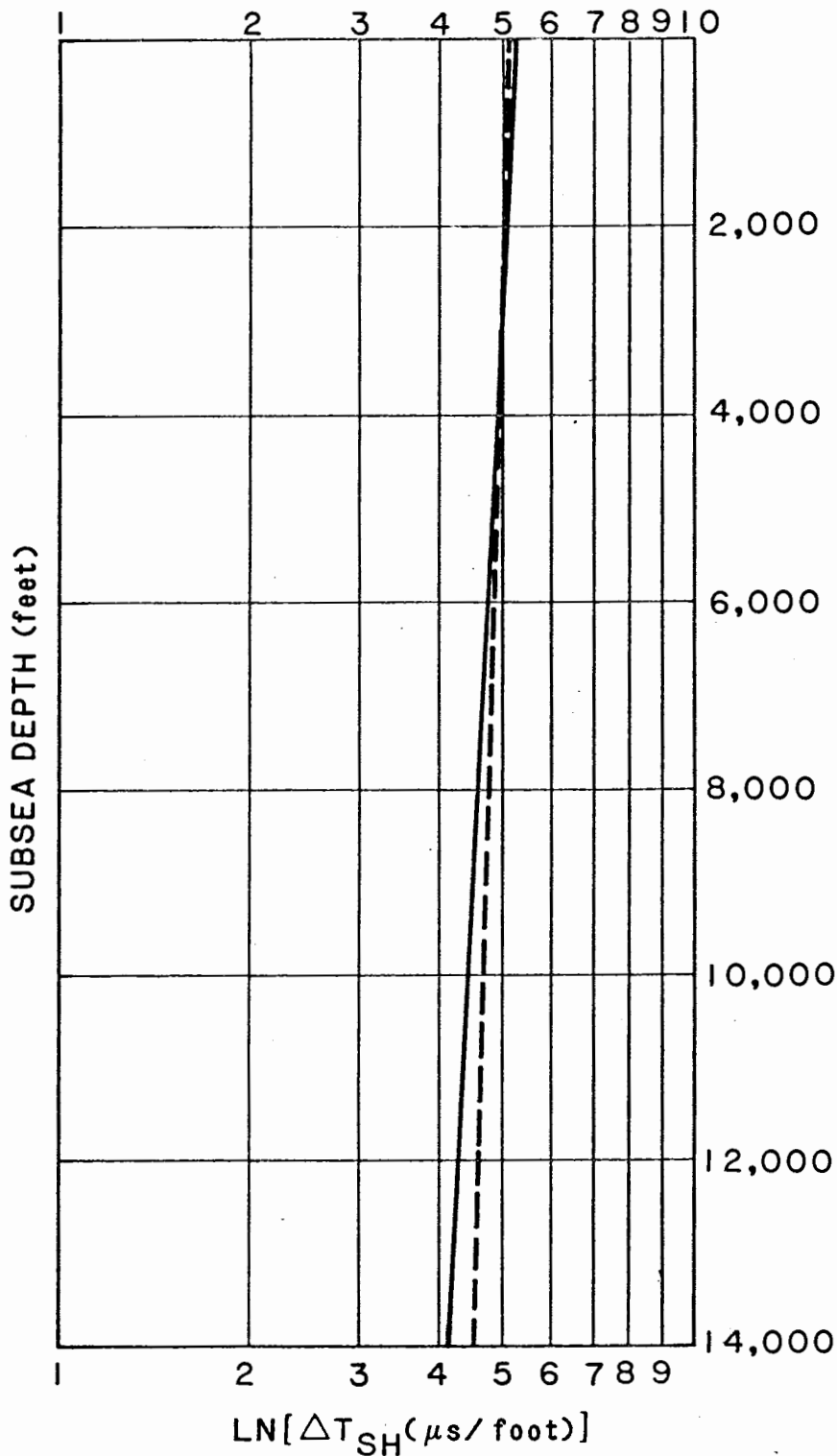


**FIGURE 58.**

BERING SEA TERTIARY SHALE ACOUSTIC TRANSMISSION AS A FUNCTION OF DEPTH,  $\text{LN}(\Delta T) = 5.267 - (\text{DEPTH} / 12,061 \text{ FEET})$ , AS OBTAINED IN PLATE 2. Bering Sea curve shown as solid line. Dashed curve is shale transmission versus burial depth for Miocene and Oligocene shales of the upper Texas and southern Louisiana Gulf Coast (adapted from Hottmann and Johnson, 1965, p. 719, fig. 2).

seconds/foot. However, no representative data are available to evaluate possible nonlinearity of the curve at these depths.

Shale velocity data for the Navarin Basin COST No. 1 well are presented with the Bering shelf shale velocity compaction curve in figure 59. A dramatic departure of shale velocities from the normal trend is clearly present below approximately 9,430 feet. The travel-time anomaly increases downward from 9,430 to approximately 14,500 feet, where it then begins to decrease. At total depth (16,400 feet), shale velocities have nearly returned to values normal for that depth. The data also suggest a zone of slight overpressure from approximately 2,500 to 3,840 feet.

Shale velocity data are presented in a different format in figure 60 along with superimposed evaluation curves for pore fluid pressure gradient (after McClure, 1977). The evaluation curves may be used to estimate pore pressures directly, as is done in a separate section below. This plot (fig. 60) also suggests the existence of a very significant shale velocity anomaly below 9,430 feet. The evaluation curves indicate formation pressure gradients as high as 16.5 ppg mud weight equivalent.

#### SHALE RESISTIVITY

Shale resistivity data for three Bering Sea wells are presented in plate 2 along with nomographic curves for evaluating pore pressure. Resistivity data exhibit more scatter than velocity data, probably because of their greater sensitivity to subtle variations in shale mineralogy (particularly the presence of iron-rich minerals like chlorite and glauconite). A clustering of data points is clearly present down to approximately 9,300 feet SSD, with very good agreement between the Navarin No. 1 and St. George No. 2 data sets. Below this depth, the normal positive relationship between shale resistivity and burial depth is clearly reversed in the Navarin Basin COST No. 1 well. If the shale resistivity curve for the St. George Basin COST No. 2 well is conditionally accepted as a normal configuration for the Bering shelf, then the point of reversal in the Navarin data trend is also the point of departure from "normal." Thus, the shale resistivity data appear to confirm the conclusion drawn from the shale velocity analysis that a major zone of abnormal pore pressure exists below 9,430 feet in the Navarin well.

Depressed shale resistivity values in the interval from 2,500 to 3,840 feet suggest the presence of an additional zone of excess pore pressure. This resistivity anomaly, however, may be due in part to high resistivities in response

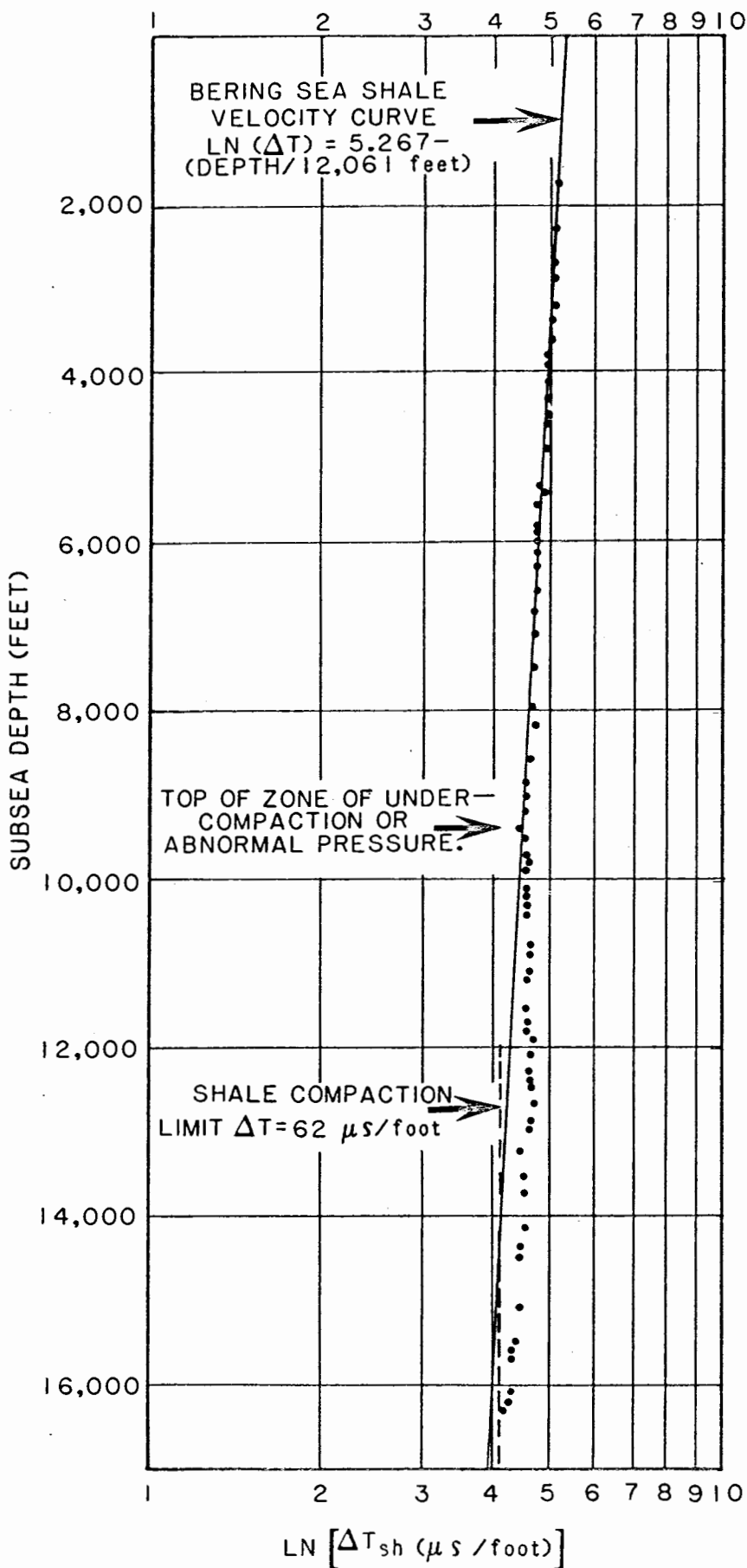


**FIGURE 59.**

SHALE TRAVEL TIME VERSUS DEPTH FOR NAVARIN BASIN COST NO. 1 WELL. The solid line is a composite of shale data from St. George Basin COST No. 1 well, St. George Basin COST No. 2 well, and Navarin Basin COST No. 1 well, as obtained in the analysis presented in plate 2. The solid line represents the normal relationship of shale velocity to burial depth in Tertiary sediments of the Bering Sea shelf. Shales which plot to the right of this curve are considered to be undercompacted or to possess abnormally high pore pressures. The top of the zone of abnormally high pore pressures lies at approximately 9,345 feet subsea depth (9,430 feet measured depth) in the Navarin Basin COST No. 1 well. This reversal in compaction trend corresponds to similar reversals in wireline log resistivity and density curves and actual shale density measurements (plate 2; figs. 60, 61). The dashed line in the lower part of the graph corresponds to the theoretical shale compaction limit at  $\Delta T = 62$  microseconds/foot.

to fresh (nonsaline) pore fluids in the interval above 2,500 feet. Examples of this commonly observed effect are illustrated by Fertl (1976, p. 220, fig. 5.38).

### SHALE DENSITY

Shale density data were also examined for evidence of trend reversal or anomalous densities in the zones of suspected overpressure identified by the resistivity and velocity data. Two data sets were analyzed: (1) shale densities obtained from the Schlumberger Compensated Formation Density (FDC) log and (2) density measurements obtained at the well site by Exploration Logging (USA), Inc. (EXLOG), personnel using the fluid density gradient column technique. Well site shale density data are recorded on the "Drilling Data Pressure Log," incorporated with the Final Well Report submitted to the operator (ARCO) by EXLOG (1983). Both data sets are plotted against burial depth in figure 61, along with evaluation curves for fluid pressure gradient (after McClure, 1977).

Shale densities depart from a normal compaction configuration in the interval from 2,500 to 3,840 feet. The density deficit suggests the presence of excess pore pressures. The evaluation curves suggest counterbalance mud weight gradients as high as 13 ppg in this interval (fig. 61). Densities progressively increase with burial depth between 3,840 and 9,430 feet, where a value of approximately 2.4 grams/cubic centimeter ( $\text{g/cm}^3$ ) is reached. Below 9,430 feet, instead of increasing with burial depth, densities remain constant at  $2.4 \text{ g/cm}^3$  down to the basal Tertiary unconformity at 12,780 feet (12,695 feet SSD). Shale density slowly increases with depth within the tilted Cretaceous strata, but does not return to a normal compaction gradient until a depth of approximately 15,700 feet. The evaluation curves (after Pennebaker, in McClure, 1977) superimposed on figure 61 indicate the presence of fluid pressure gradients as high as 12.5 ppg mud weight equivalent in the zone below 9,430 feet.

In conclusion, shale density data also suggest the presence of large sections of overpressured rock from 2,500 to 3,840 feet and from 9,430 to 15,700 feet, confirming the results of shale resistivity and shale velocity analyses.

### DRILLING EXPONENT

Concurrent with the drilling of the Navarin Basin COST No. 1 well, EXLOG continuously monitored formation pressure through the drilling exponent method. This is an empirical method of pressure detection with some theoretical basis that has proven useful in many areas. The fundamental assumption

underlying the drilling exponent method (or "d" exponent method) is that the rate of penetration is directly dependent upon the differential pressure at the rock face being drilled. Differential pressure is here defined as the difference between formation pore fluid pressure and the pressure exerted at the bottom of the hole by the column of drilling fluids in the well bore. An underbalanced condition (where formation pore pressure is greater) generally promotes faster and more efficient drilling as long as hole stability is maintained. However, an underbalanced condition poses the risk of movement of formation fluids into the well bore. Conversely, overbalanced conditions result in slower penetration rates, but improved hole stability and control of formation fluids. Therefore, if all drilling parameters (including mud weight, viscosity, bit weight, bit type, bit dullness, jet ports, rotation rate, hole size and orientation, downhole drilling assembly, and lithology) are kept constant, the penetration rate should significantly increase when the well bore passes from a normally pressured section into a section with excess pore pressures. The greatest difficulty in the use of this outwardly simple empirical method involves proper evaluation of the individual and interactive effects of the numerous drilling variables on penetration rate. These variables change constantly because of the very nature of the operations. Thus, one must evaluate whether a sudden jump in penetration rate is due to overpressure, or to one or several other factors. An excellent summary of the basic method is found in Jordan and Shirley (1966). Specific details of the normalized technique used by EXLOG are published in EXLOG manuals MS-156 and MS-196.

The results of the EXLOG pore pressure computations are summarized in figure 62. A dashed line representing the normal hydrostatic gradient derived from actual pressure test data is also shown. Minor pore pressure anomalies appear to be present as "bulges" in the distribution of data in the intervals from 2,500 to 3,840 feet and from 6,800 to 8,100 feet. These "bulges" correspond to anomalies in the shale velocity data (fig. 60). However, only the upper anomaly between 2,500 and 3,840 feet is supported by the shale density data (fig. 61). In their final report, EXLOG (1983) noted that a normal compaction trend was observed between 1,509 and 5,300 feet. They also identified the possible presence of excess pore pressures in the interval from 6,540 to 7,520 feet on the basis of drilling exponent trends, tight hole problems, splintery cuttings, mud pit gains, and increased gases associated with overpull on connections. Actual pressure measurements in the uppermost part of this interval, however, indicate

**FIGURE 60.** SHALE INTERVAL TRAVEL TIME VERSUS DEPTH FOR THE NAVARIN BASIN COST NO. 1 WELL. The composite normal curve for Bering shelf shales of Eocene to Holocene age (as obtained in plate 2) is also depicted along with a set of calibration curves for pore pressure gradients through the zones of apparent  $\Delta T$  anomaly and abnormal pore pressure from 2,500 to 3,800 feet and from 9,345 to 16,200 feet (subsea depth). The pressure gradient curves are those formulated by E. S. Pennebaker, Jr., and published as pressure reader charts by McClure (1977, p. IV-7, 8, and appendixes). The distribution of shale velocity data indicates that mud weight gradients as high as 16.5 pounds per gallon would be needed to balance formation pore pressures in some zones below 9,345 feet (subsea depth).

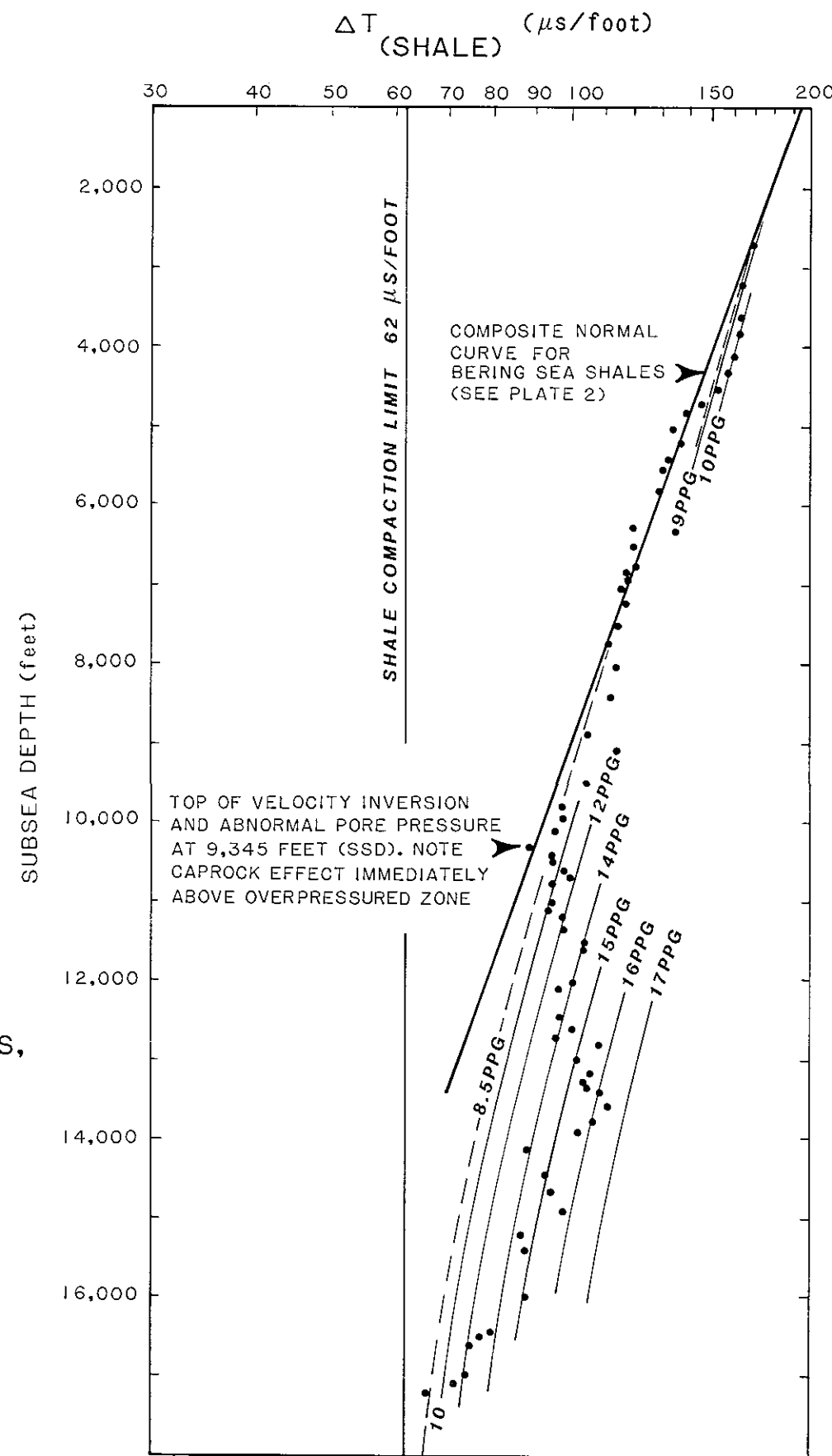


**FIGURE 60.**

**FIGURE 61.** PLOT OF SHALE DENSITY VERSUS SUBSEA DEPTH FOR NAVARIN BASIN COST NO. 1 WELL. Nomographic curves for apparent pore pressure gradient are depicted through zones exhibiting anomalous densities due to overpressured conditions. This analysis of the shale density data indicates that mud weight gradients as high as 13.0 pounds per gallon would be needed to control formation pore pressure in some zones below 9,345 feet (subsea depth) and in the interval between 2,000 and 3,800 feet (subsea depth). The pressure gradient curves are those formulated by E. S. Pennebaker, Jr., and published as pressure reader charts by McClure (1977, p. IV-7, 8, and appendixes).

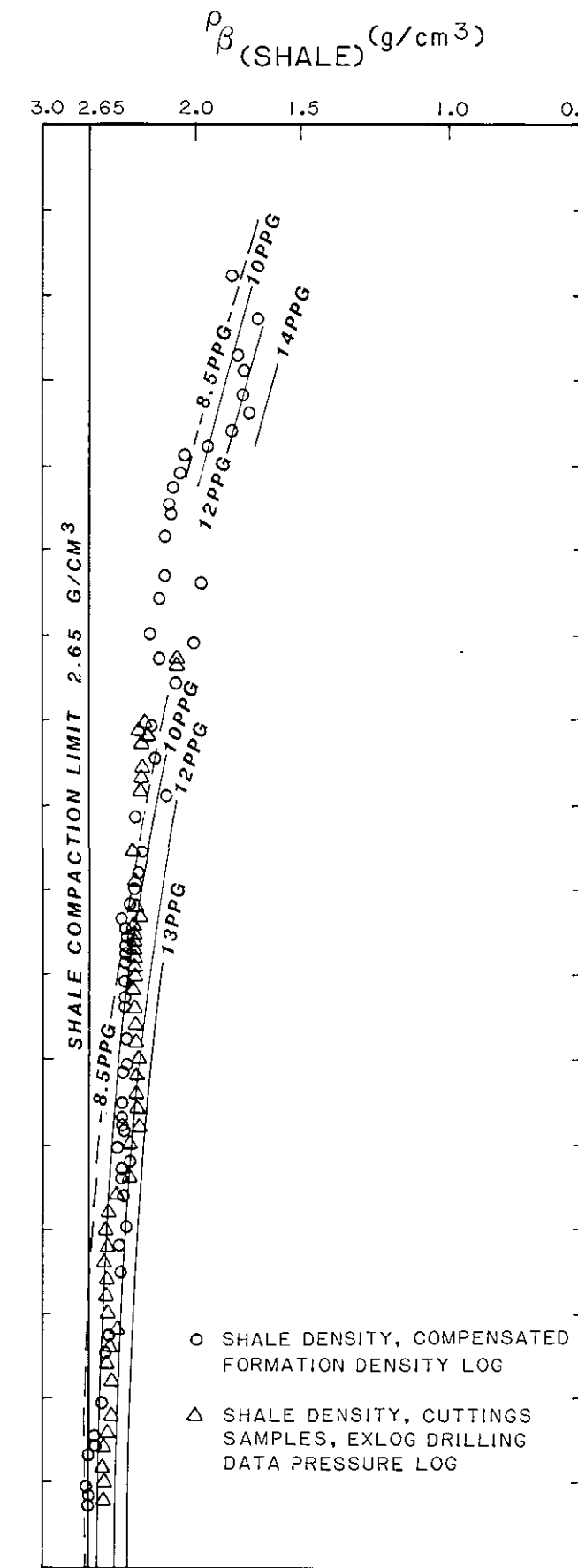


**FIGURE 61.**

**FIGURE 62.** PORE PRESSURE ESTIMATES FROM DRILLING PARAMETERS, NAVARIN BASIN COST NO. 1 WELL. Pore pressures were obtained by Exploration Logging, Inc., concurrent with the drilling of the well. The pore pressure data are modified after those presented in the pressure evaluation log included with the final well report submitted by Exploration Logging, Inc. The theory and methods of this technique for pressure evaluation are presented in Manuals MS-156 and MS-196, published by Exploration Logging, Inc. Small anomalies in the intervals from 2,500 to 3,800 feet and from 6,800 to 8,100 feet suggest overpressuring, and a very large increase in pore pressure is identified for the depth interval below 12,000 feet. The drilling-parameter method apparently failed to identify the zone of significant overpressure between 9,335 and 12,000 feet, which is clearly identified on wireline logs.

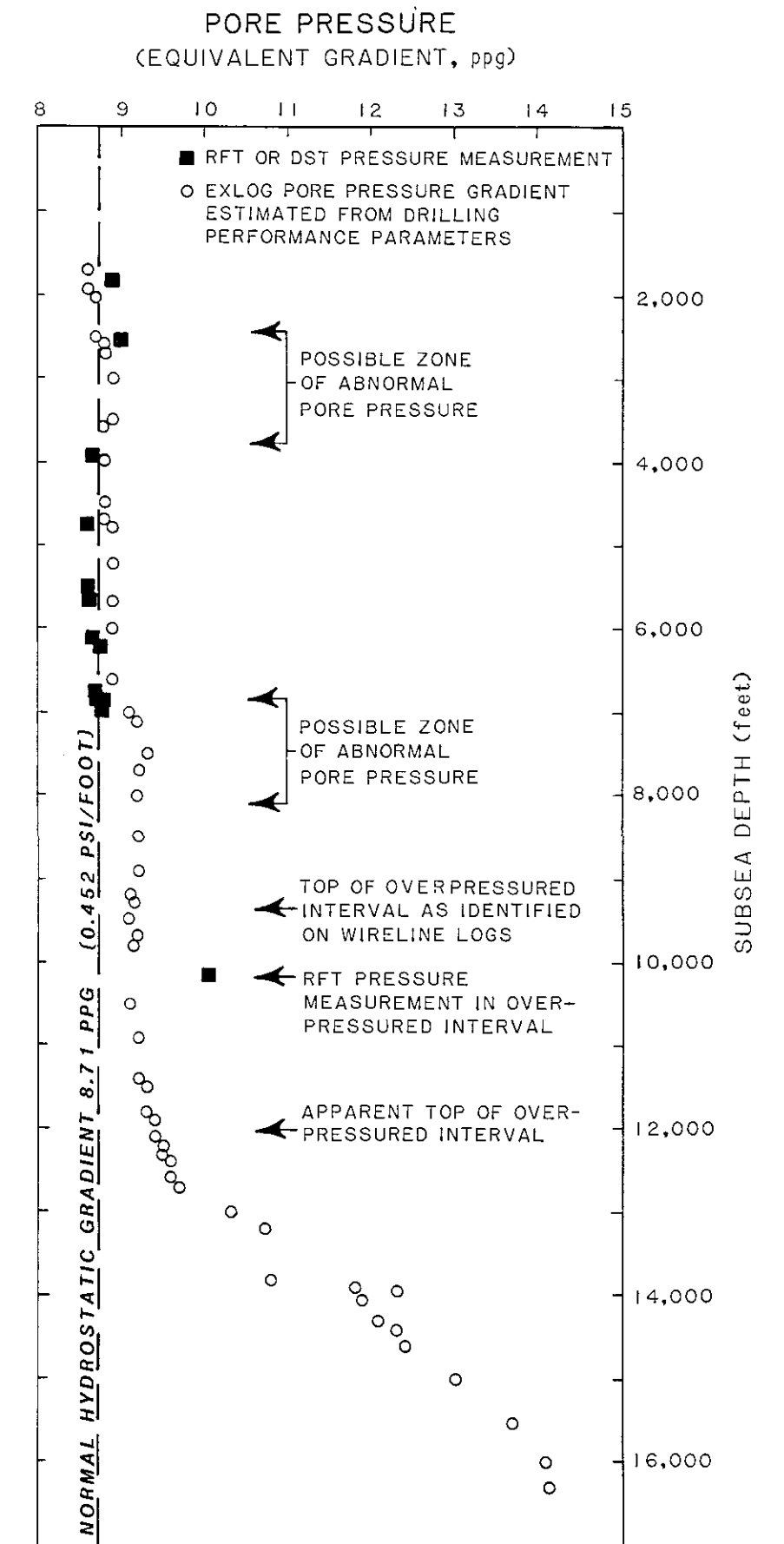


**FIGURE 62.**

normal pressures consistent with gradients measured above 6,540 feet (figs. 56 and 62). No direct pressure measurements were obtained in the interval exhibiting the apparent anomaly between 2,500 and 3,840 feet.

The top of the major overpressured zone at 9,430 feet is clearly defined on wireline log data. It is not, however, reflected in the drilling parameter pore pressure analysis. In their summary on formation pressures for this part of the well, EXLOG (1983) comments that:

"between 9100 feet and 10,000 feet, a strongly positive trend developed, with a flattened middle section reflecting lithological variations. Pore pressures were estimated at lying between 9.1 lb/gal and 9.2 lb/gal . . . From 10,000 feet to 12,834 feet, a flattened, more vertical trend was calculated from the predominantly siltstone lithology. This transition trend occurred with little rise in pore pressure to 11,500 feet."

However, in their operations summary EXLOG (1983) notes that:

"the region from 12,000 feet to 12,880 feet exhibited slight overpressure. Due to large trip gases, occasionally cutting the mud weight to 9.1 lb/gal from 10.6 lb/gal, diminishing kick tolerance, and some tight hole sections from 12,600 feet to 12,880 feet, the decision was made to set casing."

Below the casing shoe at 12,834 feet, where the operator raised the mud weight from 10.1 ppg to 10.9 ppg, an underbalanced condition appears to have been manifested by negative drill exponent trends (EXLOG, 1983), high flow check, connection and trip gases, and unstable hole conditions. These conditions led to a stuck and abandoned drill string, which necessitated a sidetrack at 13,537 feet. At the sidetrack, the operator raised the mud weight to 12.1 ppg.

As the deeper part of the hole was drilled, balanced to underbalanced conditions were suggested by increasing connection and trip gases, background gas, and occasional tight sections of hole, although mud weight was eventually raised to greater than 14 ppg by total depth (16,400 feet). Most of the gas associated with pipe pickup operations appears to have originated from coal seams (EXLOG, 1983) within the Cretaceous sequence below the unconformity at 12,780 feet. Frequent flow checks on drilling breaks failed to find evidence of flow, although a short-lived mud resistivity anomaly at 16,012 feet suggested a brief saltwater influx (EXLOG,

1983) against 14.1 ppg mud. No evidence of flow was detected elsewhere in the mud chloride content, which remained essentially constant below the 13 3/8-inch casing seat at 4,833 feet (see Operational Summary chapter).

#### FORMATION TEMPERATURE DATA

No effort was made to analyze flowline temperature data for characteristic thermal signatures associated with zones of excess pore pressure in the manner suggested by Wilson and Bush (1973). This type of study was not done because of difficulties associated with estimating the effects on returning-mud temperatures of mud circulation at varying annular velocities through a 500-foot marine riser (McClure, 1977, p. III-27). Temperatures obtained from wireline borehole surveys (see Geothermal Gradient chapter) are subject to error because of well bore effects. The measurements are also too infrequent to allow identification of the elevated geothermal gradients which typify zones of abnormal pore pressure (Wilson and Bush, 1973).

#### ESTIMATED MAGNITUDE OF ABNORMAL PORE PRESSURE

Pressure plots derived from analysis of shale resistivity, velocity, and density data were prepared for the Navarin Basin COST No. 1 well following guidelines provided by McClure (1977), Hottmann and Johnson (1965), and Stewart (1983). These are presented as a series of diagrams in plate 3. A pressure plot prepared from drilling exponent data (fig. 62) is also presented in plate 3E. Each plot shows actual pressure data, hydrostatic and lithostatic gradients, circulating dynamic mud pressure, and pore pressure calculations. Reference pressure gradients are posted in the lower right part of each plot.

#### Shale Resistivity Analysis

Estimation of pore pressures from shale resistivity data was done following guidelines suggested by Stewart (1983) and the set of evaluation curves shown in plate 2. This evaluation method has three properties: (1) the evaluation curve is depth fixed; (2) constant salinity is assumed; and (3) the accuracy of the method is generally 0.5 ppg where data are well controlled. Shale resistivity values are first posted versus depth at the scales shown. This plot is then overlaid on the evaluation curves at a zero depth (subsea) match. The data set is then "fit" by sliding left or right so that the predominant points fall to the right of the normal compaction curve (the 9 ppg

line, plate 2). Pressures (in mud weight equivalent) for points on or left of the normal compaction curve can be read directly; those depth points where shale values fall to the right of the 9 ppg curve are presumed to have a normal (9 ppg) pore pressure gradient.

This approach to data fitting has been slightly modified here. Available direct pressure measurements were converted to equivalent mud gradient and posted with the set of evaluation curves. Shale resistivity data were then shifted horizontally along the depth match to obtain the best visual fit between shale resistivity and pressure data. Such fitting was made difficult by the high scatter exhibited by the resistivity data.

Two other alternatives exist for a data fit. The first option is to slide the data to the right so that all points above the point of inversion at 9,430 feet fall on or to the right of the 9 ppg curve. This would result in the computation of normal pore pressures for approximately 3,000 feet of the obviously overpressured section beneath this inversion point. This approach seems far too conservative and ignores the direct pressure measurement, which yielded an equivalent gradient of 10.01 ppg at 10,163 feet (SSD). The second data-fitting option regards the 1,000 feet of section immediately above the inversion point as "normal." Shale resistivity data are then superimposed on the evaluation curves so that the inversion point matches the 9 ppg curve. However, the inversion point then appears to lie within overconsolidated "caprock" (see discussion below), and use of the point as a base line yields radically high pressure estimates which violate direct pressure data both above and below the inversion point. For these reasons, both of these alternative fit options were rejected. The data fit illustrated in plate 2 appears to most closely honor all available data.

A pore pressure plot prepared from this analysis of the resistivity data is presented in plate 3A. These calculations identified a zone of abnormal pore pressure in the interval from 2,500 to 3,840 feet. Because of data scatter, "caprock" effects, and the fitting technique, excess pore pressure values were not derived by this method for the upper 2,770 feet of the major overpressured zone below 9,430 feet.

The conclusion reached from these efforts is that shale resistivities in the Navarin Basin COST No. 1 well offer the least satisfactory wireline log method for quantification of formation pressure.

## Shale Velocity Analysis

Two separate approaches were used in the analysis of shale velocity data. The first approach involved the comparison of actual shale velocity data to that predicted for a given burial depth by the Bering shelf "normal" compaction gradient on plate 2. By this means, a velocity anomaly was computed for each depth-versus-travel-time shale point. Where a positive anomaly (excessively high travel time or low velocity) was identified, a pore pressure estimate was graphically obtained by using the relationship between pore pressure and travel-time anomaly published for the Oligocene-Miocene of the Gulf Coast by Hottmann and Johnson (1965, p. 720, fig. 5). Hottmann and Johnson's graph is reproduced in figure 63. The results of this analysis are shown in plate 3B along with direct pressure measurements and mud weight data.

Although these shale-velocity pore pressures fit constraining pressure data fairly well above 7,000 feet (SSD), unrealistically high pressures are derived for all deeper points. Theoretical pore pressures for the depth of the RFT test at 10,163 feet (SSD) exceed by 1,500 psi the actual pressure obtained in the test. Two possible explanations may be offered for the excessively high pressures obtained by this treatment of the shale velocity data:

- (1) The shale velocity anomaly versus pore pressure graph (fig. 63) compiled by Hottmann and Johnson (1965) for the Gulf Coast is not directly applicable to Bering shelf sediments. Indeed, shale velocity anomalies at 10,163 feet (SSD), where an excess pore pressure measurement was obtained, yield a point that plots well off the Hottmann and Johnson curve. A single control point is not adequate to justify a shift or correction of the Hottmann and Johnson curve, so the construction of a proper curve for Bering shelf sediments must await additional data.

- (2) At depths below 13,750 feet (SSD), the Bering shelf curve extrapolates to shale travel times less than 62 microseconds/foot, the theoretical compaction limit. As discussed above, the compaction function probably departs from linearity near this depth and asymptotically approaches the 62 microseconds/foot theoretical limit. Therefore, the use of the linear function below 13,750 feet results in erroneously large travel-time anomalies and derived pore pressures.

A separate evaluation of pore pressures from shale velocity data was conducted by using evaluation curves constructed by Pennebaker (1968a, 1968b; in McClure, 1977) for worldwide evaluations of formation pressures. The technique consists of

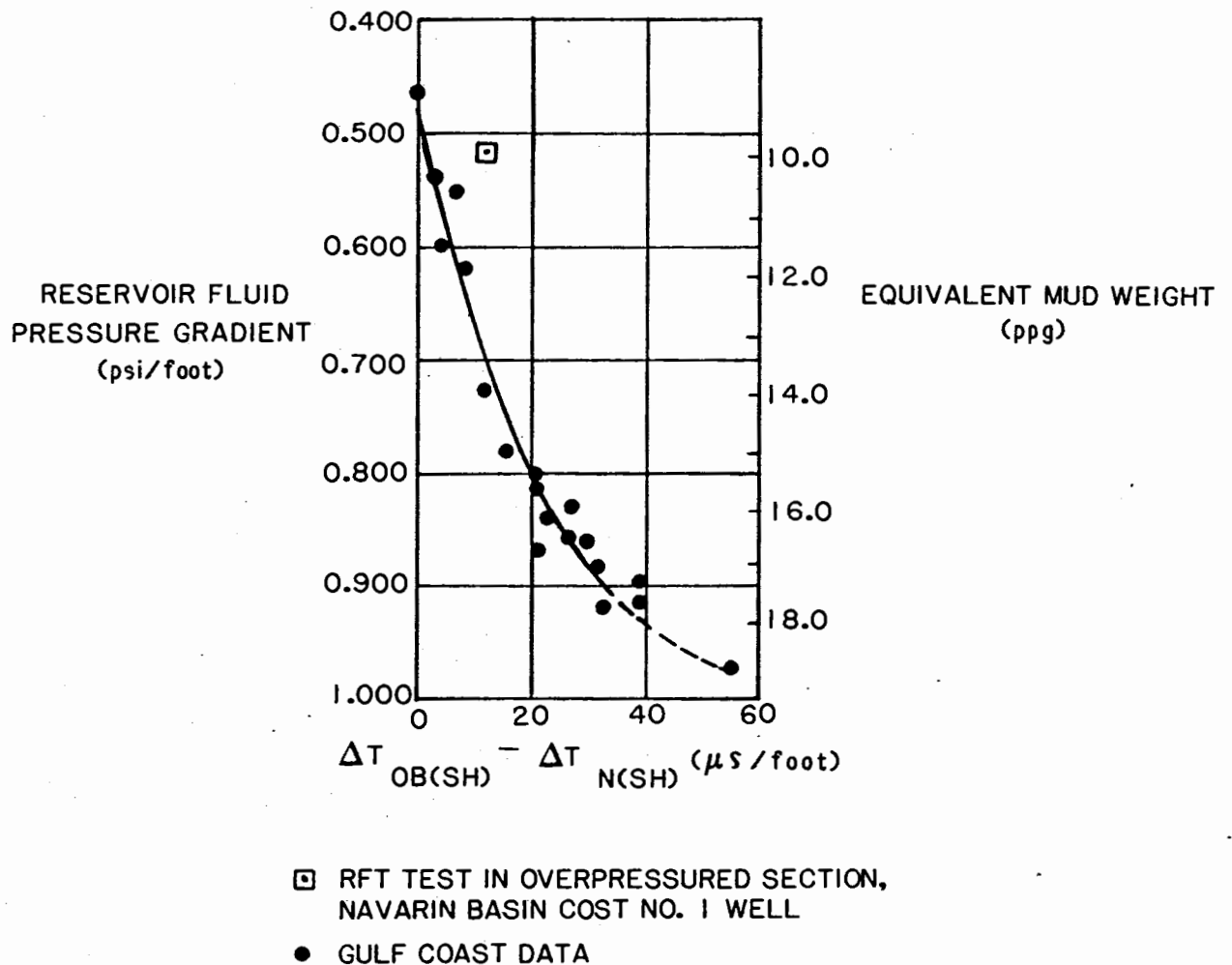


**FIGURE 63.**

HOTTMANN AND JOHNSON'S CURVE FOR THE RELATIONSHIP BETWEEN SHALE TRAVEL TIME ANOMALY AND PORE PRESSURE IN THE OLIGOCENE-MIOCENE OF THE GULF COAST OF LOUISIANA AND TEXAS. (HOTTMANN AND JOHNSON, 1965, p.720,fig. 5). This curve was used to obtain the unrealistically high pore pressures shown in plate 3B. The single direct pressure measurement available for the overpressured interval in the Navarin Basin COST No. 1 well is posted as a small open square (travel time anomaly = 11.5; pressure gradient = 0.524). In the Gulf Coast, this magnitude of travel-time anomaly would be associated with a pore pressure gradient of 0.700. The Hottmann and Johnson curve evidently must be shifted or corrected to be applicable to Bering Sea sediments.

overlaying the curves on the shale velocity data and shifting one or the other vertically (matched along the 100 microseconds/foot line) to obtain a satisfactory visual match between the 8.5-ppg line and the normally pressured sediments in the few thousand feet above the overpressured interval. This fit is illustrated in figure 60. Pennebaker's empirical curves depart from linearity at depth as the shale compaction limit is asymptotically approached by the 8.5-ppg or "normal" compaction profile. At depths below 13,750 feet (SSD), this curve is superior to the Bering shelf curve as a base line. A pressure plot derived from this analysis of velocity data is presented in plate 3C. Computed theoretical pore pressures agree well with actual pressure data. Comparison of the curve for mud column pressure to the theoretical pore pressure data suggests that the well was drilled in an underbalanced condition from 10,000 to 12,830 feet, where deteriorating hole conditions necessitated the setting of a casing string. This plot suggests that an underbalance of approximately 3,000 psi existed at the bit when drilling was resumed after the casing run. Continuing hole problems that led to a stuck and abandoned drilling assembly and the subsequent sidetrack at 13,537 feet prompted successive increases in mud weight (eventually in excess of 14 ppg) as the hole was drilled to total depth. At total depth (16,400 feet) the plot indicates that a maximum underbalance of approximately 800 psi (or 1.5 ppg mud weight) existed in the uncased part of the well between 12,830 and 15,500 feet. An overbalanced condition existed below 15,500 feet in the well bore when the well reached total depth.

Of all the wireline log techniques, this treatment (plate 3C) of shale velocity data yielded pore pressure estimates most consistent with the operational data and independent pressure information.

#### Shale Density Analysis

Shale densities were also analyzed by using the evaluation curves published by McClure (1977), which are identical in form to those employed in the analysis of velocity data. The density data and the configurations of the Pennebaker evaluation curves are shown in figure 61. Pore pressure estimates obtained from this analysis are shown in plate 3D. As found in the other analyses, a narrow zone of excess pore pressure is present in the interval from 2,500 to 3,840 feet. Theoretical pore pressures agree well with actual pressure data in the normally compacted sections, but are too conservative at the pressure measurement taken just below the top of the overpressured zone. These theoretical pore pressures suggest that the well was drilled in an underbalanced condition (up to 700 psi or 1.3 ppg

differential) between 10,000 and 12,830 feet, before the 9 5/8-inch casing run. The theoretical pore pressures further indicate that the mud weights employed between the casing shoe and total depth were ample to counterweight formation pressures in that interval. Pore pressures obtained from analysis of shale densities are probably too conservative. The pressure relationships in plate 3D are inconsistent with the underbalanced conditions suggested by the chronic problems with pick-up gas and unstable hole conditions encountered between 12,830 and 16,400 feet.

All wireline log methods of pore pressure estimation suggest that the zone of overpressure extends without detectable interruption well below the basal Tertiary unconformity at 12,780 feet. Density values for shale cuttings rise perceptibly below this unconformity but are still relatively low for these depths (fig. 61). The stratigraphic column presented in plate 3H indicates that the major zone of abnormal pore pressure contains rocks of Oligocene, Eocene, and Late Cretaceous age.

#### Drilling Exponent Analysis

Pore pressure gradients calculated from drilling response parameters by EXLOG (fig. 62) are portrayed as pressure data in the pressure plot of plate 3E. These estimates agree well with the direct pressure measurements in the shallow section, but are deficient by approximately 10 percent, or 500 psi, at the depth of the RFT pressure test at 10,163 feet (SSD). The EXLOG pore pressure analysis failed to identify the top of the overpressured zone at 9,430 feet (clearly delineated by sonic and density analysis), and their estimates appear to be too conservative in the deeper parts of the well.

#### POSSIBLE CAUSES OF ABNORMAL PORE PRESSURE

The analyses presented above identified two principal zones (2,500 to 3,840 feet and 9,430 to 15,300 feet) where abnormally high pore pressures appear to be present. The actual cause of this abnormal pore pressure is unknown, but sufficient data are available to warrant some speculation.

In his studies of the mechanics of oil expulsion and migration, Burst (1969) identified three separate stages or pulses of water mobilization and expulsion during the progressive burial and diagenesis of shales. The first stage of dewatering is primarily a kinetic process during which pore water and excess interlayer water (greater than two molecular layers) is expelled in response to the mechanical redistribution of solid particles and concomitant reduction

in pore space. This process reduces the total water content of the sediments (initially 70 to 80 percent) to approximately 30 percent (20 to 25 percent interlayer water and 5 to 10 percent residual pore water). This initial pulse of fluid expulsion occurs within the first few thousand feet of burial and is accompanied by an increase in bulk density in Gulf Coast sediments from 1.32 to 1.95 g/cm<sup>3</sup> (Burst, 1969, p. 106, fig. 6). In the logged section of the Navarin Basin COST No. 1 well from 1,500 to 3,565 feet, shale densities remain fairly constant at 1.75 g/cm<sup>3</sup> (fig. 61). From 3,565 to 3,840 feet, shale densities increase to 1.95 g/cm<sup>3</sup>. Below 3,840 feet, shale densities are approximately 2.1 g/cm<sup>3</sup>. These data are consistent with Burst's (1969) model for mechanical compaction as a contributing source for the excess pore fluids in this interval.

However, these sediments are generally rich in siliceous microfossils which locally constitute more than 50 percent of the bulk volume of diatomaceous oozes (AGAT, 1983, D4231, fig. 9). As discussed in the Bottom-Simulating Reflector chapter, diatom tests exhibit progressively greater fragmentation, corrosion, and pitting of exterior surfaces at depths greater than 3,690 feet, and siliceous diatoms are very sparse below 3,870 feet. These observations suggest that the opaline tests are undergoing solution attack with loss of structural integrity and subsequent collapse in response to overburden pressure. This occurs at a depth which corresponds very closely to the base of the zone of abnormal pore pressure. Isaacs and others (1983) and Hein and others (1978) have documented significant mineralogical changes in diatomaceous sediments which appear to be controlled primarily by temperature (specifically the opal-A to opal-CT transformation corresponding to a temperature range of 109° to 122° F). The depth of wholesale diatom test destruction corresponds to a temperature of 125° F (plate 3G) in the Navarin COST No. 1 well and is therefore consistent with independent data for the threshold temperature of opal-A instability. Water released by this reaction and the excess pore waters resulting from the mechanical collapse of pore space in the interval from 3,690 to 3,870 feet may have been an additional source for the excess pore fluids in the overlying zone of abnormal pore pressure. Conversely, the mobilization of retained fluids out of pores at 3,840 feet as a consequence of independent processes may have led to siliceous microfossil dissolution and mechanical crushing of tests in response to a greater share of lithostatic weight being shifted to grain contacts.

The reason for retention of these fluids in the overlying zone is unknown. Perhaps the transformation depth (3,840 feet) represents a threshold overburden pressure required for spontaneous autofracturing and lateral or downward expulsion.

In the Navarin well, shales below 3,840 feet are well consolidated and follow a normal compaction profile. Their mechanical properties contrast sufficiently with the overlying abnormally pressured sequence to produce a seismic reflector (seismic horizon A) near their mutual boundary at 3,565 feet (plate 3H). This reflector can also be correlated with a bottom-simulating reflector at some distance from the well. Seismic records show that the overpressured zone above the reflector is characterized by poor reflectors or low signal strength within the zone (fig. 44).

After the initial pulse of mechanical dewatering, pore water escape paths are severely reduced and relatively little additional pore water is given up with increasing burial depth. The second major pulse of shale dehydration is thermochemically controlled and is primarily a process of desorption of thermally energized water from crystal lattice faces into intergranular pores (Powers, 1967). This new pore water apparently requires 40 to 50 percent more room than it did as intracrystalline water, which results in an excess volume of pore water. This process is accompanied by major changes in crystal-lattice dimensions and is part of the transformation of expandable clays, or smectites, into illite, a nonexpandable clay. The transformation is observed over a temperature range of 200° to 300° F (Powers, 1967), with an average critical dehydration temperature threshold of 221° F (Burst, 1969). Burst (1969, p. 106, fig. 6) indicates that this transformation is accompanied by an increase in the bulk density of shales from 1.96 to 2.28 g/cm<sup>3</sup>. In the Navarin well, shale densities rise to 2.4 g/cm<sup>3</sup> in the "caprock" at the top of the overpressured interval (fig. 61) and from there remain constant down to the unconformity at 12,780 feet. Below the unconformity, shale densities rise to approximately 2.5 g/cm<sup>3</sup>, then remain constant down to the apparent base of the overpressured zone at 15,300 feet, where shale densities rapidly increase to the compaction limit of 2.65 g/cm<sup>3</sup>.

Two independent observations suggest that thermally activated stripping of interlayer water from smectites during illitization may be the primary process responsible for the zone of abnormal pore pressure below 9,430 feet:

(1) X-ray diffraction mineralogical studies of shale samples from cores conducted by AGAT, Inc. (1983), identified a major change in bulk mineralogy that roughly corresponds to the upper surface of the abnormal pressure zone. In core 10, above 9,686 feet, approximately 50 percent of the clay fraction in shales is smectite. In core 11, below 9,948 feet, only mixed-layer clays are found, and the illite proportion of the clay fraction rises significantly (plate 3F). The depth interval of this transformation (9,686 to 9,948 feet) corresponds approximately to the top of the overpressured zone at

9,430 feet. New pore water released by this transformation probably generated the excess pore fluids present in the overpressured section.

(2) Burst (1969) and Schmidt (1973, p. 330) suggest a temperature threshold of 221° F (on average) for the dehydration of smectites, although Burst (1969, p. 116, fig. 10) postulated a range of 198° to 232° F. The geothermal profile for the Navarin Basin COST No. 1 well, reproduced in plate 3G (see also Geothermal Gradient chapter), predicts the occurrence of temperatures of 220° F at a subsea depth of 9,100 feet (9,185 feet measured depth). Thus, the critical threshold temperature for smectite illitization appears to be achieved a very short distance (245 feet) above the top of the major zone of abnormal pore pressure.

### CAPROCK

Zones of abnormal hardness or compaction, commonly referred to as "caprock," are often found directly over sections with abnormal pore pressures. Such zones depart from normal compaction gradients on conventional wireline log profiles and appear to be overcompacted. Caprock is characterized (fig. 57) by high resistivity, low sonic travel times (high velocity), and high density (Fertl, 1976, p. 226, fig. 5.44). Caprock zones can exceed 1,000 feet in thickness (Fertl, 1976, p. 214, fig. 5.32) and often cause difficulties in the selection of a "normal" compaction trend in an unfamiliar province. Caprock may exhibit cementation by common agents such as quartz, calcite, siderite, zeolites, and perhaps sulfates. Caprock lithologies are often described as "hard, limey shale."

In the Navarin Basin COST No. 1 well, resistivity data (plate 2) suggest the presence of a caprock in the interval from 8,500 to 9,550 feet. Above 9,200 feet, shales are described as "clay, gray, soft, soluble, amorphous, silty, and bentonitic" (Formation Evaluation Log, in EXLOG, 1983). At 9,450 feet, EXLOG describes apparent caprock as "shale, light to medium gray, hard, silty, non- to slightly-calcareous, with abundant fossil material." Below 9,800 feet, lutites are described as "clay, gray, sticky, plastic, and soluble," properties that are common in overpressured shales. X-ray diffraction analysis of conventional core samples by AGAT (1983, table 1, D-423-7 to D-423-11) yielded the following average total carbonate (calcite, ankerite, and siderite) contents:

	Core Number	Depth Interval	Average Carbonate Content
Caprock Interval	7	7,600 to 7,626 feet	1.0%
	8	8,639 to 8,649 feet	1.4%
	9	9,402 to 9,430 feet	3.5%
	10	9,656 to 9,686 feet	7.7%
	11	9,949 to 9,984 feet	2.7%

These data suggest an increase in the carbonate content of shales in the suspected caprock zone, although core 10, just beneath the apparent caprock, also exhibits a high carbonate content. The analysis of core 10 was probably biased by the inclusion of a few coquinoid horizons that were rich in biogenic carbonate (up to 33 percent), so the arithmetic average obtained from this data is somewhat misleading.

#### SUMMARY

The wireline log and formation test data clearly identify a major zone of abnormal formation pore pressure in the interval below 9,430 feet in the Navarin Basin COST No. 1 well. A shallow zone of excess pore pressure between 2,500 and 3,840 feet also appears to be present. Only a single direct pressure measurement was obtained in confirmation of abnormal pressure in the lower interval. Estimation of the actual magnitude of overpressure therefore relies heavily on the evaluation of wireline log data. The interpretation of this data is somewhat subjective, and in the absence of complete pressure test confirmation, the pressure estimates derived from wireline logs must be regarded as approximations.

Of the various methods of pressure analysis applied to the wireline log data, the analysis of shale velocity data following the procedure of McClure (1977) appears to have yielded results that most closely conform to independent test and operational data (fig. 60 and plate 3C).

The upper zone of overpressure may be associated with diagenesis of diatomites and inefficiencies in mechanical expulsion of pore fluid from compacting shales. Mineralogical, thermal, and density data suggest that at least part of the excess pore fluids in the lower zone of abnormal pore pressure are generated as a by-product of smectite-illite transformations.

Both zones of excess pore pressure correspond to intervals that exhibit poor internal reflectivity on CDP seismic panels (fig. 44). The base of the upper zone of overpressure correlates with a high-amplitude positive reflection observed on seismic records. The boundaries of

the lower zone are not associated with any particular event on seismic records. At the well site, the basal Tertiary unconformity does not correspond to any identifiable continuous reflector, probably because of reduced acoustic impedance caused by excess pore pressures both above and below the unconformity.

Overpressured sections present potential hazards to drilling operations. Careful analysis of velocity data from seismic surveys in the vicinity of proposed wells may provide clues to the depths at which overpressured zones may occur, and casing programs can then be designed to protect drilling operations. Pore pressure estimates calculated from drilling responses failed to identify the top of the major zone of overpressure in the Navarin Basin COST No. 1 well, and over 2,000 feet of overpressured section was penetrated before the problem was detected. Any suggestion of an overbalanced condition while drilling, such as increasing background or pickup gas (connection, flow check, trip, etc.), tight or sloughing hole, or increasing penetration rate on a dulling bit, should prompt the cessation of drilling and the running of a sonic log as a pressure check. Pressures obtained from analysis of the sonic log would then dictate the operational response to the problem.

The presence of excess pore pressures in the geothermal environment of the lower zone (below 9,430 feet) enhances the prospects for hydrocarbon accumulations in the Navarin Basin. The top of the lower overpressured interval roughly corresponds to the level of peak oil generation (Hunt, 1979, p. 146, fig. 4-26) at a temperature of 212° F (100° C). The availability of excess pore waters in shales as an expulsion vehicle for simultaneously evolving hydrocarbons is recognized as a very important factor in the migration of hydrocarbons from their source into potential traps (Burst, 1969; Hunt, 1979). Excellent source beds for liquid hydrocarbons are found near the base of the Tertiary sequence and within the zone of abnormally high pore pressure. Should these intervals also coincide in areas where faulting provides escape avenues for the excess pore fluids, potential traps in communication with the faults can be reasonably expected to be charged with hydrocarbons (Weber and others, 1978). In the Navarin Basin COST No. 1 well, the only potential reservoir beds are found above the "caprock" from approximately 5,000 to 7,000 feet. Faults which postdate these beds would provide natural conduits for the migration of hydrocarbons into these beds from sources at greater depth.

## GEOHERMAL GRADIENT

by

Gary C. Martin

The thermal gradient for the Navarin Basin COST No. 1 well was determined by using the High Resolution Thermometer log (HRT), bottom hole temperatures (BHT) from the logging runs, and formation fluid temperatures from the drill stem test (DST) and from the Repeat Formation Tester log (RFT). True formation temperatures were estimated from each logging run by extrapolating BHT measurements obtained from successive log suites to a static formation temperature.

The analytical extrapolation technique consists of a linear regression applied to the suite of BHT measurements versus the logarithm of the expression:

$$\frac{dt}{t + dt}$$

where for each measurement,  $dt$  = time after circulation stopped (hours) and  $t$  = circulating time (hours). The extrapolation of the obtained line to the temperature reached when

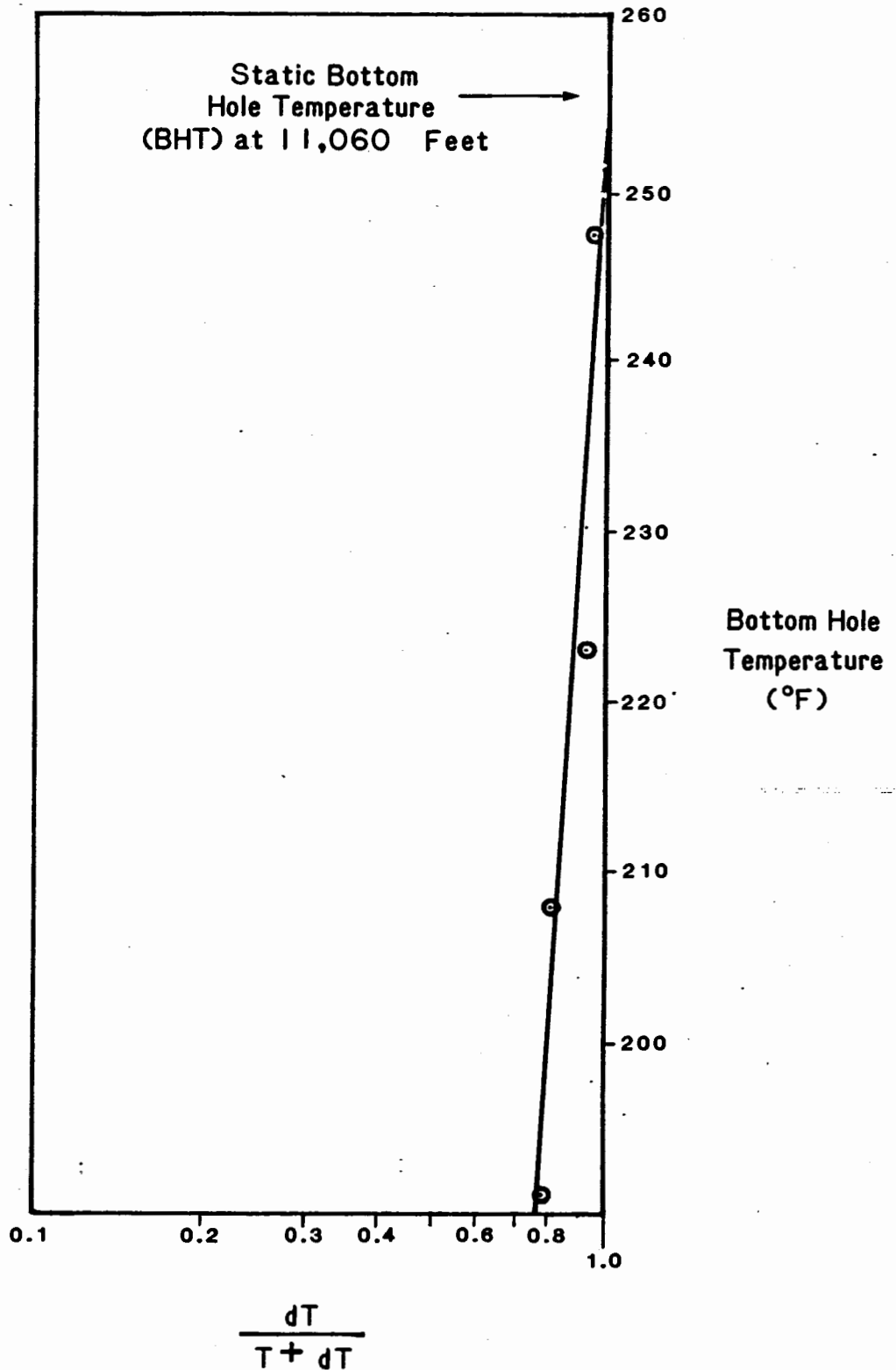
$$\frac{dt}{t + dt} = 1$$

should define true, static formation temperature (fig. 64).

This technique is based on the observation that temperature rise after circulation has stopped is similar to static pressure buildup and thus may be analyzed in a similar manner (Fertl and Wichmann, 1977). In practice, this technique yields accurate estimates of true static formation temperature except when circulation times are in excess of 24 hours.

After static BHT was calculated from each logging run, a plot of temperature versus depth was constructed by using all available temperature data (fig. 65). After comparing the various data and noting the characteristics of heat transfer between drilling fluids and formation lithology and fluids, it was determined that the true thermal gradient was best approximated by the static BHT and DST data.

The thermal gradient obtained from the HRT log is anomalously high. This log was run through the cased section of the hole (from the sea floor to 12,834 feet) after total depth had been reached. Drilling mud heated by the higher temperatures at the bottom of the hole was circulated past



T equals circulating time in hours and  
 dT equals elapsed time after circulation stopped.

**FIGURE 64.** GRAPH SHOWING THE EXTRAPOLATION OF BOTTOM HOLE TEMPERATURES (BHT) TO DETERMINE STATIC BHT FOR LOGGING RUN 2, NAVARIN BASIN COST NO. 1 WELL.

the well casing string for 63 days before reaching total depth. This heat was readily conducted from the mud through the casing and heated the upper borehole above true formation temperature. Theoretically, this effect should increase uphole and probably accounts for the progressive divergence upward of the HRT thermal gradient from the estimated true geothermal gradient in figure 65.

The RFT temperature data were also found to be generally unsatisfactory for calculating the true geothermal gradient. This is probably a function of the small amount of formation fluid sampled in an RFT test and the resulting susceptibility of this test to near-borehole thermal modification. RFT data were apparently affected by a process similar to the one that affected the HRT data; that is, the heat transfer in the upper sections of the borehole was from the mud to the formation (warming the formation), but the heat transfer in the lower sections of the borehole was from the formation to the mud (chilling the formation). This process of thermal modification may account for the slight positive uphole divergence of the RFT temperatures in logging run 1 from the calculated true geothermal gradient.

Thermal modification also probably accounts for the low RFT temperatures obtained in runs 2 and 3. These low temperatures were obtained from relatively deeper sections of the well at the time logging runs 2 and 3 were recorded and are due to the relatively cool circulating mud chilling the formation adjacent to the borehole. RFT temperatures in the extensively sampled sandy interval from 5,000 to 7,000 feet approximate the flowline mud temperatures recorded during drilling. This suggests thermal equilibration (cooling) of the formation with the well bore through contact with the relatively cool circulating mud. RFT temperatures in this sandy interval are farther displaced from the calculated geothermal gradient than those measured in the underlying mudstone interval (7,000 to 10,300 feet). This is probably due to the inherently greater thermal conductivities of the sandstones.

The single DST temperature was assumed to represent in situ formation temperature because the DST extracted a large volume (55 barrels) of formation fluid and thus sampled fluid a sufficient distance from the borehole. The DST temperature falls very close to the geothermal gradient calculated from the BHT data.

Linear regression (least squares) was applied to the static BHT and DST data to determine the average geothermal gradient shown in figure 65. This yielded a gradient of

1.78° F per 100 feet from total depth (16,400 feet) to about 3,800 feet. Above 3,800 feet, the gradient is higher and is estimated to be 2.5° F per 100 feet, on the basis of an assumed sea-floor temperature of 40° F. This higher gradient is attributed to the change in lithology and degree of compaction at 3,800 feet. The unconsolidated, undercompacted diatomaceous sediments above 3,800 feet appear to be overpressured (see Abnormal Formation Pressure chapter) and have an excessively high fluid content. Because of the overpressuring and because water has a lower thermal conductivity than sediment, this interval has a lower average thermal conductivity than the more compacted rocks below 3,800 feet. This effect has apparently produced the characteristic higher geothermal gradient observed here.

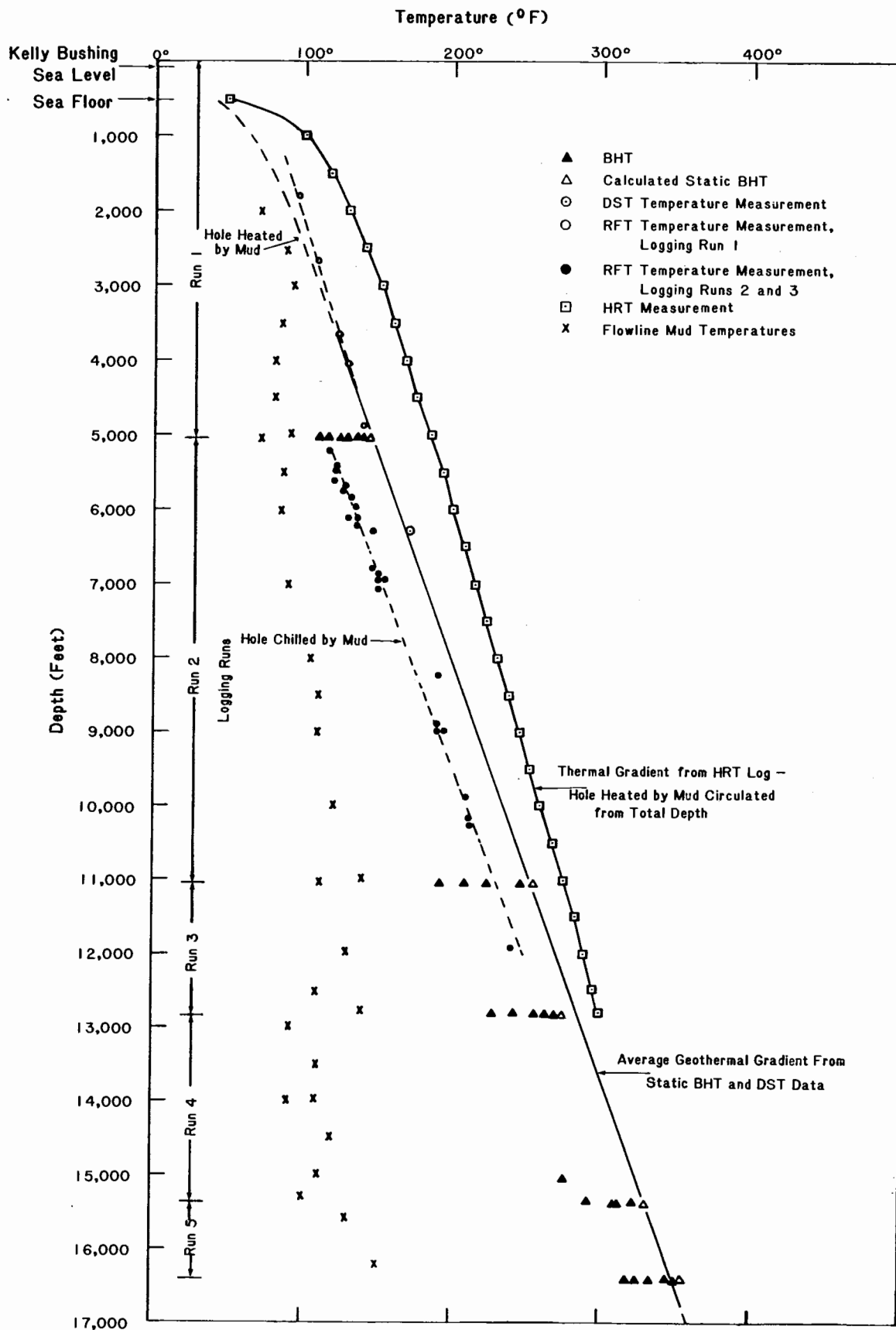


**FIGURE 65.** THERMAL GRADIENT FOR THE NAVARIN BASIN COST NO. 1 WELL.



# ORGANIC GEOCHEMISTRY

by  
Taber O. Flett

## INTRODUCTION

Organic geochemical analyses, approved by Atlantic Richfield Company (ARCO), were performed upon samples from the Navarin Basin COST No. 1 well by Exploration Logging (USA), Inc. (EXLOG), and Robertson Research (US), Inc. The elapsed time from the actual sampling at the well to analysis in the laboratory probably did not exceed 1 week. Zephiran was added to the canned cuttings samples. No evidence of bacterial methane was reported. The results discussed in this report are taken from Dow and Coleman (1983) and from Russ (1983). A description of the fluorescence of drilling mud and cuttings as a result of ultraviolet irradiation and a summary of mud gas analyses are included in the Well Log Interpretation chapter. All depths are measured from the Kelly Bushing, which was 85 feet above mean sea level and 517 feet above the sea floor.

Samples selected by ARCO and sent to Robertson Research (U.S.), Inc., included canned cuttings samples collected at 60-foot intervals, sidewall cores taken at approximately 100-foot intervals, and representative plugs and chips from 20 conventional cores. Headspace gas from canned cuttings samples was analyzed for light (C<sub>1</sub>-C<sub>6</sub>) hydrocarbons; the cuttings were then washed, described, and a representative sample analyzed for total organic carbon content (TOC). Samples with approximately 0.4 weight percent or more TOC were analyzed with Rock-Eval pyrolysis (hereafter referred to as pyrolysis). Sidewall cores taken at about 100-foot intervals plus representative plugs and chips from the 20 conventional cores were analyzed in the same manner except that light hydrocarbon analysis was not included. Cuttings and sidewall core samples were selected at approximately 300-foot intervals and from each conventional core for kerogen isolation, vitrinite reflectance (R<sub>0</sub>), spore coloration index (SCI), and elemental analysis. A few samples contained insufficient kerogen for elemental analysis. Soxhlet extraction, elution chromatography, and saturate-fraction gas chromatography were performed upon conventional core samples and upon selected cuttings samples from 12,060 to 15,120 feet. Soxhlet extraction with dichloromethane was performed upon weighed samples for 18 hours. The asphaltenes were separated on a silica-alumina chromatographic column with hexane, and the hexane-soluble fraction was separated into saturates, aromatics, and NSO (nitrogen, sulfur, and oxygen) compounds by successive elutions with hexane, benzene, and benzene-methanol. The saturate fraction in the C<sub>15</sub> to C<sub>40</sub> range was analyzed by using gas chromatographic techniques.

The study performed by EXLOG included analysis of cuttings, conventional cores, and mud samples for TOC and by pyrolysis to the total depth of 16,400 feet. The results of these analyses agree favorably with data obtained by Robertson Research. TOC values produced by EXLOG are included on plate 4 at approximately 500-foot intervals to show the reproducibility of the measurements and where Robertson Research data are unavailable. Pyrolysis data from both laboratories are presented in this report for separate profiles, but similar data sets are not provided for comparison because procedural differences may yield a difference in separate analyses performed upon the same sample. The general appearance of profiles produced by the two laboratories is, however, in good agreement, and all of the original data are available for examination at this office.

The hole was sidetracked at about 13,260 feet. Data presented in this report from depths greater than 13,900 feet are taken from the sidetracked portion of the hole. There were no serious discrepancies in the geochemical data where the two segments overlap (13,260 to 13,900 feet).

#### ORGANIC CARBON

Total organic carbon content (TOC) from sidewall and conventional cores is displayed on plate 4 with sample descriptions. Sidewall and conventional core values are generally more representative of the range of values for the various lithologies than cuttings samples, which are a blend of samples over an interval. In this case, EXLOG analyses of cuttings samples have been included at intervals of about 500 feet to demonstrate the reproducibility of these measurements.

A minimum organic carbon content of 0.5 percent in shales is generally regarded as necessary to generate oil for a commercial accumulation (Hunt, 1979; Tissot and Welte, 1978). Most source rocks, according to Hunt, are in the range of the gray shales, having from 1 to 2 percent organic carbon plus several hundred parts per million (ppm) hydrocarbon. Additionally, the amount of organic carbon required to generate commercial amounts of hydrocarbons depends upon the type of organic matter from which it was derived, because this determines the amount of hydrogen available to combine with the carbon.

Geochemical analyses to a depth of approximately 2,000 feet in this well are of dubious value because of cement contamination. From about 2,000 to 7,600 feet, TOC values tend to be less than 0.5 percent and somewhat erratic. From about 7,600 to 11,700 feet, TOC values range between 0.5 and 1.0 percent and the values exhibit less variability.

Samples analyzed between 2,000 and 11,700 feet were derived largely from gray-brown siltstone and fine- to medium-grained sandstone.

From 11,700 feet to the major unconformity at 12,780 feet, maximum TOC ranges generally between 1.0 and 2.0 percent, with the values still exhibiting a relatively low degree of variability. Samples in this interval were drawn generally from gray to dark-gray mudstone and shale. Conventional core 14 (12,715 to 12,743 feet) produced TOC values from 1.31 to 1.89 percent.

Between 12,780 and 15,200 feet, the organic carbon content of samples is extremely erratic. Measurements as low as 0.06 percent from a sidewall core (13,510 feet) and as high as 32.67 percent from conventional core 17 (13,889 feet) were recorded. These samples were taken from sandstones (some volcanic), siltstones, shales, and coals. The greater variety of lithologies probably accounts for the higher scatter of the data. Both EXLOG and Robertson Research washed coal from some of their samples in an effort to obtain geochemical data from shale. Unless other samples were unavailable, analyses of these washed samples were not included in the well profiles in this report. Where washed sample analyses are given, such as in some of the pyrolysis data or perhaps a few of the canned cuttings samples, they are clearly indicated.

If coal is known to be present, one can anticipate the nature of analyses that are likely to occur and make certain inferences about the petroleum potential of the rock that the samples represent. If a sample has been treated in some way before analysis, however, one cannot be absolutely certain that all of the coal has been removed or that other materials have not been removed which should properly have been included in the analysis. Vitrinite is the most common maceral observed in coal, and it is found in 80 to 90 percent of all well cuttings (Hunt, 1979). When vitrinite is washed from a sample, it is impossible to determine whether it was autochthonous vitrinite derived from indigenous coal, allochthonous vitrinite derived from clastic coal fragments, or vitrinite from a kerogen contained in a shale.

From 15,200 to 16,400 feet (TD), TOC values from sidewall and conventional cores are about 0.5 percent and exhibit a relatively low range of values. TOC analyses of cuttings in this interval are high and erratic, probably the result of caving and mixing. The sampled lithology that yielded these analyses appears to have been composed mostly of hard, gray-brown siltstone, mudstone, and shale, with traces to minor amounts of coal.

If one considers organic carbon content alone, good potential source material exists between about 11,700 and 15,200 feet. However, below the unconformity at 12,780 feet, most of the high organic content seems to be derived from coal.

#### DESCRIPTION OF KEROGEN

Kerogen was examined in reflected and transmitted light by Robertson Research. Results of the reflected-light petrography, the hydrogen index from pyrolysis performed by EXLOG, and the H/C ratio from elemental analysis performed by Robertson Research are presented in figure 66.

Three petrographic classes of kerogen plus amorphous material, a subgroup within the exinite or liptinite category, are reported in this study. They are:

1. Amorphous (algal or structureless, colloidal matter)
2. Exinite (herbaceous, lipid-rich relics)
3. Vitrinite (woody and humic components)
4. Inertinite (hard, carbon-rich, nonreactive, brittle particles).

There is good overall agreement between the reflected-light and transmitted-light microscopy, although some allowances must be made for inherent differences in the natures of the two techniques. The maceral identification in transmitted light is not presented in this report, but it is available for examination at this office if the information is required.

A comparison of visual percentage estimates of kerogen types with chemical data on a large number of samples has shown that kerogens with less than about 35 visual percent of amorphous material plus exinite tend to be gas prone, whereas oil sources usually contain over 65 percent of these maceral types (Dow and O'Connor, 1982).

From 1,680 to 7,000 feet, the sum of amorphous material plus exinite ranges from about 20 to 65 percent of all kerogens. The humic kerogen groups, vitrinite and inertinite, constitute about 60 to 65 percent of the total kerogens. The hydrogen indices from pyrolysis are low, generally less than 100 milligrams of hydrocarbons per gram of organic carbon, and these values are reflected in the H/C ratios computed from elemental analyses, which tend to be less than 1.0. In immature sediments, H/C ratios from humic kerogens are normally not greater than about 1.0 (Hunt, 1979).

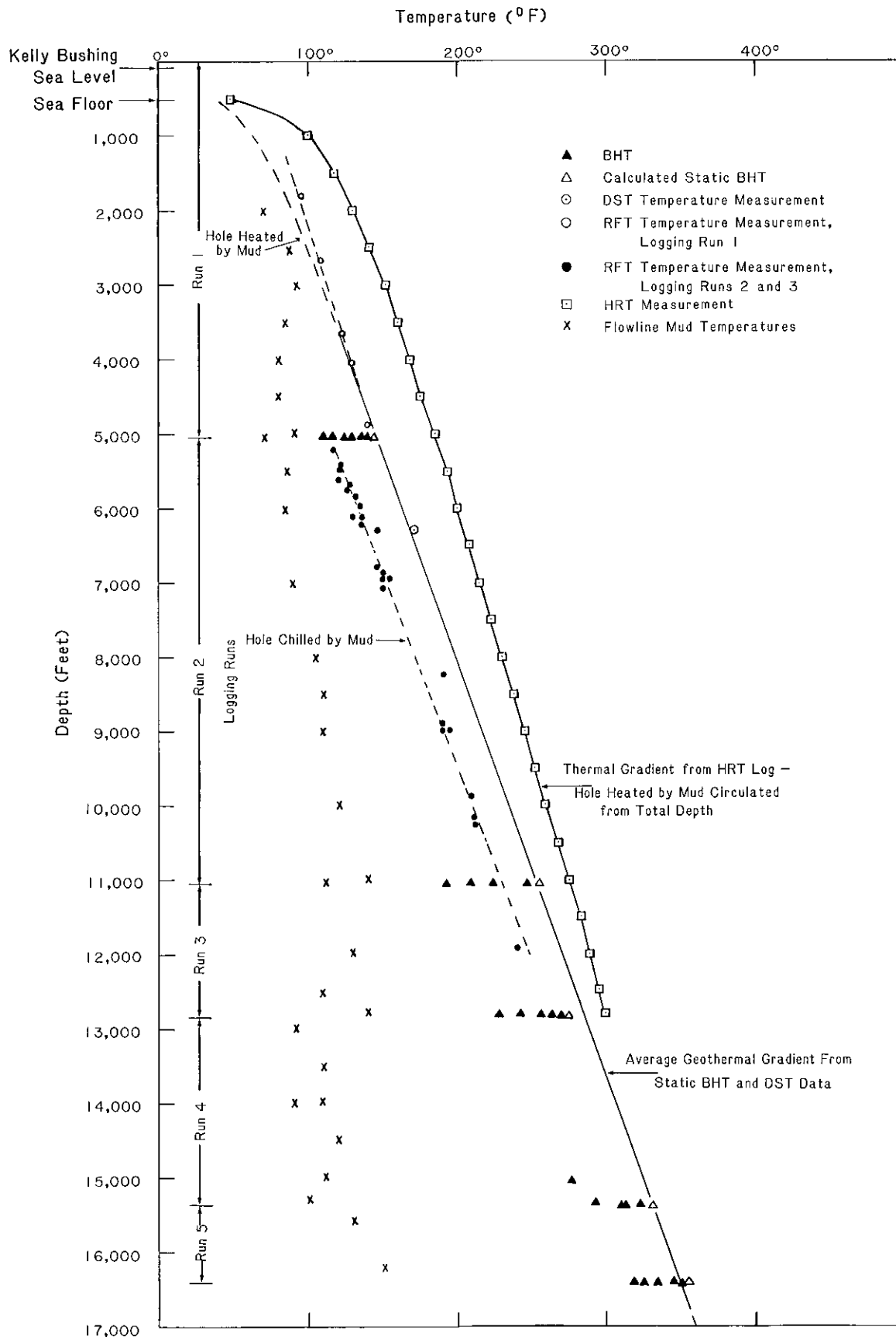


FIGURE 65. THERMAL GRADIENT FOR THE NAVARIN BASIN COST NO. 1 WELL.

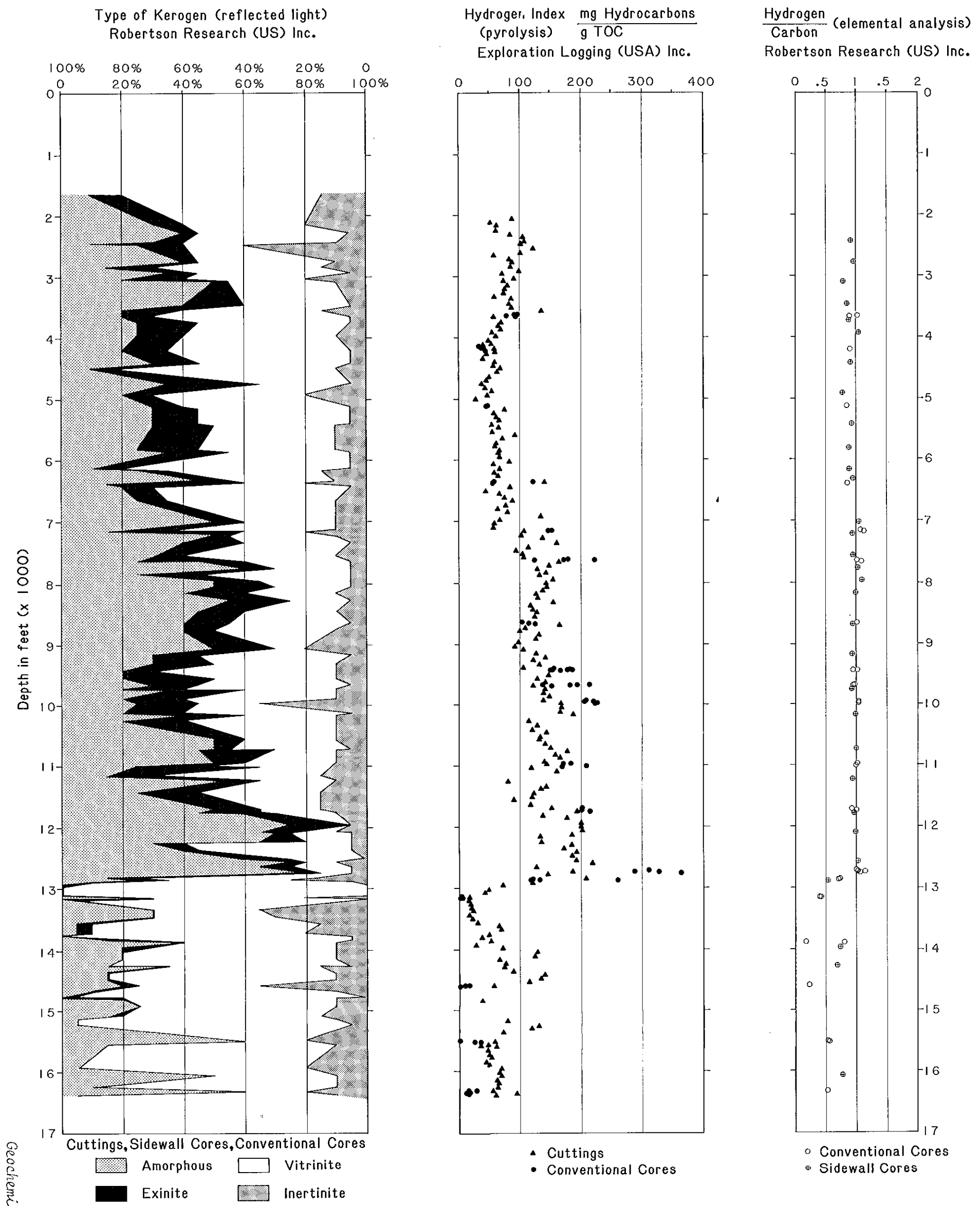
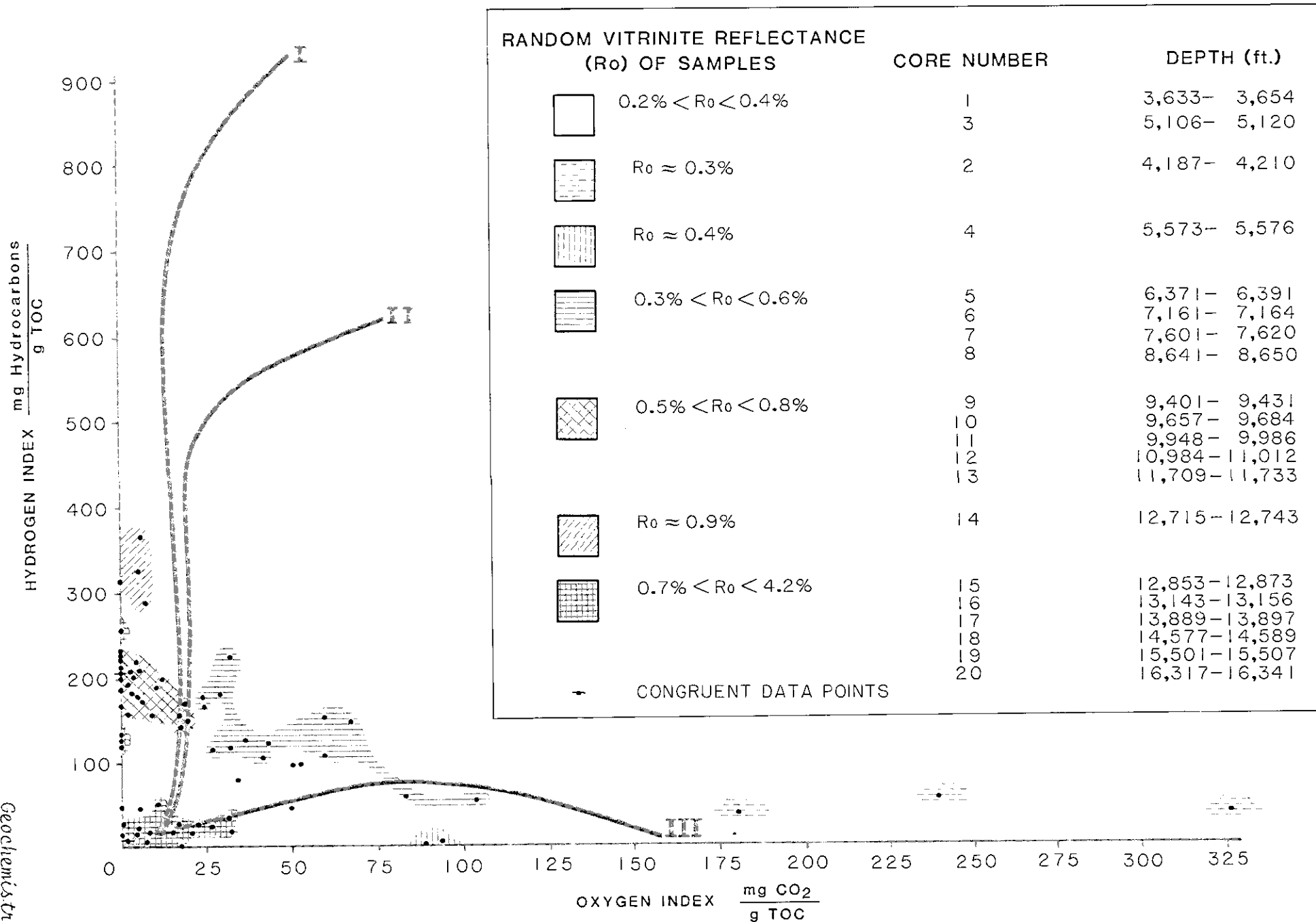
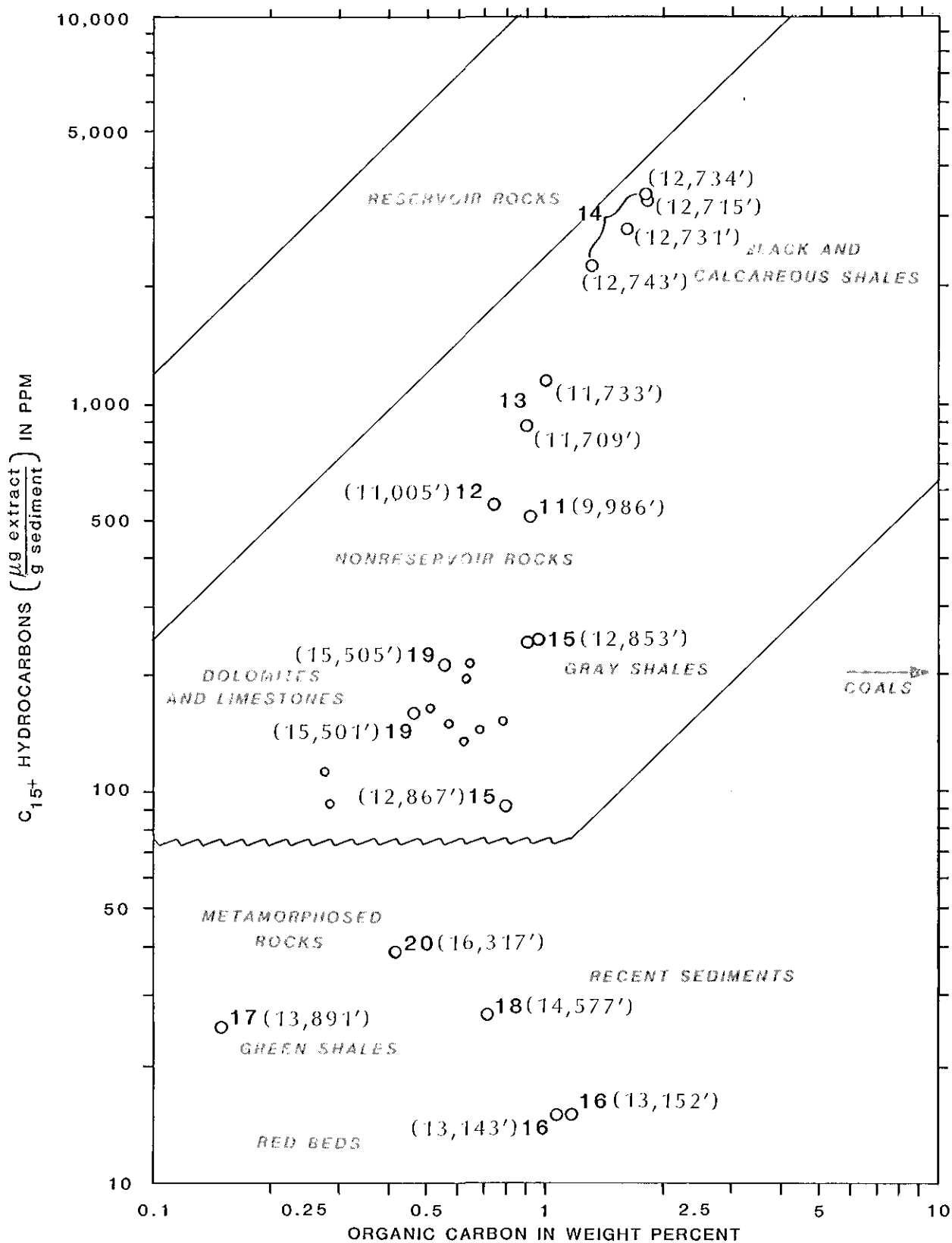


FIGURE 66. CLASSIFICATION OF ORGANIC MATTER



**FIGURE 67.** MODIFIED VAN KREVELEN DIAGRAM. DATA FROM ROCK EVAL PYROLYSIS OF CONVENTIONAL CORE SAMPLES PERFORMED BY EXPLORATION LOGGING (USA), INC.





INTERPRETATIONS BASED ON DATA FROM VARIOUS SEDIMENTARY BASINS (HUNT, 1979)  
 O 16 (13,152') - CONVENTIONAL CORE      o - CONVENTIONAL CORES 1-10  
 NUMBER AND DEPTH

**FIGURE 69.** TOTAL ORGANIC CARBON AND EXTRACTABLE C<sub>15+</sub> HYDROCARBONS. ANALYZED BY ROBERTSON RESEARCH (US) INC.

In the interval from about 7,000 feet to the unconformity at 12,780 feet, average values for sapropelic kerogen and hydrogen content are significantly higher, and both exhibit a dramatic decrease at 12,780 feet. The hydrogen index seems to exhibit a closer correspondence to the kerogen content than does the H/C ratio from elemental analysis. However, the H/C ratios are generally slightly higher within this lithologic sequence than they are in superjacent sediments. This suggests that when the kerogen was originally deposited, it must have had a more sapropelic character than subsequently deposited organic material. The chemical reactions that collectively constitute the process termed "maturation" would have significantly reduced the H/C ratio of a kerogen buried in Eocene time. The apparent failure of these values to decrease, indeed the modest increase in the H/C ratio which has occurred, agrees favorably with the reflected-light microscopy and implies a change with depth from a humic to a sapropelic kerogen (Dow and O'Connor, 1982).

The most favorable part of the interval occurs between about 11,700 and 12,780 feet. Values for amorphous material plus exinite are frequently in excess of 65 percent, and the hydrogen indices range around 200 milligrams of hydrocarbons per gram of organic carbon. Conventional core 14 (12,715 to 12,743 feet) contains kerogen consisting of 75 to 85 percent sapropelic material, with hydrogen indices between 286 and 362 milligrams of hydrocarbons per gram of organic carbon, and with elemental H/C values from 0.72 to 1.15. The random vitrinite reflectance level at this depth is approximately 0.9 percent. Seismic evidence suggests that time-equivalent lithologies may be found to greater depth and may have developed to greater thickness to the northwest of this well site and in other parts of the Navarin Basin.

Below 12,780 feet in the well, kerogen generally contains in excess of 50 percent vitrinite. The hydrogen indices and H/C values drop abruptly at this depth, the hydrogen indices remaining generally less than 100 milligrams of hydrocarbons per gram of organic carbon and the H/C ratios remaining below 0.8 with only a few exceptions. Coal is conspicuous in samples to about 15,200 feet, and most well logs, particularly the neutron density and sonic logs, indicate the presence of coal beds. Thicknesses of coal beds displayed on these logs range from 2 feet, the limit of detectability, to about 28 feet near the bottom of the interval. From about 15,200 to 16,400 feet (TD), coal is no longer present in sidewall or conventional cores, but it is present in cuttings samples. Anomalous TOC values from cuttings samples also reflect this condition. It is reasonable to assume that coal from overlying strata has contaminated cuttings in the lower part of the well. However, very thin coal laminae could also account for these observations.

The hydrogen and oxygen indices from pyrolysis performed by EXLOG on conventional core samples are plotted on a modified Van Krevelen diagram (fig. 67). EXLOG hydrogen indices are slightly higher than similar Robertson Research data, but the general trends of the plotted data are very similar. Pyrolysis data for samples from cores 1 through 13 generally fall along a type III maturation curve. The hydrogen indices derived from these cores appear to increase slightly as the relative level of thermal maturity implied by both  $R_0$  and the oxygen indices increases, core 4 excepted. Core 14 produced three out of four hydrogen indices in excess of 300 milligrams hydrocarbons per gram of organic carbon. Robertson Research indicated only one value out of four in excess of 300 for the same conventional core. These values suggest a type I or, more probably, a type II kerogen on the basis of microscopy and paleontology. Below 12,780 feet the hydrogen indices drop rapidly and cluster near the origin of the modified Van Krevelen diagram. Some of these samples are overmature with  $R_0$  values as high as 4.2 percent (core 17, 13,889 feet). Other sediments, such as core 3 (5,117 feet), with only 0.45 percent TOC and very little hydrogen and oxygen, were probably organically lean when they were originally deposited.

#### THERMAL MATURATION

The level of thermal maturation reached by carbon-bearing sediments can be evaluated in a variety of ways. In figure 68, well profiles of the random vitrinite reflectance ( $R_0$ ), spore coloration index (SCI), kerogen fluorescence intensity, carbon preference index (CPI), and  $T_2$ -max from the second pyrolysis response are displayed.

Robertson Research reported that the only significant problems with the  $R_0$  data were the presence of high rank, recycled organic matter in some shallow samples, occasional oxidized vitrinite, solid bitumen, pseudovitrinite, and contamination due to caving in some of the cuttings samples. It is significant, however, that the mean number of reflectance observations averaged to produce each point on the profile down to the unconformity at 12,780 feet is only 8.5. In many instances only two or three values are identified as the mode, and the maximum number of observations used to compute the mean vitrinite reflectance for this interval never exceeds 20. The number of  $R_0$  measurements available beneath the unconformity at 12,780 feet is frequently more adequate because of the presence of coal. The  $R_0$  values project a relatively continuous curve from the surface to the bottom of the well, implying that the unconformity at 12,780 feet does not represent sufficient erosion to have caused a maturity anomaly. Alternatively, an inadequate population of reflectance measurements

HYDROGEN INDEX  $\frac{\text{mg Hydrocarbons}}{\text{g TOC}}$

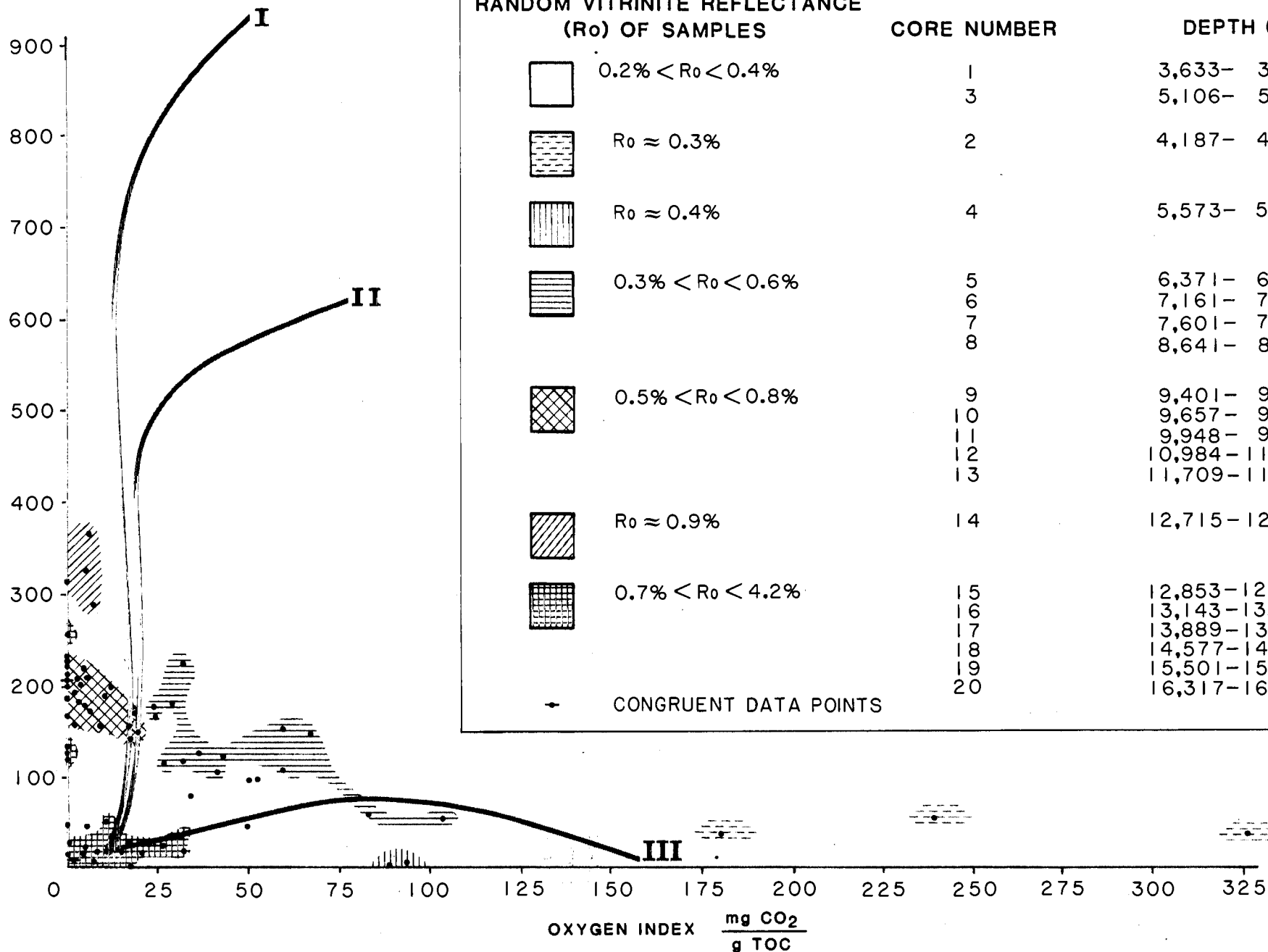


**FIGURE 67.** MODIFIED VAN KREVELEN DIAGRAM. DATA FROM ROCK EVAL PYROLYSIS OF CONVENTIONAL CORE SAMPLES PERFORMED BY EXPLORATION LOGGING (USA), INC.



may have masked an anomaly, or perhaps the coal measures just beneath the unconformity actually represent Paleocene deposition. The generally good agreement of the  $R_0$  profile with the other measures of thermal maturity suggests that the  $R_0$  profile is valid. The lack of paleontologic evidence for Paleocene deposition at the well site (and good evidence for Maastrichtian deposition) leads to the conclusion that a minimum amount of erosion at the well site may be the most satisfactory explanation for the absence of an  $R_0$  anomaly.

$R_0$  values reach 0.6 percent, the generally recognized threshold for commercial oil generation (Hunt, 1979), at about 10,000 feet. At an  $R_0$  of about 1.35 percent, liquid hydrocarbons deteriorate to gaseous hydrocarbons at a significant rate. This threshold occurs slightly below 15,000 feet in this well. Except for a limited stratigraphic range in which anomalously high levels of thermal maturity were attained, wet gas would probably be generated to the bottom of this well, given the presence of adequate amounts of sapropelic kerogen.

Anomalously high  $R_0$  values, up to 4.0 percent, are present between 13,000 and 14,000 feet and also at 14,577 and 14,764 feet.  $R_0$  profiles of this nature are characteristic of contact metamorphism in sediments adjacent to igneous intrusives (Dow, 1977). According to Robertson Research, sediments at these depths exhibit natural coking. Samples sent for geochemical analyses were described by Robertson Research as volcanic, but more detailed petrography by AGAT (1983) indicated that they contain diabase (see Lithology chapter). Potassium-argon analyses, performed by Teledyne Isotopes, yielded radiometric ages of about twenty million years for the several diabase samples, which appear to represent Miocene sills that were intruded into Late Cretaceous sediments.

Robertson Research also studied spore and pollen slide preparations in transmitted light. A value ranging from 1 to 10 on the spore coloration index (SCI) was assigned on the basis of the color of the sample. These colors, which range from "straw to pale yellow" for SCI=1, to "glassy black/graphitized" for SCI=10, reflect the degree of thermal maturity reached by the sediment sample. The technique is an adaptation of Staplin's thermal alteration index (Staplin, 1969).

Robertson Research reports that the abundance of terrestrial kerogen produced very good SCI data. Most samples yielded strong, unimodal SCI populations which resulted in a well profile very similar to that derived from the  $R_0$  measurements. These data also showed the apparent lack of missing section at 12,780 feet, the contact metamorphism that occurs in sediments below approximately 13,000 feet, and the general development of thermal maturity with depth.

The SCI reached 3.5 by about 6,500 feet, which is the threshold for peak oil generation (Dow and Coleman, 1983). This value seems a bit high when compared with  $R_0$  data. These slightly higher values may be due to the presence of recycled sediments, or they may be a function of the subjectivity of color perception by the observer. At 10,000 feet, the SCI value increased to only 4.0. Below 13,000 feet, igneous activity drove the SCI values up from 7 to 10. Where igneous activity was not present below 13,000 feet, the SCI values are a bit erratic. They exceed 7.0 in apparently unmetamorphosed sediments from 14,500 to 15,000 feet. For the purpose of evaluating thermal maturity, an SCI value of 7.0 is roughly equivalent to an  $R_0$  of 1.35 percent (Dow and Coleman, 1983). These SCI values also imply, therefore, that at depths greater than 15,000 feet, wet gas is more likely to be generated than liquid petroleum.

Coal petrographers have observed that bitumens, petroleum-like substances, form from liptinites and vitrinites. This first coalification jump (or "bituminization") corresponds with the most prolific phase of crude oil formation in petroleum source rocks, that is  $R_0$  from 0.5 percent to about 1.3 percent (Stach and others, 1982). Radke and others (1980) documented a series of dramatic changes in rank trends at about 0.9 percent  $R_0$ . They suggested that the coincidence of changes in liptinite and vitrinite fluorescence with changes in the yield and composition of soluble organic matter, at near-equal stages of thermal maturity, implies a common cause. They interpreted this common cause to be the shift from predominantly generating to predominantly degrading chemical reactions, such as the dealkylation of aromatics and the cracking of alkanes. According to this study, vitrinite fluorescence tends to increase to a maximum at an  $R_0$  of about 1.0 percent, after which it decreases radically.

Qualitative descriptions of kerogen background fluorescence observed by Robertson Research indicate that ultraviolet fluorescence increased gradually and remained very high from 7,620 to 14,242 feet, after which it decreased very rapidly. Almost no fluorescence was observed between 13,000 and 14,000 feet, but most  $R_0$  values in this interval are well above 1.0 percent. Temperatures that were high enough to coke sediments could be expected to volatilize the aromatic compounds that are generally believed to be associated with the ultraviolet fluorescence of hydrocarbons.

Radke and others (1980) observed that in coals the odd-even predominance of n-alkanes from  $C_{15+}$  bitumen extracts, as expressed by the carbon preference index (CPI 25-31), exhibits a gradient change between  $R_0$  values of 0.9 and 1.0 percent. The CPI becomes asymptotic to about 1.0 or 1.1 within this range of thermal development. Robertson Research,

using soxhlet extraction and gas chromatography to isolate and quantitatively measure the n-alkanes, computed a similar ratio using the original Bray and Evans (1961) formula (CPI 24-34).

CPI values computed by Robertson Research from conventional core samples appear to become asymptotic at about 13,000 feet. CPI values from cuttings appear to be slightly erratic, perhaps because of uncertainty as to the exact depth from which the samples were cut. This corresponds with an  $R_0$  value of 0.9 percent at 13,000 feet.

Barker (1974), Claypool and Reed (1976), and Espitalie and others (1977) have suggested that  $T_2$ -max, the temperature at which maximum evolution of thermal hydrocarbons occurs during pyrolysis, can be used to characterize the degree of thermal maturation of kerogen. However, these measurements are influenced by the individual testing laboratory's instrumentation and technique, the rate of heating, the type of kerogen, the presence of recycled or oxidized organic matter, downhole contamination, and the presence of solid bitumen (Tissot and Welte, 1978; Dow and Coleman, 1983).

Pyrolysis was performed upon samples by both EXLOG and Robertson Research. The results of the two sets of analyses were quite similar. The  $T_2$ -max profile in figure 68 was constructed from EXLOG data.

Pyrolysis is frequently performed in such a manner that amorphous and liptinitic organic material will yield  $T_2$ -max values between 435° and 470° C when the kerogen is at its most favorable level of maturity for the formation of crude oil. EXLOG identified the interval between 12,540 and 14,940 feet as the oil generation window (Russ, 1983), which implies that their equipment and procedures were also calibrated for these threshold levels. Despite the fact that most of these analyses were performed on cuttings samples, the variation in the measurements is low, and the data yield a continuous profile down to the major unconformity at 12,780 feet. At greater depths, reworked sediments, coal fragments, and sediments exposed to igneous activity combine to produce a very discontinuous curve, with one measurement as high as 536° C. In both the EXLOG and Robertson Research data from below 13,000 feet, conventional core and sidewall core analyses tend to produce somewhat higher  $T_2$ -max values than cuttings. This suggests that the cuttings may contain uphole contaminants. It is reasonable to conclude from these data that hydrocarbon gas is more likely to form than liquid petroleum at depths greater than 15,000 feet.

There is good agreement between the indicators of thermal maturity that sufficient maturity for peak oil generation occurs between approximately 10,000 and 15,000 feet, and that wet gas would be preserved to at least 16,400 feet (TD). The continuous nature of the profiles across the unconformity at 12,780 feet and the projection of the  $R_0$  data to a value of about 0.2 percent at the surface suggest that deposition has been relatively continuous and that large amounts of section have not been lost at unconformities. All of the data, with the exception of the CPI profile, indicate a zone of high thermal maturity between 13,000 and 14,000 feet, and locally between 14,500 and 15,000 feet. These zones are of metamorphic grade and probably reflect the contact metamorphism of sediments by igneous intrusions.

#### HYDROCARBON SOURCE POTENTIAL

Plate 4 displays geochemical data and selected profiles, including sample descriptions, TOC (from sidewall cores, conventional cores, and cuttings at about 500-foot intervals), the genetic potential ( $S_1+S_2$ ) and transformation ratio ( $S_1/S_1+S_2$ ) from pyrolysis,  $C_{15+}$  bitumen and hydrocarbon extract from conventional cores and cuttings, and the volume and wetness ratio of headspace gas from canned cuttings samples. Wetness (in percent) is defined in this report as:

$$\left[ \frac{C_2+C_3+C_4}{C_1+C_2+C_3+C_4} \right] \times 100$$

Appendix 1 contains a summary of abbreviations excerpted from Mitchell and Maher (1957) that are used in the sample descriptions.

The total organic carbon content of these sediments has been examined, and the interval between 11,700 and 12,780 feet has been identified as the most promising section of potential source rock. Higher organic carbon contents are present at greater depth, but these tend to be associated with coal-bearing sediments having kerogen distributions and hydrogen levels characteristic of a terrigenous origin.

Rock-Eval pyrolysis is performed by heating whole rock samples at a predetermined rate in an inert atmosphere. Free or adsorbed hydrocarbons present in the rock are volatilized first at a moderate temperature. As the temperature increases, pyrolysis of kerogen generates hydrocarbons and hydrocarbon-like compounds. Finally, oxygen-bearing volatiles such as carbon dioxide and water are evolved. Relative amounts of the evolved hydrocarbons are measured by a flame ionization detector and quantities of oxygen-bearing compounds by a thermal conductivity detector. These measurements are usually



reported in weight-to-weight ratios of evolved gas to rock sample and are abbreviated by the symbols  $S_1$ ,  $S_2$ , and  $S_3$ , respectively. The temperature  $T_2$ -max in degrees centigrade, already referred to in the maturation section of this chapter, is the temperature at which the maximum evolution of pyrolytic hydrocarbons (the  $S_2$  peak) occurs. The hydrogen and oxygen indices plotted on the modified Van Krevelen diagram (fig. 67) are defined as the quotients  $S_2/TOC$  and  $S_3/TOC$ , respectively, and are reported in milligrams of gas per gram of organic carbon.

Studies by Claypool and Reed (1976) indicate that the  $S_1$  peak is directly proportional to the concentration of extractable  $C_{15+}$  hydrocarbons and the  $S_2$  peak is approximately proportional to the organic carbon content of the rock. The sum  $S_1+S_2$  is termed the genetic potential by Tissot and Welte (1978) because it accounts for both type and abundance of organic matter. They suggest the following threshold values for evaluating the oil and gas potential of source rock.

Table 14. Suggested threshold values for genetic potential ( $S_1+S_2$ ) from pyrolysis (from Tissot and Welte, 1978).

Genetic Potential ( $S_1 + S_2$ in ppm)	Hydrocarbon Source Rock Potential
Less than 2000	No oil. Some gas.
2000 to 6000	Moderate source rock.
Greater than 6000	Good source rock.

The genetic potential profile for this well, presented on plate 4, was constructed from Robertson Research data. The EXLOG observations are not included but yielded a very similar profile. Values in excess of 2,000 parts per million (ppm) occur from about 11,700 feet to the major unconformity at 12,780 feet. Values in excess of 6,000 ppm are present from about 12,450 to 12,780 feet.

The transformation ratio, or "productivity index" ( $S_1/S_1+S_2$ ), is usually regarded as an indicator of thermal maturity. However, it also responds to the composition of the kerogen if the level of maturity is high enough to generate hydrocarbons from favorable organic matter. Anomalously high values can also indicate the presence of nonindigenous hydrocarbons. In the Navarin well, the transformation ratio is generally less than 0.25 and exhibits only slight variation to a depth of about 10,000 feet. It then increases gradually to the unconformity at 12,780 feet, more or less mirroring the

genetic potential. This increase probably reflects a combination of the effects of increased thermal maturity and more favorable kerogen. Beneath the unconformity, the transformation ratio becomes erratic and increases to as much as 0.803 in response to the igneous activity and probably to methane generated by coal. The relatively low but slightly erratic wetness ratios from the headspace gas tend to support this hypothesis. An interesting feature of this profile is the low level of the transformation ratio between the surface and about 6,000 feet. The relatively large amounts of methane detected in canned cuttings samples and recorded on the mud log throughout this interval are not apparent in the fine-grained, organic-rich material selected for analysis by pyrolysis. Presumably this methane was contained in the diatomaceous ooze and siltstone and sandstone that represent much of the Neogene lithology, and is of either a biogenic or a nonindigenous origin.

Various empirical threshold values have been suggested to define anomalous levels of C<sub>15</sub>+ extractable hydrocarbons. Bayliss and Smith (1980) regard 200 to 400 ppm on a weight-to-weight basis as a good anomaly, and anything in excess of 800 ppm to be an excellent anomaly. Hunt (1979) considers 50 to 150 ppm to be adequate, but Phillippi (1957) placed the threshold of a good anomaly as high as 500 ppm. Bayliss and Smith (1980) suggest that 1,000 to 2,000 ppm extractable bitumen constitutes a good anomaly and that values in excess of 4,000 ppm are excellent. Conventional core 11 (at 9,986 feet) yields the first C<sub>15</sub>+ extractable hydrocarbon value in excess of 400 ppm, and below this point there seems to be a rather dramatic increase in both C<sub>15</sub>+ total extract and C<sub>15</sub>+ extractable hydrocarbons. The C<sub>15</sub>+ extractable hydrocarbons exceed 800 ppm at a depth of 11,709 feet (conventional core 13). Below the major unconformity at 12,780 feet, C<sub>15</sub>+ hydrocarbon and total extract values fall to background levels once again. Conventional core 17 (at 13,889 feet) appears to be slightly anomalous but this is probably due to the presence of coal. Note the corresponding high organic carbon content and relatively low value for the wetness ratio from this sample.

The amount of C<sub>15</sub>+ hydrocarbons and C<sub>15</sub>+ bitumens is frequently evaluated relative to the amount of organic carbon available to generate these substances. Tissot and Welte (1978) warn against the possibility of migrated or nonindigenous bitumen. Such an accumulation "is marked by abnormally high bitumen to organic carbon ratios (above 200 mg per g of organic carbon)." Although the bitumen to organic carbon ratio does exceed 0.2 in samples from conventional core 14, the S<sub>1</sub>/S<sub>1</sub>+S<sub>2</sub> ratio from pyrolysis does not suggest

that the amount of hydrocarbons which occur could not have been generated by the organic material incorporated in these sediments.

Hunt (1979) cites a study of Mesozoic-Cenozoic rocks in the western Ciscaspian region (Larskaya and Zhabrev, 1964) indicating that the "bitumen coefficient," the ratio between chloroform-soluble carbon and total organic carbon, is related to temperature. These investigations concluded that where the rocks they studied contained predominantly coal particles, the "bitumen coefficient" was very small and changed very little with increasing temperature. Where amorphous matter occurred, the "bitumen coefficient" was high and increased rapidly with temperature. Their studies imply that bitumen yields of fine-grained rocks in sedimentary basins are related to kerogen type. The C<sub>15</sub>+ organic extract data plotted on plate 4, particularly between about 11,700 and 12,780 feet, appear to correspond very well with these observations.

Hunt (1979) has plotted the C<sub>15</sub>+ hydrocarbon extract versus TOC from various sedimentary basins. His diagram is reproduced in a modified form in figure 69 with data from conventional core samples from the Navarin well substituted for the original data. There is a steady increase in the organic carbon in cores 11, 12, 13, and 14 to nearly the amount observed in reservoir rock. The amount of organic carbon drops sharply in core 15, and in subsequent cores the TOC content is similar to that observed in metamorphic rocks. The sample from core 17 (13,889 feet) that produced slightly higher amounts of C<sub>15</sub>+ bitumen contained 36.67 percent organic carbon and fell completely off this diagram in the direction of the field indicated for coals.

Relatively large amounts of headspace gas are present in the sediments above 6,000 feet in this well. This gas was detected in the drilling mud, as well as in the canned cuttings samples, and is composed almost completely of methane. Robertson Research suggests that this gas is of biogenic origin because of its high methane content. No carbon isotope ratios are presently available.

From approximately 6,000 to 12,780 feet, the amount of headspace gas relative to TOC is lower. A slight increase occurs between about 12,250 and 12,780 feet. Wetness, however, increases steadily from near 0 to 91 percent at about 11,910 feet, and it remains high to 12,780 feet.

From the major unconformity at 12,780 feet to about 14,250 feet, the gas content of cuttings is relatively high and the values are erratic. However, wetness is generally low, for the most part less than 20 percent, and with one

exception, all values are less than 40 percent. From 14,250 feet to the bottom of the well, both cuttings gas content and wetness are low.

These data suggest that thermogenic hydrocarbons have indeed been generated in the interval between 10,000 and 12,780 feet, where an adequate level of thermal maturity exists and organically rich sediments are present. The base of this interval apparently contains the most favorable potential source rocks.

#### SUMMARY AND CONCLUSIONS

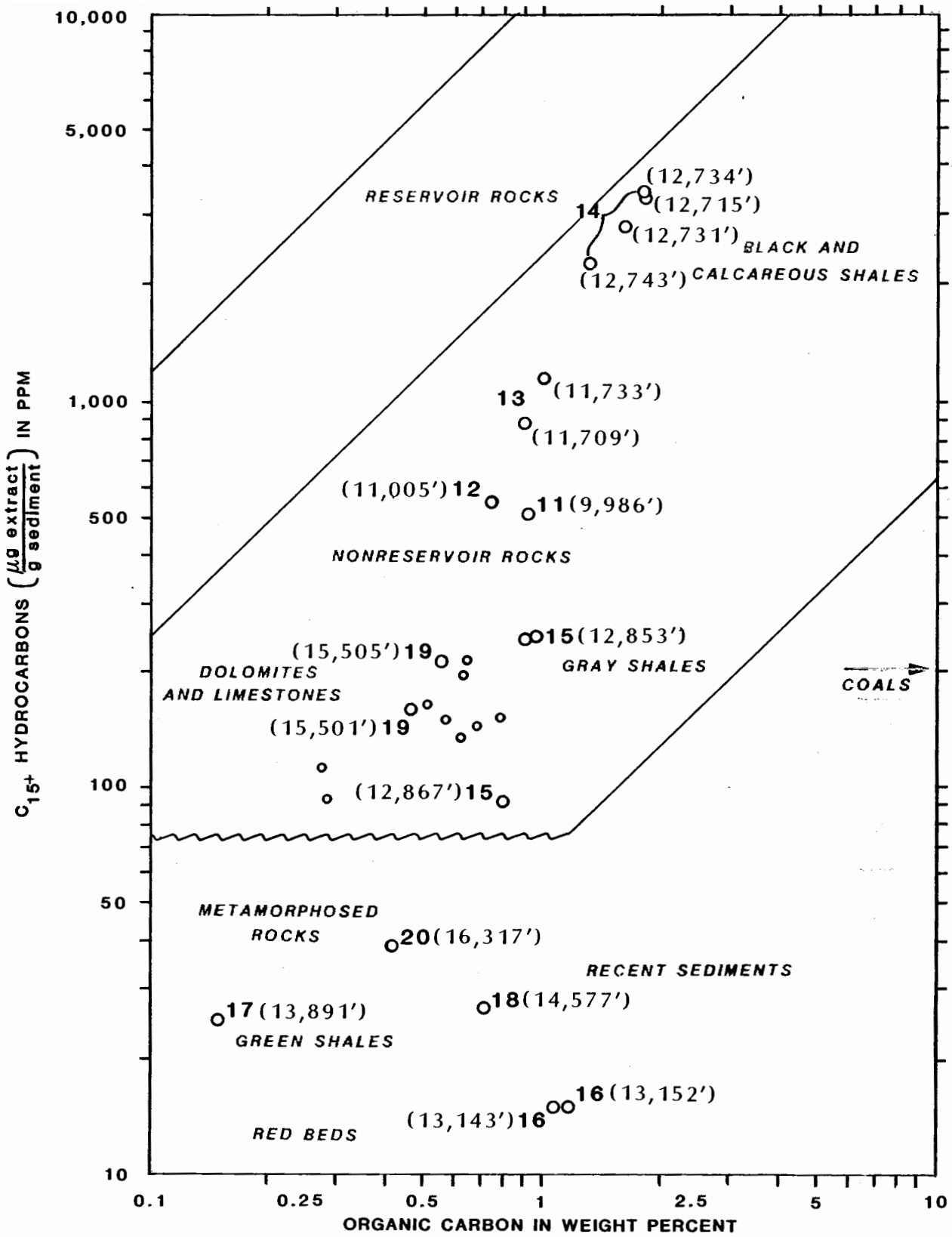
Geochemical data from the Navarin Basin COST No. 1 well indicate a sequence of Neogene rocks to a depth of about 5,700 feet that contains a predominantly type III kerogen. The Paleogene sequence, from approximately 5,700 to 12,780 feet, seems to contain progressively greater amounts of sapropelic kerogen with increased depth, and conventional core 14 yielded analyses from 12,715 to 12,742 feet that are characteristic of a type II kerogen. The kerogen changes abruptly at the major unconformity (12,780 feet) to a type III kerogen, and coal is common in samples from beneath this unconformity. Type III kerogen persists to the bottom of the well.

Type III kerogen is the product of Demaison's (1981) "type C" organic facies, and type II kerogen is derived from what he terms a "type B" organic facies.

A "type C" organic facies is typically the product of a mildly oxidic depositional environment and may include both marine and nonmarine sediments, slope and rise deposits, and exinite-rich coals. Hydrocarbons formed in this type of environment tend to be gas prone, sometimes with condensate hydrocarbons.

A "type B" organic facies is the product of an anoxic marine environment. It may occur where a regional oxygen minimum layer intersects the continental slope and shelf. It can also occur in silled basins such as the Black Sea or where upwelling seawater is rich in nutrients but under-saturated in oxygen. The Monterey Formation in California is considered to be an example of the latter setting. Transgressive marine shales and type II kerogen are associated with this facies, and they often constitute excellent oil source rocks.

The geochemical characteristics of these organic facies at an  $R_0$  of 0.5 percent are given in table 15 with similar analyses of samples from the Navarin well at a depth of 8,000 feet, where  $R_0$  is also approximately 0.5 percent.



INTERPRETATIONS BASED ON DATA FROM VARIOUS SEDIMENTARY BASINS (HUNT, 1979)  
 O 16 (13,152') - CONVENTIONAL CORE NUMBER AND DEPTH      o - CONVENTIONAL CORES 1-10

**FIGURE 69.** TOTAL ORGANIC CARBON AND EXTRACTABLE  $C_{15+}$  HYDROCARBONS. ANALYZED BY ROBERTSON RESEARCH (US) INC.



Table 15. Geochemical characteristics of Demaison's "type B and C" organic facies and analogous values from the Navarin Basin COST No.1 well.

	Type C Organic Facies R <sub>0</sub> =0.5%	COST No.1 Well R <sub>0</sub> =0.5%	Type B Organic Facies R <sub>0</sub> =0.5%
H/C	0.8 to 1.0	1.0	1.2 to 1.4
Hydrogen Index ( $\frac{\text{mg Hydrocarbon}}{\text{g TOC}}$ )	25 to 125	140 to 150	450 to 600
Oxygen Index ( $\frac{\text{mg CO}_2}{\text{g TOC}}$ )	50 to 200	15	20 to 60

It would appear that this kerogen more nearly resembles organic matter found in a "type C" organic facies. But organic characteristics and paleobathymetry suggest that at about 8,000 feet there is a gradational change from sediments with a greater terrestrial influence deposited in an upper bathyal environment to sediments with greater sapropelic kerogen content deposited in a middle bathyal environment. Between about 11,700 and 12,780 feet, Paleogene sediments include at least several tens of feet of "type B" organic facies. If this lithologic sequence thickens deeper in the basin, significant amounts of oil-prone source rock at a favorable level of thermal maturity may be present.

Sufficient thermal maturity for the development of crude oil exists below 10,000 feet, and degeneration of hydrocarbons due to thermal cracking probably does not occur above 15,000 feet except in sediments exposed to igneous activity. No significant oil shows were encountered in this stratigraphic test, but relatively greater amounts of methane did occur in sediments down to about 6,000 feet. This methane is believed to be of biogenic origin. With the possible exception of this light gas, there is no evidence to suggest that any of the hydrocarbons and organic extracts analyzed were not indigenous to the lithology penetrated by this well.

## ENVIRONMENTAL CONSIDERATIONS

By

Allen J. Adams

ARCO Exploration Company, as operator for itself and other participants, submitted a letter to the Minerals Management Service (MMS) (formerly Conservation Division, U.S. Geological Survey) dated June 18, 1981, for the proposed drilling of a deep stratigraphic test well in the Navarin Basin of the Alaska Outer Continental Shelf (OCS). Documents submitted in support of this proposal included a Drilling Plan, an Environmental Report, an Oil-Spill Contingency Plan (OSCP), and a Coastal Zone Consistency Certification. Site-specific biological surveys and geohazards/geotechnical surveys at the primary and alternate sites were required to investigate and document environmental conditions before approval of the geological and geophysical (G & G) permit application for the deep stratigraphic test well. The primary and alternate sites are located 120 miles and 133 miles, respectively, west of Pinnacle Island in the St. Matthew Hall Island group. The applicant followed requirements of 30 CFR Part 251 in submitting the G & G Permit application for this well.

A deep stratigraphic test well is drilled to acquire geological and engineering data that are used to determine the potential for hydrocarbon generation and retention within a proposed lease sale area. Deep Stratigraphic wells are commonly drilled off-structure and are not intended to locate hydrocarbon accumulations. The Navarin Basin COST No. 1 well was drilled off-structure. The information gathered from this test well was used to evaluate the hydrocarbon potential of the area covered by Navarin Basin Lease Sale No. 83 held in April 1984.

As part of the permit application review process, MMS prepared an Environmental Assessment (EA) under National Environmental Policy Act (NEPA) directives. The EA serves as a decision-making document to determine if the proposed action is or is not a major Federal action significantly affecting the quality of the human environment in the sense of NEPA, Section 102(2)(C). The EA evaluates the proposed action, the affected environment, environmental consequences, alternatives to the proposed action, unavoidable adverse environmental effects, and controversial issues.

MMS took site-specific geological, meteorological, oceanographic, biological, and cultural conditions into consideration before approving the drilling plan and monitored these conditions during drilling operations.

## GEOLOGY

A site-specific shallow drilling geohazards/geotechnical survey (Nekton, Inc., 1980b) was conducted in accordance with MMS requirements. It showed the sea floor at the proposed primary and alternate sites to be nearly flat and relatively featureless. The three geologic basins in the Navarin Province were formed by faulting, subsidence, and infilling with Late Mesozoic through Holocene age sediments. The northern basin is the largest, and the central basin the smallest. Both the primary and the alternate drill sites are on the eastern flank of the southern basin. The sea-floor sediment consists of soft Holocene clayey silts. Growth faults are present near the flanks of the basins. Several minor growth faults cut the underlying Pleistocene and Pliocene sediments at the well sites, but do not displace surface sediments. Displacement occurs to within 23 feet of the sea floor, with observed offsets as great as 10 feet. Pliocene reflectors at the alternate site contain evidence of amplitude anomalies, or bright spots, which suggest the presence of gas-charged sediments.

## GEOLOGICAL CONSIDERATIONS

The EA addressed the following types of geological hazards: shallow gas, faulting, seismicity and sediment instability, volcanism, abnormal pressure, and hydrogen sulfide.

The shallow drilling hazards survey indicated the presence of shallow gas at the alternate site only. Shallow gas, usually biogenic in origin, was not anticipated at the primary site and is not a problem at normal pressure.

Minor "active" growth faults occur at the sites, but did not cut the surface. Minimal offset between bedding and the gradual extension of this type of fault indicate that large, rapid displacement does not occur.

Seismicity in the area is historically low. Six earthquakes have been recorded in the Navarin Basin, the most recent in 1974. All were less than magnitude 6.0 on the Richter scale. An earthquake in the Navarin area could cause liquefaction or mass movement. However, because the topography of the proposed well sites was nearly flat, mass movement would not be expected. Liquefaction might occur, but the effects would probably be limited to anchors, wellhead, or riser connections and would be minor. An earthquake of sufficient magnitude to cause liquefaction, although unpredictable, was considered unlikely to occur during drilling operations.

The Navarin Basin is on the fringe of an area that could be affected by a large, explosive eruption in the Aleutian Arc System. Such an event was unlikely to occur during operations. Even if a major eruption had occurred, only minor ashfall would have occurred at the sites.

On the basis of preliminary geological and geophysical studies, abnormal pressure was not expected at the two potential well sites. Well location, well design, and safety procedures were designed to alleviate potential adverse conditions caused by abnormal pressure. The possibility of encountering high-pressure hydrocarbons at depth was also considered unlikely because the well was drilled off-structure.

Hydrogen sulfide ( $H_2S$ ) was not expected to be present. Had the drill rig monitoring system detected the presence of  $H_2S$ , the proper precautions would have been taken, in accordance with the  $H_2S$  Contingency Plan.

#### METEOROLOGY AND OCEANOGRAPHY

Most of the Bering Sea lies in subarctic latitudes, and a cyclonic atmospheric circulation predominates. Cloudy skies, moderately heavy precipitation, and strong surface winds characterize the marine weather. The weather is controlled by high pressure over the Pacific and Arctic Oceans and over Siberia, which causes the Aleutian low. Oceanic current flow is northerly, ranging from 0.5 knot in the south to 1.0 knot in the north, where the flow is accelerated toward the Bering Strait. Waves greater than 5 feet occur less than 50 percent of the time from June through September, 75 percent of the time in October, and more than 75 percent of the time in November. The well location is ice free from May through December, with up to 85 percent ice coverage from January through April.

Because limited meteorological and oceanographic data were available, the operator was required to collect meteorological, oceanographic, and performance data, pursuant to OCS Order No. 2, to aid in future operations in the area. During set-up and drilling operations, climatic and sea-state conditions were monitored to ensure that they did not exceed rig tolerances or jeopardize human safety. Winds, barometric pressure, air and water temperatures, waves, and currents were monitored and recorded. All environmental data collected during drilling operations are available to the public.

## BIOLOGY

The Bering Sea shelf edge and, to a lesser extent, the rest of the Navarin Planning Area are characterized by high primary productivity. This is due to the upwelling of nutrient-rich oceanic water, which supports a complex ecosystem of culturally and commercially valuable stocks of fish, invertebrates, and marine mammals. St. Matthew and Hall Islands, a wilderness area approximately 30 miles east of the planning area boundary, support a large number of bird species. These islands have been nominated as an area meriting special attention in the Alaska Coastal Management Plan.

A site-specific marine biological survey was designed by MMS in concert with other Federal and State agencies to obtain biological data at both the primary and alternate proposed deep stratigraphic test sites. Through the use of underwater video and photographic documentation, plankton tows, infaunal sampling, and trawling, ARCO (Nekton, 1980a) determined the relative abundance and types of organisms present in various habitats. These surveys were conducted from August 15 to August 17, 1980. The results are summarized as follows:

1. Copepods were the most abundant element of the plankton, accounting for about 99 percent of the total organisms. Smaller amounts (approximately 1 percent) of euphausiids (shrimp-like crustaceans) and chaetognaths (arrow worms) were also found. Decapod crustaceans (crabs) accounted for less than 1 percent of all samples. No fish eggs or fish larvae were found at either site.
2. Epibenthic invertebrates were the numerically dominant component of the trawl catch at both sites. The most abundant invertebrates were asteroids (sea stars) and ophiuroids (brittle stars). One commercial shrimp species was taken in low numbers at both sites.
3. Video and still photography of the seabed at both sites revealed, in decreasing order of abundance, eelpouts, roundfish, near-bottom plankton organisms, sea stars, and sea snails. Benthic grabs at both sites revealed that polychaete annelids (bristled worms) were the dominant phyla, followed by arthropods, priapulids (small wormlike animals), and echinoderms.

The biological survey conducted by Nekton, Inc., indicated that the area contained no unique habitats or species that would require rejection or modification of the drilling program.

It was determined that normal operations at either of the two sites would not adversely affect the environment. No additional biological resources were discovered during drilling operations. No adverse impacts on existing biological resources were apparent from well activities.

#### MARINE MAMMALS, ENDANGERED SPECIES, AND BIRDS

Marine resources of the Navarin Planning Area include overwintering whales and pinnipeds (seals and walrus); migrating whales; and migrating and resident sea birds and other waterfowl.

Few endangered mammals frequent the Navarin Planning Area. Bowhead whales overwinter in the vicinity of the ice front; beluga whales may also be present; and sperm whales feed along the shelf break along the western boundary of the area.

The proposed drilling program was submitted to the National Marine Fisheries Service (NMFS) and the U.S. Fish and Wildlife Service for review and comment regarding potential impacts of the operation on living resources in the area. A letter was received from NMFS, included as an attachment to the EA, recommending stipulations to be carried out in concert with the Alaska OCS Orders. NMFS recommended minimum approach distances for air and surface support craft, gave guidelines for reinitiation of consultation, and recommended continued cetacean research.

Eleven species of birds were observed at the primary site, and ten species at the alternate site. The most abundant bird species at both sites was the northern fulmar. Other species frequently encountered at the primary site included tufted puffins, common murre, fork-tailed storm petrels, black turnstones, Aleutian terns, Arctic terns, and black-legged kittiwakes, and at the alternate site, black-legged kittiwakes and common murre.

#### FISHERIES

The Navarin Planning Area contributes significantly to Bering Sea fisheries production. In the past, Bering Sea fishery resources have been largely exploited by Japanese, Korean, and Soviet fishing fleets, but with the advent of the Federal 200-mile extended jurisdiction, NMFS predicted that these resources would be intensively harvested by U.S. fishermen. Approximately 315 species of fish are present in the Bering Sea, of which 25 are commercially valuable. Herring, salmon, cod, halibut, ocean perch, and various flatfish are

the most important of the commercial species. Noteworthy also are the productive groundfish stocks, valuable populations of king and Tanner crab, and western Alaska salmon.

#### CULTURAL RESOURCES

It was determined that cultural and archeological surveys would not be required for the Navarin Basin well sites because the sites were located in a low probability area for cultural resources. If the TV transects, side-scan sonar, or magnetometer surveys had indicated unexplained anomalies, a review of the data would have been performed by a qualified marine archeologist. No anomalies were detected, and no cultural resources were identified during drilling operations.

#### DISCHARGES INTO THE MARINE ENVIRONMENT

The applicant disposed of drill cuttings and waste drilling mud into the ocean in compliance with MMS and Environmental Protection Agency (EPA) regulations. Past studies on the disposition and effects of routine discharges from offshore oil and gas activities indicated that such discharges were not likely to significantly affect the marine environment.

Bentonite was a continuous additive to the drilling mud. Barite was added as necessary for increasing mud weight. Bentonite and barite are insoluble, nontoxic, and inert. Other additives were used in minor concentrations, and most were used only under special conditions. These other additives would be either nontoxic or chemically neutralized in the mud or upon contact with seawater. No oil-based drilling mud was used.

Some excess cement was introduced into the marine environment while cementing shallow casing strings up to the sea floor.

Liquid wastes, including treated sewage, gray water, and some drilling by-products were discharged in accordance with regulations set forth by the EPA.

#### CONTINGENCY PLAN FOR OIL SPILLS

Procedures for preventing, reporting, and cleaning up oil spills were addressed in the OSCP, which was part of the Drilling Plan. The OSCP listed the equipment and material available to the permittee and described the capabilities of

the equipment under different sea and weather conditions. The plan also included a discussion of logistical support and identified specific individuals and their responsibilities in implementing the OSCP. Two response levels were organized: an onsite oil-spill team and an onshore support organization. The onsite oil-spill team was structured to provide immediate containment and cleanup capability for operational spills, such as may result from the transfer of fuel oil, and to initiate containment actions for larger, uncontrolled spills. The onshore support organization was to provide additional equipment and manpower to clean up large spills if they occurred.

One thousand feet of containment boom, an oil-spill skimmer, sorbents, oil storage containers, dispersants, collectants, and chemical application equipment were located on the drilling vessel. Additional equipment located on the emergency support barge offshore from St. Matthew Island included 300 feet of containment boom, an oil-spill skimmer, a diaphragm pump, and sorbents. Several oil-spill training drills were conducted to ensure familiarization with this equipment by each onsite oil-spill team. The operation also had access to additional oil-spill response equipment located at onshore staging points. The OSCP also identified all equipment that was available from other response organization sources, agreements to commit these resources, and requirements for obtaining the equipment. No spills resulted from this drilling operation.

The operator drilled the well according to the OCS Orders and utilized standard well control equipment and procedures. The casing and cementing programs (OCS Order No. 2) and subsequent abandonment requirements (OCS Order No. 3) were designed to prevent leakage or contamination by fluids within a permeable zone. Upon completion of the well, the site was cleared of all pipe and other material on or above the ocean floor.

As part of the EA process, the proposed deep stratigraphic test well program was submitted for comments to the appropriate Federal and State agencies, as well as to other interested parties. Responses were included as part of the EA. On the basis of the EA, on October 26, 1981, the Deputy Conservation Manager, Alaska Region, with the concurrence of the Conservation Manager, signed a Finding Of No Significant Impact (FONSI) on ARCO's proposed action, and determined that an Environmental Impact Statement was not required. A notice was issued to that effect. The Office of the Deputy Conservation Manager (now Regional Supervisor, Field Operations) consequently issued a letter to ARCO approving their Drilling Plan and G & G Permit. The State of Alaska found the operation to be consistent with its Coastal Zone Management Program on September 17, 1981, before MMS approved the Application for

Permit to Drill. The EA and FONSI documents are available for review in the public file in the office of the Regional Supervisor, Field Operations, U.S. Minerals Management Service, 800 A Street, Anchorage, Alaska 99501.

## SUMMARY AND CONCLUSIONS

by  
Ronald F. Turner

The ARCO Navarin Basin COST No. 1 Well was drilled to a measured depth of 16,400 feet. The Kelly Bushing was 85 feet above sea level. The water depth was 432 feet. The well site is approximately 457 miles southwest of Nome, Alaska. Drilling commenced on May 26, 1983, and was completed on October 22, 1983. Four strings of casing were set during drilling: 30-inch casing at 614 feet; 20-inch casing at 1,508 feet; 13 3/8-inch casing at 5,016 feet, and 9 5/8-inch casing at 12,834 feet. The drilling fluid for the first 1,536 feet was seawater; the drilling mud thereafter varied from 8.8 pounds/gallon to 14.1 pounds/gallon.

Logging runs were made from 5,032 to 1,497 feet, 11,046 to 5,004 feet, 12,834 to 5,004 feet, 15,341 to 12,815 feet, and 16,385 to 12,815 feet. The types of well logs run are listed in the Operational Summary chapter; geological analyses of most of the logs are presented in the Well Log Interpretation chapter. Twenty conventional cores, 668 sidewall cores, and well cuttings collected at 30-foot intervals (from 1,536 to 16,400 feet) were analyzed, variously, for porosity, permeability, lithology, organic geochemistry, paleontology, radiometric age, and paleomagnetism.

As required by 30 CFR 251, the operator (ARCO) filed a Drilling Plan, Environmental Report, Oil-Spill Contingency Plan, and Coastal Zone Consistency Certification. In addition, the MMS (formerly USGS, Conservation Division) required a geohazards survey, geotechnical survey, and site-specific biological survey. The zooplankton, infauna, epifauna, vagile benthos, and pelagic fauna were collected and analyzed. Particular emphasis was placed on protecting local and migratory marine mammals and avifauna. Waste discharges into the environment were minimal, nontoxic, and in compliance with Federal environmental protection regulations.

Sea-floor instability and gas-charged sediments are major geologic hazards in the Navarin Basin planning area. The well was drilled in an area not affected by these potential geohazards. Wireline log and formation test data clearly identify a potentially dangerous major zone of abnormal formation pore pressure from 9,430 to 15,300 feet. Thermally activated stripping of interlayer water from smectitic clays during illitization may be the primary process responsible for the abnormal pressures in this interval. Log analysis methods of assessing abnormal pressures are discussed at some length in the Abnormal Formation Pressure chapter. Caprocks associated with overpressured zones might function

as hydrocarbon traps, and the excess pore fluids might aid in the expulsion and migration of hydrocarbons.

Stratigraphic units in the well were defined on the basis of microfossil content, lithology and well log characteristics, and absolute dating techniques. The well penetrated Pliocene (1,536 to 3,180 feet), Miocene (3,180 to 5,704 feet), Oligocene (5,704 to 12,280 feet), Eocene (12,280 to 12,780 feet), and Cretaceous (12,780 to 16,400 feet) age sediments. The unsampled interval above 1,536 feet probably contains Plio-Pleistocene and Holocene sediments. The paleontology, paleobathymetry, and paleoecology of the section penetrated by the well are discussed in the Paleontology and Biostratigraphy chapter. The sedimentary section was divided into 11 lithologic zones on the basis of composition, source, and physical characteristics (see Lithology and Well Log Interpretation chapters). With the exception of a Late Cretaceous coal-bearing section, the fine-grained clastic sediments encountered were all deposited in marine environments. Reservoir characteristics are generally poor, and the best potential reservoirs are located considerably above the oil window. Porosity and permeability have been reduced by compaction, cementation, diagenesis, and authigenesis.

Time-depth curves generated from Long-Spaced Sonic (LSS) log data and nearby CDP stacking velocities differ by no more than 4 percent. The steeper time-depth curve calculated from LSS log data apparently is a result of nongeologic influences such as invalid assumptions relating stacking velocities to  $V_{RMS}$  and  $V_A$ , and the inherent travel path differences between the two methods. The effects of velocity anisotropy commonly associated with fine-grained sediments are not present.

Five regional depositional sequences were recognized on CDP sections, mapped, and correlated to the wells, in part by means of a synthetic seismogram generated from the Long-Spaced Sonic Log. The character and significance of these seismic sequences are discussed in the Seismic Stratigraphy chapter.

An average geothermal gradient of 1.78° F per 100 feet was calculated from 3,800 to 16,400 feet. The anomalously higher gradient of 2.5° F per 100 feet above 3,800 feet is probably due, at least in part, to the effects of an overpressured zone associated with the complex diagenetic alteration of diatomaceous sediments.

A bottom-simulating reflector (BSR) apparently related to biogenic silica diagenesis is present in the basin. In the well, this reflector is represented by lithologic Zone A-2. Such seismic reflections may be useful as markers of potentially dangerous abnormally pressured zones.

Sufficient thermal maturity for the development of crude oil exists below 10,000 feet. Degeneration of hydrocarbons due to thermal cracking probably does not occur above 15,000 feet except in sediments exposed to igneous activity. No significant oils shows were encountered in this stratigraphic test, but relatively greater amounts of methane did occur in sediments down to about 6,000 feet. This methane is believed to be of biogenic origin. With the possible exception of this light gas, there is no evidence to suggest that any of the hydrocarbons and organic extracts analyzed were not indigenous to the lithologies sampled. Between about 11,700 and 12,780 feet, the early Oligocene and late Eocene section includes a "type B" (anoxic marine) organic facies. If this lithologic sequence thickens deeper in the basin, significant amounts of oil-prone source rock at a favorable level of thermal maturity would be present.

The Navarin Basin consists of three en echelon subbasins filled with more than 26,000 feet of layered Tertiary sedimentary rock. The subbasins formed as a result of extensional deformation associated with strike-slip motion between the Kula and the North American Plates in the Late Cretaceous to early Tertiary. By the late Eocene, movement of the Kula Plate was isolated by subduction at the present Aleutian Arc. Subbasin subsidence in response to structural downdropping probably remained active until the late Oligocene. Regional subsidence in response to crustal cooling eventually led to sedimentation beyond the structurally defined subbasins. Beginning in the late Eocene, the three subbasins were filled with marine mudstones, siltstones, and minor sandstones. Sea level lowerings in the "middle" and late Oligocene, however, exposed older Tertiary and Mesozoic basement highs to wave-base erosion which resulted in the deposition of coarser grained material along the subbasin flanks.

Paleocene, Eocene, and Oligocene marine mudstones and sandstones with good source and reservoir potential may well be present in the deeper parts of the basin.

## REFERENCES

- AGAT Consultants, Inc. 1983. Reservoir quality study, ARCO Navarin Basin COST Well No. 1. 8 vols. Denver. Independent consultant report prepared for ARCO Exploration Company.
- Al-Chalabi, Mahboub. 1974. An analysis of stacking, RMS, average, and interval velocities over a horizontally layered ground. *Geophysical Prospecting* 22:458-75.
- Al-Chalabi, Mahboub. 1979. Velocity determination from seismic reflection data. In *Developments in Geophysical Exploration Methods-1*. London: Applied Science Publication Ltd.
- Anstey, N. A. 1977. *Seismic interpretation: The physical aspects*. Boston: International Human Resource Development Corp.
- ARCO Alaska, Inc. 1981. Environmental report for Navarin Basin COST No. 1. Anchorage. Report submitted to U.S. Minerals Management Service, Alaska OCS Region.
- Asquith, G. E., and Gibson, C. G. 1982. Basic well log analysis for geologists. Tulsa: AAPG.
- Badaut, Denise, and Risacher, Francois. 1982. Authigenic smectite on diatom frustules in Bolivian saline lakes. *Geochimica et Cosmochimica Acta* 47: 363-75.
- Banik, N. C. 1983. Velocity anisotropy of shales and depth anomalies in the North Sea. In 53rd Annual International Society of Exploration Geophysicists meeting, September 11-15, 1983, Las Vegas, Nevada: Expanded abstracts with biographies, 1983 Technical Program, 540-42. Tulsa.
- Barker, Colin. 1974. Pyrolysis techniques for source-rock evaluation. *AAPG Bulletin* 58:2349-61.
- Barron, J. A. 1980. Lower Miocene to Quaternary diatom biostratigraphy of Leg 57, off northeastern Japan, Deep Sea Drilling Project. In *Initial reports of the Deep Sea Drilling Project, vol. 56, 57, part 2*, 507-38. Washington, D.C.: National Science Foundation.
- Barron, J. A. 1981. Late Cenozoic diatom biostratigraphy and paleoceanography of the middle latitude eastern Pacific, Deep Sea Drilling Project. In *Initial reports of the Deep Sea Drilling Project, vol. 63*, 507-73. Washington, D.C.: National Science Foundation.

- Barron, J. A., and Keller, G. 1982. Widespread Miocene deep-sea hiatuses: Coincidence with periods of global cooling. *Geology* 10:577-81.
- Bayliss, G. S., and Smith, M. R. 1980. Source rock evaluation reference manual. Houston: Geochem Laboratories.
- BioStratigraphics Consulting Micropaleontology. 1983. ARCO Navarin Basin COST No. 1, Bering Sea, Alaska. 5 parts. Ventura, Calif: BioStratigraphics, a unit of McClelland Engineers.
- Blow, W. H. 1969. Late middle Eocene to Recene planktonic foraminiferal biostratigraphy. In Proceedings, first International Conference of Planktonic Microfossils, Geneva, 1967, vol. 1, 199-422. Leiden: E. J. Brill.
- Bolli, H. M. 1957. Planktonic foraminifera from the Oligocene-Miocene Cipero and Lengua Formations of Trinidad, B.W.I.: U.S. National Museum Bulletin, No. 215, 97-123.
- Bray, E. E., and Evans, E. D. 1961. Distribution of n-paraffins as a clue to recognition of source beds. *Geochemica et Cosmochimica Acta* 22:2-15.
- Burckle, Lloyd. 1981. Paleomagnetic data on the Dictyochoa aspera/D. fibula crossover in the equatorial Pacific. *Micropaleontology* 27:332-34.
- Burst, J. F. 1969. Diagenesis of Gulf Coast clayey sediments and its possible relation to petroleum migration. *AAPG Bulletin* 53:73-93.
- Byun, B. S. 1983. Characteristics of reflection traveltimes for layer models. In 53rd Annual International Society of Exploration Geophysicists meeting, September 11-15, 1983, Las Vegas, Nevada: Expanded abstracts with biographies, 1983 Technical Program, 447-48. Tulsa.
- Carlson, P. R.; Fischer, J. M.; Karl, H. A.; and Larkin, Christopher. 1983. Isopach map of unit A, youngest sedimentary sequence in Navarin Basin. In Surface and near-surface geology, Navarin Basin province: Results of the 1980-81 field seasons, ed. H. A. Karl and P. R. Carlson. U.S. Geological Survey Open-File Report 84-89.
- Carlson, P. R., and Karl, H. A. 1981. Seafloor geologic hazards, sedimentology, and bathymetry: Navarin Basin province, northwestern Bering Sea. U.S. Geological Survey Open-File Report 81-1217.

- Carlson, P. R.; Karl, H. A.; Fischer, J. M.; and Edwards, B. D. 1982. Geologic hazards in Navarin Basin province, northern Bering Sea. In Fourteenth annual Offshore Technology Conference, proceedings, paper 4172.
- Carlson, P. R., and Marlow, M. S. 1984. Discovery of a gas plume in Navarin Basin. *Oil and Gas Journal* 82 (2 April):157-58.
- Claypool, G. E., and Reed, P. R. 1976. Thermal-analysis technique for source rock evaluation: Quantitative estimates of organic richness and effects of lithologic variation. *AAPG Bulletin* 60:608-26.
- Core Laboratories, Inc. 1983. Core analysis report for ARCO Alaska, Inc., Navarin COST No. 1 stratigraphic test, Navarin Basin, Alaska. Dallas.
- Davey, R. J.; Downie, Charles; Sarjeant, W. A. S.; and Williams, G. L. 1966. Studies on Mesozoic and Cainozoic dinoflagellate cysts. *Bulletin of the British Museum (Natural History), Geology, Supplement 3*. London.
- Deffeyes, K. S. 1959. Zeolites in sedimentary rocks. *Journal of Sedimentary Petrology* 29:602-9.
- Demaison, G. J. 1981. Stratigraphic aspects of source bed occurrence: The organic facies concept. In *Geochemistry for geologists. Short Course Notes*. Dallas: AAPG.
- Dix, C. H. 1955. Seismic velocities from surface measurements. *Geophysics* 20:68-86.
- Dow, W. G. 1977. Kerogen studies and geological interpretations. *Journal of Geochemical Exploration* 7(2):79-99.
- Dow, W. G., and Coleman, S. H. 1983. Geochemical analysis of Navarin Basin #1 COST well, Alaska. Houston: Robertson Research (U.S.), Inc. Prepared for ARCO Exploration Co., Anchorage.
- Dow, W. G., and O'Connor, D. J. 1982. Kerogen maturity and type by reflected light microscopy applied to petroleum exploration. In *How to assess maturation and paleotemperatures*, 133-57. SEPM Short Course no. 7. Tulsa: Society of Economic Paleontologists and Mineralogists.
- Dresser Atlas, Dresser Industries, Inc. 1979. Log interpretation charts. Houston.

- Dundo, O. P. 1974. Stratigraphic scheme of the Cretaceous deposits of the Koryak highlands (design of unified and correlational schemes). In Stratigraphy and lithology of the Cretaceous, Paleogene, and Neogene deposits of the Koryak-Anadyr District, 5-15. Leningrad: Scientific Research Institute of Arctic Geology (NIIGA), Ministry of Geology of the USSR.
- Elsik, W. C. 1977. Paralecaniella indentata (Defl. and Cooks. 1955) Cookson and Eisenack 1970 and allied dinocysts. *Palynology* 1:95-102.
- ERT biostrat. 1983. Micropaleontology report, Navarin Basin COST well program, Bering Sea, Alaska. Fort Collins, Colo.: ERT biostrat, a division of Environmental Research and Technology, Inc.
- Espitalie, J.; Laporte, J. L.; Madec, M.; Marquis, F.; Leplat, P.; Paulet, J.; and Boutefeu, A. 1977. Methode rapide de caracterisation des roches meres, de leur potentiel petrolier et de leur degre d'evolution. *Revue de l'Institute Francais Petrolier* 32:23-42.
- Exploration Logging (USA), Inc. 1983. Final operational report, ARCO Alaska, Inc., Navarin Basin COST well #1, May 1983 to October 1983. Anchorage.
- Exploration Logging (USA), Inc., see also Russ, 1983, Geochemical final well report.
- Fertl, W. H. 1976. Abnormal formation pressures. *Developments in Petroleum Science*, 2. New York: Elsevier.
- Fertl, W. H., and Wichmann, P.A. 1977. How to determine static BHT from well log data. *World Oil* 184:105-6.
- Folk, R. L. 1974. *Petrology of sedimentary rocks*. Austin, Tex.: Hemphill.
- Fullam, T. J.; Supko, P. R.; Boyce, R. E.; and Stewart, R. J. 1973. Some aspects of Late Cenozoic sedimentation in the Bering Sea and north Pacific Ocean. In *Initial reports of the Deep Sea Drilling Project*, vol. 19, ed. P. R. Supko, 887-96. Washington, D. C.: National Science Foundation.

- Geological Society of America. 1970. Rock color chart, by E. N. Goddard, P. D. Trask, R. K. DeFord, O.N. Rove, J. T. Singewald, Jr., R. M. Overbeck. Boulder.
- Gladenkov, Y. B. 1977. Stages in the evolution of mollusks and subdivisions of the North Pacific Neogene. In Proceedings of the first International Congress on Pacific Neogene stratigraphy, Tokyo, 1976, ed. Tsunemasa Saito and Hiroshi Ujiie, 89-91. Tokyo: International Union of Geological Sciences, Science Council of Japan, and Geological Society of Japan.
- Gladenkov, Y. B. 1980. Stratigraphy of marine Paleogene and Neogene of northeast Asia (Chukotka, Kamchatka, Sakhalin). AAPG Bulletin 64:1087-93.
- Gretener, P. E. 1981. Pore pressure: Fundamentals, general ramifications, and implications for structural geology (revised). Education Course Note Series no. 4. Tulsa: AAPG.
- Hammond, R. D., and Gaither, J. R. 1983. Anomalous seismic character - Bering Sea shelf. Geophysics 48:590-605.
- Harland, Rex. 1978. Quaternary and Neogene dinoflagellate cysts. In Distribution of biostratigraphically diagnostic dinoflagellate cysts and miospores from the northwest European continental shelf and adjacent areas, ed. Bindra Thusu, 7-17. Continental Shelf Institute Publication no. 100. Trondheim, Norway.
- Hedberg, H. D. 1976. Relation of methane generation to under-compacted shales, shale diapirs and mud volcanoes. AAPG Bulletin 58:661-73.
- Hein, J. R.; O'Neil, J. R.; and Jones, M. G. 1979. Origin of authigenic carbonates in sediment from the deep Bering Sea. Sedimentology 26:681-705.
- Hein, J. R., and Scholl, D. W. 1978. Diagenesis and distribution of late Cenozoic volcanic sediment in the southern Bering Sea. Geological Society of America Bulletin 89:197-210.
- Hein, J. R.; Scholl, D. W., Barron, J. A.; Jones, M. G.; and Miller, Jacquelyn. 1978. Diagenesis of late Cenozoic diatomaceous deposits and formation of the bottom simulating reflector in the southern Bering Sea. Sedimentology 25:155-81.
- Hottmann, C. E., and Johnson, R. K. 1965. Estimation of formation pressures from log-derived shale properties. Journal of Petroleum Technology (June 1965): 717-22.

- Hunt, J. M. 1979. Petroleum geochemistry and geology. San Francisco: W. H. Freeman.
- Iijima, Azuma. 1980. Geology of natural zeolites and zeolitic rocks. *Pure and Applied Chemistry* 52:2115-30.
- Iijima, Azuma, and Utada, Minoru. 1983. Recent developments in the sedimentology of siliceous deposits in Japan. In *Siliceous deposits in the Pacific region*, ed. A. Iijima, J. R. Hein, and R. Siever, 45-64. *Developments in Sedimentology* no. 36. Amsterdam: Elsevier.
- Isaacs, C. M.; Pisciotto, K. A.; and Garrison, R. E. 1983. Facies and diagenesis of the Miocene Monterey Formation, California: A summary. In *Siliceous deposits in the Pacific region*, ed. A. Iijima, J. R. Hein, and R. Seiver, 247-82. *Developments in Sedimentology* no. 36. Amsterdam: Elsevier.
- Jacobson, R. A. 1984. Age determination of dredge samples. Denver: Jacobson Consulting, Inc.
- Jones, D. M.; Kingston, M. J.; Marlow, M. S.; Cooper, A. K.; Barron, J. A.; Wingate, F. H.; and Arnal, R. E. 1981. Age, mineralogy, physical properties, and geochemistry of dredge samples from the Bering Sea continental margin. U.S. Geological Survey Open-File Report 81-1297.
- Jorden, J. R., and Shirley, O. J. 1966. Application of drilling performance data to overpressure detection. AIME-SPE Paper no. 1407. *Journal of Petroleum Technology* 18:1387-94.
- Karl, H. A., and Carlson, P. R. 1984. Surface and near-surface geology, Navarin Basin province: Results of the 1980-1981 field seasons. U.S. Geological Survey Open-File Report 84-89.
- Keigwin, Lloyd, and Keller, Gerta. 1984. Middle Oligocene cooling from equatorial Pacific DSDP site 77B. *Geology* 12:16-19.
- Keller, Gerta. 1983. Biochronology and paleoclimatic implications of middle Eocene to Oligocene planktonic foraminiferal faunas. *Marine Micropaleontology* 7(6):463-86.
- Keller, Gerta, and Barron, J. A. 1983. Paleooceanographic implications of Miocene deep-sea hiatuses. *Geological Society of America Bulletin* 94:590-613.
- Kerr, R. A. 1984. Ice cap of 30 million years ago detected. *Science* 224(13 April):141-42.

- Koizumi, Itaru 1973. The Late Cenozoic diatoms of sites 183-193, Leg 19 Deep Sea Drilling Project. In Initial reports of the Deep Sea Drilling Project, vol. 19, ed. P. R. Supko, 805-55. Washington, D. C.: National Science Foundation.
- Korotkevich, V. D. 1974. Late Cretaceous spore-pollen assemblages of the Koryak highlands. In Stratigraphy and lithology of the Cretaceous, Paleogene, and Neogene deposits of the Koryak-Anadyr District, 31-37. Leningrad: Scientific Research Institute of Arctic Geology (NIIGA), Ministry of Geology of the USSR.
- Kvenvolden, K. A., and McMenamin, M. A. 1980. Hydrates of natural gas: A review of their geologic occurrence. U.S. Geological Survey Circular 825.
- Larskaya, Y. S., and Zhabrev, D. H. 1964. Effects of stratal temperatures and pressures on the composition of dispersed organic matter from the example of the Mesozoic-Cenozoic deposits of the western Ciscaspian region. Dokl. Akad. Nauk SSSR 157(4):135-39.
- Lentin, J. K., and Williams, G. L. 1977. Fossil dinoflagellates: Index to genera and species. Bedford Institute of Oceanography Report Series BI-R-77-8. Dartmouth, Canada.
- Levin, F. K. 1978. The reflection, refraction, and diffraction of waves in media with an elliptical velocity dependence. Geophysics 48:528.
- Ling, H. Y. 1973. Silicoflagellates and Ebridians from Leg 19. In Initial reports of the Deep Sea Drilling Project, vol. 19, ed. P. R. Supko, 751-75. Washington, D. C.: National Science Foundation.
- Ling, H. Y. 1977. Late Cenozoic silicoflagellates and Ebridians from the eastern North Pacific region. In Proceedings of the first International Congress on Pacific Neogene Stratigraphy, Tokyo, 1976, ed. Tsunemasa Saito and Hiroshi Ujiie, 205-33. Tokyo: International Union of Geological Sciences, Science Council of Japan, and Geological Society of Japan.
- MacGregor, J. R. 1965. Quantitative determination of reservoir pressures from conductivity log. AAPG Bulletin 49:1502-11.
- Marks, J. G. 1983. Molluscan fossils from third Alaska deep test, a report for ARCO Exploration Company: Preliminary reports and summary. Englewood, Colo.

- Marlow, M. S.; Carlson, P.; Cooper, A. K.; Karl, H.; McLean, H.; McMullin, R.; and Lynch, M. B. 1981. Hydrocarbon resource report for proposed OCS sale No. 83, Navarin Basin, Alaska. U.S. Geological Survey Open-File Report 81-252.
- Marlow, M. S.; Cooper, A. K.; and Childs, J. R. 1983a. Tectonic evolution of Gulf of Anadyr and formation of Anadyr and Navarin Basins. AAPG Bulletin 67:646-65.
- Marlow, M. S.; Vallier, T. L.; Cooper, A. K.; Barron, J. A.; and Wingate, F. H. 1983b. A description of dredge samples collected in 1982 from the Bering Sea continental margin west of Navarin Basin. U.S. Geological Survey Open-File Report 83-325.
- Mason, Brian, and Sand, L. B. 1960. Clinoptilolite from Patagonia: The relationship between clinoptilolite and heulandite. American Mineralogist 45:341-50.
- Matthews, R. K., and Poore, R. Z. 1980. Tertiary  $^{18}\text{O}$  record and glacio-eustatic sea-level fluctuations. Geology 8:501-4
- McClure, L. J. 1977. Drill abnormal pressure safely. Manual for a short course offered by the author. Houston.
- McLean, Hugh. 1979a. Review of petroleum geology of Anadyr and Khatyrka Basins, U.S.S.R. AAPG Bulletin 63:1467-77.
- McLean, Hugh. 1979b. Sandstone petrology: Upper Jurassic Naknek Formation of the Alaska Peninsula and coeval rocks on the Bering shelf. Journal of Sedimentary Petrology 49:1263-68.
- Meyer, B. L., and Nederlof, M. H. 1984. Identification of source rocks on wireline logs by density/resistivity and sonic transit time/resistivity crossplots. AAPG Bulletin 68:121-29.
- Meyers, Herbert. 1976. A historical summary of earthquake epicenters in and near Alaska. U.S. National Oceanic and Atmospheric Administration Technical Memorandum EDS NGSDC-1.
- Mitchell, J. G., and Maher, J. C. 1957. Suggested abbreviations for lithologic descriptions. AAPG Bulletin 41:2103-7.
- Murata, K. J.; Friedman, I.; and Gleason, J. D. 1977. Oxygen isotope relations between diagenetic silica minerals in Monterey shale, Temblor Range, California. American Journal of Science 277:259-72.

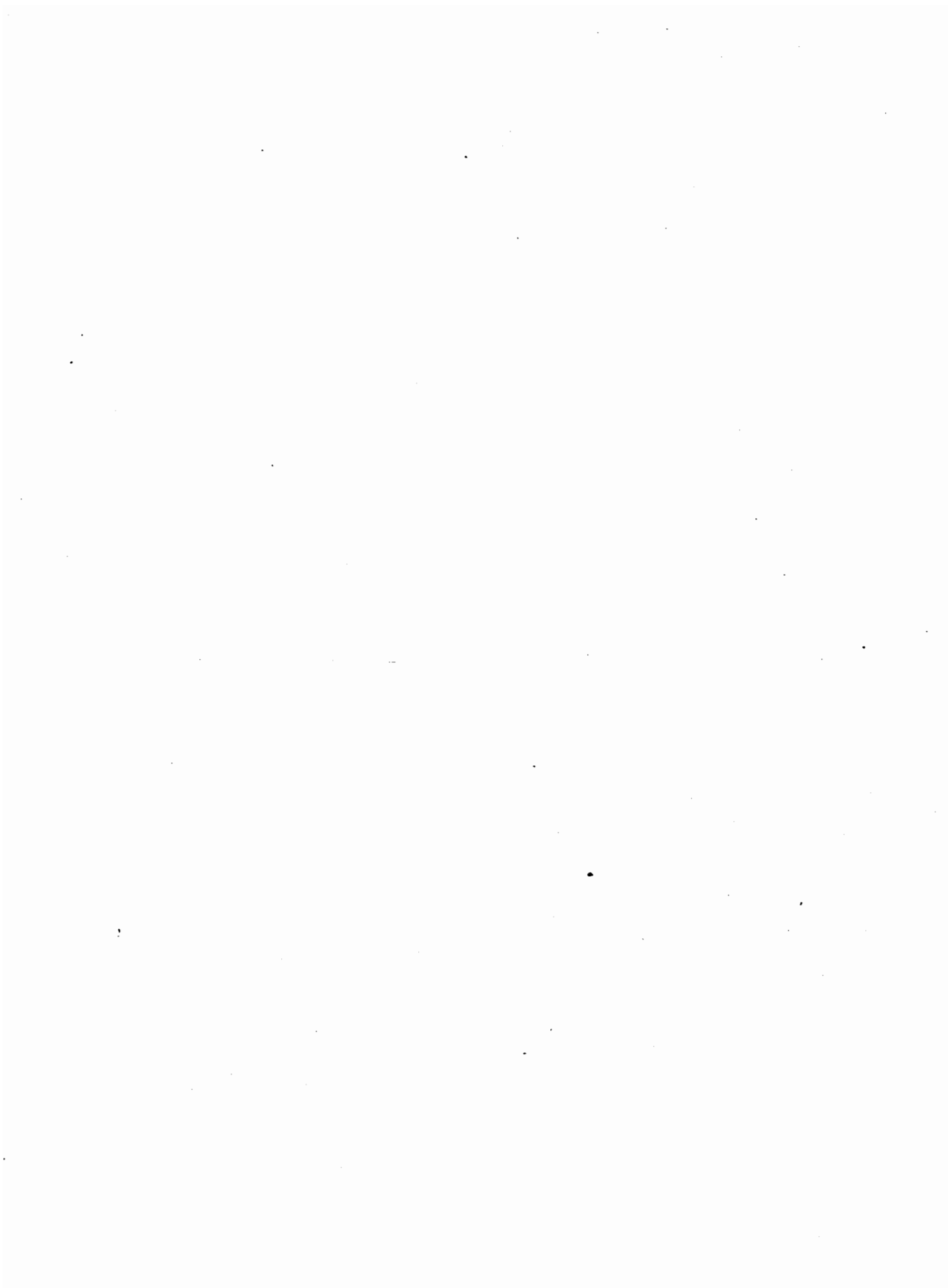
- Murata, K. J., and Whiteley, K. R. 1973. Zeolites in the Miocene Briones Sandstone and related formations of the central Coast Ranges, California. *Journal of Research of the U.S. Geological Survey* 1:255-65.
- Nardin, T. R.; Hein, F. J.; Gorsline, D. S.; and Edwards, B. D. 1979. A review of mass movement processes, sediment and acoustic characteristics, and contrasts in slope and base-of-slope systems versus canyon-fan-basin floor systems. In *Geology of continental slopes*, ed. L. J. Doyle and O. H. Pilkey, 61-73. Society of Economic Paleontologists and Mineralogists Special Publication no. 27. Tulsa.
- Nekton, Inc. 1980a. Biological survey: proposed continental offshore stratigraphic test No.1, Navarin Basin, Alaska. San Diego. Report to ARCO Oil and Gas Company.
- Nekton, Inc. 1980b. Shallow drilling hazards survey: proposed continental offshore stratigraphic test No. 1, Navarin Basin, Alaska. San Diego. Report to ARCO Oil and Gas Company.
- Patton, W. W., Jr.; Lanphere, M. A.; Miller, T. P.; and Scott, R. A. 1975. Age and tectonic significance of volcanic rocks on St. Matthew Island, Bering Sea, Alaska. U.S. Geological Survey Open-File Report 75-150.
- Pennebaker, E. S. 1968a. An engineering interpretation of seismic data. SPE 2165, 43rd AIME Fall Meeting, Houston, Texas. Dallas: Society of Petroleum Engineers of AIME.
- Pennebaker, E. S. 1968b. Seismic data indicate depth, magnitude of abnormal pressures. *World Oil* 166:73-78.
- Phillipi, G. T. 1957. Identification of oil source beds by chemical means. In 20th International Geological Congress, proceedings, Mexico City, Sec. 3, 25-28.
- Pisciotta, K. A. 1981. Distribution, thermal histories, isotopic compositions, and relection characteristics of siliceous rocks recovered by the Deep Sea Drilling Project. In *Society of Economic Paleontologists and Mineralogists Special Publication no. 32*, 129-147.
- Powers, M. C. 1967. Fluid-release mechanisms in compacting marine mudrocks and their importance in oil exploration. *AAPG Bulletin* 51:1240-54.
- Radke, Matthias; Schaffer, R. G.; Leythaeuser, Detlev; and Teichmuller, Marlies. 1980. Composition of soluble organic matter in coals: Relation to rank and liptinite fluorescence. *Geochemica et Cosmochemica Acta* 44:1787-1800.

- Robertson Research (U.S.), Inc., see Dow and Coleman, 1983.
- Robinson, G. S. 1970. Change of the bathymetric distribution of the genus *Cyclammina*. In Vol. 20, Transactions, Gulf Coast Association of Geological Societies, ed. N. G. Shaw, 201-9. Shreveport.
- Rouse, G. E. 1977. Paleogene palynomorph ranges in western and northern Canada. In Contributions of stratigraphic palynology (with emphasis on North America): Vol. 1, Cenozoic palynology, ed. W. C. Elsik, 48-65. American Association of Stratigraphic Palynologists Contribution Series no. 5 A.
- Russ, Tony. 1983. Geochemical final well report, ARCO Alaska, Inc., Navarin Basin COST No. 1. Anchorage: Exploration Logging (USA), Inc.
- Schlumberger Well Services, Inc. 1972. Log interpretation manual. Vol. 1, Principles. Houston.
- Schlumberger Well Services, Inc. 1974. Log interpretation manual. Vol. 2, Applications. Houston.
- Schmidt, G. W. 1973. Interstitial water composition and geochemistry of deep Gulf Coast shales and sandstones. AAPG Bulletin 57:321-37.
- Scholl, D. W., and Creager, J. S. 1973. Geologic synthesis of Leg 19 (DSDP) results: Far North Pacific, and Aleutian Ridge, and Bering Sea. In Initial reports of the Deep Sea Drilling Project, vol. 19, ed. P. R. Supko, 897-913. Washington, D. C.: National Science Foundation.
- Schrader, Hans. 1973. Cenozoic diatoms from the northeast Pacific, Leg 18. In Initial reports of the Deep Sea Drilling Project, vol. 18, 673-797. Washington, D. C.: National Science Foundation.
- Serova, M. Y. 1976. The *Caucasina eocaenica kamchatica* Zone and the Eocene-Oligocene boundary in the northwestern Pacific. In Progress in micropaleontology: Selected papers in honor of Prof. Kiyoshi Asano, ed. Yokichi Takayanagi and Tsunemasa Saito, 314-28. New York: The American Museum of Natural History, Micropaleontology Press.
- Sheriff, R. E. 1978. A first course in geophysical examination and interpretation. Boston: International Human Resource Development Corp.
- Stach, E.; Mackowsky, M.-Th.; Teichmüller, M.; Taylor, G. H.; Chandra, D.; and Teichmüller, R. 1982. Stach's textbook of coal petrology. Berlin: Gebrüder Borntraeger.

- Staplin, F. L. 1969. Sedimentary organic matter, organic metamorphism, and oil and gas occurrence. *Bulletin of Canadian Petroleum Geology* 17:47-66.
- Stewart, M. I. 1983. Well planning, part I. Seminar given at U.S. Minerals Management Service, Alaska OCS Region, Anchorage, Alaska, August 1-5, 1983.
- Stoll, R. D.; Ewing, J.; and Bryan, G. M. 1971. Anomalous wave velocity in sediments containing gas hydrates. *Journal of Geophysical Research* 76:2090.
- Stone, D. B., Panuska, B.C., and Packer, D. R. 1982. Paleolatitudes versus time for southern Alaska. *Journal of Geophysical Research* 87(no.B5):3697-3707
- Stover, L. E., and Evitt, W. R. 1978. Analyses of pre-Pleistocene organic-walled dinoflagellates. *Stanford University Publications Geological Sciences* vol. 15. Stanford.
- Teledyne Isotopes. 1983. Potassium-argon age determination on three samples from the ARCO Navarin Basin COST well No. 1 for ARCO Alaska, Inc. Westwood, N.J.: Teledyne Isotopes.
- Tipsword, H. L.; Setzer, F. M.; and Smith, F. L., Jr. 1966. Interpretation of depositional environment in Gulf Coast petroleum exploration from paleoecology and related stratigraphy. *Transactions, Gulf Coast Association of Geological Societies*, vol. 16, ed. F. W. Bates, 119-30. Houston.
- Tissot, B. P., and Welte, D. H. 1978. *Petroleum formation and occurrence*. New York: Springer-Verlag.
- Turner, R. F.; Bolm, J. G.; McCarthy, C. M.; Steffy, D. A.; Lowry, Paul; and Flett, T. O. 1983a. Geological and operational summary, Norton Sound COST No. 1 well, Norton Sound, Alaska. U.S. Geological Survey Open-File Report 83-124.
- Turner, R. F.; Bolm, J. G.; McCarthy, C. M.; Steffy, D. A.; Lowry, Paul; Flett, T. O.; and Blunt, David. 1983b. Geological and operational summary, Norton Sound COST No. 2 well, Norton Sound, Alaska. U.S. Geological Survey Open-File Report 83-557.

- Turner, R. F.; McCarthy, C. M.; Comer, C. D.; Larson, J. A.; Bolm, J. G.; Banet, A. C., Jr; and Adams, A. J. 1984a. Geological and operational summary, St. George Basin COST No. 1 well, Bering Sea, Alaska. OCS Report MMS 84-0016. Anchorage: U.S. Department of the Interior, Minerals Management Service.
- Turner, R. F.; McCarthy, C. M.; Comer, C. D.; Larson, J. A.; Bolm, J. G.; Flett, T. O.; and Adams, A. J. 1984b. Geological and operational summary, St. George Basin COST No. 2 well, Bering Sea, Alaska. OCS Report MMS 84-0018. Anchorage: U.S. Department of the Interior, Minerals Management Service.
- U.S. Minerals Management Service, Alaska OCS Region, Field Operations. 1981. OCS environmental assessment No. AK 81-6. Anchorage. Photocopy.
- Vail, P. R.; Mitchum, R. M., Jr; and Thompson, S., III. 1977. Seismic stratigraphy and global changes of sea level, part 4: Global cycles of relative changes of sea level. In Seismic stratigraphy: Applications to hydrocarbon exploration, ed. C. E. Payton, 83-97. American Association of Petroleum Geologists Memoir 26. Tulsa.
- Vallier, T. L.; Underwood, M. B.; Jones, D. L.; and Gardner, J. V. 1980. Petrography and geologic significance of Upper Jurassic rocks dredged near Pribilof Islands, southern Bering Sea continental shelf. AAPG Bulletin 64:945-50.
- Van Alstine, D. R. 1983. Paleomagnetism of core from the Navarin Basin COST well No. 1. Vol 1, Interpretation. Walnut Creek, Calif.: Z Axis, a subsidiary of Woodward-Clyde Consultants. Prepared for the Bering Sea COST Group.
- Van Bennekom, A. J., and Van der Gaast, S. J. 1976. Possible clay structures in frustules of living diatoms. *Geochimica et Cosmochimica Acta* 40:1149-52.
- Vogel, T. M., and Kvenvolden, K. A. 1981. Hydrocarbon gases in Navarin Basin province sediments. In Sea floor geologic hazards, sedimentology, and bathymetry: Navarin Basin province, northwestern Bering Sea, ed. P. R. Carlson and H. A. Karl, 80-99. U.S. Geological Survey Open-File Report 81-1217.
- Voloshinova, N. A., and Budasheva, A. I. 1961. Lituolids and trochamminids from the Tertiary deposits of Sakhalin Island and the Kamchatka Peninsula. Microfauna of the USSR, Trudy sbornik 12, vol. 170, p. 199, Leningrad (VNIGRI).

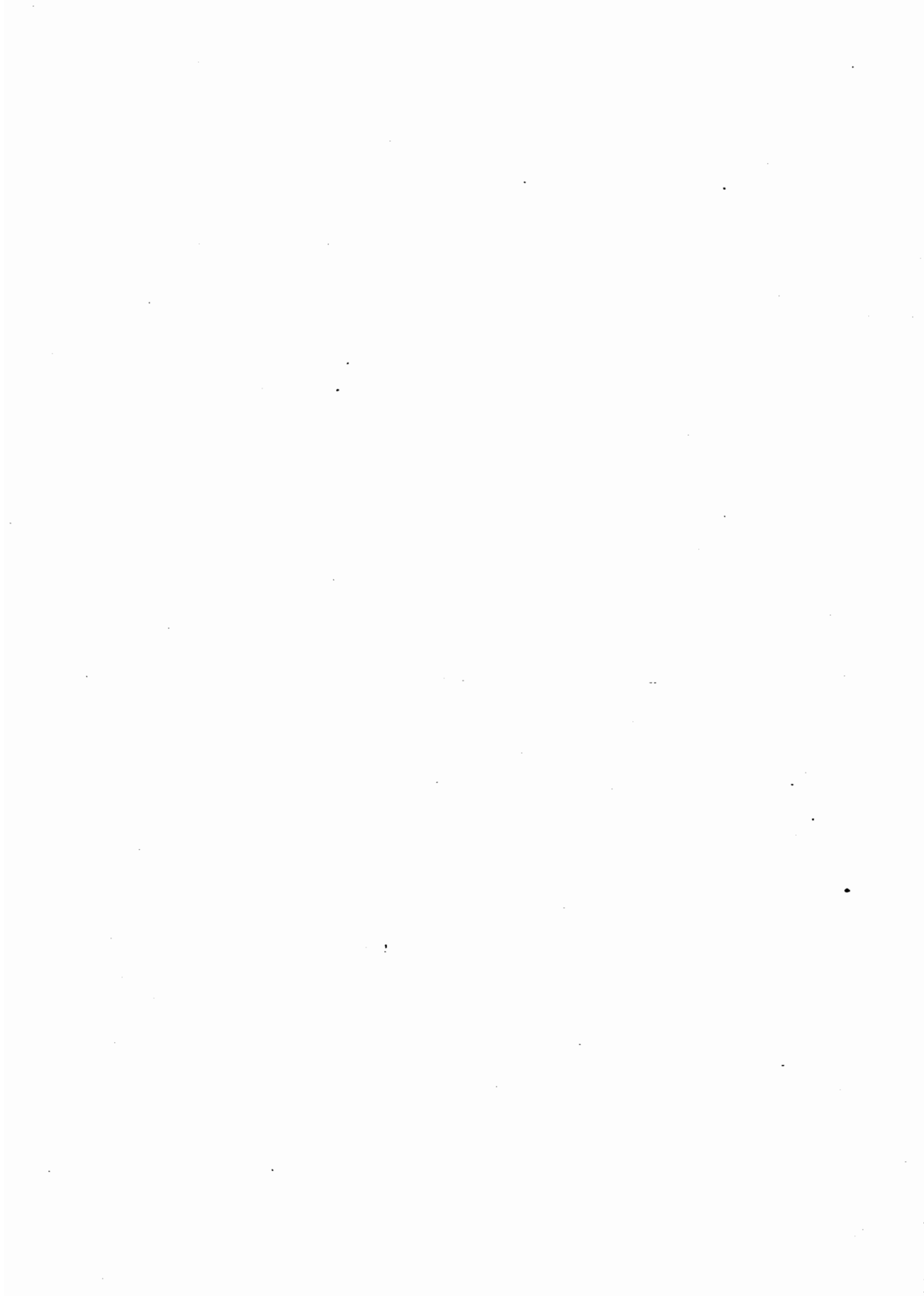
- Voloshinova, N. A.; Kuznetsova, V. N.; and Leonenko, L. S. 1970. Neogene Foraminifera of Sakhalin: Proceedings of the All Union Petroleum Scientific Research, Geological Exploration Institute. 3 Vols. National Translations Center TT 76-53241. Washington, D. C.: Smithsonian Institution and National Science Foundation; Translated from Russian.
- Von Rad, U., and Rosch, H. 1972. Mineralogy and origin of clay minerals, silica and authigenic silicates in Leg 14 sediments. In Initial reports of the Deep Sea Drilling Project, vol. 14, ed. A. C. Pimm, 727-51. Washington, D. C.: National Science Foundation.
- Wall, David, and Dale, Barnie. 1971. A reconsideration of living and fossil Pyrophacus Stein, 1883 (Dinophyceae). *Journal of Phycology* 7:221-35.
- Wallace, W. E. 1965. Application of electric log measured pressures to drilling problems and a new simplified chart for well site pressure computation. *Log Analyst* 6:26-38.
- Weber, K. J.; Mandl, G.; Pilaar, W. F.; Lehner, F.; and Precious, R. G. 1978. The role of faults in hydrocarbon migration and trapping in Nigerian growth fault structures. In Tenth Annual Offshore Technology Conference, proceedings, paper 3356.
- Whitney, J. W., and Wallace, W. K. 1984. Oceanic plate motions and tectonic evolution of the Bering Sea shelf. In 80th Annual meeting, Cordilleran Section, Geological Society of America, May 30-June 1, 1984, Anchorage, Alaska: Abstracts with programs, 340.
- Williams, G. L. 1975. Dinoflagellate and spore stratigraphy of the Cenozoic, offshore eastern Canada. *Geological Survey of Canada*, paper 74-30, 2, 107-161.
- Williams, G. L., and Bujak, J. P. 1977. Cenozoic palynostratigraphy of offshore Eastern Canada. In Contributions of stratigraphic palynology (with emphasis on North America): Vol. 1, Cenozoic palynology, ed. W. C. Elsik, 14-48. American Association of Stratigraphic Palynologists Contribution Series no. 5A.
- Wills, J. C.; Bolm, J. G.; Stewart, G. H.; Turner, R. F.; Lynch, M. B.; Petering, G. W.; Parker, John; and Schoof, Brian. 1978. Geological and operational summary, Atlantic Richfield Lower Cook Inlet, Alaska, COST well No. 1. U.S. Geological Survey Open-File Report 78-145.
- Wilson, G. J., and Bush, R. E. 1973. Pressure prediction with flowline temperature gradients. AIME-SPE Paper no. 3848. *Journal of Petroleum Technology* 25:135-42.



APPENDIX 1

Suggested Abbreviations for Lithologic Descriptions  
Excerpted from Mitchell and Maher, 1957

arg	Argillaceous
blk	Black
brn	Brown
calc	Calcite, calcareous
carb	Carbonaceous
cly	Clay, clayey
clyst	Claystone
cmt	Cement, cemented
dk	Dark
f	Fine, finely
fos	Fossil, fossiliferous
frag	Fragment, fragmental
fri	Friable
frs	Fresh
glau	Glaucinite, glauconitic
gn	Green
gr	Grain, grained
gy	Gray
hd	Hard
ig	Igneous
intr	Intrusion, intrusive
lam	Laminated
ls	Limestone
lstr	Luster
lt	Light, lighter
m	Medium
mas	Massive
mdst	Mudstone
mica	Mica, micaceous
mts	Matrix
pyr	Pyrite, pyritized
qtz	Quartz
sd	Sand
sdv	Sandy
sft	Soft
sh	Shale
shy	Shaly
sl	Slight, slightly
sltst	Siltstone
slty	Silty
ss	Sandstone
tr	Trace
tuf	Tuffaceous
v	Very
vf	Very fine
vgt	Variegated



## APPENDIX 2

### Well Data and Consultants Reports Available for Public Inspection, Navarin Basin COST No. 1 Well

#### Schlumberger Offshore Services Anchorage, AK

- 2 in. Dual Laterolog/Micro-Spherically Focused Log  
Runs 1, 2, 3, 4, 5
- 5 in. Dual Laterolog/Micro-Spherically Focused Log  
Runs 1, 2, 3, 4, 5
- 2 in. Dual Induction Laterolog/Spherically Focused Log Linear  
Correlation  
Runs 1, 3, 4, 5
- 2 in. Borehole Compensated Sonic Log  
Runs 1, 2, 3, 4, 5
- 5 in. Borehole Compensated Sonic Log  
Runs 1, 2, 3, 4, 5
- 2 in. Compensated Neutron/Formation Density Log  
Runs 1, 2, 3, 4, 5
- 5 in. Compensated Neutron/Formation Density Log  
Runs 1, 2, 3, 4, 5
- 2 in. Compensated Formation Density  
Runs 1, 2, 3, 4, 5
- 5 in. Compensated Formation Density  
Runs 1, 2, 3, 4, 5
- 2 in. Natural Gamma Ray Spectrometry Tool  
Runs 1, 2, 3, 4, 5
- 5 in. Natural Gamma Ray Spectrometry Tool  
Run 1, 3, 4, 5
- 2 in. Long-Spaced Sonic Log  
Runs 1, 2, 3, 4, 5
- 5 in. Long-Spaced Sonic Log  
Run 1, 2, 3, 4, 5

5 in. Sonic Waveforms -- 8 ft.  
Runs 1, 2, 3, 4, 5

2 in. Proximity-Microlog  
Run 3

5 in. Proximity-Microlog  
Runs 2, 3, 4

High Resolution Dipmeter Tool  
Run 1

5 in. Stratigraphic High Resolution Dipmeter Tool  
Run 5

5 in. Stratigraphic High Resolution Dipmeter Tool Cyberdip  
Runs 5

5 in. Dipmeter  
Runs 2, 4, 5

Repeat Formation Tester  
Runs 1, 2, 3

Repeat Formation Tester Quicklook  
Runs 2, 3

60 in. Repeat Formation Tester  
Run 3

2 in. High Resolution Thermometer  
Run 5

5 in. Cement Bond/Variable Density Log  
Run 5

2 in. Profile Caliper  
Run 3

Polar Plat  
Run 1

5 in. Arrow Plot from Cluster Program  
Runs 1, 2, 3, 4

Core Laboratories, Inc.  
Anaheim, CA

Special Core Analysis Studies  
Core Analysis Permeability and Porosity  
Core Photographs  
Correlation Coregraph

PBT, Inc.  
Golden, CO

Compressional and Shear Wave Velocities of Cores

ARCO Alaska, Inc.  
Anchorage, AK

Core Descriptions  
Core Gamma Data  
Sidewall Sample Descriptions  
Vertical Seismic Profiles  
Head Space Gas Analysis  
Calibrated Sonic Log  
Vertically Stacked Seismic Traces  
Deviation Plot of Travel Times  
Two-Way Travel Time Log

ERT Biostrat  
Fort Collins, CO

Biostratigraphic Weekly Reports

Z-Axis Exploration Inc.  
Walnut Creek, CA

Paleomagnetism of Cores, Interpretation and Data

Baroid  
Anchorage, AK

Mud Report

University of Colorado  
Boulder, CO

Paleontology Report Core No. 7

Jay Marks  
Englewood, CO

Paleontology Report

Eastman Whipstock  
Anchorage, AK

Core Orientation Reports

Production Services  
Anchorage, AK

Drill Stem Tests

Robertson Research (U.S.), Inc.  
Houston, TX

Geochemical Analysis  
Supplemental Geochemical Analysis of Cuttings and Core No. 14

Biostratigraphics  
San Diego, CA

Palynology Report  
Radiolaria Report  
Calcareous Nannofossil Report  
Biostratigraphic Summary  
Siliceous Nannofossil Report  
Foraminifera Report  
Charts  
    Diatoms  
    Spores and Diatoms  
    Foraminifera

Hughes Tool  
Anchorage, AK

Bit Record

Exploration Logging (USA), Inc. (Exlog)  
Anchorage, AK

Formation Evaluation Log  
Gemdas Logging Reports  
Geochemical Final Well Report

Teledyne Isotopes  
Westwood, NJ

K-Ar Age Determinations

Christensen Diamond Products  
Salt Lake City, Utah

Coring Logs

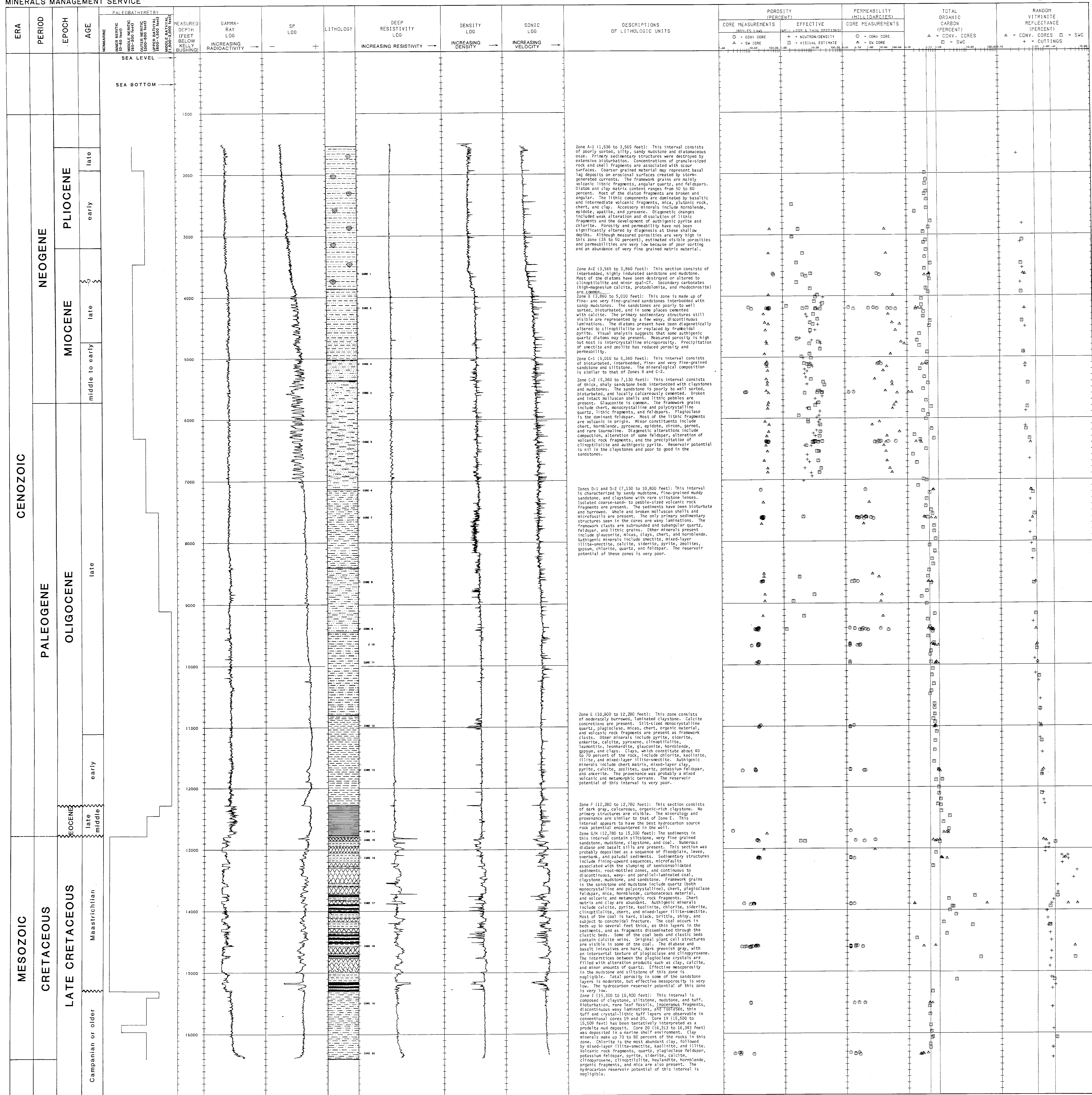
Birdwell  
Anchorage, AK

Calibrated Velocity Log

Seismograph Service Corp.  
Tulsa, OK

Seismic Velocity Survey

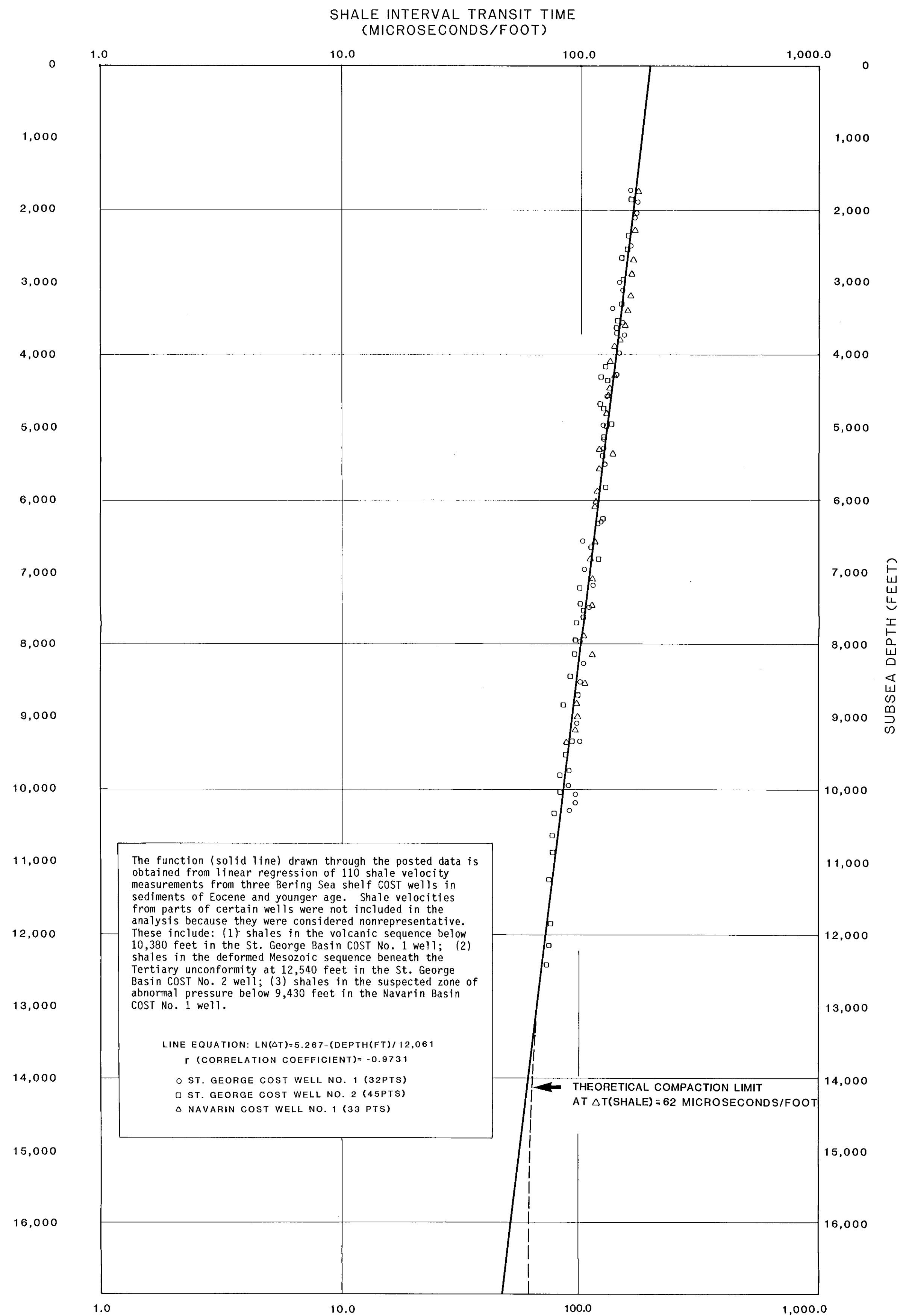
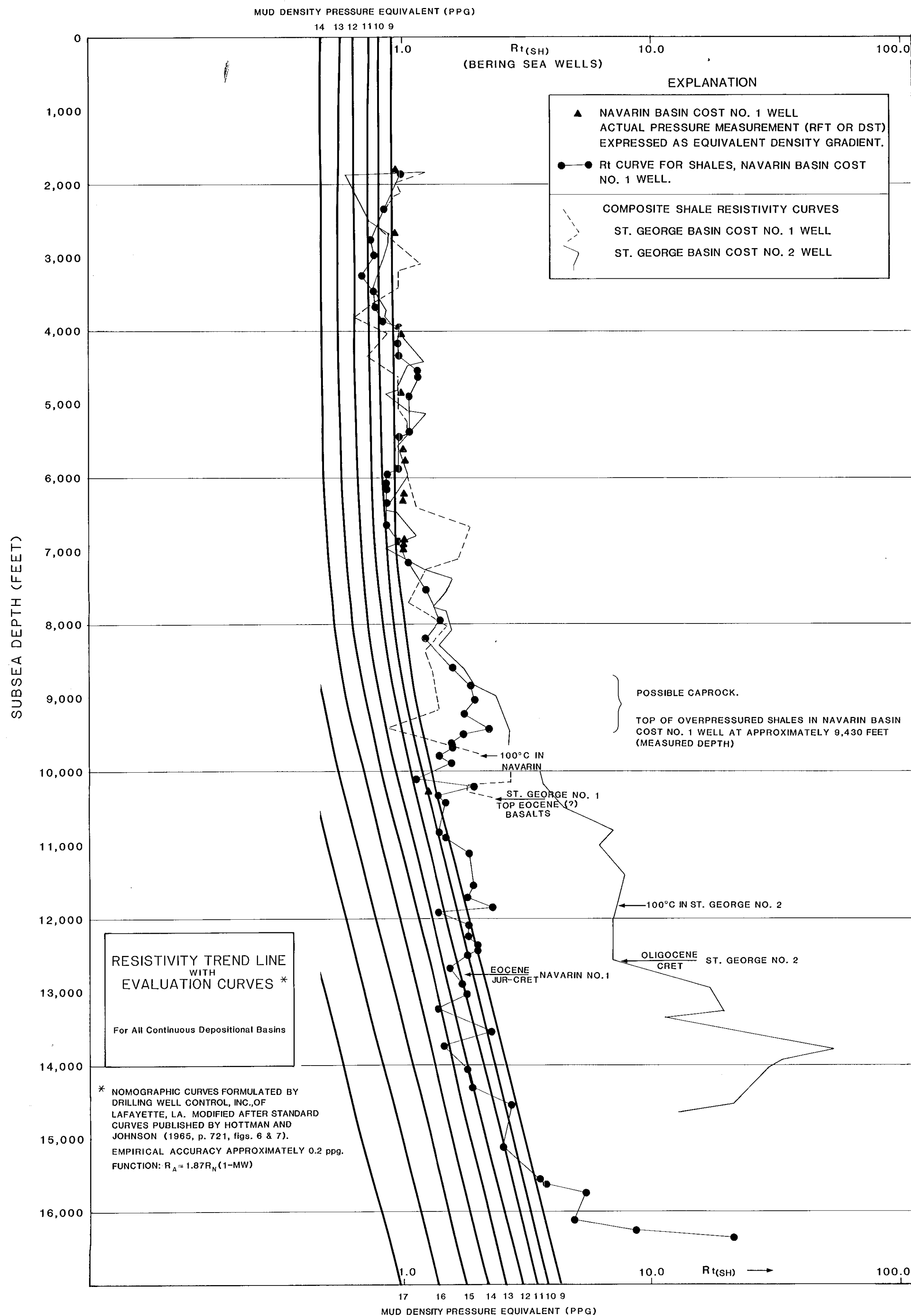




STRATIGRAPHIC COLUMN AND SUMMARY CHART OF GEOLOGIC DATA, NAVARIN BASIN COST NO. 1 WELL, BERING SEA, ALASKA

BERING SEA SHELF COMPOSITE SHALE RESISTIVITY CURVES FOR  
SEDIMENTS OF HOLOCENE THROUGH CRETACEOUS (?) AGE

BERING SEA SHELF COMPOSITE SHALE ACOUSTIC TRANSMISSION  
CURVE FOR SEDIMENTS OF HOLOCENE THROUGH EOCENE AGE



SHALE RESISTIVITY AND SHALE VELOCITY CURVES, BERING SEA SHELF, ALASKA.

**RESISTIVITY LOG**

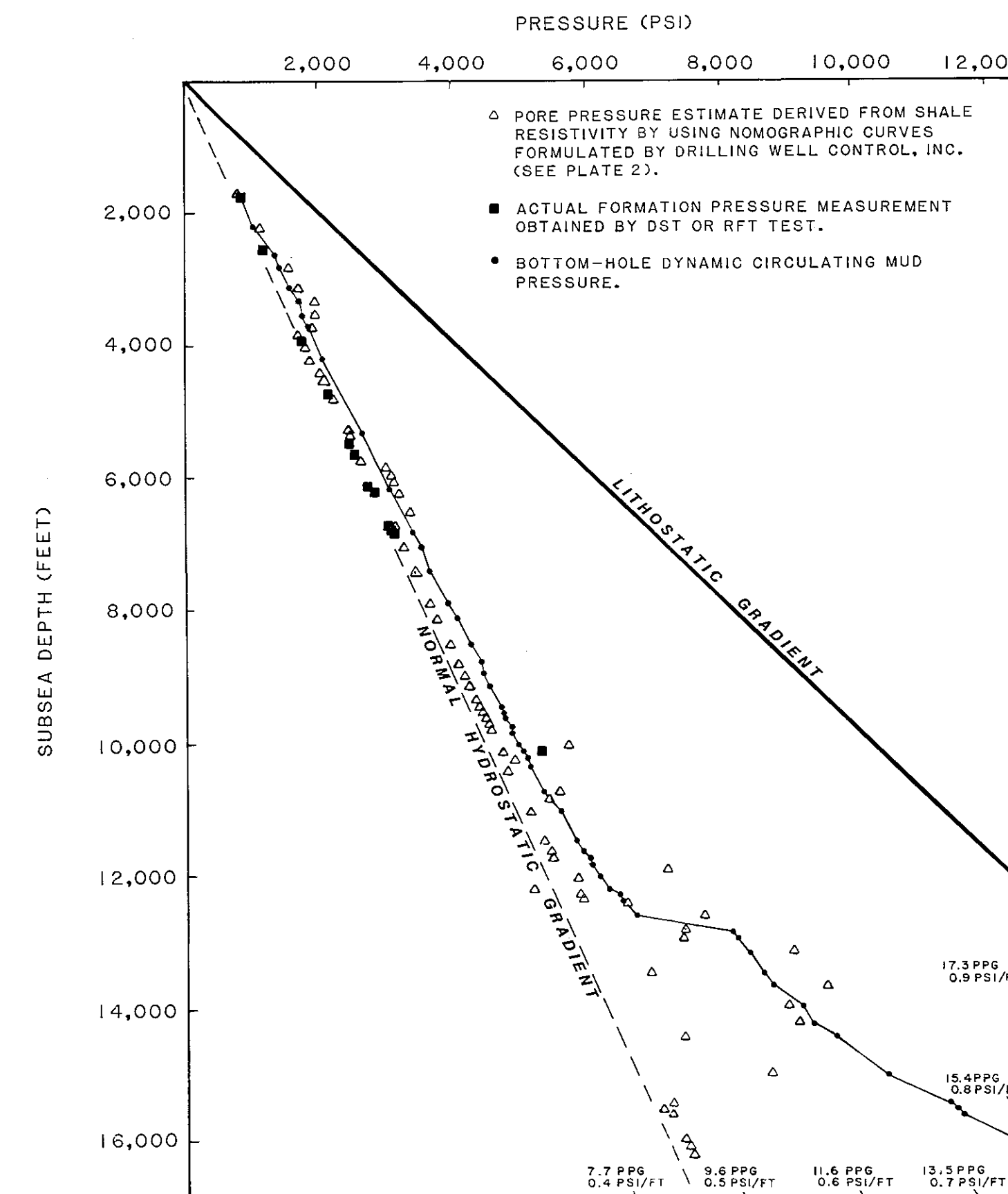


DIAGRAM A: PRESSURE PLOT DERIVED FROM SHALE RESISTIVITY DATA.

**SONIC LOG**

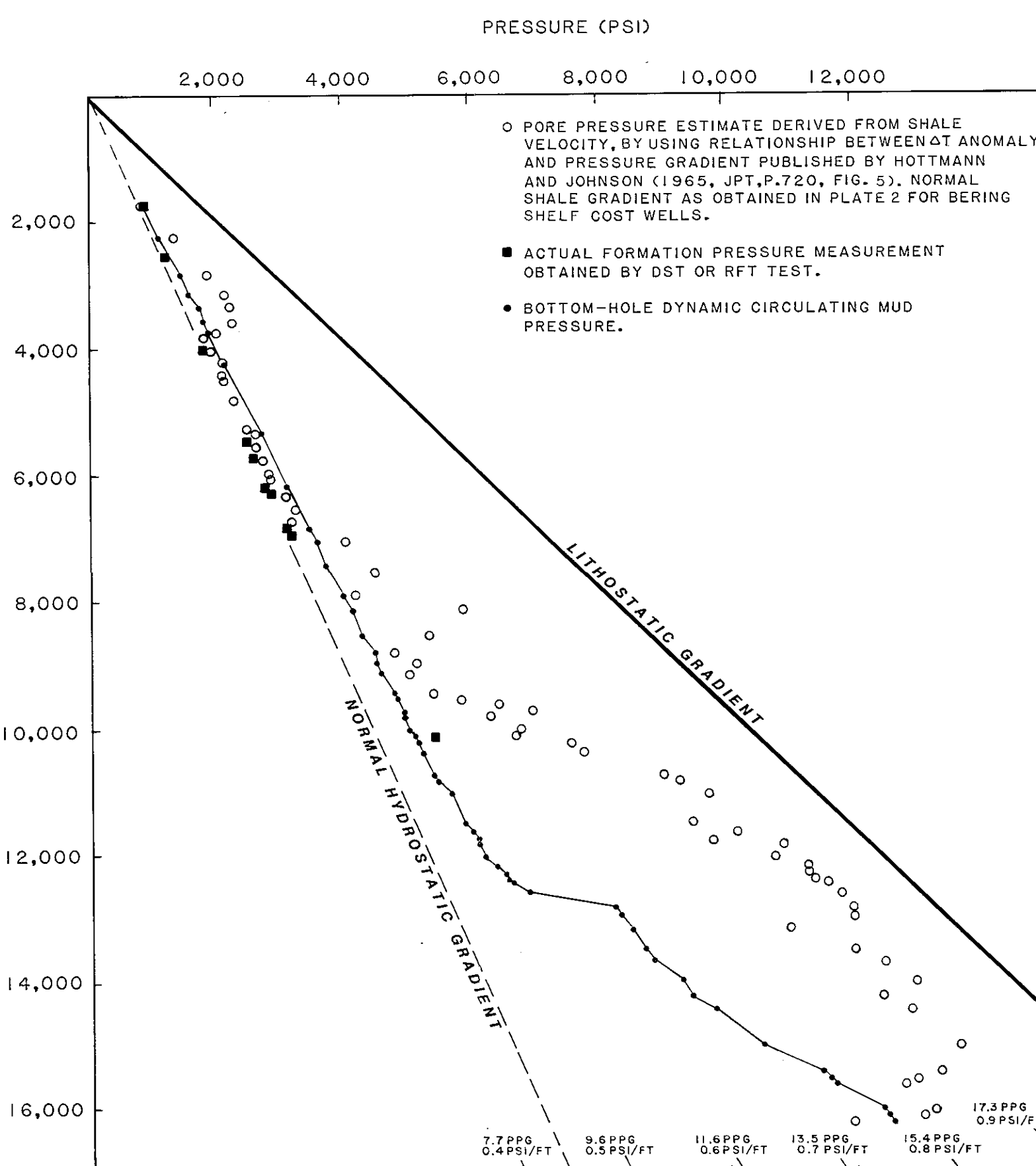


DIAGRAM B: PRESSURE PLOT DERIVED FROM SHALE ACOUSTIC DATA AND BERING SEA COMPACTION CURVE BY USING RELATIONSHIP BETWEEN  $\Delta T$  (NORMAL) -  $\Delta T$  (ACTUAL), OR  $\Delta T$  ANOMALY, AND PORE PRESSURE GRADIENT PUBLISHED BY HOTTMANN AND JOHNSON (1965, P. 720, FIG. 5).

**SONIC LOG**

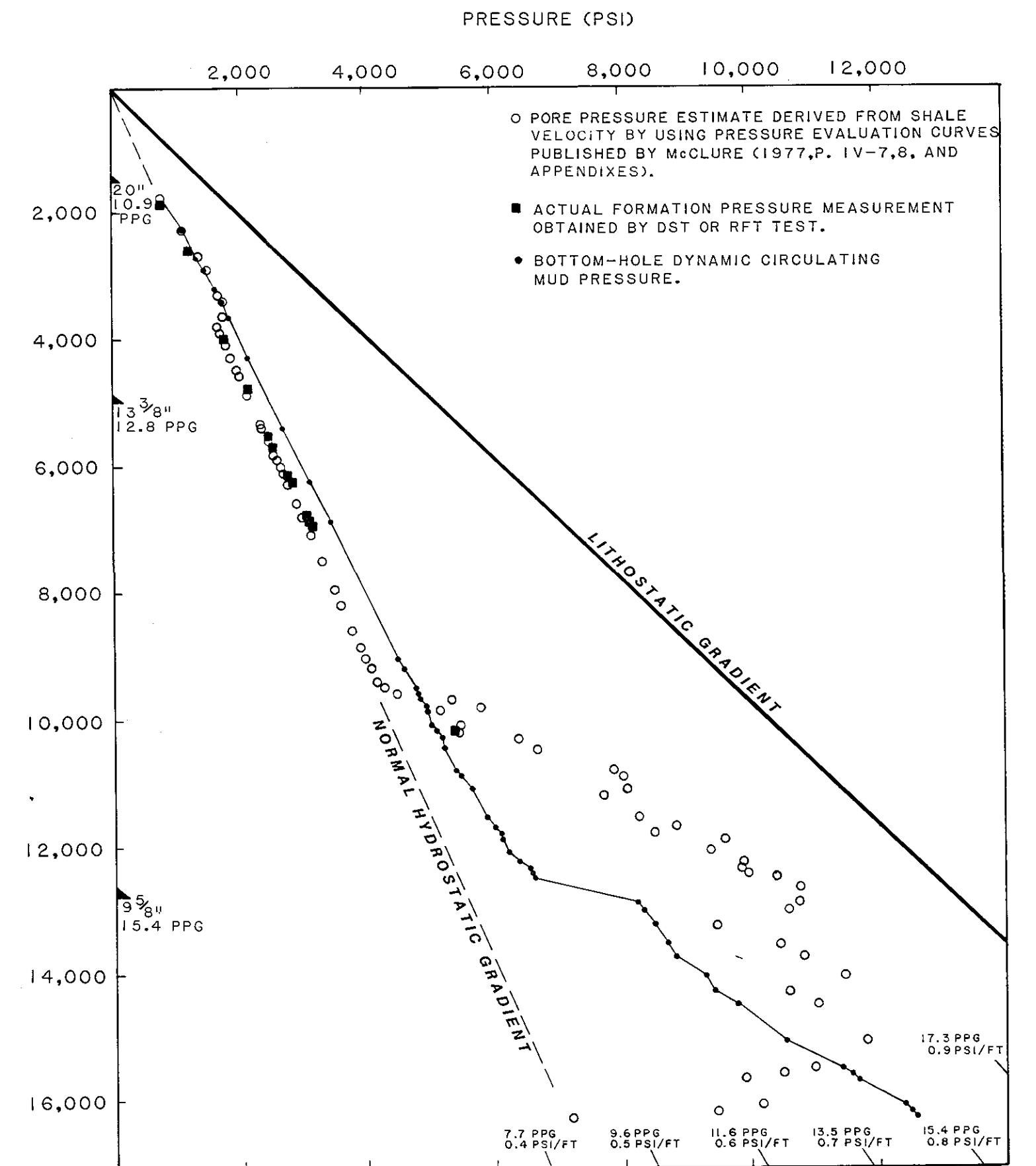


DIAGRAM C: PRESSURE PLOT DERIVED FROM SHALE ACOUSTIC DATA BY UTILIZING PRESSURE EVALUATION CURVES (SEE FIGURE 60) PUBLISHED BY McCLURE (1977, P. IV-7,8 AND APPENDICES). CASING POINTS AND LEAK-OFF FRACTURE GRADIENTS ARE POSTED ON THE LEFT SIDE OF THE DIAGRAM.

**DENSITY**

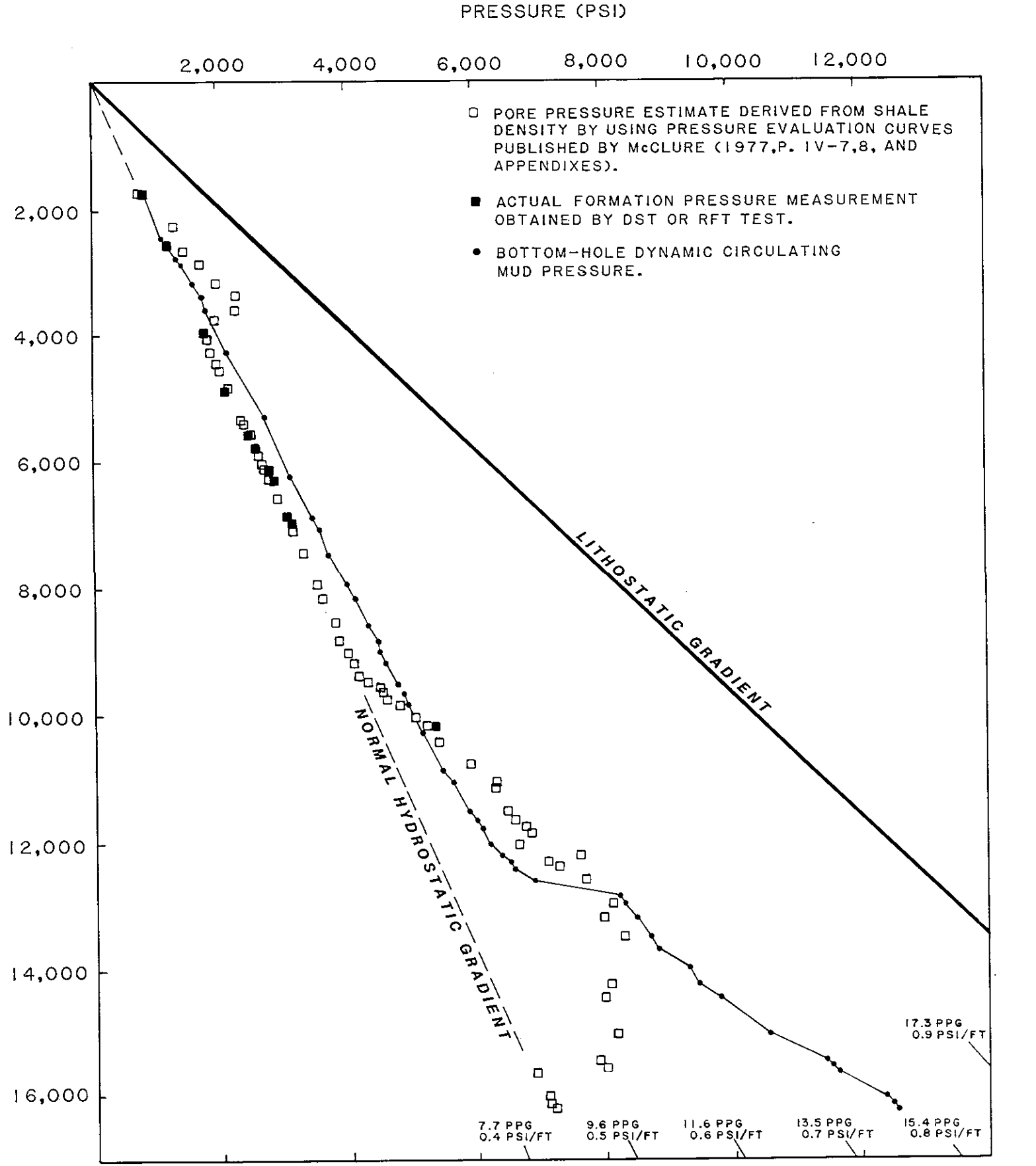


DIAGRAM D: PRESSURE PLOT DERIVED FROM SHALE DENSITY DATA BY UTILIZING PRESSURE EVALUATION CURVES (SEE FIGURE 60) PUBLISHED BY McCLURE (1977, P. IV-7,8, AND APPENDICES).

**DRILLING EXPONENT**

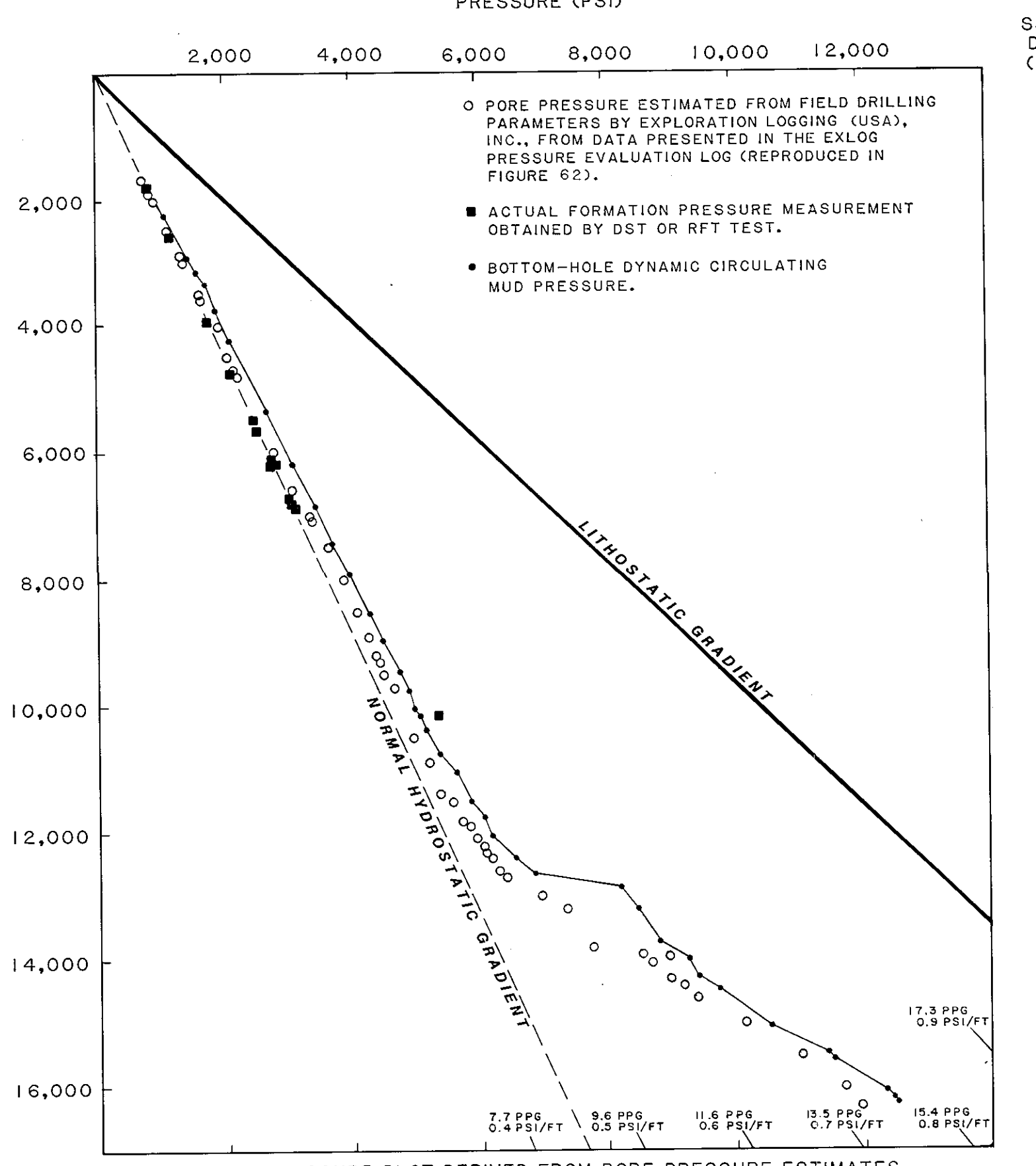


DIAGRAM E: PRESSURE PLOT DERIVED FROM PORE PRESSURE ESTIMATES CALCULATED FROM FIELD DRILLING PARAMETERS BY EXPLORATION LOGGING (USA), INC., AS SUMMARIZED IN FIGURE 62.

**CLAY MINERALOGY**

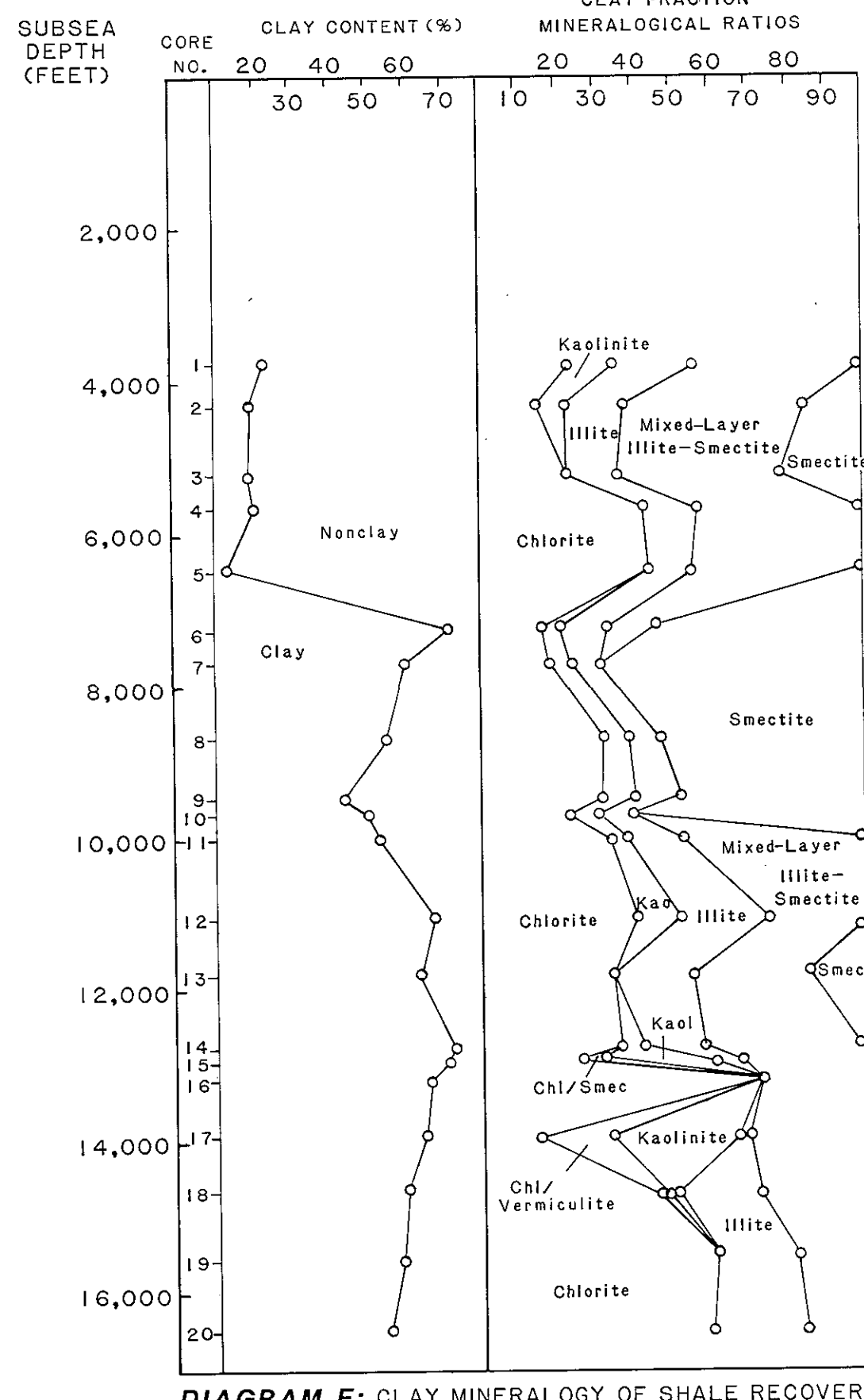


DIAGRAM F: CLAY MINERALOGY OF SHALE RECOVERED IN CONVENTIONAL CORES. MODIFIED AFTER AGAT CONSULTANTS, INC. (1983, D-423-1, FIG. 5).

**TEMPERATURE**

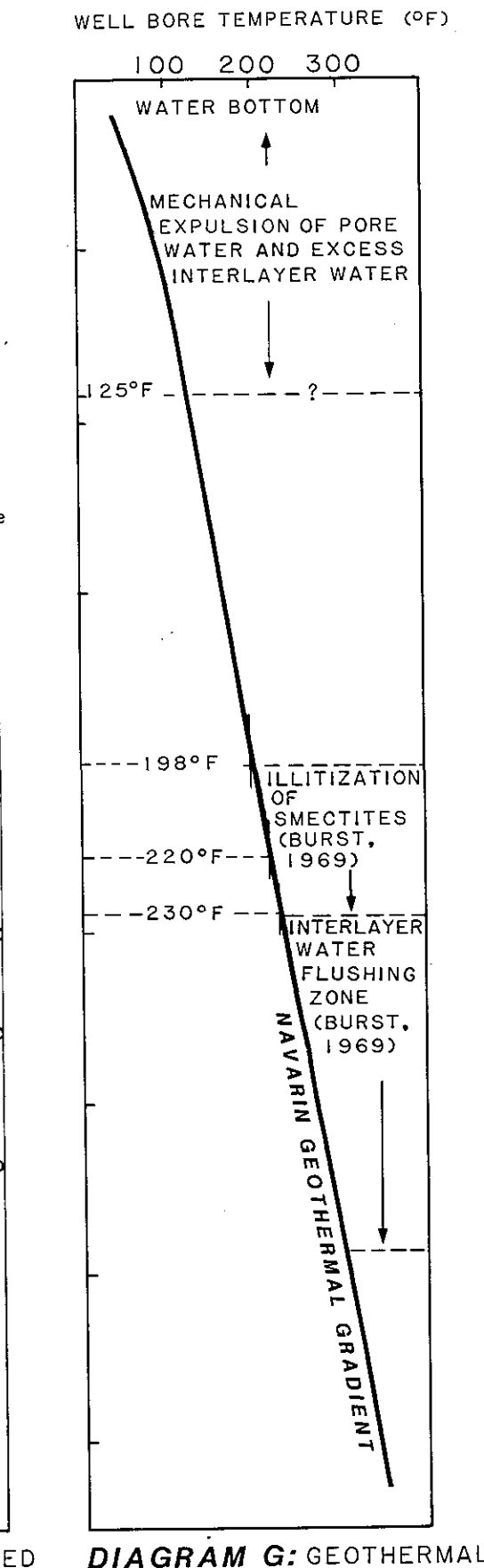


DIAGRAM G: GEOTHERMAL GRADIENT IN THE NAVARIN BASIN COST NO. 1 WELL (THIS REPORT).

**AGE DATA**

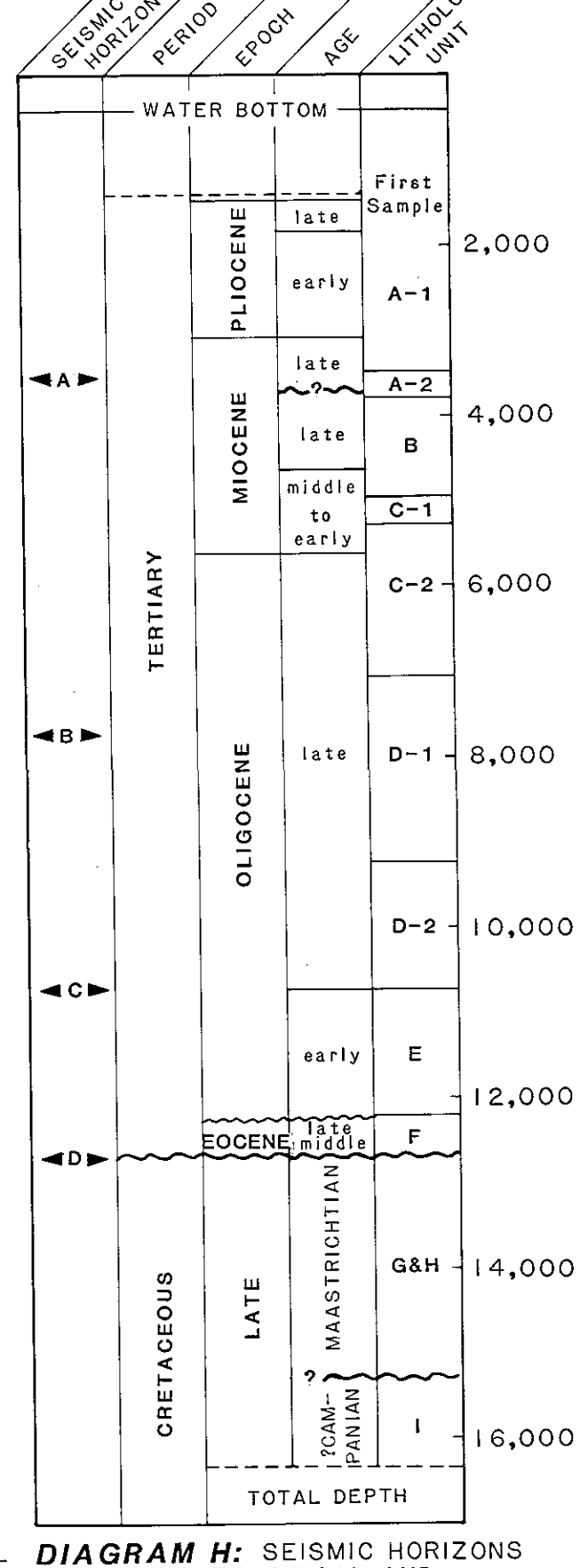


DIAGRAM H: SEISMIC HORIZONS AND PALEONTOLOGICAL AND LITHOLOGICAL ZONATION IN THE NAVARIN BASIN COST NO. 1 WELL (THIS REPORT).

